Propagation of Tau pathology in Alzheimer disease

Dissertation

zur

Erlangung des Doktorgrades (Dr. rer. nat.)

der

Mathematisch-Naturwissenschaftlichen Fakultät

der

Rheinischen Friedrich-Wilhelms-Universität Bonn

vorgelegt von

Sara Ferreira Rodrigues

Braga, Portugal

Bonn

2020

Angefertigt mit Genehmigung der Mathematisch-Naturwissenschaftlichen Fakultät der Rheinischen Friedrich-Wilhelms-Universität Bonn

1. **Gutachter: Prof. Dr. Eckhard Mandelkow**
2. **Gutachter: Prof. Dr. Walter Witke**

Tag der Promotion: 02.06.2020

Erscheinungsjahr: 2020

To my parents and brother

“Para ser grande, sê inteiro: nada

Teu exagera ou exclui.

Sê todo em cada coisa. Põe quanto és

No mínimo que fazes.

Assim em cada lago a lua toda

Brilha, porque alta vive”

Ricardo Reis

Abbreviations

ºC – degree Celsius

µg – microgram

µL – microliter

µM – micromolar

AD – Alzheimer disease

AAV – adeno-associated virus

Aβ – amyloid beta

APP – amyloid precursor protein

BBB – blood brain barrier

BCA – bicinchoninic acid

BSA – bovine serum albumin

BW – body weight

CA1 – cornu ammonis 1

CA2 – cornu ammonis 2

CA3 – cornu ammonis 3

CAMKII – calmodulin kinase II

Cdk5 – cyclin-dependent kinase 5

DAB – 3,3'-Diaminobenzidine

DG – dentate gyrus

EC – entorhinal cortex

FTD – frontotemporal dementia

gcl – granule cell layer

GFAP – glial fibrillary acidic protein

GSK3β – glycogen synthetase kinase 3β

htau – human tau

IF – immunofluorescence

IHC – immunohistochemistry

i.p. – intra-peritoneal

KO – knockout

LEC – medial entorhinal cortex

MAP – microtubule associated protein

ml – molecular layer

mM – milimolar

MAP – microtubule-associated protein

MEC – medial entorhinal cortex

MT – microtubule

MWM – Morris water maze

NFTs – neurofibrillary tangles

Nop - Neuropsin

NOR – novel object recognition

OF – open field

PaS – parasubiculum

PBS – phosphate-buffered saline

pcl – pyramidal cell layer

PHF – paired helical filaments

p. i. – post-injection

PP – perforant pathway

PrS – presubiculum

PSD95 – post-synaptic density 95

PSP – progressive supranuclear palsy

pTau – Tau phosphorylation

PVDF – polyvinylidenedifluoride

RPM – rotations per minute

RT – room temperature

SDS – sodium dodecyl sulfate

slm – *stratum lacunosum moleculare*

so – *stratum oriens*

sr – *stratum radiatum*

TBS – tris-buffered saline

tetO – tetracycline operator

ThS – thioflavin S

TKO – Tau-knouckout

tTA – tetracycline transactivator

WB – western blot

WT – wild type

Summary

Clinical and experimental evidences suggest that the spreading of tau protein throughout the brain may underlie the stereotypical progression of pathology in the brains of Alzheimer disease (AD) patients and concomitant cognitive decline. Although previous studies showed that tau protein can be released and taken up by cells, several open questions regarding the spreading of tau pathology still exist. The nature of the tau species that are able to spread across cells is still unknown. Furthermore, it is still debatable if the tau species that propagate across cells are the species responsible for the pathological changes. Recently, the involvement of other processes in the pathological mechanisms of AD, like neuroinflammation, further contributed to this debate. Therefore, this doctoral thesis monitored the potential involvement of the aggregation propensity of tau on the spreading of the protein across cells, and in the extent of pathology developed. This was achieved by using transgenic mouse models expressing mutant human tau (htau) with a pro-aggregant (ΔK280) or anti-aggregant (ΔK280-2P) mutation, restricted to the entorhinal cortex (EC). This study showed that the propagation of tau is independent of the protein's aggregation potential, as both pro- and anti-aggregant htau propagate from the EC to other brain regions. In contrary, markers of tau pathology (phosphorylation, pathological conformation) did not spread further than the EC axon terminals located in the middle molecular layer of the dentate gyrus (DG). We also observed marked astrogliosis in the hippocampal region of mice expressing pro-aggregant htau, suggesting that neuroinflammatory processes may precede the spreading of tau pathology from the EC to the hippocampus.

Based on the principle that inhibiting tau aggregation may be a promising therapeutic target, we additionally tested the efficacy of BSc3094, a tau aggregation inhibitor, in reducing tau pathology using transgenic mice expressing mutant human P301L tau. BSc3094 reduced the levels of tau phosphorylation and insoluble tau, and improved cognition in some behavioral tasks as well.

Altogether, these results provide novel evidence about the mechanisms underlying the propagation of tau pathology, and highlight BSc3094 as a promising compound for a future therapeutic approach for AD.

List of figures

Figure 1 - Schematic representation of a healthy neuron (right) and an AD neuron (left) summarizing the typical cellular cascades affected in AD. 4

Figure 2 - Genomic structure of the human MAPT gene and the splicing isoforms of tau in the human brain. 7

Figure 3 - Dual role of tau phosphorylation in the cell. 10

Figure 4 - Schematic representation of the residues in the longest tau isoform that can be phosphorylated and epitopes specific for major tau antibodies. 11

Figure 5 - Functions of tau protein. 14

Figure 6 - Formation of tau fibrils. 16

Figure 7 - Trans-synaptic propagation of tau pathology and Braak staging, illustrating the progression of tau pathology in AD. 19

Figure 8 - Prion-like propagation of tau pathology. 20

Figure 9 - Mechanisms for tau transfer between cells. 21

Figure 10 - The perforant pathway provides the major input to the hippocampus from the entorhinal cortex. 23

Figure 11 - Layers of the EC on the mouse brain. 24

Figure 12 - Organization of the rodent dentate gyrus. 25

Figure 13 - The hippocampal mossy cell. 26

Figure 14 - Different cell types are involved in tau-induced neuroinflammation. 28

Figure 15 - Potential therapeutic strategies to reduce tau aggregates. 32

Figure 16 - Blood-brain-barrier. 33

Figure 17 - Tau transgene expression in the experimental mouse models. 47

Figure 18 - *In vivo* bioluminescence imaging of luciferase activity in the mouse brain. 49

Figure 19 - Implantation of Alzet osmotic pumps for direct intraventricular drug delivery. 52

Figure 20 - Nesting test. 52

Figure 21 - A mouse in a burrowing tube. 53

Figure 22 – Expression of mutant human tau-ΔK280 and tau-ΔK280-2P is restricted to the entorhinal cortex. 64

Figure 23 - Body weight of gender-mixed WT, pro- and anti-aggregant tau transgenic mice. 65

Figure 24 - Expression of mutant human tau in the neuropsin mice at different ages. 67

Figure 25 - Expression of mutant human tau in the neuropsin mice at 24 months of age. 68

Figure 26 - Total tau levels in the entorhinal cortex of neuropsin pro- and anti-aggregant mice. 69

Figure 27 - Phosphorylation of tau on the Ser262/Ser356 epitope is more pronounced in the pro-aggregant mice compared to anti-aggregant mice. 69

Figure 28 - Tau phosphorylation at Ser262/Ser356 in pro-aggregant, anti-aggregant and wild-type mice at different ages. 70

Figure 29 - Tau phosphorylation at Thr231/Ser235 in pro-aggregant, anti-aggregant and wild-type mice at different ages. 71

Figure 30 - Expression of tau with pathological conformation over time. 73

Figure 31 - Expression of tau with pathological conformation in the neuropsin mice at 24 months of age. 74
Figure 32 - No significant alterations in astrogliosis observed in the dentate gyrus of pro- and anti-aggregant mice compared to wild-type mice. 75
Figure 33 - No significant alterations in microglia expression observed in the dentate gyrus of pro- and anti-aggregant mice compared to wild-type mice.. 76
Figure 34 - No significant alterations in neuroinflammation markers in the DG and EC of neuropsin mice at 24 months of age. 77
Figure 35 - Experimental design of the project. 78
Figure 36 - Body weight in all experimental groups at 5 months of age (before AAV injection) and at 18 months post-injection. 79
Figure 37 - Total tau levels in non-injected mice and mice injected with AAV-K2 and AAV-K3. 80
Figure 38 - Trans-synaptic spreading of tau protein in pro- and anti-aggregant neuropsin mice 3 months after AAV injection. 81
Figure 39 - Trans-synaptic spreading of tau protein in WT mice injected with AAV encoding pro- and anti-aggregant mutant human tau 3 months after AAV injection. 82
Figure 40 - Trans-synaptic spreading of tau protein in TKO mice injected with AAV encoding pro- and anti-aggregant mutant human tau 3 months after AAV injection. 83
Figure 41 - Expression of GFP and human tau (Tau Y9) in a WT mouse injected with AAV-K2 (pro-aggregant htau) at 18 months post-injection. 84
Figure 42 - Phosphorylation of tau at Ser396/Ser404, detected with PHF-1 antibody in the EC region of AAV-injected mice, 3 months after AAV injection. 85
Figure 43 - Phosphorylation of tau at Ser396/Ser404, detected with PHF-1 antibody, only propagates from the EC to other brain regions in WT mice. 86
Figure 44 - Expression of tau with pathological conformation (antibody MC1) in neuropsin mice 18 months post-injection. 87
Figure 45 - Expression of tau with pathological conformation in WT mice injected with AAV-K2 or AAV-K3 at 18 months post-injection. 88
Figure 46 - Expression of tau with pathological conformation in TKO mice injected with AAV-K2 or AAV-K3 at 18 months post-injection. 89
Figure 47 - Expression of GFAP and Iba1 in pro- and anti-aggregant neuropsin mice at 3 months post-injection. 91
Figure 48 - Levels of inflammatory markers in neuropsin pro- and anti-aggregant mice over time. 92
Figure 49 - Expression of GFAP and Iba1 in WT mice injected with AAV-K2 and AAV-K3 at 3 months post-injection. 93
Figure 50 - Levels of inflammatory markers in WT mice injected with AAV-K2 and AAV-K3 over time. 94
Figure 51 - Expression of GFAP and Iba1 in TKO mice injected with AAV-K2 and AAV-K3 at 3 months post-injection. 95
Figure 52 - Levels of inflammatory markers in TKO mice injected with AAV-K2 and AAV-K3 over time. 96

FIGURE 53 - LEVELS OF INFLAMMATORY MARKERS IN WT AND TKO MICE INJECTED WITH AAV-K2 OVER TIME. 97
FIGURE 54 - LEVELS OF PRE- AND POST-SYNAPTIC MARKERS IN NEUROPSIN PRO- AND ANTI-AGGREGANT MICE OVER TIME. 98
FIGURE 55 - LEVELS OF PRE- AND POST-SYNAPTIC MARKERS IN WT MICE INJECTED WITH AAV-K2 AND AAV-K3 OVER TIME. 99
FIGURE 56 - LEVELS OF PRE- AND POST-SYNAPTIC MARKERS IN TKO MICE INJECTED WITH AAV-K2 AND AAV-K3 OVER TIME. 100
FIGURE 57 - LEVELS OF PRE- AND POST-SYNAPTIC MARKERS IN WT AND TKO MICE INJECTED WITH AAV-K2 OVER TIME. 101
FIGURE 58 - INTRAVENOUS ADMINISTRATION OF BSC3094 DEMONSTRATES POOR BLOOD-BRAIN-BARRIER PERMEABILITY, BUT DIRECT INTRACEREBRAL ADMINISTRATION OF THE DRUG SIGNIFICANTLY REDUCES SARKOSYL-INSOLUBLE TAU. 104
FIGURE 59 - EXPERIMENTAL DESIGN FOR TESTING THE PUTATIVE THERAPEUTIC EFFECT OF BSC3094........ 105
FIGURE 60 - TOTAL BRAIN AND BODY WEIGHT IN RTG4510 AND CONTROL MICE USED IN THE STUDY........ 106
FIGURE 61 - BURROWING AND NESTING TESTS SHOWED THAT BSC3094 DOES NOT RESCUE THE BEHAVIORAL DEFICITS IN RTG4510 MICE. 107
FIGURE 62 - NO MOTOR IMPAIRMENTS OBSERVED IN RTG4510 MICE, BUT A SLIGHT INCREASE IN ANXIETY-LIKE BEHAVIOR COMPARED TO CONTROL MICE. 108
FIGURE 63 - BSC3094 TREATMENT REVERSED THE MEMORY DEFICITS IN RTG4510 MICE IN THE NOVEL OBJECT RECOGNITION TEST. 109
FIGURE 64 - BSC3094 DID NOT IMPROVE SPATIAL REFERENCE MEMORY IN RTG4510 MICE. 110
FIGURE 65 - BSC3094 TREATMENT SLIGHTLY IMPROVED LONG-TERM MEMORY IN THE MWM TEST. 111
FIGURE 66 - TREATMENT WITH BSC3094 SIGNIFICANTLY REDUCED TAU PHOSPHORYLATION IN RTG4510 MICE. 113
FIGURE 67 - BSC3094 DID NOT REVERSE THE LOSS OF GLUTAMATE RECEPTOR 1 IN RTG4510 MICE. 114
FIGURE 68 - BSC3094 TREATMENT DID NOT REVERSE THE LOSS IN THE EXPRESSION OF SYNAPTIC MARKERS IN RTG4510 MICE. 115
FIGURE 69 - SCHEMATIC REPRESENTATION OF THE SPREADING OF TAU PROTEIN AND TAU PATHOLOGY. 132

List of tables

TABLE 1 - SUMMARY FOR ALL EXPERIMENTAL GROUPS REGARDING TAU MARKERS: HUMAN TAU (TAU Y9), PHOSPHORYLATED TAU (PHF-1) AND PATHOLOGICAL CONFORMATION OF TAU (MC1). 90

TABLE 2 - SUMMARY FOR ALL EXPERIMENTAL GROUPS REGARDING THE EXPRESSION OF THE NEUROINFLAMMATORY MARKERS IBA1/CD11B (FOR MICROGLIA) AND GFAP (FOR ASTROGLIA) OBTAINED BY IMMUNOFLUORESCENCE OR WESTERN BLOT IN DIFFERENT BRAIN REGIONS AND TIME POINTS. 98

TABLE 3 - SUMMARY OF THE EXPRESSION OF PRE-SYNAPTIC (SYNAPTOPHYSIN) AND POST-SYNAPTIC (PSD95) MARKERS IN THE ENTORHINAL CORTEX AND HIPPOCAMPUS IN ALL EXPERIMENTAL GROUPS. 102

List of supplementary figures

SUPPL. FIG. 1 - PLASMID MAPS OF THE ADENO-ASSOCIATED VIRUS USED IN THE STUDY. 161

SUPPL. FIG. 2 - VOLUME OF LUCIFERIN TO BE INJECTED IN THE MICE BEFORE BLI MEASUREMENT ACCORDING TO THE BODY WEIGHT TO ACHIEVE AN INJECTION CONCENTRATION OF 150 MG/KG. 163

SUPPL. FIG. 3 - DOSAGE OF ANALGESIA (CARPROFEN) TO BE ADMINISTRATED TO THE MICE BEFORE SURGERY, ACCORDING TO THE ANIMAL'S BODY WEIGHT. 164

SUPPL. FIG. 4 - SCORE SHEET FOR EVALUATING THE MICE AFTER STEREOTAXIC INJECTION OF AAV, AS APPROVED BY THE GERMAN AUTHORITY FOR ANIMAL WELFARE LANUV UNDER THE ANIMAL APPLICATION NUMBER 84-02.04.2016-A278. 165

SUPPL. FIG. 5 - SCORE SHEET FOR EVALUATING THE MICE AFTER IMPLANTATION AND REPLACEMENT OF ALZET OSMOTIC PUMPS, AS APPROVED BY THE GERMAN AUTHORITY FOR ANIMAL WELFARE LANUV UNDER THE ANIMAL APPLICATION NUMBER 84-02.04.2017-A405. 166

Index

SUMMARY IX

LIST OF FIGURES XI

LIST OF TABLES XV

LIST OF SUPPLEMENTARY FIGURES XV

INDEX XVII

1. INTRODUCTION 3

- 1.1. ALZHEIMER DISEASE EPIDEMIOLOGY 3
- 1.2. CLINICAL SYMPTOMS AND PATHOLOGICAL MECHANISMS OF ALZHEIMER DISEASE 3
- 1.3. TAU PROTEIN 5
  - *1.3.1. Genomic structure and tau isoforms 5*
  - *1.3.2. Physiological functions 8*
  - *1.3.3. Tau phosphorylation 8*
  - *1.3.4. Sorting mechanisms of tau 11*
  - *1.3.5. Pathological roles of tau protein 12*
  - *1.3.6. Toxicity of different tau species 14*
- 1.4. MOUSE MODELS FOR THE STUDY OF ALZHEIMER DISEASE 15
- 1.5. PROPAGATION OF TAU PATHOLOGY IN ALZHEIMER DISEASE 17
- 1.6. THE PERFORANT PATHWAY 22
  - *1.6.1. Entorhinal cortex 22*
  - *1.6.2. Hippocampus 24*
- 1.7. NEUROINFLAMMATION AND AD - ROLE OF GLIAL CELLS IN THE PROPAGATION OF TAU PATHOLOGY 26
- 1.8. THERAPEUTICAL INTERVENTIONS TO HALT THE PROPAGATION OF TAU PATHOLOGY 29
  - *1.8.1. BSc3094 as a potential therapeutic agent for AD 30*
  - *1.8.2. The blood-brain-barrier as an obstacle for drug delivery 31*

2. AIMS OF THE STUDY 37

3. MATERIALS AND METHODS 41

- 3.1. MATERIALS 41
  - *3.1.1. Primary antibodies 41*
  - *3.1.2. Secondary antibodies 42*
  - *3.1.3. Molecular weight markers 42*
  - *3.1.4. Kits 42*
  - *3.1.5. Centrifuges 43*
  - *3.1.6. Microscopes 43*
  - *3.1.7. Surgery equipment 43*
  - *3.1.8. Others 44*
- 3.2. METHODS 45
  - *3.2.1. Animals 45*
  - *3.2.2. Housing conditions 47*
  - *3.2.3. Fresh ex-vivo brain slices and measurement of luciferase bioluminescence 47*

3.2.4. In vivo bioluminescence of human tau expression ... 48
3.2.5. Adeno-associated virus (AAV) ... 49
3.2.6. AAV injections ... 50
3.2.7. Determination of BSc3094 concentration in the brain ... 50
3.2.8. Implantation of Alzet osmotic pumps ... 51
3.2.9. Behavioral assessment ... 52
3.2.10. Histological analysis ... 55
3.2.11. Immunofluorescence ... 56
3.2.12. Microscopy ... 57
3.2.13. Brain homogenization and protein quantification ... 57
3.2.14. Sarkosyl extraction ... 57
3.2.15. Western blotting ... 58
3.2.16. Statistical analysis ... 58
4. RESULTS ... 63
4.1. PROPAGATION OF TAU PATHOLOGY IN MICE EXPRESSING TAU UNDER THE NEUROPSIN PROMOTER 63
4.1.1. Transgenic mice expressing pro- and anti-aggregant human tau under the neuropsin promoter ... 63
4.1.2. Absence of trans-synaptic spreading in neuropsin pro- and anti-aggregant mice up to 24 months of age ... 65
4.1.3. Tau phosphorylation is increased in pro-aggregant mice compared to anti-aggregant mice 69
4.1.4. Only pro-aggregant mice present pathological conformation of tau, which is restricted to the EC 72
4.1.5. Inflammatory processes are not altered in pro- or anti-aggregant mice compared to WT non-transgenic mice ... 75
4.2. PROPAGATION OF TAU PATHOLOGY IN AAV-INJECTED MICE ... 77
4.2.1. Body weight of all experimental groups ... 78
4.2.2. Tau protein can spread across cells independently of the aggregation propensity ... 79
4.2.3. Is GFP also spreading across cells? ... 84
4.2.4. Phosphorylation of tau is more pronounced in pro-aggregant mice ... 85
4.2.5. Pathological conformation of tau observed in pro-aggregant mice, but restricted to the EC and perforant pathway ... 87
4.2.6. Pro-aggregant mice have increased astrogliosis, and this may precede the trans-synaptic spreading of tau pathology ... 90
4.3. THERAPEUTIC INTERVENTION TO HALT THE PROPAGATION OF TAU PATHOLOGY BY A TAU AGGREGATION INHIBITOR ... 102
4.3.1. BSc3094 has poor BBB permeability, but direct intraventricular administration reduces sarkosyl-insoluble tau in transgenic mice ... 103
4.3.2. rTg4510 mice have decreased brain and body weight compared to littermate controls, which is not reversed by BSc3094 treatment ... 105

4.3.3. BSc3094 treatment does not reverse the impairments in burrowing and nest building in rTg4510 mice ... 106
4.3.4. rTg4510 transgenic mice do not show motor impairment, but anxiety-like behavior in the open field ... 107
4.3.5. BSc3094 treatment reverses the memory impairment in rTg4510 mice in the novel object recognition test, but not in the y-maze test ... 109
4.3.6. BSc3094 improves long-term memory in the Morris Water Maze test ... 110
4.3.7. BSc3094 treatment reduces the level of phosphorylated tau species in rTg4510 mice 112
4.3.8. BSc3094 treatment has no effect on the expression of glutamate receptor and synaptic markers ... 113
5. DISCUSSION ... 119
5.1. PROPAGATION OF TAU PATHOLOGY IN MOUSE MODELS OF EARLY ALZHEIMER DISEASE ... 119
5.1.1. Transgenic mice expressing pro- and anti-aggregant human tau under the neuropsin promoter as models of tau spreading ... 120
5.1.2. Combining AAV-directed gene transfer with neuropsin mice to boost the propagation of tau pathology ... 122
5.1.3. The propagation of tau protein is independent of the aggregation potential ... 123
5.1.4. Absence of trans-synaptic propagation of markers of tau pathology ... 125
5.2. ROLE OF NEUROINFLAMMATION IN THE ONSET AND PROPAGATION OF TAU PATHOLOGY ... 127
5.2.1. Neuroinflammation may precede the propagation of tau pathology ... 128
5.3. THERAPEUTIC INTERVENTION TO HALT THE PROPAGATION OF TAU PATHOLOGY ... 133
5.3.1. Tau aggregation inhibitors as therapeutical agents for AD and other tauopathies ... 133
5.3.2. BSc3094 as a promising therapeutical agent for tau-related neurodegeneration ... 134
5.3.3. Treatment with BSc3094 failed to reverse the body and brain weight loss in rTg4510 mice 135
5.3.4. Treatment with BSc3094 significantly reduced the levels of phosphorylated and insoluble tau, and partially improved cognition ... 135
6. CONCLUSIONS ... 141
7. REFERENCES ... 145
8. APPENDIX ... 161

1

INTRODUCTION

1. Introduction

1.1. Alzheimer disease epidemiology

According to worldwide demographic records, the number of elderly people has been rising substantially over the last century, due to an increase in life expectancy of the population (Alzheimer's Association, 2017). Since the incidence of dementia rises with age, this demographic change is leading to an increase of dementia. The 2018 World Alzheimer Report presents dramatic numbers: every three seconds one person develops dementia worldwide, and there are about 50 million people in the world currently affected by the disease. This number is predicted to rise to about 152 million people by 2050 (Alzheimer's Disease International, 2018).

The most common type of dementia is Alzheimer disease (AD), accounting for 2/3 of all dementia cases (Alzheimer's Disease International, 2018). AD is a progressive age-related neurodegenerative disorder characterized by impairments in memory, thinking and behavior. Symptoms usually develop slowly and aggravate over time, interfering with the person's daily tasks (Holtzman et al., 2012). The high prevalence of the disease creates a massive strain on the health care systems and families' budget. The current cost of the disease is about a trillion US dollars a year, which is forecast to double by 2030 (Alzheimer's Disease International, 2018). This amount includes an estimated cost for "informal" caregivers, the people who suddenly find themselves acting as 24-hour nurses to family relatives. Worth mentioning, AD caregivers are often at an increased risk for significant health problems, experiencing depression, high levels of stress, sadness, anxiety, loneliness, and exhaustion (Heinrich et al., 2014; Mausbach et al., 2014).

Considering this, many governments around the world have increased research and clinical efforts to find new preventive and therapeutic strategies for AD.

1.2. Clinical symptoms and pathological mechanisms of Alzheimer disease

AD is clinically characterized by a gradual and progressive impairment in cognitive functions. The outstanding clinical feature of AD patients is the impairment in short-term memory, disabling the retention of new information (Thies & Bleiler, 2011).

Furthermore, there are also disturbances in executive functions involving judgment, planning or solving problems, difficulty completing familiar tasks, confusion with time or place, problems with words in speaking and writing, and changes in mood and personality (Alzheimer’s Association, 2019).

Several brain changes occur in AD, but the two major histopathological hallmarks of the disease are the extracellular deposition of senile plaques containing amyloid-β (Aβ), and the hyperphosphorylation and aggregation of the protein tau inside neurons, leading to the formation of neurofibrillary tangles (NFTs) (figure 1).

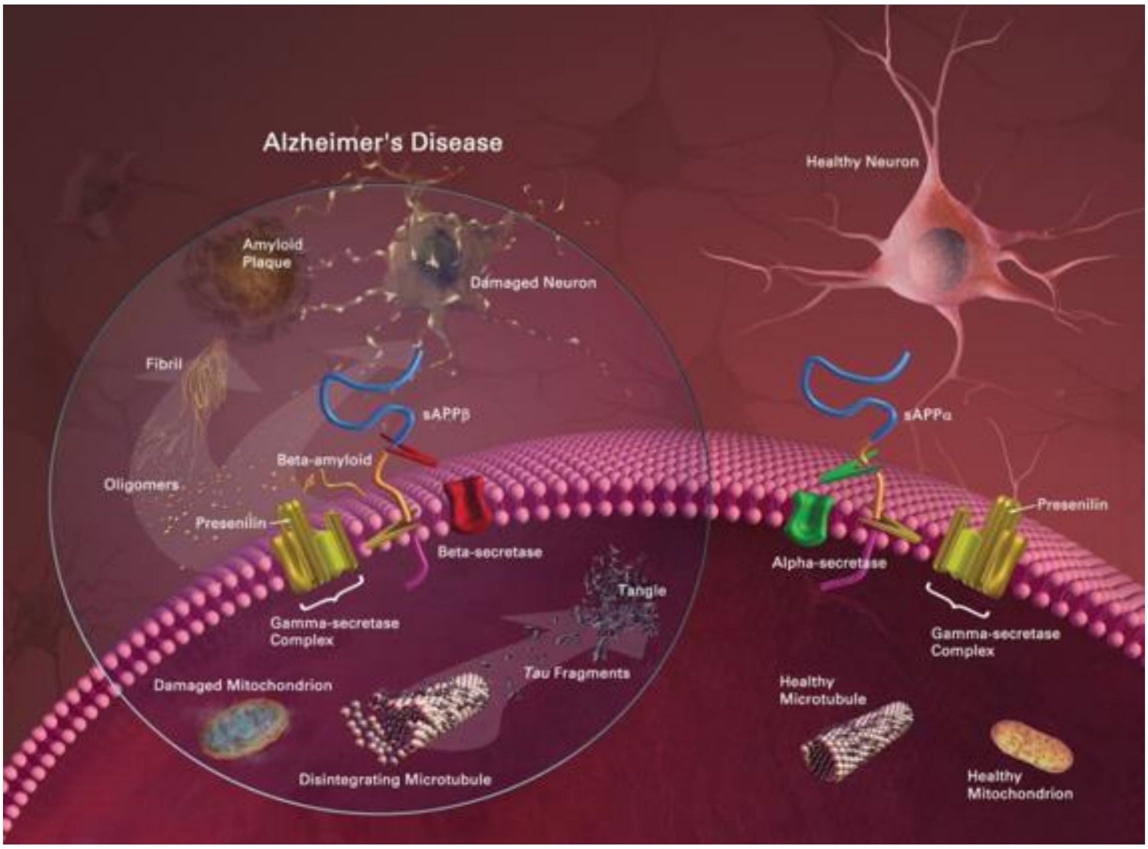
Alzheimer's Disease
Healthy Neuron
Amyloid Plaque
Damaged Neuron
Fibril
sAPPβ
sAPPα
Beta-amyloid
Oligomers
Presenilin
Beta-secretase
Presenilin
Alpha-secretase
Tangle
Gamma-secretase Complex
Gamma-secretase Complex
Tau Fragments
Damaged Mitochondrion
Healthy Microtubule
Disintegrating Microtubule
Healthy Mitochondrion

Figure 1 - Schematic representation of a healthy neuron (right) and an AD neuron (left) summarizing the typical cellular cascades affected in AD.
In healthy neurons, APP is cleaved by α-secretase, preventing the production of neurotoxic Aβ. Tau protein binds and stabilizes microtubules. In contrast, AD neurons are characterized by the sequential cleavage of APP by β-secretase and γ-secretase, resulting in Aβ production and release into the extracellular space, where it eventually accumulates in senile amyloid plaques. Furthermore, hyperphosphorylated tau detaches from microtubules, leading to their disruption. The free, unbound tau accumulates and aggregates, leading to the formation of NFTs. (Image courtesy of the National Institute on Aging/National Institutes of Health; https://www.nia.nih.gov/alzheimers/alzheimers-scientific-images-and-video).

Studies have demonstrated that misprocessed amyloid precursor protein (APP) and Aβ trigger synaptic malfunction, neuronal atrophy and synaptic loss (Catania et al., 2009; Almeida et al., 2005; Roselli et al., 2005). While still debated, it is suggested that

Aβ triggers abnormal tau hyperphosphorylation as well, leading to the formation of NFTs and neuronal loss in AD (Huang and Jiang, 2009). On the other hand, accumulating data suggests the involvement of tau in the detrimental effects of Aβ, as different *in vitro* and *in vivo* studies have provided compelling evidence that tau is necessary for Aβ-induced neurotoxicity, since the absence of tau blocked the neurotoxic effects of Aβ in tau-knockout (KO) mice (Rapoport et al., 2002; Roberson et al., 2007; Ittner et al., 2010; Zempel et al., 2013; Vossel et al., 2015). Furthermore, recent studies demonstrated that synaptic dysfunction/atrophy and memory loss are accompanied by synaptic accumulation of hyperphosphorylated tau (Hoover et al., 2010; Kimura et al., 2010). Indeed, tau is present in synapses acting as a scaffold protein that interacts with different proteins/receptors to modulate synaptic signaling and mechanisms of synaptic plasticity (Ittner et al., 2010; Kimura et al., 2014). As an example, P. Verstreken and collaborators have identified Synaptogyrin-3 as binding partner of tau on synaptic vesicles, revealing a new presynapse-specific tau interactor, which may contribute to early synaptic dysfunction in neurodegenerative diseases associated with tau (McInnes et al., 2018). Indeed, reduction of Synaptogyrin-3 prevents the association of presynaptic tau with vesicles, alleviating tau-induced defects in vesicle-mobility and restoring neurotransmitter release in fly and mouse models of tauopathy. In addition, while Aβ deposition does not correlate with the clinical progression of AD, the diffusion of NFTs, followed by neuronal and synaptic loss, matches the clinical progression of the disease (Braak & Braak, 1991; Murayama & Saito, 2004). Therefore, blocking tau aggregation and NFTs formation is considered a promising approach to prevent AD progression. Based on the above, the present thesis focuses on clarifying the role of tau protein in the mechanisms that precipitate AD pathology and its spreading throughout the brain, as well as on potential therapeutical strategies to halt the propagation of tau pathology.

1.3. Tau protein

1.3.1. Genomic structure and tau isoforms

Tau protein (Uniprot P10636, human tau), originally discovery by M. Kirschner and colleagues (Weingarten et al., 1975) is predominantly expressed in the axons of mature and growing neurons (Götz et al., 2013), but is also present at lower levels in astrocytes and oligodendrocytes (Lopresti et al., 1995; Gorath et al., 2001). Tau protein belongs to the family of microtubule-associated proteins (MAPs) (Dehmelt and Halpain, 2005). MAPs interact with heterodimers of α- and β-tubulin to assemble microtubules (MT) which, together with actin and intermediate filaments, establish and maintain the overall internal architecture of the cytoplasm, comprising a major determinant of overall cell shape (Goodson and Jonasson, 2018).

The human tau (htau) gene is located on chromosome 17q21.1, and comprises at least sixteen exons resulting from alternative splicing (Neve et al., 1986; Himmler, 1989) (figure 2). The gene produces three transcripts of 2, 6 and 9 kb, which are differentially expressed in the nervous system depending on the stage of neuronal maturation and neuron type (Andreadis, 2005; Couchie et al., 1992; Yan Wang & Loomis, 1993). By alternative mRNA splicing of exons 2, 3 and 10, six tau isoforms are produced in the central nervous system (CNS), resulting in six different polypeptide chains with molecular weights between 35 and 70 KDa. The six tau isoforms differ in the presence or absence of one or two short inserts in the amino-terminal half (0N, 1N and 2N, respectively), and have either three or four MT-binding semi-conserved repeats (~31 amino acid residues each) in the carboxy-terminal half (3R and 4R-tau), which form the MT-binding domain. The 4-repeat tau isoform (4R tau, with exon 10) shows higher affinity for MT than the 3R tau (without exon 10) isoform, and is therefore more efficient in promoting MT assembly (Goedert and Jakes, 1990; Goode and Feinstein, 1994). The expression of the different htau isoforms is developmentally regulated: in the adult human brain, six isoforms of tau are expressed, whereas in the fetal brain only the shortest tau is expressed. In the adult human brain, levels of 3R and 4R forms are roughly equal, but the 2N isoform is underrepresented compared with the others (Goedert and Jakes, 1990). Furthermore, the expression of tau in the human brain also shows considerable regional variation (Boutajangout et al., 2004; Trabzuni et al., 2012), which may contribute to the differential vulnerability of distinct brain regions to tau pathology, as it will be discussed later in the present dissertation. In the C-terminal tail, residues 369-400 are weakly homologous to the MT-binding repeats and, therefore, some authors refer to this region as R’ (or fifth repeat) (Gustke et al., 1994).

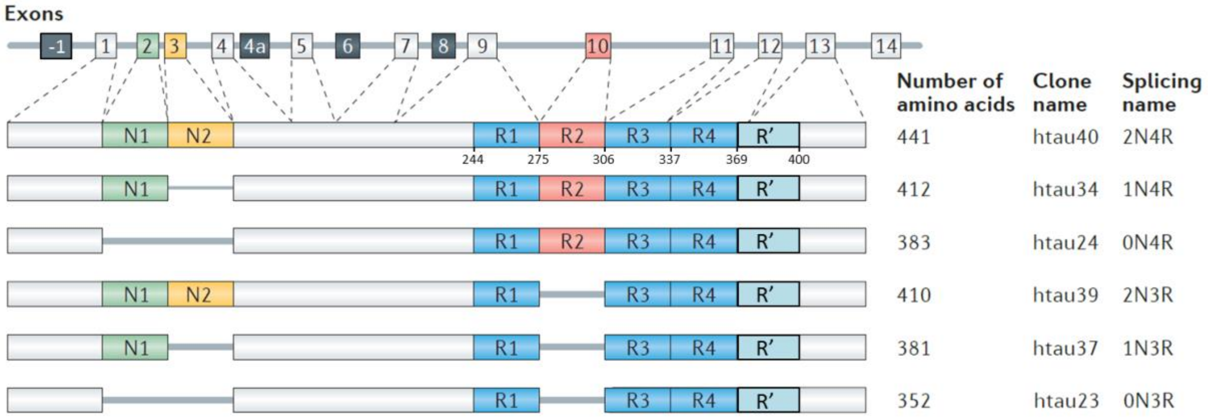

Figure 2 - Genomic structure of the human MAPT gene and the splicing isoforms of tau in the human brain.
The MAPT gene, which encodes htau, contains 16 exons. Exons 1, 4, 5, 7, 9, 11, 12 and 13 are constitutive (represented as grey boxes), while the others are subject to alternative splicing. A total of six mRNAs are generated by alternative splicing of exons 2, 3 and 10. These tau isoforms differ according to the presence of 0, 1 or 2 near-amino-terminal inserts (0N, 1N or 2N, respectively) and the presence of repeat R2, yielding 3 or 4 carboxy-terminal repeat domain tau species (3R or 4R, respectively). The residues 369-400 are weakly homologous to the repeats, and therefore named by some authors as R' (or fifth repeat). (Adapted from Wang & Mandelkow, 2016).

Tau is a highly hydrophilic, natively unfolded protein which remains soluble even under high temperatures. Despite being overall a basic protein, the ~120 N-terminal residues are predominantly acidic, and the ~40-residue C-terminus is roughly neutral (Gustke et al., 1994). This asymmetry of charges is important for interactions with MT and other partners, for internal folding and for aggregation (Mandelkow and Mandelkow, 2012). Although tau is the main component of paired-helical filaments (PHFs) found in AD (Grundke-Iqbal et al., 1986) and other tauopathies, it has little tendency for aggregation due to its hydrophilicity and flexibility (Mukrasch et al., 2009). However, when tau binds to other interacting proteins and partners (such as MT), certain conformations may become stabilized, which promote physiological or pathological states (Grüning et al., 2014; Kadavath et al., 2015). As an example, when tau protein is bound to MT, the amino acid residues critical for aggregation are stabilized in an alternative conformation (hairpin) and are not readily available, preventing the aggregation of the protein (Kadavath et al., 2015). This suggests that stabilizing the MT-bound conformation of tau may be a potential therapeutic approach, by delaying tau aggregation (Ballatore et al., 2012). Furthermore, in solution, the tau molecule tends to spontaneously change its conformation and favor a paperclip-like structure. This may prevent the self-aggregation of tau protein by masking the regions crucial for this process, suggesting another possible therapeutic approach (Jeganathan et al., 2008; Mroczko et al., 2019).

1.3.2. Physiological functions

By regulating dynamics of MT growth and shrinkage, tau plays an essential role in establishing neuronal cell polarity and axonal outgrowth during development, besides maintaining axonal morphology and axonal transport in mature cells (Shahani and Brandt, 2002). Tau may also regulate axonal transport indirectly: 1) by influencing the function of the motor proteins dynein and kinesin, which are responsible for transporting cargoes towards the cell body and the axon terminals, respectively (Stamer et al., 2002; Dixit et al., 2008); 2) by reducing the number of motors engaged with cargoes and thus interfere with axonal transport of cargoes (Vershinin et al., 2007)**;** 3) by competing with other cargoes for available kinesin and thereby affecting their axonal transport (Utton et al., 2005; Konzack et al., 2007)**;** among others (Magnani et al., 2007; Kanaan et al., 2011). Tau also plays an essential role in axonal elongation and maturation, as tau knockdown in cultured rat neurons inhibits neurite formation (Caceres and Kosik, 1990), whereas tau overexpression promotes the formation of neurites even in non-neuronal cells (Knops et al., 1991). Tau-KO mice have also highly contributed to the discovery of novel functions of tau protein. Although it was initially observed that Tau-KO mice do not present any obvious phenotype, probably due to the compensatory increase in MAP1 levels in axons (Hirokawa et al., 1996; Dawson et al., 2001), recent studies revealed pathological changes in this mouse line that also implicate tau in the regulation of neuronal activity (Roberson et al., 2007; Ittner et al., 2010; Leroy et al., 2012; Holth et al., 2013; Gheyara et al., 2014), neurogenesis (Fuster-Matanzo et al., 2009; Hong et al., 2010), iron export (Lei et al., 2012) and long-term depression (LTD) (Ahmed et al., 2014; Kimura et al., 2014).

1.3.3. Tau phosphorylation

Tau protein can suffer several types of post-translational modifications (PTMs), including glycosylation, ubiquitination, glycation, acetylation and phosphorylation. PTMs influence the protein's structure, functions and further cellular processing (Buée et al., 2000; Guo et al., 2017). Overall, phosphorylation has received most attention, since it is an early marker of tau pathology. It is believed that tau pathology arises, at least partially, from the impaired ability of hyperphosphorylated tau to bind MT, leading to the accumulation of tau and formation of fibrils, which are often accompanied by neuronal degeneration and loss (Gong and Iqbal, 2008). As an example, tau phosphorylation at Ser262 strongly reduces binding of tau to MT (Biernat et al., 1993).

Tau phosphorylation and dephosphorylation is a normal cellular event found in healthy cells, as a dynamic process essential for neurite outgrowth, axonal transport and MT assembly, stabilization and dynamics, meaning that it is not restricted to pathological states (Buée et al., 2000; Johnson and Stoothoff, 2004) (figure 3).

Despite this, the phosphorylation of tau is exacerbated in several tauopathies, resulting in a highly reduced ability of the protein to efficiently bind MT, as compared to normal tau (Yoshida and Ihara, 1993; Hanger et al., 2002). Therefore, hyperphosphorylation of tau at certain sites is thought to exert a neurotoxic function by interfering with MT stability and assembly, compromising dendritic plasticity and axonal transport (Biernat et al., 1993; Salehi et al., 2003). These changes are thought to lead to the disruption of the neuronal cytoskeleton and polymerization of phosphorylated tau in NFTs (Gong, 2000), which later cause neurodegeneration and cell death (figure 3).

Besides the disruption of MT-binding, hyperphosphorylation of tau may induce pathology through additional mechanisms. First, hyperphosphorylation might lead to the missorting of tau from axons to the somatodendritic compartment, causing synaptic dysfunction (Hoover et al., 2010). Second, the phosphorylation of tau may alter its autophagic and proteasomal degradation (Chesser et al., 2013) and its truncation by proteases (García-Sierra et al., 2008; Flores-Rodríguez et al., 2015). Third, the phosphorylation of tau is often considered to enhance its aggregation propensity (Despres et al., 2017), although this is still under debate because phosphorylation at certain sites may protect against aggregation (Schneider et al., 1999). Finally, phosphorylation may change the association of tau protein with its interaction partners, interfering with axonal transport (Ittner et al., 2009).

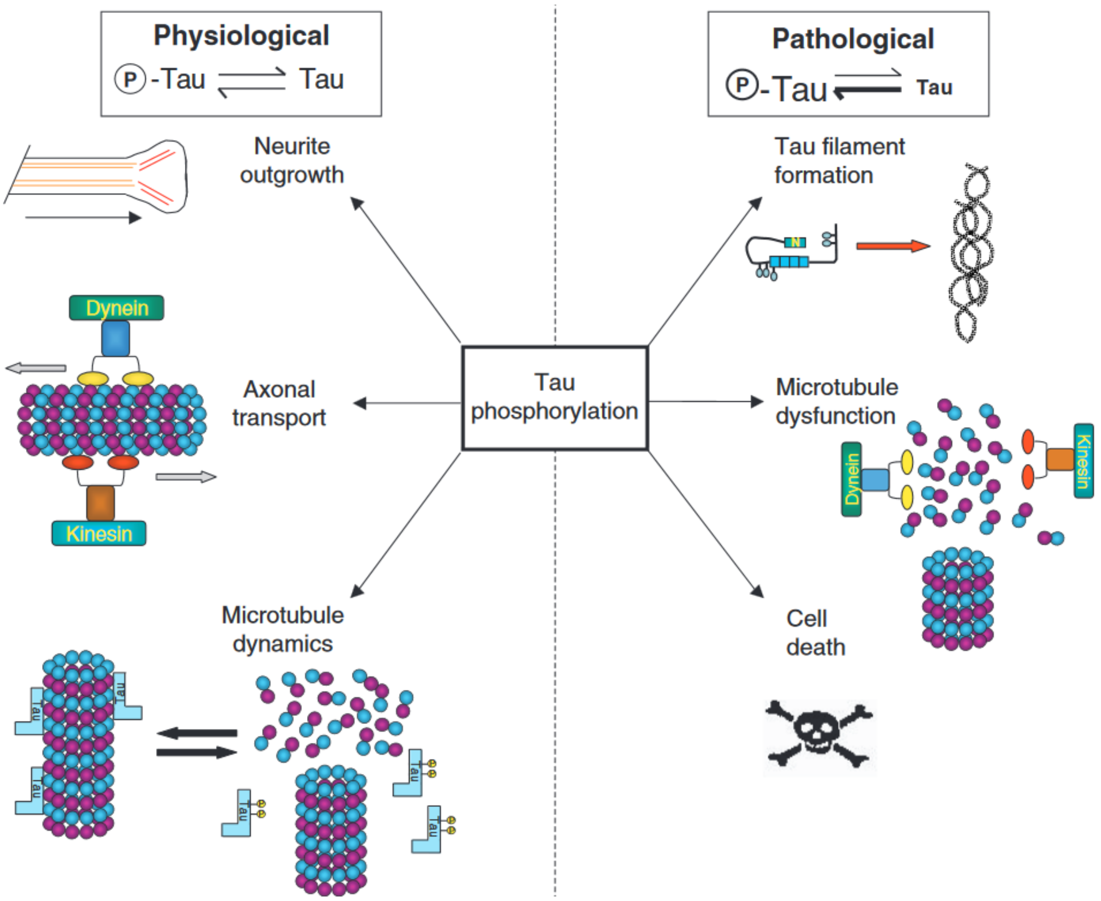
Physiological
Ⓟ-Tau ⇌ Tau
Pathological
Ⓟ-Tau ⇌ Tau
Neurite outgrowth
Tau filament formation
Dynein
Axonal transport
Tau phosphorylation
Microtubule dysfunction
Kinesin
Microtubule dynamics
Cell death
Tau

Figure 3 - Dual role of tau phosphorylation in the cell.
Appropriately coordinated tau phosphorylation is associated with physiological functions in the cell, playing a role in regulating neurite outgrowth, axonal transport and MT stability and dynamics. However, under pathological conditions (e.g. AD) there is an imbalance in the phosphorylation/dephosphorylation status of tau, which may cause the formation of NFTs, disrupt MT-based processes and eventually lead to cell death. (Adapted from Johnson & Stoothoff, 2004).

Importantly, the phosphorylation status of tau relies on the balance between protein kinases and phosphatases. Several kinases are known to phosphorylate tau, sometimes at multiple sites (Shahani and Brandt, 2002) (figure 4). Most kinases are either: 1) proline-directed kinases; e.g. glycogen synthetase kinase 3β (GSK3β), cyclin-dependent kinase 5 (cdk5), and the mitogen-activated protein kinase family or 2) non-proline-directed kinases; e.g. protein kinase A, protein kinase C, calmodulin kinase II (CamKII) and microtubule-affinity-regulating kinase (Morishima-Kawashima et al., 1995). In the AD field, GSK3β and cdk5 have been receiving special attention, due to the capacity to phosphorylate tau at multiple sites, most of them common to both kinases (Shahani and Brandt, 2002). The two enzymes are highly expressed in the brain and the colocalization of one or both kinases with hyperphosphorylated tau and NFTs, along with evidences of their active forms in pre-tangle neurons, strongly implicates them in tau pathology (Lovestone and Reynolds, 1997). MARK kinases also received special attention, due to the ability cmto phosphorylate tau at Ser262, which strongly promotes the detachment of tau from MT (Biernat et al., 1993; Drewes et al., 1997).

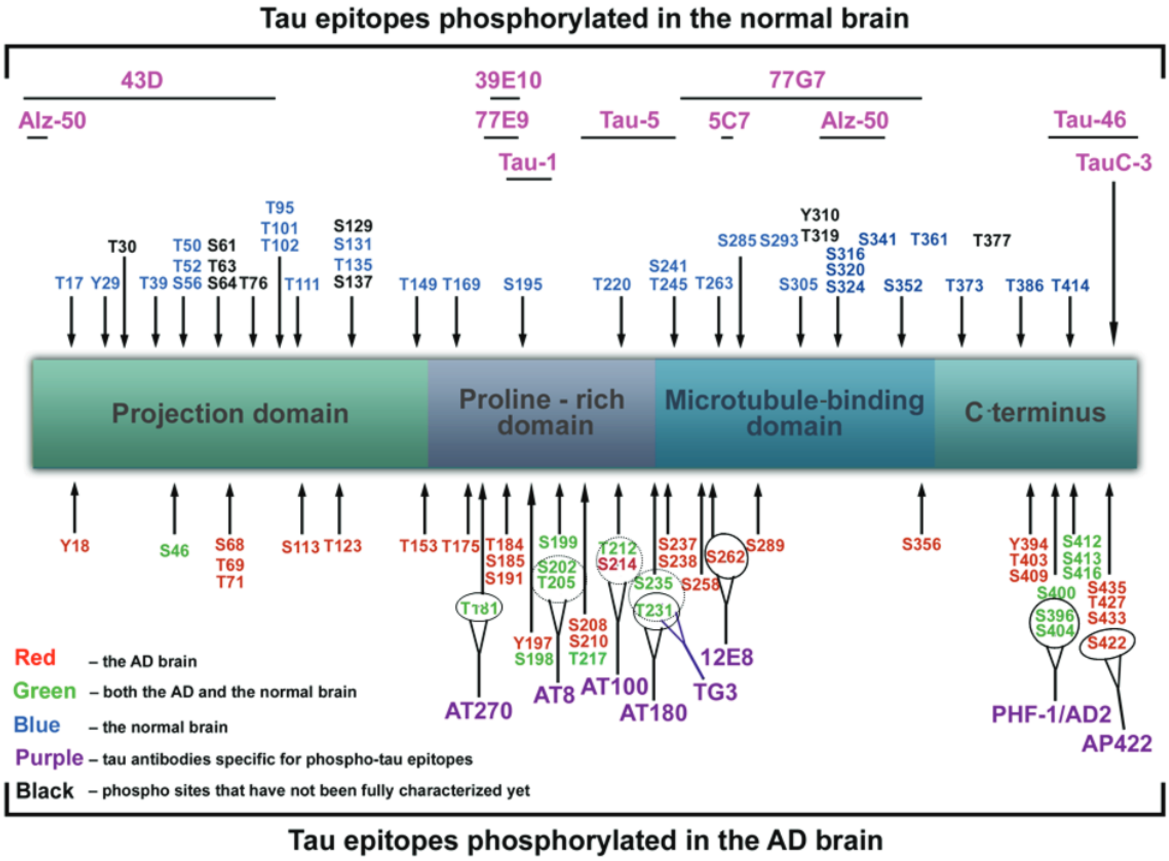
Tau epitopes phosphorylated in the normal brain
43D
39E10
77G7
Alz-50
77E9
Tau-5
5C7
Alz-50
Tau-46
Tau-1
TauC-3
T17 Y29 T30 T39 T50 S56 T52 S61 T63 S64 T76 T95 T101 T102 T111 S129 S131 T135 S137 T149 T169 S195 T220 S241 T245 T263 S285 S293 Y310 T319 S316 S320 S305 S324 S341 T361 T377 S352 T373 T386 T414
Projection domain
Proline - rich domain
Microtubule-binding domain
C-terminus
Y18 S46 S68 T69 T71 S113 T123 T153 T175 T184 S185 S191 T181 S199 S202 T205 Y197 S198 S208 S210 T217 T212 S214 S237 S238 S235 T231 S262 S258 S289 S356 Y394 T403 S409 S400 S396 S404 S412 S413 S416 S435 T427 S433 S422
AT270
AT8
AT100
AT180
12E8
TG3
PHF-1/AD2
AP422
Red – the AD brain
Green – both the AD and the normal brain
Blue – the normal brain
Purple – tau antibodies specific for phospho-tau epitopes
Black – phospho sites that have not been fully characterized yet
Tau epitopes phosphorylated in the AD brain

Figure 4 - Schematic representation of the residues in the longest tau isoform that can be phosphorylated and epitopes specific for major tau antibodies.
The amino acids that are phosphorylated in the AD brain are represented in red, while green represents amino acids that can be phosphorylated both in AD and the normal brain. Amino acids phosphorylated only in the normal brain are highlighted in blue, while black refers to phosphorylation sites that were not characterized so far. Tau antibodies specific for phosphorylated-tau epitopes are given in purple, while pink denotes antibodies specific for non-phosphorylated tau epitopes. (Adapted from Šimić et al., 2016).

1.3.4. Sorting mechanisms of tau

As previously mentioned, the subcellular distribution of tau is developmentally regulated (Drubin et al., 1984). Despite being evenly distributed in the cell body and neurites, when axons emerge and neurons are polarized, tau becomes enriched in the axons, with minor amounts found in dendrites and nuclei (Papasozomenos and Binder, 1987; Sultan et al., 2011). The processes underlying the polarized distribution of tau in adult neurons remain poorly understood, and they may occur at the level of mRNA (Litman et al., 1993; Aronov et al., 2001; Morita and Sobuě, 2009) and/or protein (Kosik et al., 1989; Hirokawa et al., 1996; Li et al., 2011). Notably, the sorting of tau seems to be isoform-dependent, as distinct tau isoforms are differentially distributed in the cellular compartments (Liu and Götz, 2013).

In human AD brains, the missorting of tau into dendrites is part of the pathological cascade and represents one of the earliest signs of neurodegeneration. However, a small amount of tau actually physiologically distributes in dendrites and, although still controversial, in dendritic spines as well (Ittner et al., 2010). The physiological role of dendritic tau has not been well characterized, but seems to be involved in the regulation of synaptic plasticity (Frandemiche et al., 2014). Tau has also been detected in the nuclei of neurons and non-neuronal cells (Loomis et al., 1990; Sjöberg et al., 2006), where it may play a role in preserving the integrity of genomic DNA and cytoplasmic/nuclear RNA (Sultan et al., 2011; Violet et al., 2014).

How the different sorting mechanisms are involved in the missorting of tau remains unclear. Given the differential distribution of tau (and tau isoforms) in different cell compartments, it is likely that the protein serves different functions in different environments. The disturbance of the sorting of tau may thus induce toxic gain of function, contributing to neurodegeneration (Zempel et al., 2010, 2017; Zempel and Mandelkow, 2014; Wang and Mandelkow, 2016; Balaji et al., 2018).

1.3.5. Pathological roles of tau protein

In spite of intense investigations, the pathways of tau-mediated neurodegeneration remain unclear. Loss of function, toxic gain of function and mislocalization of tau have each been implicated in tau-mediated neurodegeneration.

Several tau mutations have been identified within the intronic or exonic regions of the human MAPT gene, which are linked to different tauopathies, including frontotemporal dementia (FTD) with parkinsonism-17, corticobasal degeneration (CBD) and progressive supranuclear palsy (PSP) (Coppola et al., 2012; Kouri et al., 2014). Some of these mutations reduce the affinity of tau for MT or strengthen the β-structure (for instance, ΔK280 or P301L), accelerating tau aggregation both *in vitro* and *in vivo* (Hong et al., 1998; Barghorn et al., 2000; Crary et al., 2014), and contributing to pathology.

PTMs also influence tau aggregation, as mentioned before. Phosphorylation has been assumed to drive tau aggregation, as aggregated tau in patients and transgenic mice is hyperphosphorylated, and tau phosphorylation precedes aggregation (Braak, Braak, & Mandelkow, 1994). Although some phosphorylated tau species are prone to aggregation in the brain, it is not known whether other cofactors are involved in their aggregation. By contrast, phosphorylation at certain sites (e.g. in the repeat domain), protects against aggregation (Schneider et al., 1999). Furthermore, AD-like phosphorylation of tau, but not aggregation, is known to occur during anesthesia-induced hypothermia and animal hibernation (Arendt et al., 2003; Planel et al., 2007), allowing us to speculate that tau phosphorylation alone might not be enough for aggregation, but probably unknown cofactors trigger tau aggregation in the AD brain, whereas phosphorylation may accelerate aggregation indirectly by detaching tau from the MT (Wang & Mandelkow, 2012).

Mislocalization of tau is another key player in the pathological aspects of the protein, as one of the first and evident pathological abnormalities in AD is the increase in dendritic tau levels. The mislocalization of tau into postsynaptic spines might be driven by hyperphosphorylation, mutations and overexpression of tau, resulting in synaptic dysfunction (Hoover et al., 2010; Tai et al., 2014; Thies & Mandelkow, 2007). In cultured neurons, missorted dendritic tau mediates Aβ-induced toxicity by promoting the translocation of tubulin tyrosine ligase-like enzyme 6 (TTLL6) into dendrites, and the severing of MT by spastin (Zempel et al., 2013). Additionally, dendritic tau could serve as a protein scaffold to deliver the kinase Fyn to postsynaptic sites, where Fyn phosphorylates subunit 2 of the N-methyl-D-aspartate receptor (NMDAR), stabilizing the interaction of this receptor with postsynaptic density protein 95 (PSD95), potentiating glutamatergic signaling and thereby enhancing Aβ toxicity (Ittner et al., 2010) (figure 5).

In conclusion, the mechanisms underlying tau-mediated neurotoxicity have to date not been well elucidated. However, multiple therapeutic approaches have been proposed that target tau and tau function or dysfunction, based on the current understanding of these mechanisms, as it will be discussed later on the present dissertation. Nevertheless, one of the key aspects in designing therapeutical interventions targeting Tau protein is to understand which are exactly the toxic tau species, which is currently still under debate.

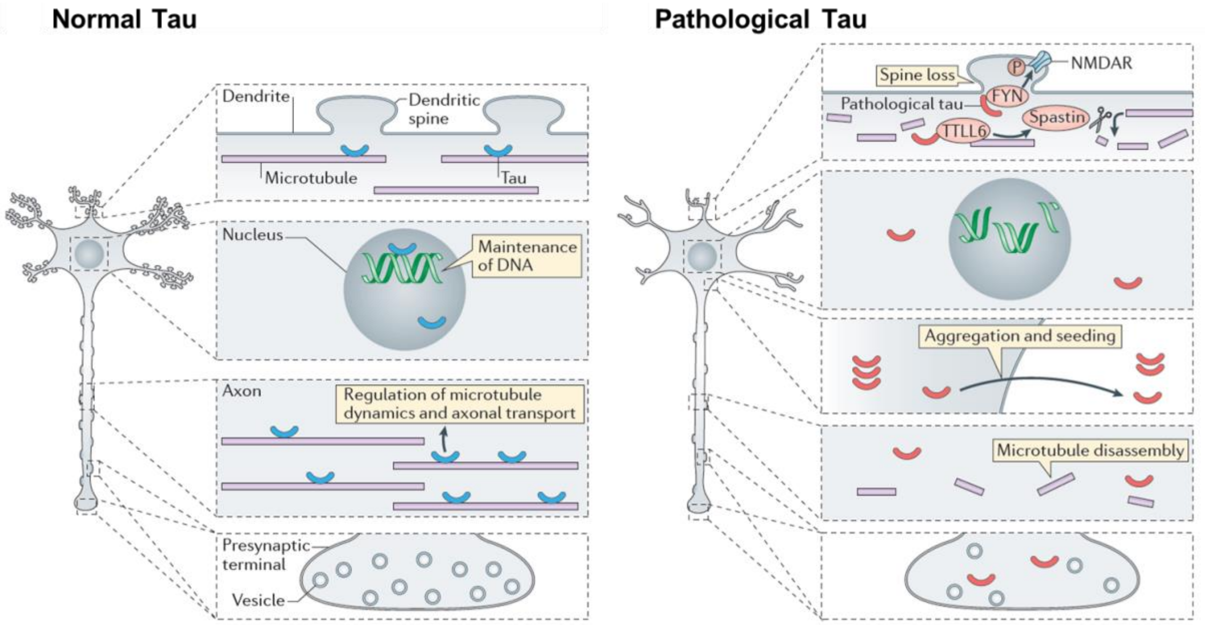
Normal Tau
Dendrite
Dendritic spine
Microtubule
Tau
Nucleus
Maintenance of DNA
Axon
Regulation of microtubule dynamics and axonal transport
Presynaptic terminal
Vesicle
Pathological Tau
Spine loss
P
NMDAR
FYN
Pathological tau
Spastin
TTLL6
Aggregation and seeding
Microtubule disassembly

Figure 5 - Functions of tau protein.
Normal tau has several physiological functions, playing an important role in stabilizing MT and regulating MT dynamics, as well as regulating axonal transport. A small amount of tau is also detected in the dendrites of healthy cells, where its function is unclear, and in the nucleus, where it may play a role in maintaining the integrity of genomic DNA. Under pathological conditions, tau detaches from MT, resulting in MT disassembly in the axons. Detached tau can mislocalize and induce synaptic dysfunction and synapse loss. As pathological tau does not enter the nucleus of the cell, this may cause DNA damage as well, due to the loss of the DNA-protective function of tau. Lastly, the formation of tau aggregates produces a deleterious effect on neuronal function. These tau aggregates can be transmitted from cell to cell, propagating the tau pathological cascade. Adapted from Wang & Mandelkow, 2016.

1.3.6. Toxicity of different tau species

Although several groups have studied the toxic properties of tau aggregates, recent evidences suggest that soluble or prefibrillar forms of aggregates, rather than higher aggregates or PHFs, are responsible for toxicity and cell death (Haass and Selkoe, 2007; Kaniyappan et al., 2017). Supporting this is the fact that, in AD patients, neuron loss in some brain regions highly exceeds the number of NFTs, implying that the majority of neurons probably die without having developed NFTs (Gomez-Isla et al., 1997). Furthermore, tangle-bearing neurons can survive and function normally for around 20 years (Morsch et al., 1999). Moreover, using transgenic mice expressing wild-type (WT) or mutant htau was also possible to demonstrate that synapse loss, impaired synaptic function and cognitive deficits occur before or without NFTs formation, suggesting that soluble tau species, rather than NFTs, are the culprit. Interestingly, switching off tau expression in transgenic mouse models expressing htau with the P301L mutation (rTg4510), or expressing full-length tau with the ΔK2810 mutation, improved memory impairment even though NFTs remained, clearly showing that tau aggregates are not sufficient for the cognitive effects and neurodegeneration typically observed in these models (SantaCruz et al., 2005; Sydow et al., 2011; Van der Jeugd et al., 2012).

Based on these evidences, recent studies pointed tau oligomers as the toxic species, and it was indeed observed that the levels of SDS-stable tau oligomers are increased in AD and PSP brains (Kimura et al., 2007; Lasagna-Reeves et al., 2012; Maeda et al., 2007; Takashima, 2015). Analyzing the temporal formation of tau fibrils *in vitro* demonstrated that there are distinct forms of tau assemblies that precede tau fibril formation and later NFTs (Takashima, 2015). In fact, monomeric tau molecules first bind to each other (probably involving disulfide bonds and other SDS-resistant interactions) to form tau oligomers that are sarkosyl-soluble (not detected by AFM). When forty tau oligomers bind together they form a β-sheet structure, which appears granular in shape and is sarkosyl-insoluble and detectable under AFM. These granular tau oligomers eventually accumulate to form tau fibrils (Maeda et al., 2007; Takashima, 2015) (figure 6).

In conclusion, exactly how tau aggregation exerts neurotoxicity remains currently unclear and, although the aggregation process seems to be neurotoxic, the possible contributions of monomeric, hyperphosphorylated, oligomeric or mutant tau to neurodegeneration may not be ruled out.

1.4. Mouse models for the study of Alzheimer disease

Due to the high prevalence of AD, and the expected large increase in the number of patients within the next years, new and improved animal models of the condition are crucial for understanding the pathophysiology of the disease and investigating potential therapeutics. Advances in genetic engineering have driven the generation of transgenic animals (Selkoe, 2006; Esquerda-Canals et al., 2017). Among vertebrates, mice are the major species for transgenic modeling due to their short lifespan, relatively low costs, and well-established procedures for genetic modification. Mutations in the MAPT gene are not found in AD, but tau mutations found in FTD promote its abnormal hyperphosphorylation and aggregation (Hong et al., 1998; Barghorn et al., 2000). Based on this, multiple transgenic mouse lines have been created for studying tau pathology in the context of AD that overexpress human 4R tau containing FTD mutations. Of these, the rTg4510 and TauΔK280 models are particularly versatile because the expression of mutant htau, and thus the pathology, can be regulated (SantaCruz et al., 2005; Mocanu et al., 2008).

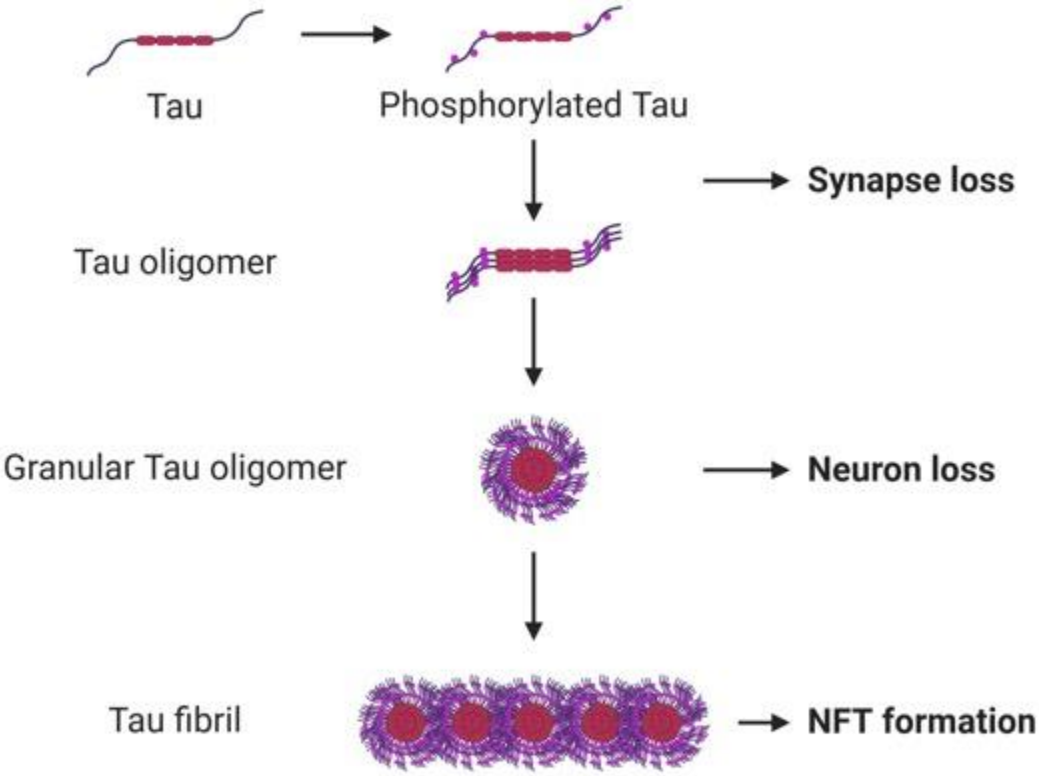

Figure 6 - Formation of tau fibrils.
Hyperphosphorylated tau protein detaches from MT and, due to its greater affinity to form tau-tau interactions, individual hyperphosphorylated tau molecules bind to each other forming oligomeric tau species (detergent-soluble and not detected by AFM). Hyperphosphorylated and oligomeric tau seem to be involved in synaptic loss. When the tau oligomer grows to about 40 molecules, it acquires a β-sheet structure and becomes a granular tau oligomer (detergent-insoluble and visible under AFM). The presence of granular tau oligomers correlates with neuronal loss. Over time, the granular tau oligomers may fuse together and form tau fibrils, which ultimately result in NFTs. (Adapted from Takashima, 2015).

The rTg4510 mouse model expresses htau (0N4R) containing the P301L mutation, which corresponds to a proline-to-leucine substitution at codon 301 (Ramsden et al., 2005; SantaCruz et al., 2005). The level of mutant htau expressed by rTg4510 mice is approximately 13 times the level of endogenous mouse tau, and these mice develop progressive age-related NFTs, neuronal loss, and behavioral deficits (Ramsden et al., 2005). Pre-tangles are observed in rTg4510 mice around 2.5 months of age, while argyrophilic tangle-like inclusions can be detected in the cortex at 4 months and in hippocampus at 5.5 months. Loss of CA1 hippocampal neurons (~60%) is observed around 5.5 months, accompanied by a pronounced loss in brain weight. Furthermore, loss of dendritic spines is detected at 8-9 months. LTP at the Schaffer collateral-CA1 synapse is impaired at 4.5 months, and deficits in spatial memory, assessed with Morris Water Maze (MWM) test, start around 2.5 to 4 months. Until 6 months of age, no motor deficits are observed. Notably, transgene suppression with Doxycycline halts neuronal death and arrests or even reverses cognitive decline (Ramsden et al., 2005; SantaCruz et al., 2005; Spires et al., 2006; Blackmore et al., 2017).

The TauΔK280 mouse model expresses full length (2N4R) htau containing the deletion mutation ΔK280, that results in tau protein lacking one lysine at the position 280 (Barghorn et al., 2000; Eckermann et al., 2007). This mutation was shown to strongly promote tau aggregation *in vitro* (Barghorn et al., 2000). *In vivo*, TauΔK280 mice present extensive pre-tangle pathology, although mature tangles are rarely observed, due to the relatively low expression of htau in the brain (~ 1-3 times the level of endogenous mouse tau). Mislocalization of tau into the cell body and dendrites, conformational alterations consistent with aggregation, as well as hyperphosphorylation at a variety of epitopes are observed in TauΔK280 mice. Expression of the mutant tau does not cause evident neuronal loss in the brain, although the mice lose synapses in the hippocampus. LTP is severely impaired in the mossy fibers (Van der Jeugd et al., 2012). Behaviorally, TauΔK280 mice develop cognitive impairments at 16 months of age, specifically in spatial learning/memory, as well as contextual learning (Van der Jeugd et al., 2012). Remarkably, transgene suppression for six weeks reversed the pre-tangle pathology in these mice.

These mouse models and others may help us gain valuable insight on the involvement of tau protein in AD-related changes, as well as understanding which tau species are responsible for toxicity and the downstream neurodegeneration. However, to fully understand the disease, it is also crucial to comprehend how tau pathology propagates throughout the brain and the mechanisms underlying the transfer of tau pathology across cells from the EC to the rest of the brain.

1.5. Propagation of tau pathology in Alzheimer disease

Because tau is a highly soluble protein and the initial aggregation phase is thermodynamically unfavorable, it is currently unclear how tau shifts from its dynamic physiological structure to a misfolded monomer prone to aggregation (Mirbaha et al., 2018; Sharma et al., 2018; Vogels et al., 2019).

Besides causing intracellular toxicity, tau oligomers and fibrils can be secreted into the extracellular space and taken up by healthy neurons (Frost et al., 2009; Guo and Lee, 2011; Kfoury et al., 2012). This process may be of critical importance as it is thought to underlie the progression of tau pathology throughout the brain. Indeed, during the clinical course of AD, filamentous tau inclusions appear sequentially throughout the brain following a stereotypical pattern, thereby providing the basis for disease staging. In AD, tau pathology is staged using the criteria defined by Braak and Braak (1991) (figure 7). Braak stages I and II correspond to the appearance of NFTs in the transentorhinal and entorhinal cortex (EC) and are not associated with clinical dementia. More pronounced involvement of both transentorhinal and entorhinal regions and formation of NFTs in the hippocampus are characteristics of stages III-IV. The degree of neuronal damage at stages III-IV may lead to the appearance of the first clinical symptoms (mild cognitive impairment). At the later stages of the disease (Braak stages V and VI) tau pathology has extensively reached the neocortex, and patients are severely demented, meeting the neuropathological criteria for the diagnosis of AD (Clavaguera et al., 2014).

Pathological conformations of tau can interact with physiological endogenous tau, leading to aggregation and, ultimately, formation of highly structured insoluble fibrils, which deposit into the cell as NFTs. This process is referred to as templated misfolding, seeded nucleation, or simply seeding (Friedhoff et al., 1998).

Using a variety of *in vitro* and *in vivo* approaches, it has been shown that tau pathology predominantly spreads along synaptic connections (de Calignon et al., 2012; Calafate et al., 2015). To support this, experimental evidences have shown that the inoculation of synthetic tau fibrils or tau aggregates isolated from brains of patients with AD or other tauopathies or from tau transgenic mice represents a trigger that causes progressive spreading of tau pathology from the injection site (or sites) to synaptically connected brain regions in htau transgenic mice, and even in WT mice (Clavaguera et al., 2009; Holmes and Diamond, 2014). Significant progress has been made recently in showing that this also occurs in the brain of Alzheimer patients: seed-competent tau is present in axons of white matter tracts and synaptosomes, and tau seeding occurs in synaptically connected areas before the occurrence of hyperphosphorylated tau in these regions (Furman et al., 2017; Kaufman et al., 2017, 2018; DeVos et al., 2018).

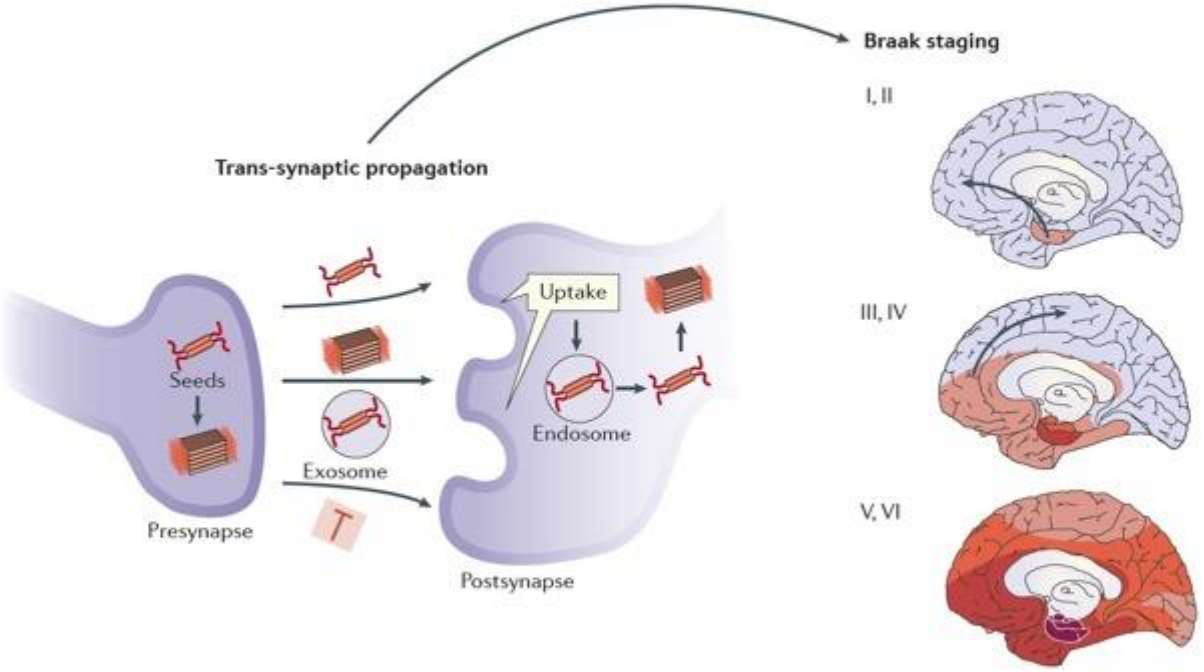

Figure 7 - Trans-synaptic propagation of tau pathology and Braak staging, illustrating the progression of tau pathology in AD.
Toxic tau can be released from the presynaptic terminal in the form of free aggregates or contained within extracellular vesicles (such as exosomes) and be taken up by other cells. This process is believed to underlie the progression of tau pathology throughout the brain, as described in the Braak stages. (Adapted from Li & Gotz, 2017).

Another hypothesis to explain the pattern of tau pathology propagation throughout the brain that Braak and Braak have described is related to selective neuronal vulnerability (Braak & Del Tredici, 2011; Demaegd, Schymkowitz, & Rousseau, 2018; Fu, Hardy, & Duff, 2018). Certain neurons may be vulnerable to the underlying pathogenic mechanisms of the disease than others (Jackson, 2014; Mattson and Magnus, 2014), perhaps due to their gene expression profiles. These vulnerable neurons may become dysfunctional and present structural abnormalities earlier than the others. Other factors that could explain the selective vulnerability of certain neurons are: poor myelination (Braak & Braak, 1996), high metabolic rates that lead to higher susceptibility to chronic oxidative stress (Yan et al., 2013), and vulnerability to toxins (Nave and Werner, 2014). However, the observation that tau protein and tau pathology can propagate to nearby cells/brain regions, but also to synaptically connected distant brain regions, strengthens the hypothesis that the hallmarks of tau pathology can be spread along anatomical connections (Hyman et al., 1984).

Additionally, other processes distinct from the cell-to-cell transmission of tau transmission have also been proposed to underlie the progression of tau pathology throughout the brain, such as the spreading of neuroinflammation via microglia, cytokine signaling, among others (Perea et al., 2018), or the spreading via neuronal activity of neurons (Wu et al., 2016).

A highly debated theory over the last years is the prion-like spreading of tau pathology (figure 8). This theory states that the propagation could occur through a “prion-like” mechanism, by analogy with the progressive aggregation of prion protein (PrP) in prion diseases (Prusiner, 1998). Importantly, the prion theory requires the presence of the normal form of the protein (PrP_{C}) in the recipient cell for the propagation of the disease, as the infectious form of the protein (PrP_{Sc}) binds to PrP_{C} and catalyzes its conversion into PrP_{Sc} (Weissmann, 2004). Similarly, the prion-like theory for the propagation of tau pathology involves the transmission of aberrant tau seeds from a “donor cell” to a “recipient cell”, and recruitment of the healthy tau in the recipient cell to generate new seeds, which may then transfer to other cells and propagate the toxic cascade (Sanders et al., 2014; Mudher et al., 2017). However, contrarily to what happens with PrP, it has been demonstrated that mice lacking endogenous mouse tau present equivalent propagation of human P301L tau from the EC to the rest of the brain compared to mice with endogenous mouse tau, clearly showing that tau cannot be strictly classified as a prion protein (Wegmann et al., 2015).

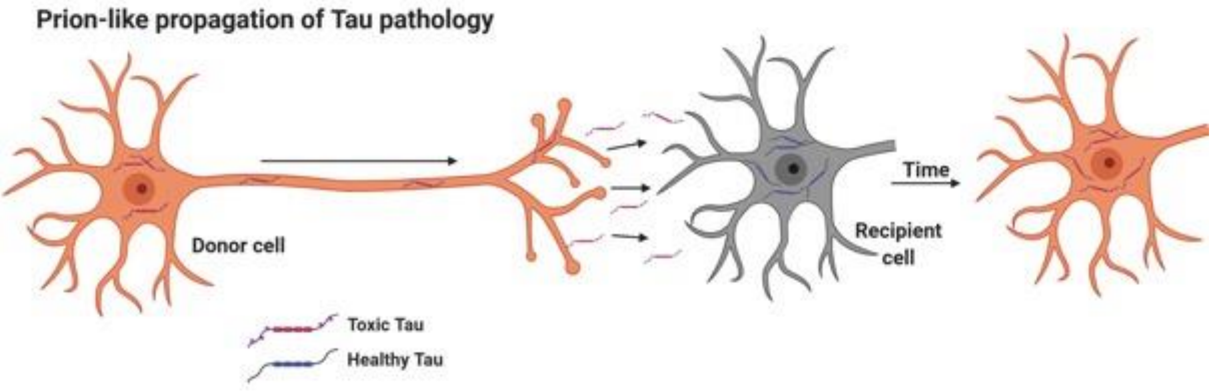

Figure 8 - Prion-like propagation of tau pathology.
This theory is based on the assumption that there are two tau species: toxic tau and healthy tau. The toxic tau species can be transferred from donor to recipient cells, where it will co-assemble with the healthy tau species present in the postsynaptic terminal, which over time will become toxic and be able to transfer to other cells, propagating the toxic cascade. (Adapted from McHugh, Morozova & Colby, 2015).

Several mechanisms for the transfer of tau protein from one cell to the other have been identified, either within the same brain region or between different regions, including exocytosis, formation of nanotubes, exosome release, mediated by microglia, and others (figure 9) (Wang & Mandelkow, 2016).

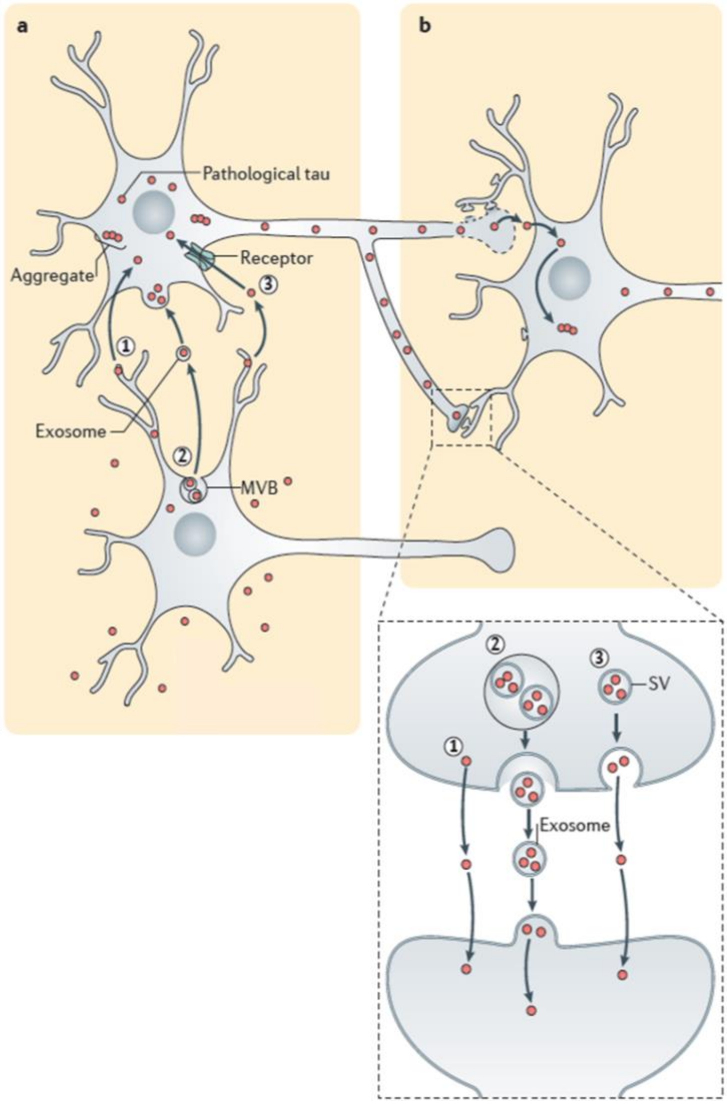

Figure 9 - Mechanisms for tau transfer between cells. Within the same brain region the transfer of tau between cells may occur through exocytosis, which allows donor neurons to release tau seeds (mechanisms 1 and 3 from part a), or through the release of exosomes (mechanism 2, part a), which can fuse and deliver their contents into recipient neurons. Recipient neurons can internalize extracellular tau seeds through endocytosis (mechanism 1, part a) or by receptor-mediated endocytosis (mechanism 3, part a). The trans-synaptic spreading of tau pathology from region a to a downstream region shown in part b may occur through 2 different mechanisms: the degeneration of presynaptic neurons can cause the leakage of the presynaptic membrane, allowing presynaptic tau seeds to diffuse across the synaptic cleft (part b, top synapse); or tau seeds may be released from the presynaptic terminal via exocytosis (mechanism 1, part b) or exosomes (mechanism 2, part b) or synaptic vesicles (SVs) (mechanism 3, part b). Once released, tau seeds can be taken up by postsynaptic neurons and subsequently initiate tau aggregation. (Adapted from Wang & Mandelkow, 2016).

Experimentally, two main approaches have been used to study the propagation of tau pathology: the use of mouse models with a brain region-specific promoter for tau expression (de Calignon et al., 2012), or the *in vivo* localized stereotaxic injection of a tau inoculum (tau synthetic fibrils, AD patients/mouse models brain homogenates or AAV encoding mutant htau) (Ahmed et al., 2014; Iba et al., 2013; Wegmann et al., 2015), followed by assessing the presence of tau pathology in adjacent tissues at later time points.

To understand the propagation of tau pathology throughout the brain according to the observation of Braak & Braak (1991), and the evidences that tau pathology spreads along anatomical connections, it is important to study the EC and the neuronal projections arising from this brain region. This may provide insights on the early stages of the development of AD, namely on the onset and progression of the disease from the EC (at Braak stage 1) to the rest of the brain (at subsequent Braak stages).

1.6. The perforant pathway

1.6.1. Entorhinal cortex

In view of the strong implications of the human EC in a variety of brain diseases, including AD (Braak & Braak, 1991; Braak & Braak, 1992; Scharfman & Chao, 2013), understanding what renders the EC vulnerable and how the pathology is transmitted from this region to others is crucial. In AD, it has been proposed that the degeneration of EC neurons may be involved in the initiation of the disease, as it occurs at an early stage of disease progression. Thus, defining the characteristics that make the EC a particularly vulnerable region is important (Scharfman & Chao, 2013).

The term “entorhinal cortex” (EC) (Brodman’s area 28) (Brodmann, 1909) is based on the fact that this brain region is partially enclosed by the rhinal (olfactory) sulcus (Witter et al, 2017). The EC is located in the medial temporal lobe in humans, participating in a widespread network involved in memory, navigation and the perception of time (Tsao et al., 2018). In rodents, the EC is located at the caudal end of the temporal lobe, adjacent to the hippocampus (Scharfman & Chao, 2013).

Interest in the EC began in the beggining of the 20th century when Ramón y Cajal described a region of the posterior temporal cortex that was strongly associated to the hippocampus (Ramón y Cajal, 1902; Witter, Kleven, & Flatmoen, 2017; Witter et al., 2017). The authors described fibers arising from the EC towards the dentate gyrus (DG) and hippocampus proper (Cornu Ammonis (CA)), which compose the perforant pathway (figure 10). This description was confirmed and extended by the studies of Lorente de Nó, 1934. Later developments of new silver impregnation techniques (Allen, 1948; Blackstad, 1956; Cragg, 1961), and later, electrophysiological studies demonstrated that axons of the perforant pathway constitute a powerful excitatory route to the hippocampus (Green and Adey, 1955; Andersen et al., 1966). Tracing studies performed in several species have confirmed that the EC projects through the perforant pathway to the DG and CA regions (Hoesen & Pandya, 1975; Witter & Amaral, 1991; Witter, Van Hoesen, & Amaral, 1989). This axonal projections "perforate" the subiculum on their way to the hippocampus, hence the name "perforant pathway" (Ramón y Cajal, 1893; Scharfman & Chao, 2013).

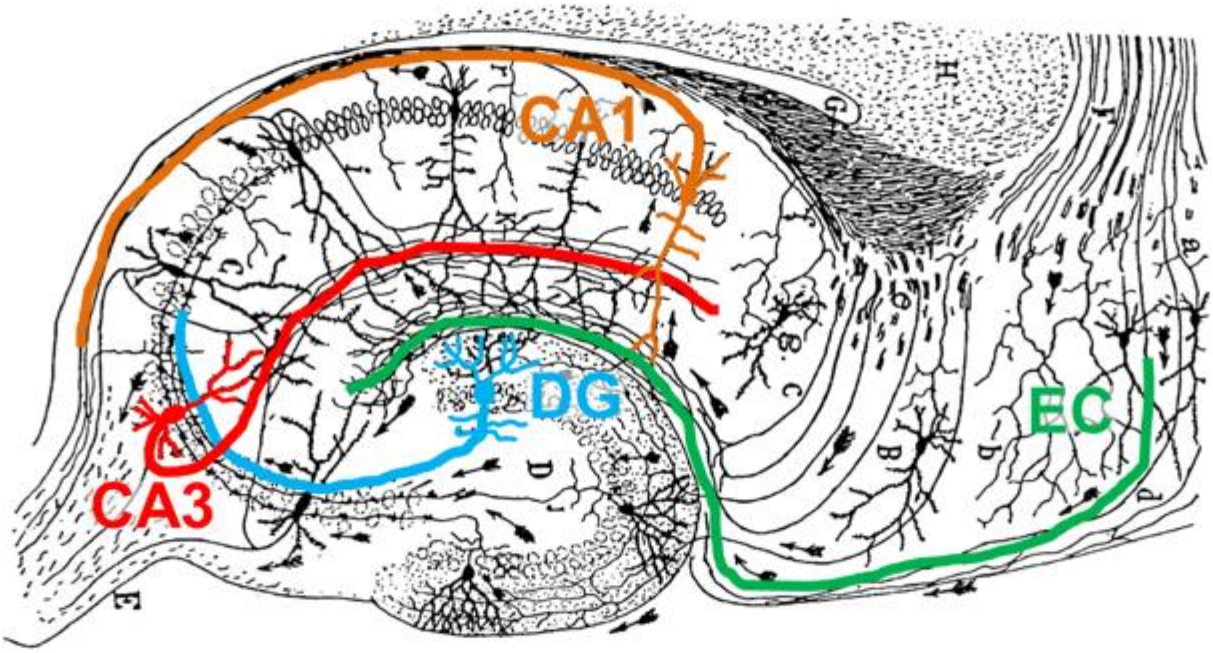

Figure 10 - The perforant pathway provides the major input to the hippocampus from the entorhinal cortex.
Modified original drawing of Ramón y Cajal, 1911 and schematic diagram of the rodent hippocampal circuitry. Neurons from EC layer II (green) project directly to the two outer thirds of the molecular layer of the DG (blue) and *stratum lacunosum moleculare* (slm) of the CA3 (red) region of the hippocampus. Neurons from EC layer III (green) send direct projections to the slm of the CA1 region (orange). The DG granule cells project to the CA3 pyramidal neurons via the mossy fibers, while CA3 axons project through the Schaffer collaterals to CA1 pyramidal neurons, which finally project to the subiculum and deep lEC IV-VI layers. (Adapted from Saura et al., 2015).

The EC has two major divisions: the medial EC (MEC), located next to the pre- and parasubiculum, and the lateral EC (LEC), adjacent to the neocortex (Scharfman & Chao, 2013) (figure 11A). LEC and MEC both project to the two outer thirds of the molecular layer of the DG. Furthermore, both also give rise to projections to CA3, CA1 and to the subiculum. In CA3 and CA1, the entorhinal terminals are in the *stratum lacunosum-moleculare*, and in the subiculum the terminals are in the outer part of the molecular layer. The EC has five cell layers, in contrast to the six layers typically observed in the neocortex. There are three superficial layers (layer I, II, III), one cell-free layer (*lamina dissecans*), and two deeper layers (V and VI) (figure 11B) (Scharfman & Chao, 2013; Scharfman, 2006; Witter et al, 1989). The entorhinal projection to the DG originates predominantly from neurons in layer II, and this projection is nearly entirely confined to the ipsilateral DG. Most of the cells in the EC region are glutamatergic neurons, including puramidal neurons (layers II, III, V and VI), and stellate cells (layer II). Interneurons can be found in all layers, similar to neocortex (Scharfman & Chao, 2013; Witter et al., 1989).

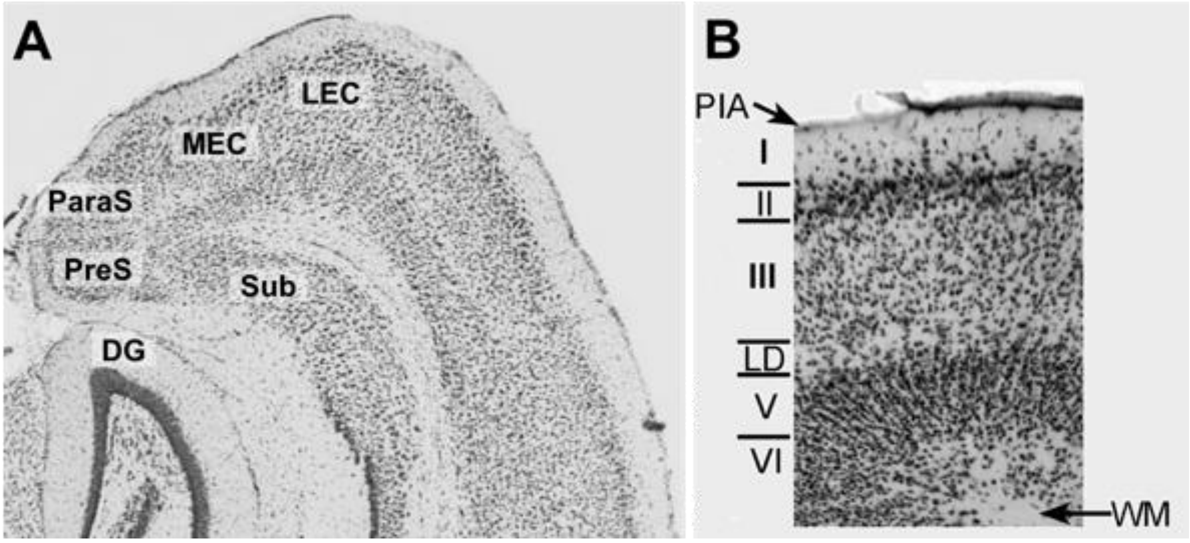

Figure 11 - Layers of the EC on the mouse brain.
A. Horizontal sections of an adult wild-type mouse showing the main subregions of the EC (MEC, medial EC; LEC, lateral EC) and neighboring areas (ParaS, parasubiculum; PreS, presubiculum; Sub, subiculum). DG = dentate gyrus. **B.** The layers of the EC are shown. The arrows denote the pial surface (PIA) and white matter (WM). LD = *lamina dissecans*. (Adapted from Scharfman & Chao, 2013).

1.6.2. Hippocampus

One of the unique features of the hippocampal formation is that many of its connections are unidirectional. Since the EC provides most of the cortical information that the hippocampus needs to carry its function, and the DG is the main termination point of the projections from the EC, it is reasonable to consider the DG as the first step in the processing of information that ultimately leads to the production of episodic memories. Furthermore, the unique neuroanatomy of the DG suggests that it is involved in an information-processing task with the information that receives from the EC and ultimately conveys to the CA3 field of the hippocampus.

The DG has three layers (figure 12), which are important to highlight when studying the spreading of tau protein or tau pathology from the EC to the DG along the perforant pathway (Amaral et al., 2007): 1) the molecular layer, a relatively cell-free layer that is mainly occupied by the dendrites of the dentate granule cells. Furthermore, perforant pathway axonal fibers, originating in the EC, are also located in this cell layer, as well as a sparse number of interneurons; 2) the granule cell layer, the principal cell layer, composed mostly by granule cell bodies. Few other neurons are also located at the boundary between the granule cell layer and the polymorphic layer, like the dentate pyramidal basket cells; 3) the polymorphic cell layer (or hilus), which constitutes the third layer of the DG. A number of different cell types are located in this layer, but the most prominent ones are the mossy cells, which regulate the DG activity and function (Oh et al., 2019). The dendrites of mossy cells are mostly confined to the hilus, but some extend to the molecular layer of the DG. Besides receiving excitatory inputs from the DG granule cells, mossy cells also receive inhibitory inputs from local interneurons and excitatory "back" projections from the CA3 pyramidal cells (Swaminathan et al., 2018). The mossy cell axon projection is complex: the axons ramify within the hilus and project to the inner molecular layer of both the ipsi- and contralateral DG (figure 13). Taken together, these anatomical features suggest a strategic role for mossy cells in relaying information in the CA3-DG network.

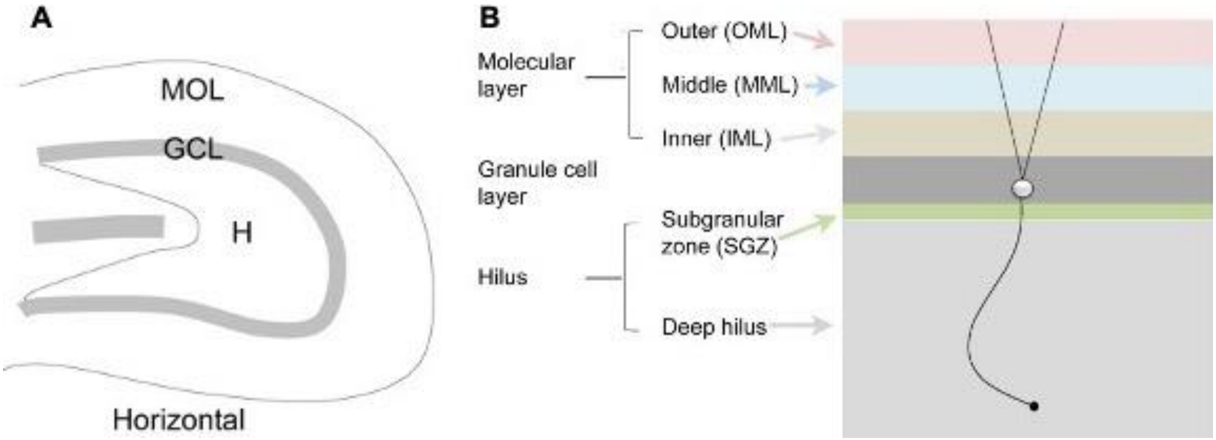

Figure 12 - Organization of the rodent dentate gyrus.
A. illustration of the horizontal view from the hippocampus. **B.** the organization of the DG is illustrated, with a granule cell showing the positioning of the dendrites and the axon, which is designated a mossy fiber. The molecular layer is subdivided in three layers: the outer molecular layer (light red), the middle molecular layer (blue) and inner molecular layer (light brown). The granule cell layer (dark grey) is composed of densely packed granule cell bodies. Below there is a small subgranular zone (green) composed by neurons from the hilus and granule cell precursors. The hilus comprises the subgranular zone and a greater area that ends where the CA3 region begins (light grey). (Adapted from Scharfman & Myers, 2013).

Considering that axons from EC neurons terminate in the two outer thirds of the molecular layer of the DG, the appearance of tau protein or tau pathology on this region cannot be defined as trans-synaptic spreading of tau, but simply transport along the axons of the perforant pathway until the axon terminal ends in the molecular layer. In this region, the synapses with the apical dendrites of granule cell layer will occur. Therefore, we can only consider trans-synaptic spreading of tau protein or tau pathology when we observe their presence in the granule cell layer of the DG, or further connections.

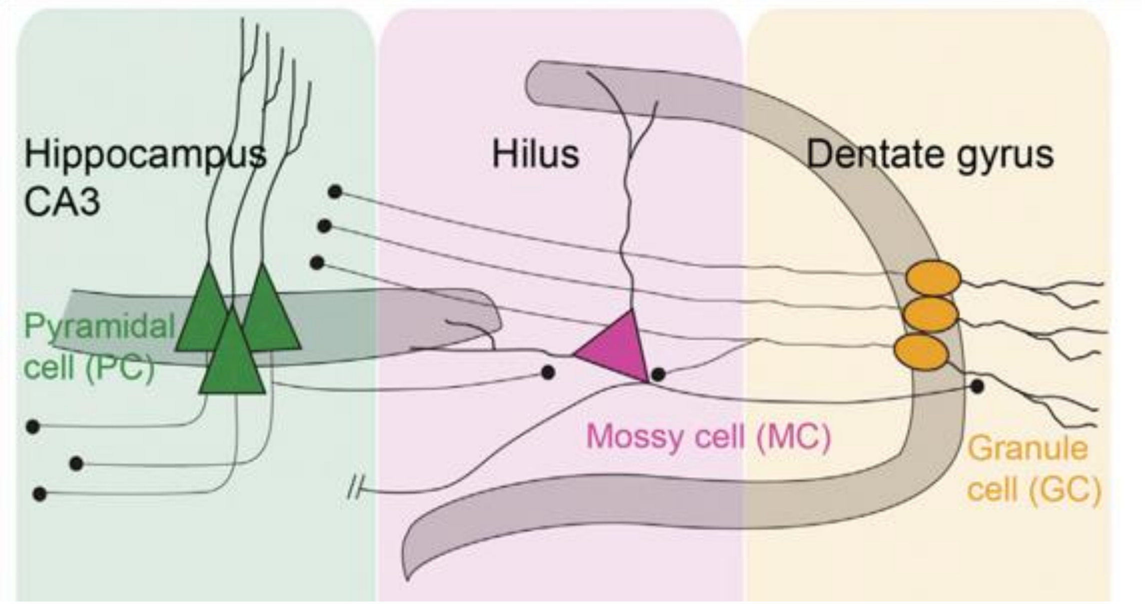

Figure 13 - The hippocampal mossy cell.
The major cell types of the DG include the granule cells, GABAergic interneurons and mossy cells. Mossy cells are located in the hilus and have large dendrites, some of which extend into the molecular layer. The mossy cells relay information in the CA3-DG network, by receiving excitatory inputs from the DG granule cells, inhibitory inputs from local interneurons and excitatory "back" projections from the CA3 pyramidal cells. Mossy cell axons ramify within the hilus and project to the inner molecular layers of both the ipsi- and contralateral DG. (Adapted from Swaminathan et al., 2018).

1.7. Neuroinflammation and AD - role of glial cells in the propagation of tau pathology

Tau pathology has been associated with chronic neuroinflammatory processes, including reactive microglia, astrocytes, and increased levels of pro-inflammatory molecules like cytokines or complement proteins (Mcgeer et al., 1989; Gerhard et al., 2004; Ishizawa et al., 2004; Ising et al., 2019; Vogels et al., 2019). Reactive microglia, reactive astrocytes, and inflammation-associated molecules are typically observed around NFTs in AD brains (Cras et al., 1991; DiPatre & Gelman, 1997; Grundke-Iqbal et al., 1990; Sheffield, Marquis, & Berman, 2000). Furthermore, it has been recently suggested that neuroinflammation may play a role on the spreading of tau pathology.

The initial purpose of the neuroinflammatory state is to remove the cause (e.g. pathogens, protein aggregates, damaged cells) and return the tissue to homeostasis. However, it is not clear if neuroinflammation in tauopathies is mostly protective or damaging and how this depends on disease stage (Vogels et al., 2019).

Microglia are of particular interest as they are the main macrophages of the CNS and exciting recent research has shown novel roles for these immune cells in both health and disease. Particularly in AD, microglia seem to play a pivotal role in the initiation and progression of tau pathology and associated neurodegeneration (Maphis et al., 2015; Hansen et al., 2018; Simon et al., 2019).

It is currently unclear if altered microglial function is a cause, consequence, or contributor to tau pathology. Secreted factors from microglia may lead to the initiation of tau aggregation in neurons (Gorlovoy et al., 2009). Indeed, it has been shown that NLRP3 inflammasome assembly inside microglia upon activation leads to increased cleavage and activity of caspase-1, plus downstream Interleukin-1β (IL-1β) release. IL-1β contributes to the worsening of tau pathology via the regulation of tau kinases and phosphatases (Ising et al., 2019). Microglia may be also involved in tau-induced synapse loss and tau spreading, and play an important role in the mechanism of action of tau immunotherapy and other therapeutics aimed at treating tauopathies (Asai et al., 2015; Funk et al., 2015; Hopp et al., 2018). However, the effects of tau pathology and microglial neuroinflammation are bidirectional. A variety of factors can potentially mediate tau-induced neuroinflammation (figure 14). The most obvious one is that tau aggregates directly activate microglia. Tau oligomers colocalize with microglia, astrocytes, and pro-inflammatory cytokines in the brains of tauopathy patients and transgenic mice (Nilson et al., 2017). It is possible that microglia first have the ability to phagocytose extracellular tau, but they are ultimately not able to keep up with degrading insoluble material around them. This leads them to become dystrophic and lose their normal homeostatic functions (Hopp et al., 2018; Streit et al., 2018). On the other hand, factors secreted from microglia can lead to abnormal patterns of PTMs and may therefore play a role in the initiation of tau aggregation (Gorlovoy et al., 2009), which will then in turn induce more inflammation, repeating the toxic cascade. Studies have shown that neuronal tau pathology leads to the accumulation of senescent microglia and astrocytes. Removal of these senescent cells from a mouse model of neuronal tauopathy led to decreased tau pathology and improved cognition (Bussian et al., 2018). The presence of dysfunctional glial cells can thus directly contribute to neuronal tau pathology. Knockout of tau also rescued inflammation-mediated neurodegeneration in mice lacking the Cx3cr1 receptor (Maphis et al., 2015), indicating that endogenous tau may protect against inflammation and its downstream effects via a yet unknown mechanism.

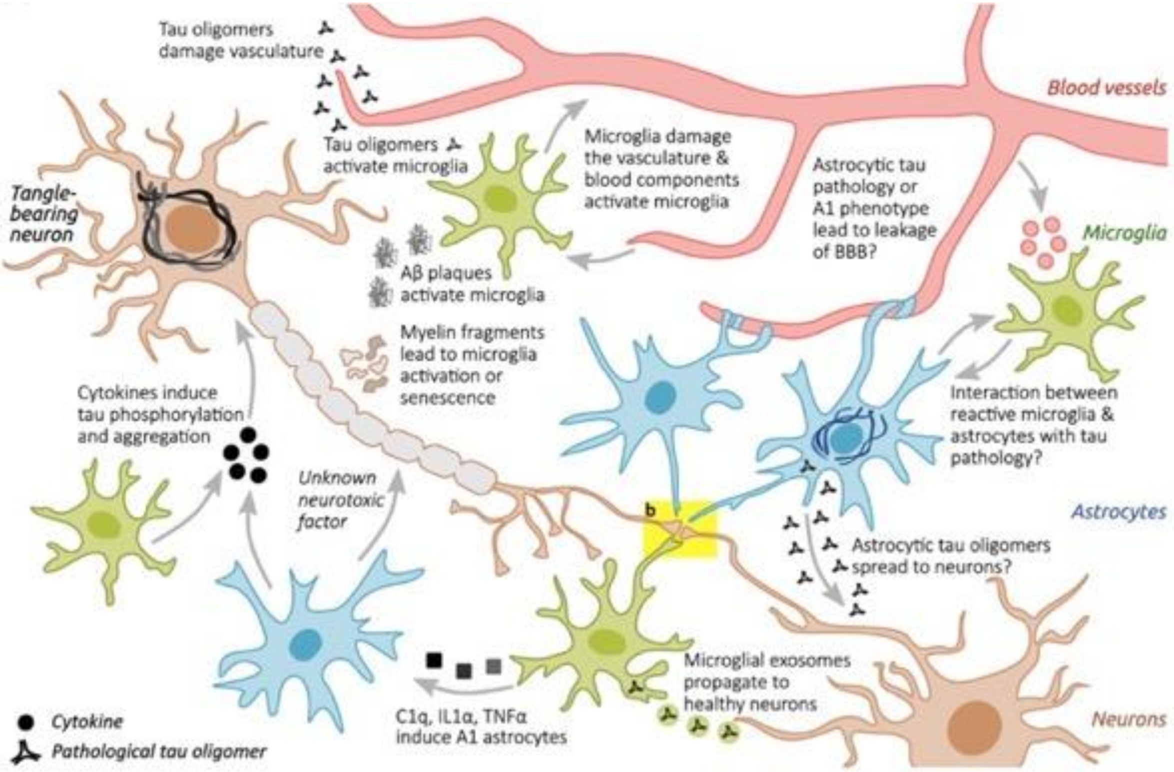
Tau oligomers
damage vasculature
Blood vessels
Tau oligomers
activate microglia
Microglia damage
the vasculature &
blood components
activate microglia
Astrocytic tau
pathology or
A1 phenotype
lead to leakage
of BBB?
Microglia
Tangle-
bearing
neuron
Aβ plaques
activate microglia
Myelin fragments
lead to microglia
activation or
senescence
Cytokines induce
tau phosphorylation
and aggregation
Interaction between
reactive microglia &
astrocytes with tau
pathology?
Unknown
neurotoxic
factor
b
Astrocytes
Astrocytic tau oligomers
spread to neurons?
Microglial exosomes
propagate to
healthy neurons
C1q, IL1α, TNFα
induce A1 astrocytes
Neurons
● Cytokine
Pathological tau oligomer

Figure 14 - Different cell types are involved in tau-induced neuroinflammation.
Neurons with tau pathology can be live phagocytosed by microglia. Neuronal tau pathology also induces neuroinflammation by shedding myelin fragments, by inducing the secretion of stress factors, tau oligomers, or via other unknown pathways. Tau oligomers can damage the vasculature directly or indirectly via microglia-induced neuroinflammation or alterations of astrocytic functions at the vasculature. All these events can potentially exacerbate the neuroinflammatory state, which in turn can aggravate tau pathology via proinflammatory cytokines. Microglia can also induce a neurotoxic phenotype in astrocytes which directly leads to neurodegeneration. Astrocytes can also accumulate tau, which may lead to mild changes in the vasculature and possibly impact microglia and synaptic function. (Adapted from Vogels et al., 2019).

Microglia may also play a critical role on the spreading of tau pathology (Asai et al., 2015). Indeed, mice injected with AAV that led to the overexpression of mutated tau in the EC presented spreading of htau from the EC to the DG observed at 1 month post-injection. Since neurons in the EC connect to neurons in the DG via the perforant pathway, this spreading was likely mediated through synaptic connections. However, depletion of microglia led to a reduction of htau detected in the DG. Knockout of TREM2 adapter protein DAP12 in a similar model also led to inhibition of synaptic tau spreading (Audrain et al., 2018). Although a portion of tau spreading might be mediated via neuron-to-neuron transfer or via glial cells such as astrocytes (Mudher et al., 2017; Martini-Stoica et al., 2018; Zanier et al., 2018), available evidence suggests that microglia might play an important role in tau spreading as well. Indeed, it was recently demonstrated that microglia contribute to the spreading of tau via exosome secretion (Asai et al., 2015).

With the currently knowledge on the biology of tau protein and all related pathways in AD, several therapeutic interventions may be underlined aiming to halt the progression of the disease throughout the brain and improve AD-related changes in behavior and cognition.

1.8. Therapeutical interventions to halt the propagation of tau pathology

Treating and preventing neurological disorders, specifically tauopathies, remains a challenge for several reasons. These include the lack of understanding of the aetiology and progression of the diseases in question, poor diagnosis at presymptomatic stages, lack of robust and sensitive biomarkers, short therapeutic windows and the inaccessibility of the degenerating brain tissue for drug delivery (Leinenga, Langton, Nisbet, & Götz, 2016; Li & Götz, 2017).

Although the mechanisms underlying tau-mediated neurotoxicity in AD have to date not been well elucidated, multiple therapeutic approaches have been proposed that target tau function or dysfunction, based on the current understanding of these mechanisms (Wang & Mandelkow, 2016). Indeed, the anti-tau pipeline has been growing over the last years, partly fueled by the lack of success targeting Aβ.

Several therapies that target tau, both directly and indirectly have been the focus of intense research activity over the past years (table 1). Important approaches that have been tested in preclinical and, eventually, clinical studies, involve: tau aggregation blockers (e.g. methylene blue, which was shown to induce autophagy and attenuate tauopathy *in vitro* and *in vivo*) (Clavaguera et al., 2014; Congdon et al., 2012; Fatouros et al., 2012; Hochgräfe et al., 2015; Lee, Brunden, Hutton, Trojanowski, 2011); reducing tau levels (e.g. siRNA or antisense oligonucleotides targeting tau) (DeVos et al., 2013; Lasagna-Reeves et al., 2016; Xu et al., 2014); vaccination (e.g. passive: antibodies PHF-1 or MC1; active: advacc1, a vaccine developed against the repeat domain of tau) (Boutajangout et al., 201AD; Chai et al., 2011; Kontsekova et al., 2014; Novak et al., 2017); targeting enzymes that regulate tau PTMs (e.g. ERK inhibitor, HDAC6 inhibitor) (Le Corre et al., 2006; Ding et al., 2008; Kilgore et al., 2010; Tran et al., 2012); targeting autophagy (e.g. autophagy inducers) (Ozcelik et al., 2013; Frederick et al., 2015); MT-stabilizers (e.g. Paclitaxel, curcumin) (Zhang et al., 2005; Miyasaka et al., 2016); among others (figure 15).

1.8.1. BSc3094 as a potential therapeutic agent for AD

BSc3094 monohydrobromide (2-[4-(4-Nitrophenyl)-2-thiazolyl]hydrazide-1H-benzimidazole-6-carboxylic acid monohydrobromide) is a phenylthiazolyl-hydrazide derivative (Pickhardt et al., 2007). BSc3094 has been used in tau protein research to study the processes underlying tau aggregation, due to its features as a potent inhibitor of tau aggregation and ability to dissolve tau preformed fibrils. Previous studies from our group have demonstrated a great efficacy for this compound to significantly reduce tau phosphorylation and aggregation, increasing at the same time cell viability and having no cytotoxic effects in an *in vitro* N2a cell model expressing pro-aggregant mutant htau (Pickhardt et al., 2015, 2017). Further studies from our group have shown that BSc3094 is also capable of inhibiting tau aggregation in a *C. elegans* model of tauopathy expressing pro-aggregant mutant htau (Fatouros et al., 2012). Recently, we also observed that BSc3094 reverses the pre-synaptic impairment in pro-aggregant tau transgenic organotypic hippocampal slices, by reversing the paired-pulse depression observed in non-treated pro-aggregant tau transgenic slices after applying a paired-pulse stimulus of the Schaffer collaterals (Dennissen et al., 2016). Taken together, these results strengthen the hypothesis that BSc3094, a powerful tau aggregation inhibitor, could be a potential therapeutical agent used to reverse tau pathology and, possibly, exert a beneficial effect in AD.

Table 1 - Examples of tau-based therapies under clinical development.
(Adapted from Li & Gotz, 2017).

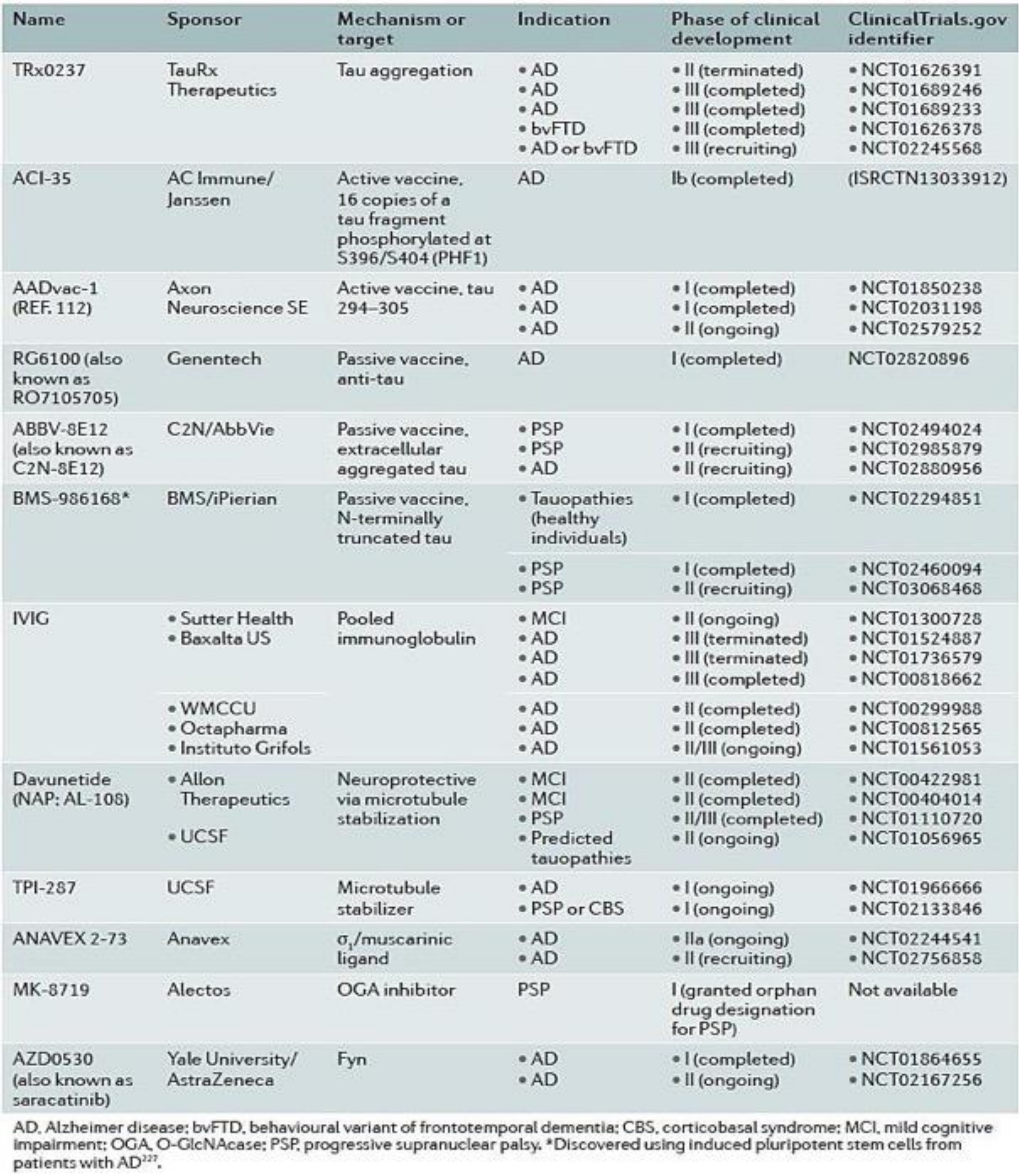

Name	Sponsor	Mechanism or target	Indication	Phase of clinical development	ClinicalTrials.gov identifier
TRx0237	TauRx Therapeutics	Tau aggregation	• AD • AD • AD • bvFTD • AD or bvFTD	• II (terminated) • III (completed) • III (completed) • III (completed) • III (recruiting)	• NCT01626391 • NCT01689246 • NCT01689233 • NCT01626378 • NCT02245568
ACI-35	AC Immune/ Janssen	Active vaccine, 16 copies of a tau fragment phosphorylated at S396/S404 (PHF1)	AD	Ib (completed)	(ISRCTN13033912)
AADvac-1 (REF. 112)	Axon Neuroscience SE	Active vaccine, tau 294–305	• AD • AD • AD	• I (completed) • I (completed) • II (ongoing)	• NCT01850238 • NCT02031198 • NCT02579252
RG6100 (also known as RO7105705)	Genentech	Passive vaccine, anti-tau	AD	I (completed)	NCT02820896
ABBV-8E12 (also known as C2N-8E12)	C2N/AbbVie	Passive vaccine, extracellular aggregated tau	• PSP • PSP • AD	• I (completed) • II (recruiting) • II (recruiting)	• NCT02494024 • NCT02985879 • NCT02880956
BMS-986168*	BMS/iPierian	Passive vaccine, N-terminally truncated tau	• Tauopathies (healthy individuals)	• I (completed)	• NCT02294851
			• PSP • PSP	• I (completed) • II (recruiting)	• NCT02460094 • NCT03068468
IVIG	• Sutter Health • Baxalta US	Pooled immunoglobulin	• MCI • AD • AD • AD	• II (ongoing) • III (terminated) • III (terminated) • III (completed)	• NCT01300728 • NCT01524887 • NCT01736579 • NCT00818662
	• WMCCU • Octapharma • Instituto Grifols		• AD • AD • AD	• II (completed) • II (completed) • II/III (ongoing)	• NCT00299988 • NCT00812565 • NCT01561053
Davunetide (NAP: AL-108)	• Allon Therapeutics • UCSF	Neuroprotective via microtubule stabilization	• MCI • MCI • PSP • Predicted tauopathies	• II (completed) • II (completed) • II/III (completed) • II (ongoing)	• NCT00422981 • NCT00404014 • NCT01110720 • NCT01056965
TPI-287	UCSF	Microtubule stabilizer	• AD • PSP or CBS	• I (ongoing) • I (ongoing)	• NCT01966666 • NCT02133846
ANAVEX 2-73	Anavex	σ_1/muscarinic ligand	• AD • AD	• IIa (ongoing) • II (recruiting)	• NCT02244541 • NCT02756858
MK-8719	Alectos	OGA inhibitor	PSP	I (granted orphan drug designation for PSP)	Not available
AZD0530 (also known as saracatinib)	Yale University/ AstraZeneca	Fyn	• AD • AD	• I (completed) • II (ongoing)	• NCT01864655 • NCT02167256

AD, Alzheimer disease; bvFTD, behavioural variant of frontotemporal dementia; CBS, corticobasal syndrome; MCI, mild cognitive impairment; OGA, O-GlcNAcase; PSP, progressive supranuclear palsy. *Discovered using induced pluripotent stem cells from patients with AD[227].

1.8.2. The blood-brain-barrier as an obstacle for drug delivery

One of the major obstacles in the development of therapeutical agents for the CNS is that many agents do not cross the blood-brain-barrier (BBB, figure 16) sufficiently well to evaluate their effects on the brain without delivering them locally. The BBB represents a barrier between the brain’s blood vessels (capillaries) and the cells and other components of the brain tissue, providing a defense against disease-causing pathogens and toxins that may be present in our blood, being also involved in maintaining brain homeostasis. This is achieved by forming a tightly regulated neurovascular unit that includes endothelial cells, pericytes and astrocytic endfeet. In the capillaries that form the BBB, endothelial cells are placed extremely close to each other, forming so called tight-junctions (Abbott, Rönnbäck, & Hansson, 2006).

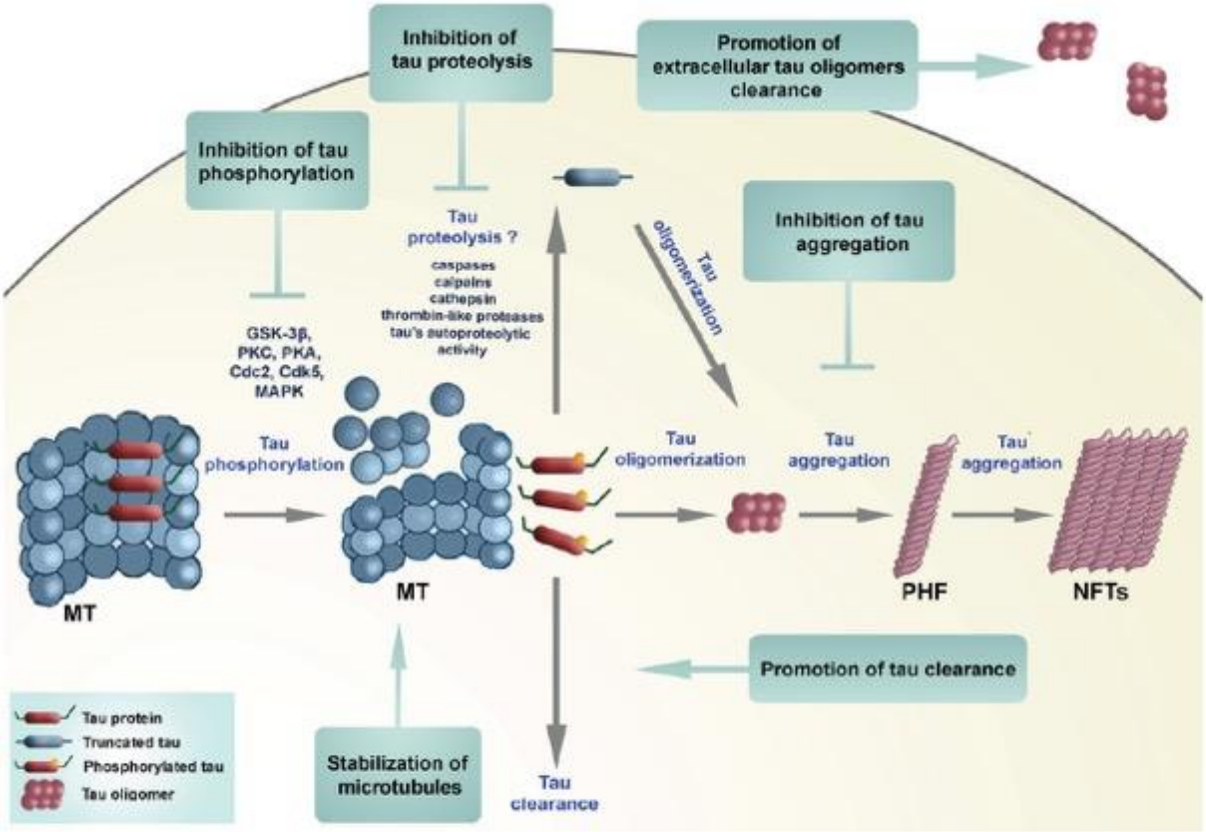
Inhibition of tau proteolysis
Promotion of extracellular tau oligomers clearance
Inhibition of tau phosphorylation
Tau proteolysis ?
caspases
calpains
cathepsin
thrombin-like proteases
tau's autoproteolytic activity
Tau oligomerization
Inhibition of tau aggregation
GSK-3β, PKC, PKA, Cdc2, Cdk5, MAPK
Tau phosphorylation
Tau oligomerization
Tau aggregation
Tau aggregation
MT
MT
PHF
NFTs
Promotion of tau clearance
Tau protein
Truncated tau
Phosphorylated tau
Tau oligomer
Stabilization of microtubules
Tau clearance

Figure 15 - Potential therapeutic strategies to reduce tau aggregates.
Different targets that interfere directly or indirectly with tau protein have been undergoing preclinical and clinical studies over the last years, including inhibitors of tau phosphorylation, inhibitors of tau proteolysis, promoters of Tau clearance, MT stabilizers, among others. (Adapted from Šimi´c et al., 2016).

A state-of-the-art technique for the local delivery of drugs into the brain of rodents is achieved with the use of Alzet osmotic pumps. This presents a major advantage by enabling the local infusion of drugs directly into the brain and at a constant rate, facilitating the generation of reliable data. The Alzet osmotic pumps, combined with a brain infusion kit, can directly target a specific brain region (e.g. the hippocampus) or the cerebral ventricles, which has the advantage of exposing a wide variety of brain regions to the drug via the cerebrospinal fluid that bathes the brain (DeVos and Miller, 2013).

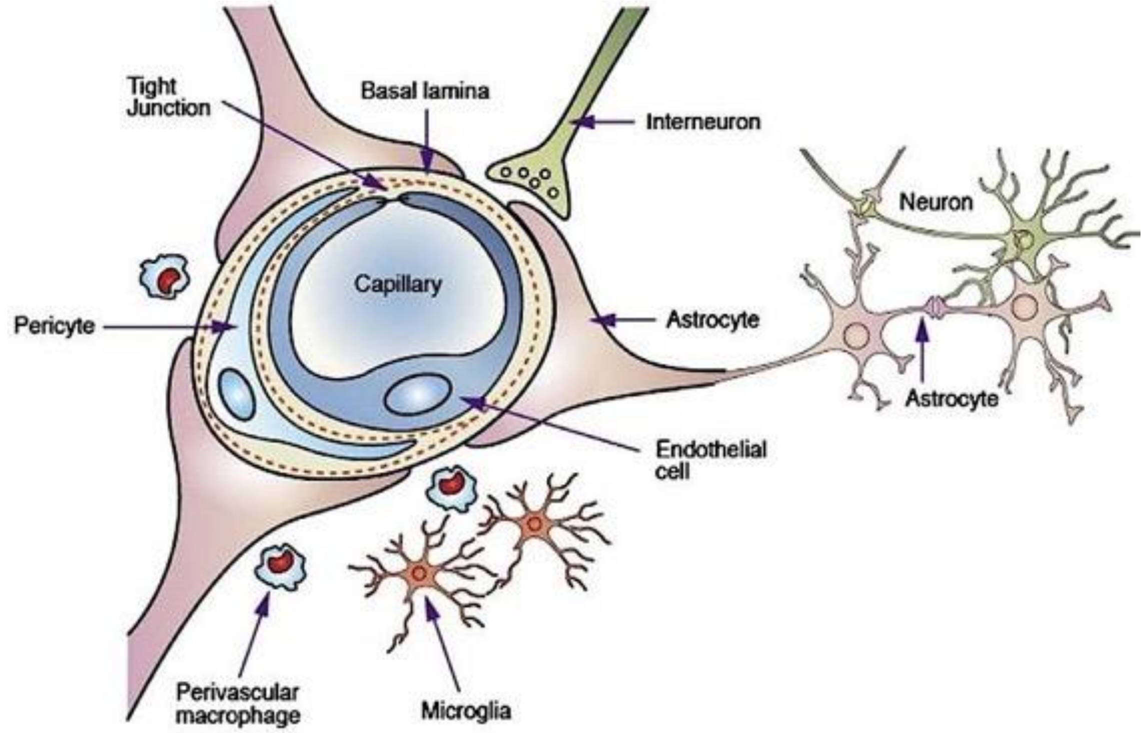
Tight Junction
Basal lamina
Interneuron
Neuron
Capillary
Pericyte
Astrocyte
Astrocyte
Endothelial cell
Perivascular macrophage
Microglia

Figure 16 - Blood-brain-barrier.
The BBB exists between the blood vessels and the cells and other components of the brain tissue providing defense against disease-causing pathogens and toxins present in our blood, and maintaining brain homeostasis. The BBB comprises a tightly regulated neurovascular unit including endothelial cells, pericytes and astrocytic endfeet. Tight-junctions are formed in the capillaries that form the BBB by placing endothelial cells extremely close to each other. (Adapted from Abbott, Rönnbäck, & Hansson, 2006).

Little is known so far about the mechanisms underlying the onset and propagation of tau pathology in AD. Furthermore, very few drugs tested proved to have a beneficial effect in patients suffering from the disease, and they mostly target the level of neurotransmitters, not tau or Aβ. Therefore, it is of major relevance to elucidate the open questions in the field, which includes questions related to the nature of the toxic tau species, the increased vulnerability of certain brain regions to the development of AD compared to others, the transfer of tau pathology from cell to cell, the role of inflammation, and others. This knowledge should help to design appropriate therapeutical strategies and possibly find an effective treatment for AD.

2

AIMS OF THE STUDY

2. Aims of the study

As previously mentioned, despite years of intense research, little is known about the mechanisms underlying the spreading of tau pathology throughout the brain, and which are exactly the tau species responsible for the development of pathology and its propagation. Initially, it was thought that the aggregated tau species were responsible for toxicity and neurodegeneration. Furthermore, it was speculated that this may also be the tau species transferred between cells to propagate the pathology. However, recent evidences pointed out the intermediate tau oligomeric species as the culprit concerning neurodegeneration, specifically in synaptic and neuronal loss, but this is still under debate. Hence, using mice expressing pro- or anti-aggregant htau restricted to the EC, we aimed to understand the molecular mechanisms that trigger the onset of tau pathology, and how this pathological process spreads throughout the brain, specifically:

- unraveling which tau species are responsible for the development of pathology;
- determining if the tau species involved in the formation of pathology are also the ones involved in the propagation of the toxic cascade throughout the brain;
- determining if the aggregation propensity of tau is a requisite for propagation, by comparing the behavior of pro- and anti-aggregant tau species (ΔK280 and (ΔK280-2P htau, respectively);
- monitoring the role of other key factors on the propagation of tau pathology, including the presence/absence of endogenous mouse tau and neuroinflammatory processes.

A further aim was to test a novel interventional therapeutic strategy to halt the propagation of tau pathology in a transgenic mouse model of the disease (rTg4510 mice), by evaluating the potential beneficial effects of the compound phenyl-thiazolyl-hydrazide derivative BSc3094, a potent tau aggregation inhibitor, in halting the propagation of tau pathology.

3

MATERIALS & METHODS

3. Materials and Methods

3.1. Materials

3.1.1. Primary antibodies

Antibody	Specificity	Dilution	Company/Ref
K9JA	Total Tau	1:20 000 (WB) 1:500 (IF)	DAKO A0024
Tau Y9	Human Tau	1:100 (IF)	Enzo Life Sciences BML-TA3119-0100
HT7	Human Tau	1:500 (IHC)	Thermo Fisher Scientific MN1000
AT8	Tau phos Ser202/Thr205	1:1000 (WB) 1:200 (IF)	Thermo Fisher Scientific MN1020
12E8	Tau phos Ser262/Ser356	1:1000 (WB) 1:100 (IHC)	ELAN Pharmaceuticals 860
PHF-1	Tau phos Ser396/Ser404	1:1000 (WB) 1:100 (IF & IHC)	Kind gift from Dr. P. Davies
AT180	Tau phos Thr231/Ser235	1:100 (IHC)	Thermo Fisher Scientific MN1040
MC1	Tau pathological conformation	1:50 (IF & IHC)	Kind gift from Dr. P. Davies
Synaptophysin	Pre-synaptic marker	1:5000 (WB)	Sigma-Aldrich S5768
PSD95	Post-synaptic density protein 95	1:1000 (WB)	Cell signaling 2507
GFAP	Glial fibrillary acidic protein	1:2000 (WB) 1:250 (IF)	Sigma-Aldrich G9269
CD11b	Cluster of differentiation molecule 11b (macrophages& microglia)	1:1000 (WB)	Abcam ab75476
Iba1	Ionized calcium binding adaptor molecule 1 (microglia & macrophages)	1:100 (IF)	WAKO 019-19-741
GluR1	Anti-Glutamate receptor 1	1:1000 (WB)	Merck AB1504
Actin	Cytoskeletal protein; used as loading control for WB	1:10 000 (WB)	Sigma-Aldrich A5441

3.1.2. Secondary antibodies

Antibody	Dilution	Company/Ref
α-mouse goat HRP	1:2000 (WB)	DAKO P0447
α-rabbit goat HRP	1:2000 (WB)	DAKO P0448
Donkey Cy3 α-mouse	1:500 (IF)	Dianova 715-165-151
Donkey Alexa 647 α-mouse	1:500 (IF)	Dianova 715-605-151
Goat Cy3 α-rabbit	1:500 (IF)	Dianova 111-165-144
Donkey Alexa 647 α-rabbit	1:500 (IF)	Dianova 711-605-152

3.1.3. Molecular weight markers

Marker	Company/Ref
Protein magic marker	Thermo Fisher Scientific LC5602
Page ruler prestained protein ladder	Thermo Fisher Scientific 26616
Smart Ladder	Eurogentec MW-1700-10

3.1.4. Kits

Kit	Company/Ref
Amersham ECL Prime Western Blotting Detection Reagent	GE Healthcare Life Sciences RPN2236
Bicinchoninic Acid Protein (BCA) Assay Kit	Sigma-Aldrich BCA-1
VECTASTAIN® Elite® ABC HRP Kit (Peroxidase, Universal)	Vector Laboratories PK-6200
DAB Quanto Chromogen and Substrate	Thermo Fisher Scientific TA-060-QHDX

3.1.5. Centrifuges

Centrifuge	Company
Eppendorf centrifuge 5415 R	Eppendorf, Germany
Ultracentrifuge Beckman CoulterTM OptimaTM MAX-E	Beckman Coulter, Germany

3.1.6. Microscopes

Microscope	Company
Light microscope BX43	Olympus, Germany
Confocal microscope FV1000 BX61	Olympus, Germany
LSM800 confocal microscope	Zeiss, Germany

3.1.7. Surgery equipment

Equipment	Company
Digital Mouse Stereotaxic Frame	World Precision Instruments (WPI), Germany
10µl NanoFil Syringe	World Precision Instruments (WPI), Germany
35 ga. blunt NanoFil needle	World Precision Instruments (WPI), Germany
100 µL Alzet Osmotic Pumps (1004)	Alzet, USA
Alzet Brain Infusion Kit 3	Alzet, USA
Hot bead sterilizer 18000-45	Fine Science Tools (FST), Germany
Micromotor High-Speed Drill	Stoelting, Germany
UltraMicroPump (UMP3) with SYS-Micro4 Controller	World Precision Instruments (WPI), Germany
Stereotax Control Panel	Leica BioSystems, Germany
Inhalation Anesthesia System	VetEquip, USA

3.1.8. Others

Equipment	Company
Shaker DOS-10L	NeoLab, Germany
Analog tuberoller RS-TR05	Phoenix Instrument, Germany
SPR 80 L Flake ice maker	Nord Cap, Germany
Analytical Lab Scale Digital Balance BP310S Delta	Sartorius, Germany
PVDF membranes (0.45µm pore size)	Millipore, Germany
Well plates (12, 24 & 96)	Corning, Germany
Vortex-Genie 2	Scientific Industries, USA
Image Quant LAS 4000 mini	GE Healthcare Life Sciences, Germany
Bio-Rad Trans-Blot SD Semi-Dry Transfer Cell	Bio-Rad, Germany
EPS 600 Electrophoresis Power Supply, 120 V	Pharmacia BioTech, USA
British Standard Microscope Slides	Thermo Fisher Scientific, Germany
Superfrost Plus™ Adhesion Microscope Slides	Thermo Fisher Scientific, Germany
Fluoromount-G® mounting medium	Southern Biotech, Germany
Roti®-Histokitt mounting medium	Carl Roth, Germany
Shandon™ Cryomatrix™ embedding resin	Thermo Fisher Scientific, Germany
Cryostat Microm HM560	MICROM International GmBH, Germany
Microtome Slide 2003	Pfm Medical AG, Germany
Vibratome VT1200	Leica, Germany
Safire microplate reader	Tecan, Germany

3.2. Methods

3.2.1. Animals

To analyze the propagation of tau pathology transgenic mice expressing mutant pro- and anti-aggregant htau were used. The tTA-EC/K2 mouse line was generated by crossing the responder line of transgenic mice co-expressing the human full-length tau protein (hTau40; 2N4R) with the FTDP-17 mutation ΔK280 (deletion of lysine 280) (figure 17A) and the reporter firefly luciferase gene under the control of a bidirectional tetO-responsive CMV promoter, with the activator mouse line Neuropsin (Nop)-tTA, which expresses the tetracycline-controlled transactivator (tTa) exclusively in the entorhinal cortex (EC) layer II, as described before (Calignon et al., 2012; Dennissen et al., 2016; Eckermann et al., 2007; Yasuda & Mayford, 2006). This yielded a regional neuron-specific expression of mutant htau and luciferase, which are confined to the MEC. In parallel, another tau transgenic mouse (tTA-EC/K3) was generated with the same constructs as the tTA-EC/K2 mouse, but with two additional prolines in the hexapeptide motifs of the repeat domain of the tau protein (figure 17A), which serve as β-sheet breakers (htau ΔK280-PP) (Eckermann et al., 2007). The tTA-EC/K2 (htau ΔK280) and tTA-EC/K3 (htau ΔK280-PP) transgenic mice are named pro-aggregant and anti-aggregant tau transgenic mice, respectively. Before starting the experiments, we selected transgenic mice with comparable tau expression by *in vivo* bioluminescence imaging to reduce inter-individual variations (Van der Jeugd et al., 2012). Wild-type (WT) C57BL-6J mice and mice lacking tau protein (B6.129X1-Mapt$_{\text{tm1Hnd}}$/J (Mapt$_{0/0}$); Tau-KO) (Dawson et al., 2001) were also used in the experiments. We analyzed gender-mixed animals. Transgenic mouse lines tTA-EC/K2 and tTA-EC/K3 were identified by PCR using the following primer pairs: htau transgene (JB309/pBI5-BN): forward 5’-GAC CTT CCG CGA GAA CGC CAA A-3’; reverse 5’-AAG AAC AAT CAA GGG TCC CCA-3’; neuropsin promoter (Nop-for/Nop-rev): forward 5’- ACC GAG AAG CAG TAC GAG A-3’; reverse 5’-ACT CGC ACT TCA GCT GCT T-3’. The following PCR programs were used:

Thermocyler Program K2 and K3 (for JB309/pBI5-BN primer):

Step	Temp. in °C	Time in sec	cycles
Initial denaturation	95	300	1
Denaturation	95	30	30
Annealing	58	60	
Extension	72	30	
Final extension	72	300	1
Hold	4	end	-

Thermocyler Program TTA (for Nop-for/Nop-rev primer):

Step	Temp. in °C	Time in sec	Cycles
Initial denaturation	94	300	1
Denaturation	94	30	35
Annealing	55	30	
Extension	72	60	
Final extension	72	600	1
Hold	4	End	-

To develop a therapeutical intervention to halt the propagation of tau pathology the rTg(tauP301L)4510 mouse model developed by K. Ashe and coworkers was used (Ramsden et al., 2005). Briefly, rTg4510 animals were produced by crossing the activator mouse line CamKII-tTA, with the responder tetO.MAPT*P301L mouse line (figure 17B). Mice having both CamKII-tTA and tau transgene expressed human mutant P301L tau (0N4R). Mice lacking the responder and the activator transgene were used as controls. Mice were screened by PCR using the following primer pairs: htau transgene (Tau mPrP_E2): forward 5’-TGA ACC ATT TCA ACC GAG CTG-3’; reverse: 5’-TAC GTC CCA GCG TGA TCT TC-3’; CamKII promoter (oIMR8746/oIMR8747): forward 5’-CGC TGT GGG GCA TTT TAC TTT AG-3’; reverse: 5’-CAT GTC CAG ATC GAA ATC GTC-3’. The following PCR program was used:

Thermocyler Program Phire 70 (for Tau mPrP_E2 & oIMR8746/oIMR8747primers):

Step	Temp. in °C	Time in sec	Cycles
Initial denaturation	98	180	1
Denaturation	98	5	30
Annealing	70	5	
Extension	72	15	
Final extension	72	60	1
Hold	4	End	1

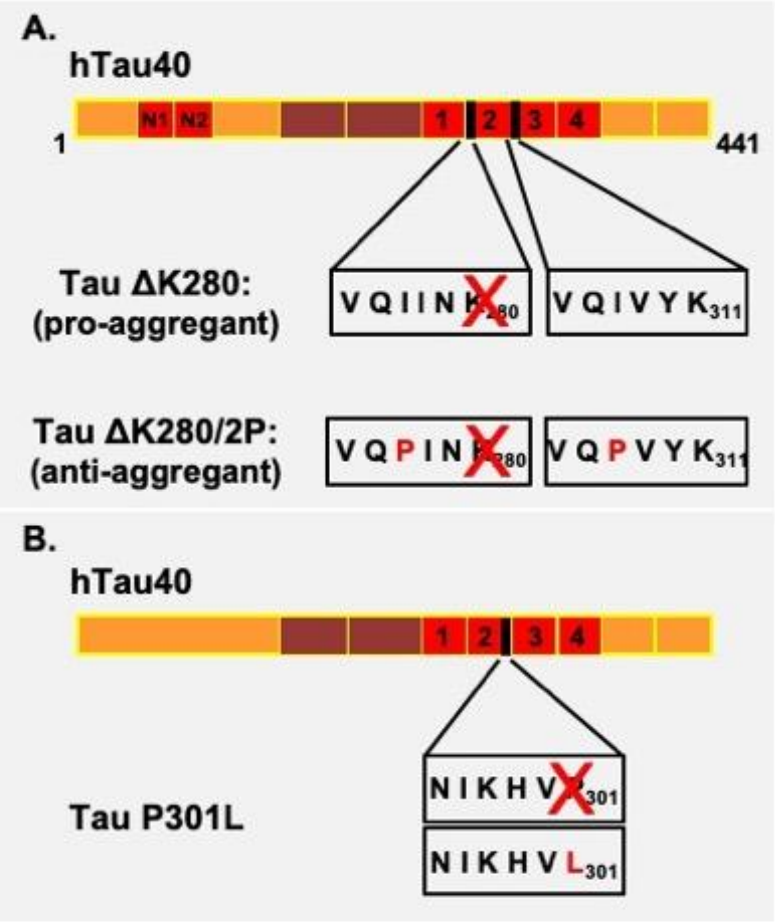
A.
hTau40
1
N1
N2
1
2
3
4
441
Tau ΔK280:
(pro-aggregant)
V Q I I N K280
V Q I V Y K311
Tau ΔK280/2P:
(anti-aggregant)
V Q P I N K280
V Q P V Y K311
B.
hTau40
1
2
3
4
Tau P301L
N I K H V P301
N I K H V L301

Figure 17 - Tau transgene expression in the experimental mouse models.
A. Bar diagrams illustrating the domains of full-length tau (2N4R, 441 residues), with the hexapeptides responsible for aggregation highlighted in black. The pro-aggregant ΔK280 mutation and the anti-aggregant proline mutations (I277P, I308P) are highlighted. **B.** The FTDP-17 mutation P301L tau is highlighted, corresponding to the substitution of a proline for a lysine at amino acid 301, which strongly favors aggregation. Adapted from Sydow et al., 2011.

3.2.2. Housing conditions

All animals were housed and handled according to standards of the German Animal Welfare Act, under the approval LANUV: 84-02.04.2016-A278 (for the spreading of Tau pathology), and LANUV: 84-02.04.2017-A405 (for the implantation of Alzet osmotic pumps). Mice were housed in groups of 2–5 animals under standard conditions (23 °C, 40–50 % humidity, *ad libitum* access to food and water) with a 12 hours light/dark cycle (with light on from 6 a.m. to 6 p.m.). After implantation of the Alzet osmotic pumps, rTg4510 mice were single housed to prevent damaging of the surgical wound.

3.2.3. Fresh *ex-vivo* brain slices and measurement of luciferase bioluminescence

Bioluminescence (BLI) can be used to characterize the spatial transgene expression pattern in detail in *ex vivo* brain slice preparations. Whole brain *ex-vivo* slices were prepared from 6 months old transgenic pro- and anti-aggregant mice to monitor luciferase BLI (and consequently htau expression), using a protocol previously described (Humpel, 2018). Briefly, mice were anesthetized (Isofluran, Piramal Critical Care, Germany) and sacrificed by cervical dislocation, and the head was removed using a pair of large scissors. After dissecting the brain, 500 µm thick horizontal brain slices were prepared using a vibratome (Leica VT1200). Slices were immediately transferred onto membrane inserts in 6-well plates and kept alive in slice culture media containing 0.15 mg/mL D-luciferin, at 37°C, 5% CO2 incubator (three whole brain sections per membrane). A subsequent BLI scan (Ivis Lumina II system; Caliper Life Science) exhibited the transgene expression pattern (Hochgräfe and Mandelkow, 2013).

3.2.4. *In vivo* bioluminescence of human tau expression

In vivo BLI was performed using an Ivis Lumina II system (Caliper Life Science) (figure 18A) according to a standardized protocol. The mice received, ten minutes before the imaging session, an intraperitoneal (i.p.) injection of 150 mg/kg of D-luciferin (Caliper Life Science) dissolved in sterile PBS. The heads of the mice were shaved to avoid optical attenuation of emitted photons. Mice were anesthetized with 2% isoflurane (Abbott) in a constant O_2 flow, which was maintained throughout the whole imaging session. Mice were placed into the heated, light-tight imaging chamber and a sequence of 6 images, taken in intervals of 2 minutes starting at 10 minutes post i.p. injection, was recorded using a highly sensitive charged coupled device camera (figure 18B). The analysis of the recorded images was accomplished using Living Image 4.0 software (Caliper Life Science). The BLI emission was normalized and the surface radiance was displayed in photons per second per square centimeter per steradian (photons/s/cm2/sr). For quantification of BLI signals, a region of interest (ROI) was defined to convert surface radiance (photons/s/cm2/sr) into total flux of the bioluminescent source (photons/s) (Hochgräfe and Mandelkow, 2013).

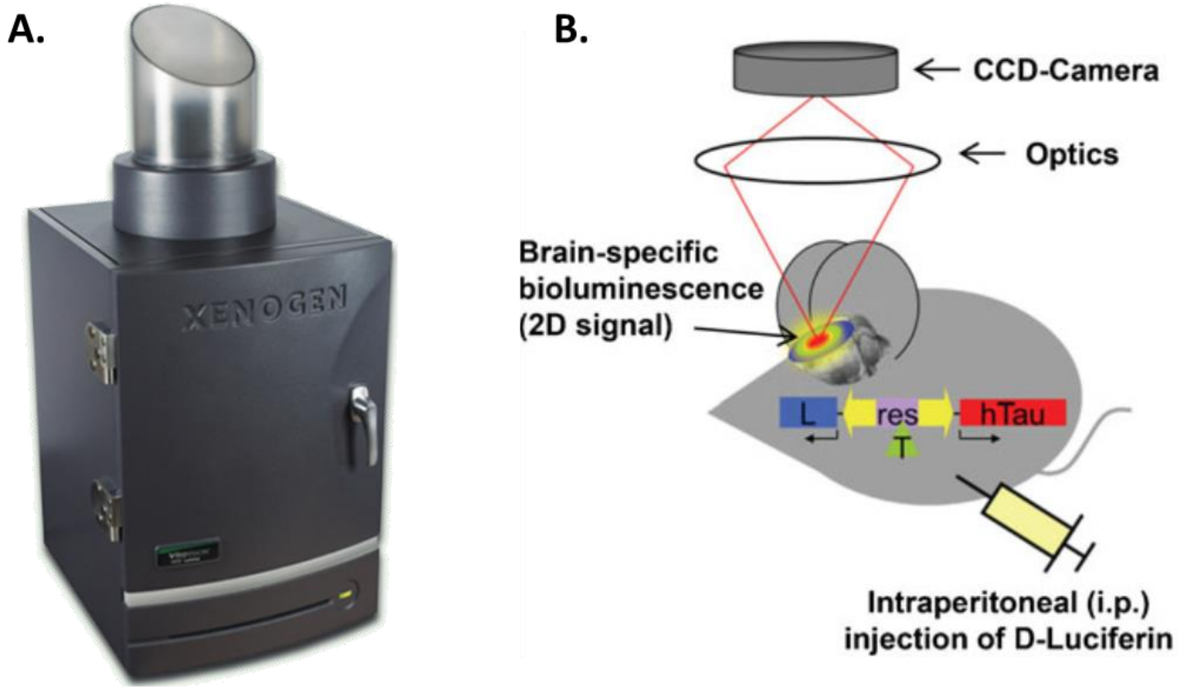

Figure 18 - ***In vivo*** **bioluminescence imaging of luciferase activity in the mouse brain.**
A. IVIS Lumina II system (Caliper Life Science); **B.** Scheme representing the workflow of BLI in tau transgenic mice expressing htau and luciferase (L) under the control of a bidirectional promoter (yellow arrows). Expression is switched on when the transactivator (T) binds to the responsive promoter element (res). Expression of the transactivator is regulated by the neuropsin promoter, resulting in EC-specific expression of luciferase and htau. After i.p. injection of 150 mg/kg D-luciferin, mice exhibit a brain-specific emission of photons, which is detected by a CCD camera system inside the BLI imaging chamber. Adapted from Hochgräfe & Mandelkow, 2013.

3.2.5. Adeno-associated virus (AAV)

Three distinct adeno-associated virus (AAV) constructs were used in the experiments: 1) AAV encoding eGFP, the translation interrupting 2a peptide(Szymczak et al., 2004), and pro-aggregant full length mutant htau ΔK280 (AAV2/8-CBA-eGFP-2a-htau40ΔK280 (named **AAV-K2**); titer = 9.71x10$_{11}$ GC/ml); 2) AAV encoding eGFP, the translation interrupting 2a peptide, and anti-aggregant full length mutant htau ΔK280-PP (AAV2/8-CBA-eGFP-2a-htau40ΔK280-PP (named **AAV-K3**); titer = 1.65x10$_{12}$ GC/ml); and 3) AAV encoding eGFP (AAV2/8.CBA.eGFP-2a WPRE.Bgh (named **AAV-GFP**)), titer 1.37x10$_{13}$ GC/ml). All AAV constructs were produced at Gene Transfer Vector Core (GTVC), Schepens Eye Research Institute and Massachusetts Eye and Ear Infirmary, Harvard Medical School. The gene of interest is expressed under the control of CMV-IE promoter as a bicistronic construct together with the GFP protein. The self-cleaving 2A peptide sequence from Porcine Teschovirus-1 virus separates both sequences, ensuring the independent expression of GFP and the gene of interest. The AAV2/8-CBA-eGFP-2a virus is classified as a mixed serotype AAV2/8, meaning that the standard plasmid used for the generation of the AAV containing the tau gene of interest has the ITRs from AAV2, but the capsid protein from serotype 8, which provides excellent targeting to neuronal cells while keeping the AAV in the lab safety level S1. The plasmid maps of the AAV used in the study are presented in the appendix section of the present thesis.

3.2.6. AAV injections

Intracerebral injections of AAV into the brain of anesthetized (Isoflurane, Piramal Critical Care, Germany) 5 month old tTA-EC/K2, tTA-EC/K3, WT and Tau-KO mice for unilateral expression of eGFP and mutant htau in the right EC were performed using classic stereotaxic procedures at the following coordinates: AP -4.7mm, ML +3.6mm (from Bregma), DV -3.0 (from *dura mater/*brain surface)). The contralateral (left) hemisphere was injected with PBS in the same brain coordinates as control. The standard injection procedure consisted in delivering 2 µL of AAV or PBS using a 10 µL glass syringe with a fixed needle (Hamilton). After reaching the injection coordinates, the needle was left in place for 2 minutes to allow the tissues to adapt. After injection at a rate of 0.2nL/min, the needle was left in place for an additional 5 minutes to prevent backflow of the injected solution.

AAV-K2 was injected into tTA-EC/K2, WT and Tau-KO mice, while AAV-K3 was injected into tTA-EC/K3, WT and Tau-KO mice. A group of WT mice was injected with AAV-GFP. Mice were sacrificed by cervical dislocation at 3, 6, 12 and 18 months post-injection (p. i.), and the brains were collected for paraffin or cryo free-floating sectioning, or western blot analysis.

3.2.7. Determination of BSc3094 concentration in the brain

To determine the ability of the drug of interest, BSc3094 (Pickhardt et al., 2007), to permeate the BBB, intravenous (i.v.) injections of BSc3094 (Sigma-Aldrich, 3 mg/kg in PEG400/water (60:40)) were performed in WT animals, and the concentration of the drug in the brain was estimated up to 24 hours post-dose.

3.2.8. Implantation of Alzet osmotic pumps

Alzet osmotic pumps (model 1004; volume: 100µL; infusion rate: 0.11µL/h; duration: 28 days) combined with the Alzet brain infusion kit 3 were implanted into anesthetized rTg4510 and control non-transgenic mice, as previously described (DeVos and Miller, 2013).

To determine the BSc3094 dose to be used in the therapeutical approach, a pilot study was performed. Alzet osmotic pumps containing vehicle (PEG400/water (60/40)) or three different concentrations of BSc3094 (0.075 mM, 0.150 mM and 1.5 mM) were implanted in 3 month old rTg4510 mice for direct infusion of the drug into the brain. The treatment lasted 28 days, after which the brain tissue was collected and total tau levels were analyzed by western blot in the sarkosyl-insoluble fraction, obtained from cortical extracts, to determine the most effective dose in reducing the levels of sarkosyl-insoluble tau.

After determining the experimental dose, the final therapeutical approach started. Alzet osmotic pumps were filled with 100µL of BSc3094 (1.5mM in 60:40 PEG400/ddH$_2$O) or vehicle. The osmotic pump and brain infusion kit were assembled together by connecting a catheter to the flow modulator of the osmotic pump reservoir, which was then connected to a cannula to be implanted at the designated coordinates. Before implantation, the fully assembled osmotic pumps (figure 19A) were placed in sterile 50mL Falcon tubes filled with saline solution and placed in a clean 37ºC water bath during 40h for priming/activation. Afterwards, the osmotic pumps were implanted into 1.5-2 months old rTG4510 or non-transgenic control mice subcutaneously. Briefly, a subcutaneous pocket was formed using blunted scissors at the base of the neck towards the left hind limb where the osmotic pump reservoir was placed. Afterwards, the cannula was placed into the correct stereotaxic coordinates using a cannula driver (AP -0.5mm, ML +0.8mm, DV -2.5 from Bregma, figure 19B). A single drop of super glue was placed on the base of the cannula, and the thin metal catheter from the cannula was driven through the skull until the plastic cannula base reached the top of the skull. When the glue was completely dry the top of the cannula was clipped off and the wound was closed using surgical suture thread. Four weeks later the osmotic pump was replaced by making a 1.5 cm incision on mouse's back, perpendicular to the pump/tubing junction, using forceps and scissors. The pump was carefully pulled out of the incision and the old pump was pulled off slowly from the flow modulator attached to the tubing and cannula. The new pump (previously primed) was slid into the flow modulator and reinserted through the incision back into the subcutaneous pocket, and the skin was sutured.

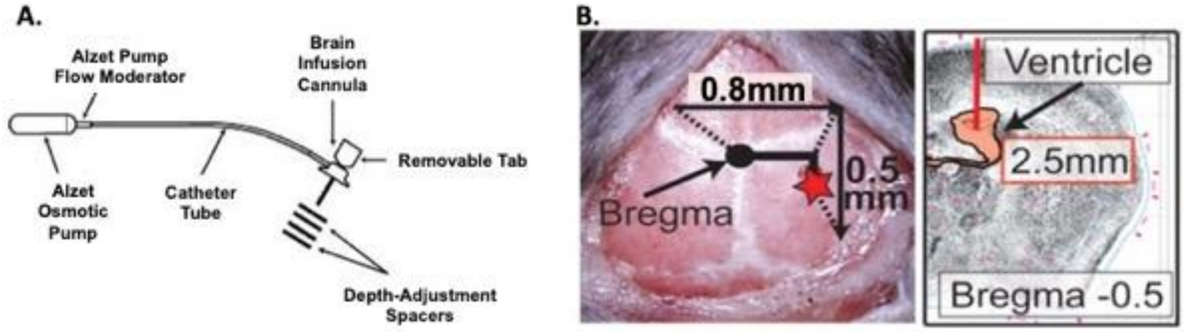
A.
Alzet Pump Flow Moderator
Brain Infusion Cannula
Removable Tab
Alzet Osmotic Pump
Catheter Tube
Depth-Adjustment Spacers
B.
0.8mm
0.5 mm
Bregma
Ventricle
2.5mm
Bregma -0.5

Figure 19 - Implantation of Alzet osmotic pumps for direct intraventricular drug delivery. **A.** Representation of the Alzet osmotic pump and brain infusion kit assembly (source: Alzet pump). **B.** Stereotaxic coordinates used for the placement of the cannula from the brain infusion kit, which is directed to the lateral ventricle, allowing the drug to reach the whole brain through the CSF flow (adapted from DeVos et al., 2013).

3.2.9. Behavioral assessment

Nesting test. To assess intrinsic nesting behavior, the mice were single-housed with one nestlet per cage (Deacon, 2012; Deacon, 2006), and monitored 2, 6 and 24 hours after the introduction of the new nestlet. The percentage of nesting was assessed at each time point $(\%\, nesting = 100 - \left(\frac{final\ weight}{initial\ weight}\right) \times 100)$, and nest-building scores defined based on the following criteria (figure 20):

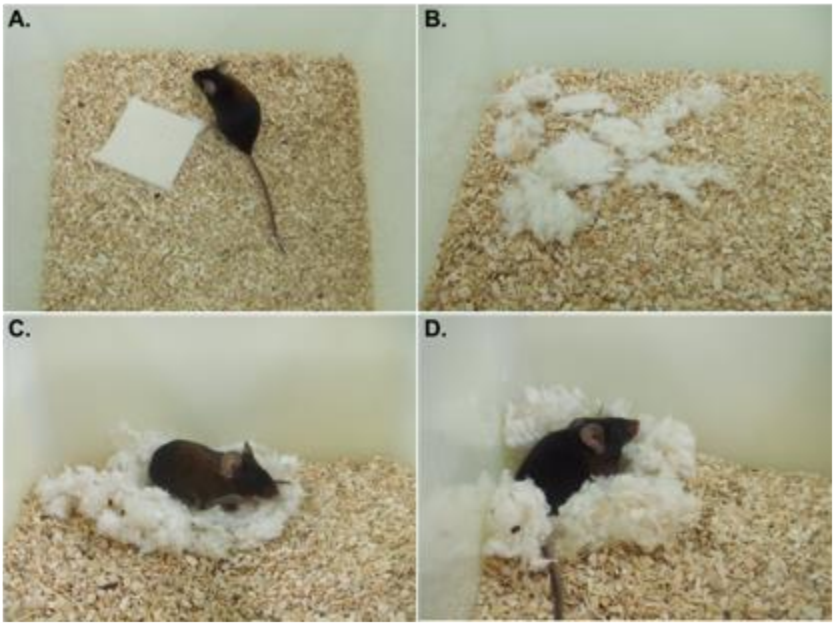

Figure 20 - Nesting test. Representation of different nesting scores, from the completely untouched nestlet (A; score 0), to the highest level of nestlet shredding with a perfect nest shape (D; score 7). Adapted from Deacon R., 2012.

- 0, nestlet untouched
- 1, less than 10% of the nestlet was shredded
- 2, 10-50% of the nestlet was shredded but there was no shape in the nest
- 3, 10-50% of the nestlet was shredded and there was shape in the nest
- 4, 50-90% of the nestlet was shredded but there was no shape in the nest
- 5, 50-90% of the nestlet was shredded and there was shape in the nest
- 6, >90% of the nest was shredded, but the nest was flat
- 7, >90% of the nest was shredded, and the walls of thenest were at least as tall as the mouse on more than 50% of its sides.

Burrowing test. Mice were single-housed and a plastic downpipe (68mm diameter; 20cm long) with one open and one closed end was placed in the cage, as previously described (Deacon, 2012; Deacon, 2009). The tube was filled with 200g of the food pellets normally supplied as diet. Machine screws were used to elevate the open end of the tube 3 cm off the floor to prevent accidental displacement of the food pellets. The test started around 4pm, 2 hours before the dark period in the holding room. The final food pellets weight was measured next morning and the percentage of burrowing determined $(\%\ burrowing = 100 - (\frac{final\ weight}{initial\ weight}) \times 100)$ (figure 21).

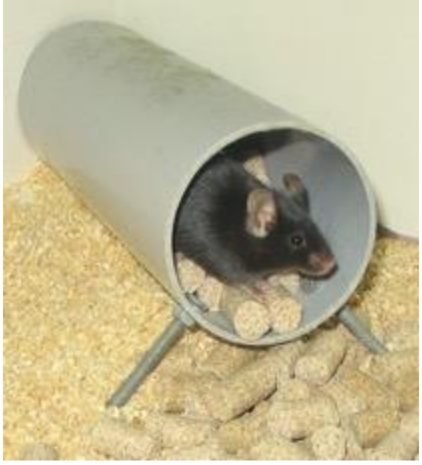

Figure 21 - A mouse in a burrowing tube.
The burrowing test is a sensitive method for detecting behavioral dysfunction in mice, as virtually all rodents display burrowing behavior. The protocol allows the quantitative measurement of burrowing in laboratory rodents, in an easy manner using an apparatus that can be placed in the home cage. The test is inexpensive to run and requires minimal experimenter training, still it is sensitive to a variety of treatments and/or cognitive deficits. Adapted from Deacon R., 2012.

Open field (OF) test. Mice were placed in the center of a 50 x 50 cm arena divided into 20 x 20 cm center, a 5 cm wall zone and a 10 cm border zone and allowed to freely explore the arena for 10 min while being tracked by a video system (EthoVision XT, Noldus Information Technology). The distance moved and the time spent in the center zone were analyzed.

Novel object recognition (NOR) test. Mice were tested in a square open field arena (50 x 50 cm) (Panlab, Spain) located in a room with dim lighting, as previously described (Dennissen et al., 2016). Briefly, the mice were habituated to the open field arena in the absence of the objects for 10min/day over two days. During the training period, the mice were placed in the open field with two identical objects for 10min. The retention test was performed 24h after the training (long-term memory) by placing the mice back in the open field for 5 min, but changing one of the familiar objects for a novel one. To record and analyze behavior the EthoVision XT video tracking system was used (Noldus Information Technology).

Y-maze test. The Y-maze behavioral test was used to assess hippocampal-dependent memory. The Y-maze used had the following dimensions: length 30 cm; width 6 cm; height 15 cm (Panlab, Spain). The test was divided in two parts, as described (Dennissen et al., 2016): the training session and the test session. During the training, one of the arms of the maze was closed (novel arm), and the mice were placed in the stem arm of the Y-maze (home arm), and allowed to explore this and the other available arm (old arm) for 10 min. After exploration, the mice were placed back in their home cage. Four hours later, the closed arm was opened, and the mice were placed in the stem arm of the Y-maze and allowed to freely explore all the arms for 5 min, to assess long-term memory. To record and analyze behavior the EthoVision XT video tracking system was used (Noldus Information Technology).

Morris Water Maze (MWM) test. The MWM test was conducted to assess spatial working memory, as previously described (Sydow et al., 2011; Sydow et al., 2016). Briefly, the test was performed as follows:

MWM pre-training: a 2 days pre-training protocol was conducted to familiarize the mice with swimming and climbing to a hidden platform (22ºC water temperature, 4 trials/day, maximum trial duration 60sec, 20min inter-trial interval). The pre-training was performed in a laboratory sink, and not in the apparatus used for the MWM (circular pool, diameter of 150 cm), to avoid any interference with the MWM learning. The pre-training platform (10 cm diameter) was placed 1 cm below the water surface.

MWM acquisition and probe trials: a 150 cm circular pool was filled with water opacified with nontoxic white paint (Biofa Primasol 3011, Germany) and kept at 22°C, as previously described (D’Hooge et al., 2005). In the middle of the target quadrant, a

15 cm round platform was hidden (1 cm beneath the water surface). The MWM room was equipped with visual cues to facilitate orientation. The pool was divided into four quadrants: target (T), right adjacent (R), opposite (O), and left adjacent (L). Each mouse performed 4 swimming trials per day (maximum duration 60 sec, 15-20 min inter-trial interval) for 5 consecutive days. Mice started the test from 4 symmetrical positions in a pseudo-randomized order across trials. When mice failed to find the submerged platform within 60 sec, they were guided to the platform, remaining there for 15 sec before returning to their cage. The escape latency, the distance traveled, and swimming speed were determined. On acquisition days 3, 4, 5, and 3 days after the end of the acquisition phase (day 8), a probe trial was conducted by removing the platform and recording the search pattern of the mice for 60s. The following learning trials 3–4 were carried out with the platform placed in the initial position on the target quadrant to avoid extinction. During acquisition and probe trials the EthoVision XT video tracking system was used (Noldus Information Technology).

3.2.10. Histological analysis

Immunohistochemistry was performed using paraffin brain sections. Briefly, mice were anesthetized (Isoflurane, Piramal Critical Care, Germany) and sacrificed by cervical dislocation. The brains were removed and fixed in histofix (Roth; 4 % PFA, pH 7.4 for 24 h) and dehydrated with ethanol and chloroform, followed by embedding in paraffin. Horizontal 5 µm thick paraffin brain sections were cut on a microtome (Microtome Slide 2003, Pfm Medical AG, Germany) and mounted onto superfrost plus adhesion microscope slides (Thermo Fisher Scientific). Sections were deparaffinized at 60ºC for 10 min and rehydrated by incubation with decreasing xylene and ethanol solutions finishing in ddH_2O. Next, antigen retrieval with citrate buffer at 80ºC for 30 min was performed, and sections were permeabilized with TBS-Triton X-100 0.1% 3x 10 min. Non-specific binding sites were blocked with 5% normal horse serum for 60 min at room temperature (RT) and slices were incubated with primary antibody in 1% blocking serum overnight at 4ºC. The following antibodies were used: HT7 (1:1000, Thermo Fisher Scientific), TauY9 (1:2000, Enzo Life Sciences), 12E8 (pS262/pS356, 1:2000, ELAN Pharmaceuticals), AT180 (pThr231/pSer235, 1:500, Thermo Fisher Scientific), AT8 (pSer202/pThr205, 1:500, Thermo Fisher Scientific), PHF-1 (pS396/pS404, 1:50, kind gift from Dr. P. Davies, Albert Einstein College of Medicine, NY), Iba1 (1:1000, Wako), GFAP (1:2000, Sigma-Aldrich). On the second day, slides were washed 3x 10 min with TBS 0.1% Triton X-100 and incubated in biotinylated secondary antibody for 60 min at RT. Slides were washed 3x 10 min in TBS 0.1% Triton X-100 and incubated with avidin-biotin-peroxidase complex (ABC) solution (Vectastain ABC kits, Vector Laboratories Inc.) in 10% blocking serum in TBS 0.1% Triton X-100 for 60 min at RT. Afterwards, sections were washed 3x 10 min in TBS 0.1% Triton X-100 and incubated in DAB solution (30 µL of DAB chromogen (reagent B) to 1 mL DAB substrate buffer (reagent A)) until staining was optimal as determined by light microscopic examination (reaction performed in the dark). The reaction was stopped in tap water and sections were dehydrated by incubation with increasing ethanol and xylene solutions and coverslips mounted with Roti®-Histokitt (Carl Roth, Germany).

3.2.11. Immunofluorescence

Mice were anesthetized (Isoflurane, Piramal Critical Care, Germany) and sacrificed by cervical dislocation. The brains were drop-fixed in 4% histofix (Roth; 4 % PFA, pH 7.4) for 3 days, cryoprotected in 30% sucrose in PBS with 0.02% sodium azide, frozen embedded in Shandon™ Cryomatrix™ embedding resin (Thermo Fisher Scientific, Germany), cut into 40 µm-thick horizontal sections, placed on 96 well-plates (filled with 0.02% sodium azide in 1X PBS solution) as free-floating sections and stored at 4ºC. Sections were washed with 1x PBS and incubated 2x 15 min in 50 mM ammonium chloride (NH_4Cl) to quench the free aldehyde groups resultant from the formaldehyde fixation. Sections were permeabilized with 1x PBS 0.5% Triton X-100 (2x 10 min) and blocked in 1x PBS + 0.2% BSA + 0.5% Triton X-100 + 0.5% FBS for 1.5 hours, followed by incubation with primary antibody in blocking buffer for 3 overnights at 4ºC with gentle agitation. The following antibodies were used: Tau Y9 (1:100, Enzo Life Sciences), MC1 (1:50, kind gift from Dr. P. Davies), PHF-1 (1:100, kind gift from Dr. P. Davies), Iba1 (1:100, WAKO), AT8 (1:100, Thermo Fisher Scientific), GFAP (1:250, Sigma-Aldrich), K9JA (1:500, DAKO). Afterwards, sections were washed 3x 10 min in 1x PBS and incubated with secondary antibodies overnight at 4ºC with gentle agitation. The following secondary antibodies were used: donkey Cy3 α-mouse (1:500), goat Cy3 α-rabbit (1:500), donkey Alexa 647 α-mouse (1:500), Donkey Alexa 647 α-rabbit (1:500). All secondary antibodies are from Dianova. Sections were washed 3x 10 min in 1x PBS, incubated 5min with Hoescht solution (Thermo Fisher Scientific, Germany) 1:10 000 in 1x PBS, washed 3x 10 min in 1x PBS and mounted onto glass slides using Fluoromount-G mounting medium (Southern Biotech, Germany) and coverslipped.

3.2.12. Microscopy

The DAB stained brain sections were observed on a BX43 light microscope (Olympus, Hamburg, Germany).

Brains sections used for immunofluorescence (AAV-injected) were visualized on an Olympus confocal microscope FV100 BX61 with a 10x, 20x, 40x and 60x objective, using lasers, beam splitters and filters according to the fluorophores. The laser power was used at 1.0% to avoid saturation of the dyes.

The AAV-injected brain sections were also observed on a LSM800 confocal microscope (Zeiss, Germany), which enables the creation of tile scans at 20x magnification. Tile scanning is useful for imaging large fields at high resolution, allowing us to image the whole brain slice or a region of interest, as the EC and hippocampus. A Z-stack of the images was taken and merged using the “maximum intensity projection” option in the Zeiss ZEN microscope software (blue edition).

3.2.13. Brain homogenization and protein quantification

After sacrificing the mice by cervical dislocation, some brains were kept for molecular analysis. Brains were collected immediately, and the following regions were dissected from both hemispheres (AAV-injected and PBS-injected) and stored at -80ºC: EC, hippocampus and cortex, which was subdivided into 2 pieces, one for western blot and the other for sarkosyl extraction. Lysis buffer was added to each Eppendorf containing the dissected brain tissues (300 µL for the EC, 600 µL to the hippocampus and cortex) and samples were sonicated 5 seconds (amplitude 40%) followed by another sonication of 3 seconds. Afterwards samples were kept in ice for 30 min, centrifuged 20 sec at 14 000 rpm (Eppendorf centrifuge 5415R) and the supernatant was collected. Protein concentration was estimated using 1 µL of the supernatant using a Bicinchoninic Acid Protein (BCA) assay kit (Sigma-Aldrich, Germany) and 40 µL Laemmli samples were prepared.

3.2.14. Sarkosyl extraction

A sarkosyl-insoluble tau fraction was isolated from brain tissue as previously described (Greenberg and Davies, 2006; Mocanu et al., 2008). Briefly, the brain tissue was weighed, homogenized in 3x volume of cold Buffer H (10mM Tris-HCl, 1mM EGTA, 0.8M NaCL, 10% sucrose, pH 7.4) and centrifuged at 26'000 rpm (Beckman CoulterTM Optima TM MAX-E) for 20 min at 4ºC. The supernatant was collected, and the resulting pellet was homogenized in buffer H and centrifuged at 26'000 rpm for 20 min at 4ºC. Both supernatants were combined, adjusted to 1% (w/v) N-lauroylsarcosine and incubated at 37ºC with shaking for 2h. After centrifugation at 61'000 rpm for 35 min at 20ºC, the supernatant was collected (sarkosyl-soluble fraction) and the pellet was resuspended in 500 µL of 1x TBS and centrifuged again at 61'000 rpm for 35 min at 20ºC, supernatant removed and pellet resuspended in 0.5 µL 1x TBS for each mg of original sample plus the same amount of 2x sample buffer and samples stored for SDS gel. Western blotting was used to analyze the supernatant (sarkosyl-soluble fraction) and the pellet (sarkosyl-insoluble fraction).

3.2.15. Western blotting

Homogenized brain tissues (EC, hippocampus and cortex), plus sarkosyl-soluble and -insoluble fractions were resolved in 10% SDS-PAGE gels, followed by semi-dry transfer to PVDF membranes. Primary antibody incubation was performed overnight at 4ºC in TBS-T (Tris-buffered saline, 0.1% Tween 20) plus 5% nonfat dry milk. The following primary antibodies were used: 12E8 (1:2000, ELAN Pharmaceuticals), PHF-1 (1:1000, kind gift from Dr. P. Davies), K9JA (1:20 000, DAKO), CD11b (1:1000, Abcam), PSD95 (1:1000, Cell signaling), Synaptophysin (1:5000, Sigma-Aldrich), GFAP (1:2000, Sigma-Aldrich), CD68 (1:1000, Thermo Fisher Scientific), GluR1 (1:1000, Merck). After washing the membranes 3x in TBS-T, the membranes were incubated with secondary antibodies for 2h at RT (anti-mouse 1:2000,or anti-rabbit 1:2000, DAKO). Antibody affinity was detected by chemiluminescence (Amersham ECL Prime Western Blotting Detection Reagent, GE Healthcare, Germany). Protein bands were visualized using Image Quant LAS 4000 mini (GE Healthcare Life Sciences, Germany), and band intensities were analyzed using Image Studio Lite 5.2 software (LI-COR Biosciences). Actin (1:10 000, Sigma-Aldrich, Germany) was used as loading control.

3.2.16. Statistical analysis

For western blotting, the mean density and area of each band were measured using at least three independent experiments in Image Studio Lite 5.2 software (LI-COR

Biosciences, Germany). The statistical analysis was completed using Graph Pad (Prism) version 7.05 software. All values are given as mean ± SEM. To compare the experimental groups a one-way or two-way ANOVA was performed, with uncorrected Fisher's LSD or Tukey's post-hoc test for multiple comparisons to evaluate statistical significance. Differences were considered statistically significant when $p < 0.05$.

For behavioral assessment, statistical comparisons between groups were accomplished by one-way or two-way ANOVA followed by post-hoc uncorrected Fisher's LSD or Tukey's multiple comparison tests. All data are presented as group mean values ± SEM. The accepted level of significance was $p < 0.05$. Statistical comparisons and graphs were performed using Graph Pad (Prism) version 7.05 software. * $p < 0.05$, ** $p < 0.01$, *** $p < 0.001$, **** $p < 0.0001$.

4

RESULTS

4. Results

4.1. Propagation of tau pathology in mice expressing tau under the neuropsin promoter

In AD, the onset and propagation of tau pathology throughout the brain follows a very well defined and predictable pattern, described by the Braak stages (Braak and Braak, 1991). Despite the scientific efforts over the last years to identify the mechanisms that underlie this pathological process, there are still several open questions in the field. In the present thesis, using well-characterized mouse models of AD, we aim to clarify the underpinnings of the onset and propagation of tau pathology. With this knowledge, we hope to develop promising therapeutic strategies, which may in the future have an impact in patients' lives.

4.1.1. Transgenic mice expressing pro- and anti-aggregant human tau under the neuropsin promoter

The trans-synaptic spreading of tau pathology was analyzed using bigenic mouse models with tau expression restricted to the EC (termed "neuropsin mice" for short in this thesis). The mice express full length htau40-ΔK280 (pro-aggregant) or htau40-ΔK280-2P (anti-aggregant) under the neuropsin promoter, restricting the expression to the EC (figure 22A). The region-specific expression of mutated htau mimics the initial steps of AD pathology, as described in the Braak stages.

Expression of human tau ΔK280 and ΔK280-2P is restricted to the entorhinal cortex

The restricted expression of both pro-aggregant (htau40-ΔK280) and anti-aggregant (htau40-ΔK280-2P) mutant tau can be monitored using different biochemical and imaging techniques. In this study, we combined a bidirectional promoter with the tau and firefly luciferase transgenes (Eckermann et al., 2007). Luciferase BLI was analyzed in fresh *ex-vivo* 500 µm thick brain slices (obtained at 6 months of age and kept alive in slice culture media containing 0.15 mg/ml D-luciferin). As shown in figure 22B, slices from both pro- and anti-aggregant neuropsin mice presented strong luciferase signals in the entorhinal region, demonstrating that luciferase expression, and consequently htau, are restricted to the EC. Slices from WT mice did not present luciferase BLI activity and, therefore, no htau expression. To differentiate transgenic from non-transgenic animals, luciferase BLI imaging *in vivo* was performed after i.p. injection of D-luciferin (150 mg/kg). Figure 22C demonstrates the presence of luciferase BLI signal in both pro- and anti-aggregant mice, reflecting positive htau expression, which is absent in WT mice.

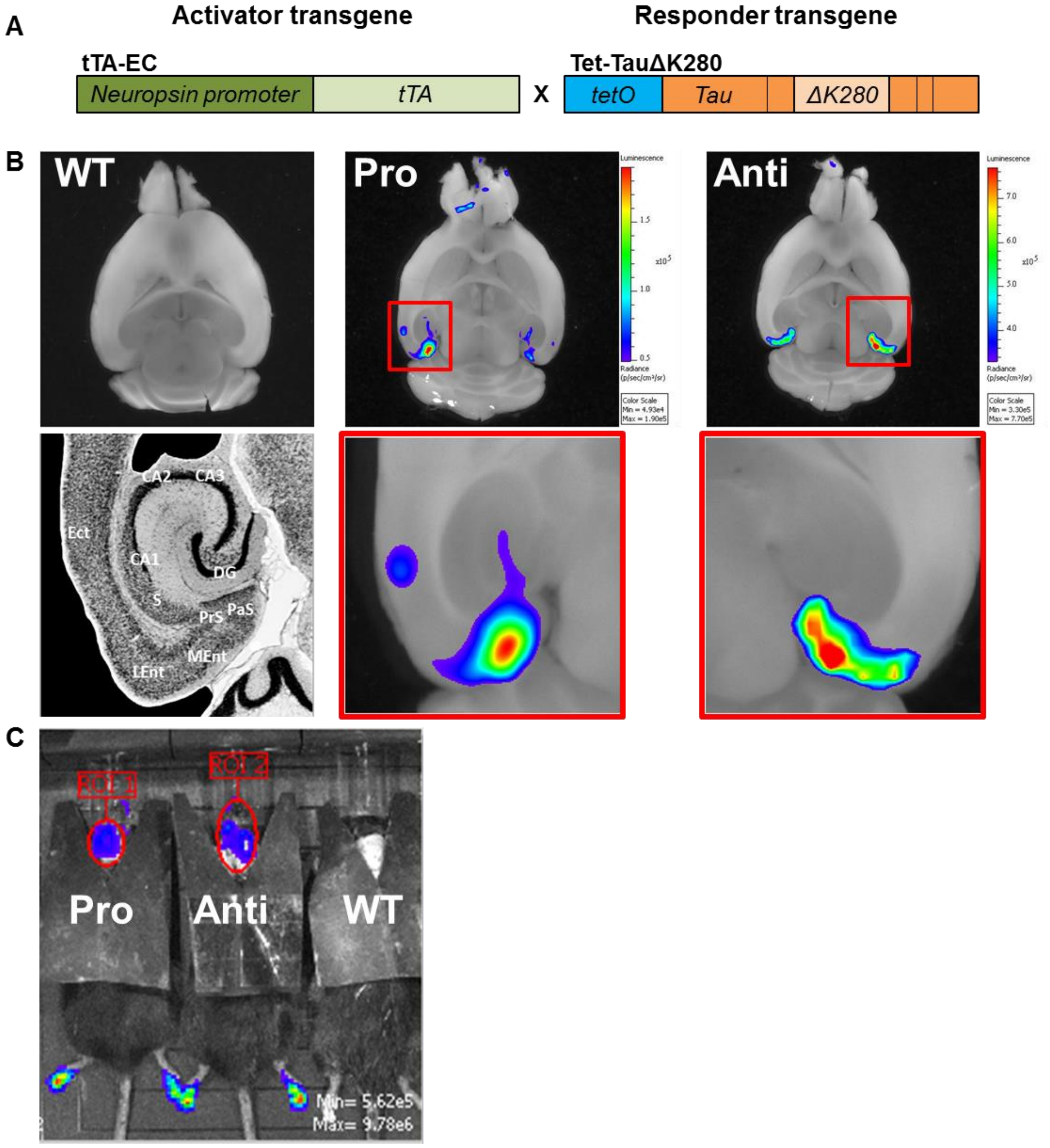
A
Activator transgene
Responder transgene
tTA-EC
Neuropsin promoter
tTA
X
Tet-TauΔK280
tetO
Tau
ΔK280
B
WT
Pro
Anti
Luminescence
Radiance (p/sec/cm²/sr)
Color Scale Min = 4.93e4 Max = 1.90e5
Color Scale Min = 3.30e5 Max = 7.70e5
CA2
CA3
Ect
CA1
DG
S
PrS
PaS
MEnt
LEnt
C
ROI 1
ROI 2
Pro
Anti
WT
Min= 5.62e5
Max= 9.78e6

Figure 22 – Expression of mutant human tau-ΔK280 and tau-ΔK280-2P is restricted to the entorhinal cortex.
A. tTA-EC transgenic mice express htau-ΔK280 or htau-ΔK280-2P under a tetO promoter and the tTA under the neuropsin promoter. **B.** BLI analysis of fresh *ex vivo* brain tissue to characterize the spatial distribution of tau transgene expression in 500 µm brain slices (obtained at 6 months of age and kept alive in slice culture media containing 0.15 mg/ml D-luciferin). Slices from pro- and anti-aggregant mice displayed BLI activity restricted to the EC, correlating with transgene expression. WT slices did not present luciferase BLI. **C.** Analysis of transgene expression *in vivo* after i.p. injection of D-luciferin (150

mg/kg) showed luciferase BLI in pro- and anti-aggregant neuropsin mice, but absence of luciferase activity (and consequently htau) in WT mice.

Impact of human tau-ΔK280 and tau-ΔK280-2P expression on the body weight

The body weight (BW) of the mice, an important biometrical parameter, was analyzed weekly. The BW provides information about the animals' welfare, which could potentially influence the experimental results and the extent or course of tau pathology to be developed. We observed no significant differences in the BW of the three experimental groups at 5 months of age (figure 23A) and at 18 months of age (figure 23B).

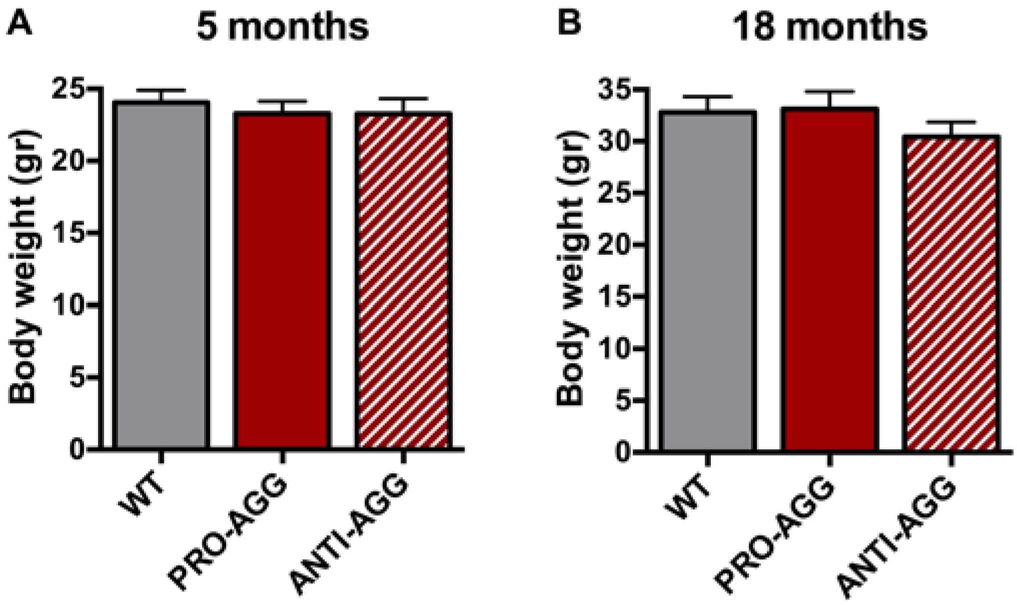

Figure 23 - Body weight of gender-mixed WT, pro- and anti-aggregant tau transgenic mice. **A.** No significant differences were observed on the BW of WT, pro- and anti-aggregant mice at 5 months of age (one-way ANOVA [F(2, 45) = 0.2334, p = 0.7928]). **B.** Likewise, at 18 months of age we observed no differences in the BW of the three experimental groups, suggesting that the expression of both pro-aggregant and anti-aggregant htau has no impact on the BW of the mice (one-way ANOVA [F(2, 40) = 0.9633, p = 0.3903]). All numerical data are shown as mean +/- SEM.

4.1.2. Absence of trans-synaptic spreading in neuropsin pro- and anti-aggregant mice up to 24 months of age

To investigate if tau aggregation is a pre-requisite for the propagation of tau pathology, and whether there is a difference in the spreading behavior of pro- and anti-aggregant tau species, we analyzed the expression of mutant htau in neuropsin mice over time. Since the hippocampus forms a unidirectional network with input from the EC, it is expected that, over time, tau propagates from the EC (where it is initially restricted) to anatomically connected regions, including the DG, CA1 and CA3. To establish a temporal pattern for the propagation of tau protein and tau pathology, we performed IHC with an htau specific antibody (HT7) and observed the expression of mutated htau in pro- and anti-aggregant mice at different ages. We observed that mutant htau, either pro-aggregant (figure 24, middle panel) or anti-aggregant (figure 24, right panel), was expressed in the EC neurons up to the axon terminals in the middle molecular layer of the DG, via the perforant pathway, at 3, 6 and 12 months of age. No htau was detected in WT mice (figure 24, left panel).

As the propagation of tau pathology in the brain is a slow process, and our mouse model expresses low levels of mutant htau, we hypothesized that perhaps the time windows previously analyzed were not enough for the trans-synaptic spreading of tau to occur. Therefore, we performed the htau specific staining in older animals, at 24 months of age. Similar to the earlier time points, pro- and anti-aggregant htau was only expressed in the EC neurons traversing the perforant pathway (figure 25, middle and lower panel, respectively). We did not observe trans-synaptic propagation of htau protein to the next level of neurons at 24 months of age in pro- or anti-aggregant mice. This means that no htau+ cells were observed in the granule cell layer of the DG or pyramidal cell layer of CA1 or CA3.

Since the level of mutant htau in the neuropsin mice used in the study is low compared to the endogenous mouse tau (approximately 20%; figure 26), we hypothesized that increasing the expression levels of mutant htau in the EC of the neuropsin mice would produce an accelerated model for the propagation of tau protein and tau pathology. This led to the second part of the study, where we performed stereotaxic injections of AAV in the neuropsin mice to increase the expression levels of mutant htau. Nonetheless, before performing the injections, we aimed to characterize tau pathology in the neuropsin non-injected mice. For this purpose, we analyzed the presence of tau phosphorylation and pathological conformation in the neuropsin mice.

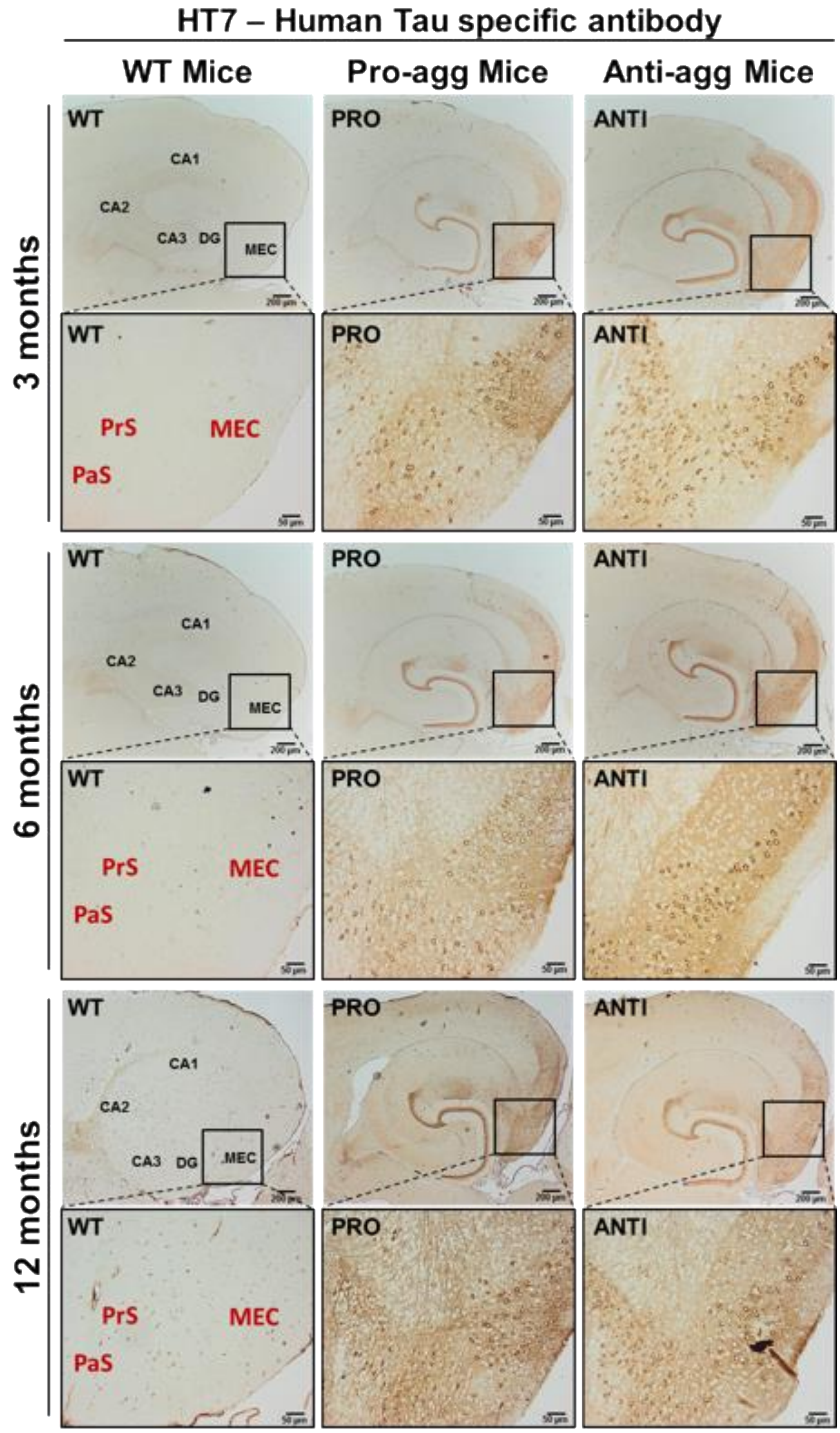
HT7 – Human Tau specific antibody
WT Mice
Pro-agg Mice
Anti-agg Mice
3 months
6 months
12 months
WT
PRO
ANTI
CA1
CA2
CA3
DG
MEC
PrS
PaS
200 µm
50 µm

Figure 24 - Expression of mutant human tau in the neuropsin mice at different ages.
Staining with HT7 antibody, specific for htau, demonstrated that in both pro- and anti-aggregant mice the expression of mutated htau is located in the EC and perforant pathway up to the axon terminal ends in the middle molecular layer of DG. These observations were consistent at 3, 6 and 12 months of age. As observed in the left panel, htau was absent in non-transgenic WT mice. MEC – medial entorhinal cortex; PaS – parasubiculum; PrS – presubiculum. Scale bar: 200 µm (upper figures); 50 µm (lower figures).

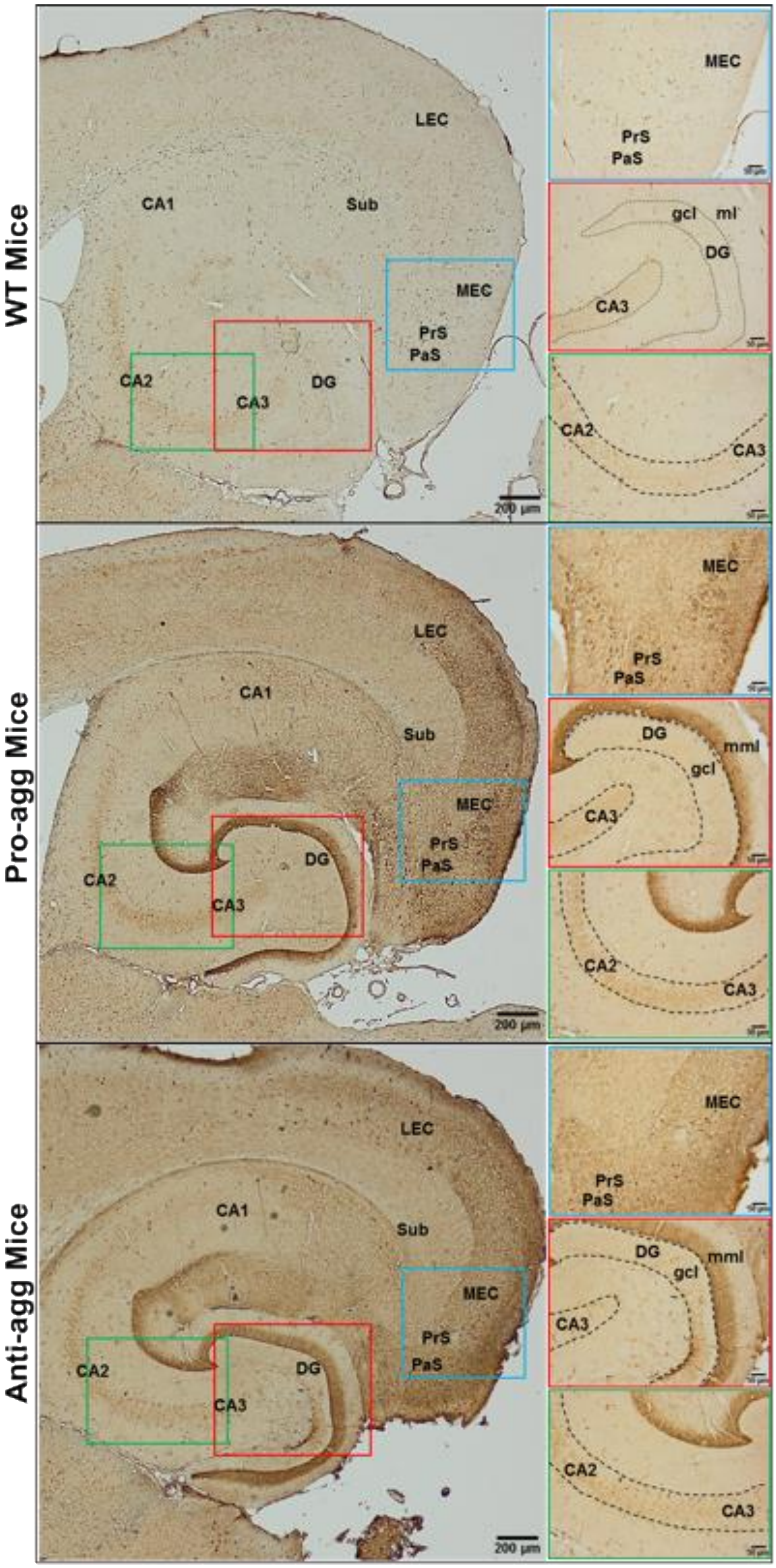
WT Mice
LEC
CA1
Sub
MEC
PrS
PaS
CA2
CA3
DG
200 µm
MEC
PrS
PaS
gcl
ml
DG
CA3
CA2
CA3
Pro-agg Mice
LEC
CA1
Sub
MEC
PrS
PaS
DG
CA2
CA3
200 µm
MEC
PrS
PaS
DG
mml
gcl
CA3
CA2
CA3
Anti-agg Mice
LEC
CA1
Sub
MEC
PrS
PaS
CA2
DG
CA3
200 µm
MEC
PrS
PaS
DG
mml
gcl
CA3
CA2
CA3

Figure 25 - Expression of mutant human tau in the neuropsin mice at 24 months of age. Staining with HT7, a specific htau antibody, showed that in both pro- and anti-aggregant mice (middle and lower panel, respectively) the expression of htau is restricted to the EC neurons and perforant pathway axons up to the middle molecular layer of the DG. No trans-synaptic spreading of tau protein to DG granule cells was observed, even at later stages (24 months), as we did not detect HT7+ cells in other brain regions distinct from the EC and perforant pathway. WT mice (upper panel) did not express htau. Scale bar: 200 µm (left figures); 50 µm (right figures).

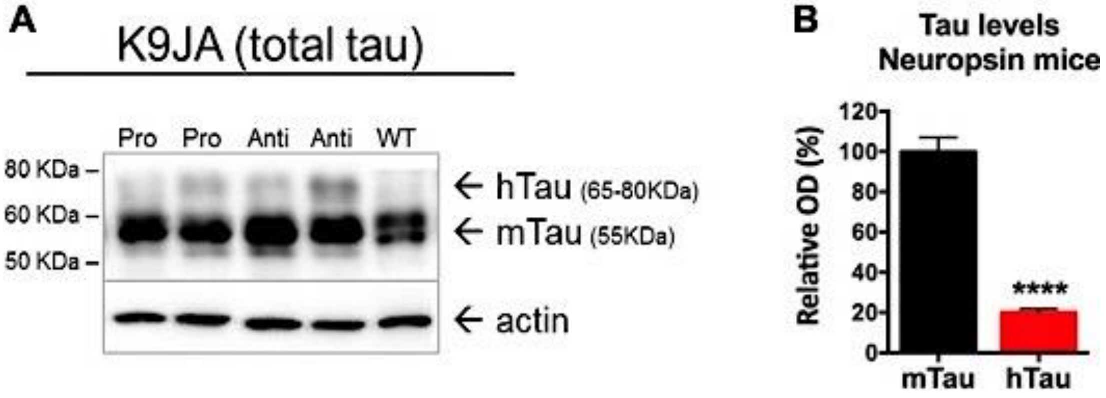

Figure 26 - Total tau levels in the entorhinal cortex of neuropsin pro- and anti-aggregant mice. **A.** WB analysis with K9JA, an antibody for total tau, showed that 12 month old pro- and anti-aggregant mice express low levels of htau compared to the endogenous mouse tau. **B.** Quantification of the levels of endogenous mtau and htau in the neuropsin mice showed that htau levels correspond to approximately 20% the levels of mtau ($p < 0.0001$). All numerical data are shown as mean +/- SEM; **** $p < 0.0001$.

4.1.3. Tau phosphorylation is increased in pro-aggregant mice compared to anti-aggregant mice

Several tau phosphorylation sites have been implicated in AD pathological mechanisms (Neddens et al., 2018). Two different phosphorylation sites were analyzed in the neuropsin mice: tau phospho Ser262/Ser356 (targets of the kinase MARK; antibody 12E8) and tau phospho Thr231/Ser235 (targets of protein kinases GSK3β or cdk5; antibody AT180). WB analysis of the EC fractions of pro- and anti-aggregant mice with the 12E8 antibody (figure 27) showed that anti-aggregant mice present lower phosphorylation of tau compared to pro-aggregant mice (approximately 35-40% lower).

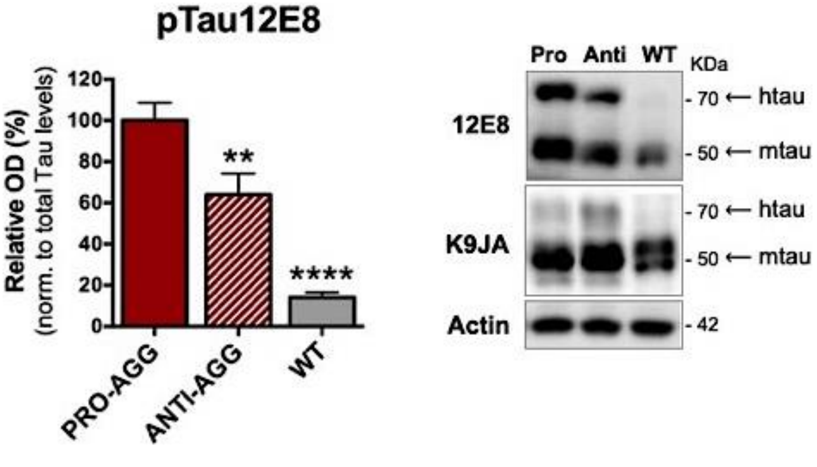

Figure 27 - Phosphorylation of tau on the Ser262/Ser356 epitope is more pronounced in the pro-aggregant mice compared to anti-aggregant mice.
WB analysis of the EC fractions of 12 month-old mice revealed that the levels of 12E8, normalized to total mtau levels, are significantly reduced in the anti-aggregant ($p = 0.0021$) and WT mice ($p < 0.0001$)

compared to the pro-aggregant mice. All numerical data are shown as mean +/- SEM; * denotes the significance compared to 100% (phospho-tau levels in pro-aggregant mice). ** $p < 0.01$; **** $p < 0.0001$.

In agreement, staining with the 12E8 antibody showed that, although 12E8 positive cells were observed in the EC of both pro- and anti-aggregant mice at all time points, tau phosphorylation was less pronounced in the anti-aggregant mice (figure 28).

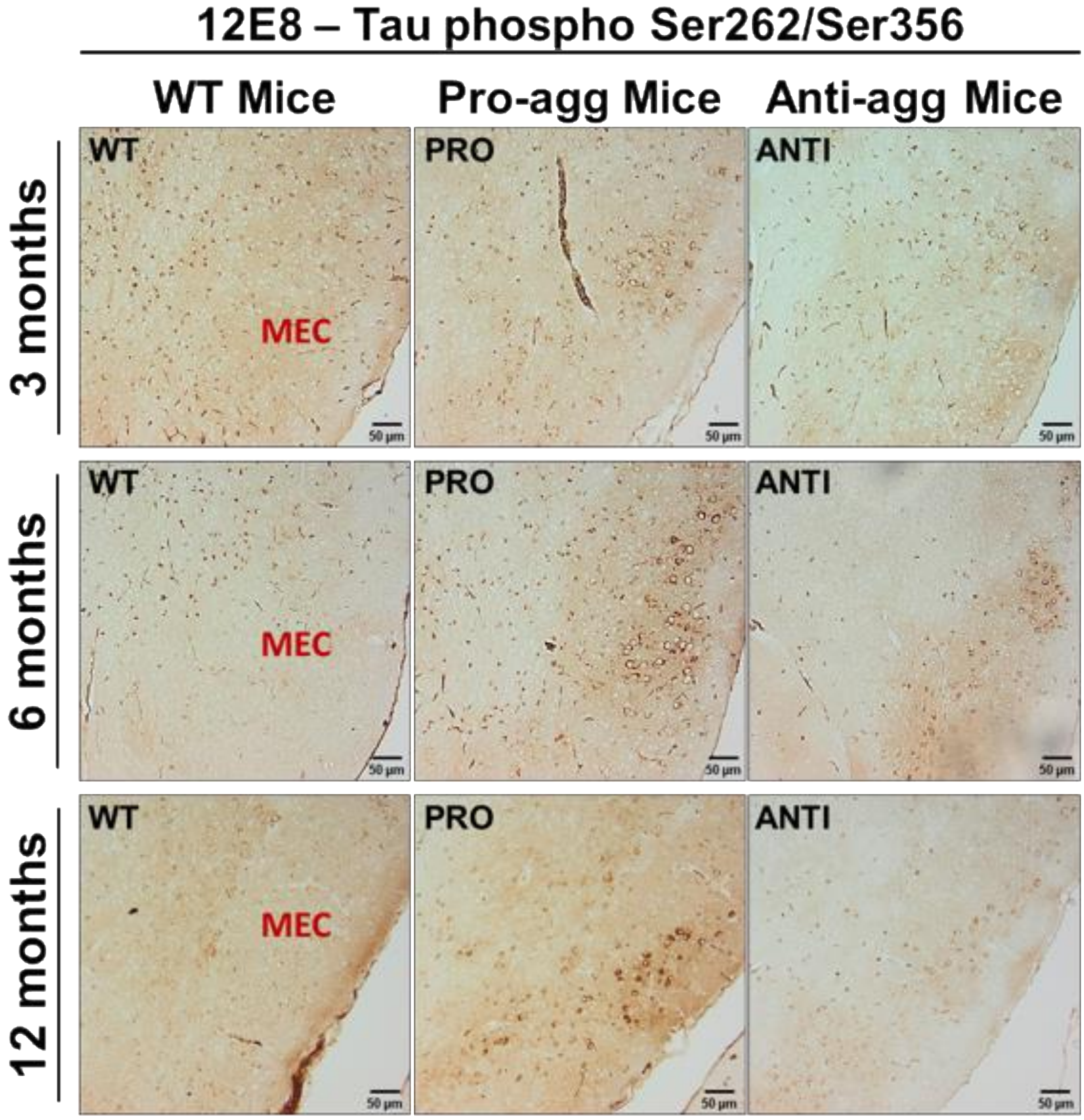
12E8 – Tau phospho Ser262/Ser356
WT Mice
Pro-agg Mice
Anti-agg Mice
3 months
6 months
12 months
WT
PRO
ANTI
MEC
50 µm

Figure 28 - Tau phosphorylation at Ser262/Ser356 in pro-aggregant, anti-aggregant and wild-type mice at different ages.
Tau phosphorylation at Ser262/Ser356, detected with 12E8 antibody, was observed in the MEC of pro-aggregant mice (middle panel) and anti-aggregant mice (right panel) at all time points analyzed (3, 6 and 12 months). Tau phosphorylation at Ser262/Ser356 was more pronounced in the pro-aggregant mice compared to anti-aggregant mice. WT mice did not present any significant pathological phosphorylation of tau (left panel). Scale bar: 50 μm.

Similarly, staining with AT180 antibody showed that both pro- and anti-aggregant mice present tau phosphorylation at Thr231/Ser235 epitope, but this is less pronounced in the animals expressing anti-aggregant htau (figure 29). WT mice present almost no tau phosphorylation on both epitopes (figures 28 and 29, right panel).

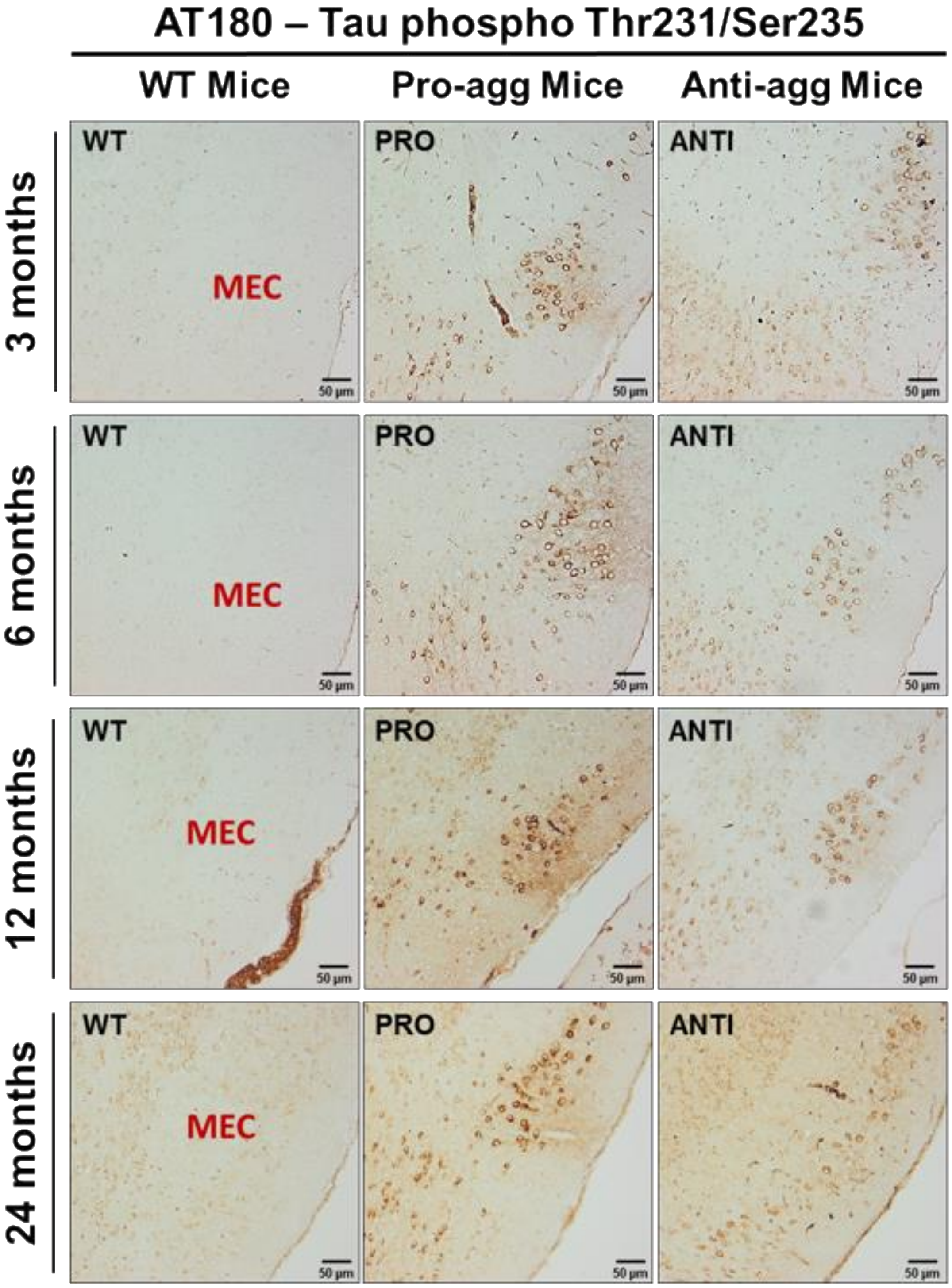
AT180 – Tau phospho Thr231/Ser235
WT Mice
Pro-agg Mice
Anti-agg Mice
3 months
6 months
12 months
24 months
WT
PRO
ANTI
MEC
50 µm

Figure 29 - Tau phosphorylation at Thr231/Ser235 in pro-aggregant, anti-aggregant and wild-type mice at different ages.
Tau phosphorylation at Thr231/Ser235, detected with AT180 antibody, was observed in the MEC of pro-aggregant mice (middle panel) and anti-aggregant mice (right panel) at all time points analyzed (3,

6, 12 and 24 months). Tau phosphorylation at Ser262/Ser356 was more pronounced in the pro-aggregant mice compared to anti-aggregant mice. WT mice did not present any significant pathological phosphorylation of tau in this brain region up to 24 months of age (left panel). Scale bar: 50 μm.

4.1.4. Only pro-aggregant mice present pathological conformation of tau, which is restricted to the EC

Conformational alterations on tau protein occur early in AD and are involved in the pathological mechanisms underlying the disease (Grüning et al., 2014; Kadavath et al., 2015). MC1 and Alz50 are the only antibodies currently existing that target a disease-specific conformational modification of tau (Vitale et al., 2018). In this study we used the MC1 antibody to evaluate the presence of tau with pathological conformation in our experimental mouse models. Pathological conformation of tau was observed in pro-aggregant mice (figure 30, middle panel), but not in anti-aggregant mice (figure 30, right panel). Furthermore, the expression of tau with pathological conformation was restricted to the EC and perforant pathway, as no trans-synaptic spreading of tau with pathological conformation was observed. This correlated with the distribution of htau (detected with HT7 antibody) over time. The pattern of expression of tau with pathological conformation was similar between all points analyzed (3, 6 and 12 months of age). WT non-transgenic mice did not present tau with pathological conformation (figure 30, left panel).

As the formation and propagation of pathological tau species is a slow process occurring in the brain, we analyzed the expression of MC1 in the neuropsin mice at 24 months of age to determine if pathological tau needs a longer time to propagate from the EC to another cell layer. However, we did not observe trans-synaptic spreading of pathological tau in the aged mice, as no MC1+ cells were observed in the granule cell layer of the DG or any other brain region outside the EC and perforant pathway (figure 31).

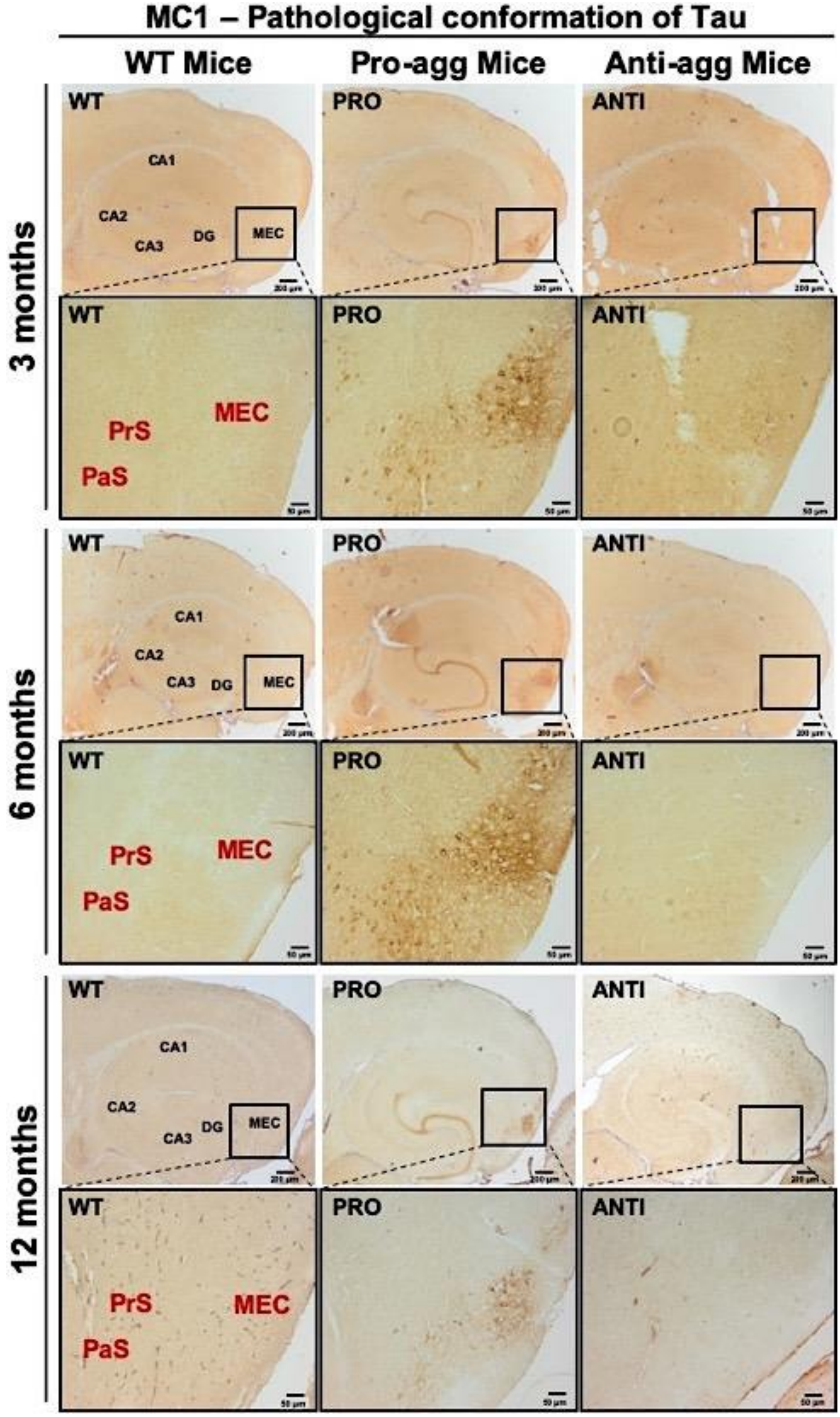
MC1 – Pathological conformation of Tau
WT Mice
Pro-agg Mice
Anti-agg Mice
3 months
6 months
12 months
WT
PRO
ANTI
CA1
CA2
CA3
DG
MEC
PrS
PaS
200 µm
50 µm

Figure 30 - Expression of tau with pathological conformation over time.
Pathological conformation of tau, detected by MC1 antibody, was observed in the EC and perforant pathway of pro-aggregant mice (middle panel), but absent in anti-aggregant mice (right panel) at all time points analyzed (3, 6 and 12 months of age). WT non-transgenic mice also did not express tau with pathological conformation at the time points analyzed (left panel). Scale bar: 200 µm (upper figures); 50 µm (lower figures).

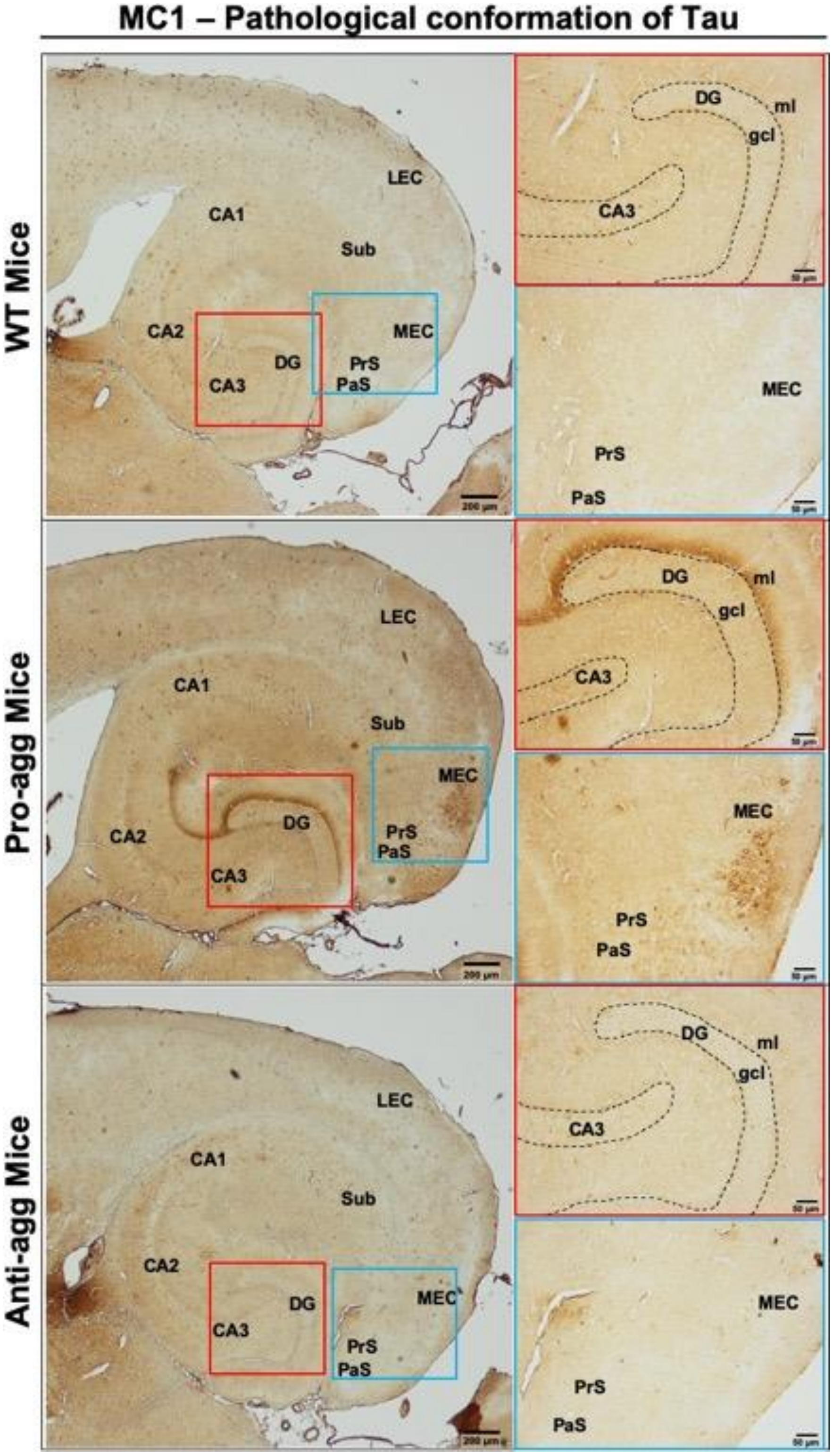
MC1 – Pathological conformation of Tau
WT Mice
LEC
CA1
Sub
CA2
MEC
DG
PrS
CA3
PaS
200 µm
DG
ml
gcl
CA3
50 µm
MEC
PrS
PaS
50 µm
Pro-agg Mice
LEC
CA1
Sub
MEC
DG
CA2
PrS
PaS
CA3
200 µm
DG
ml
gcl
CA3
50 µm
MEC
PrS
PaS
50 µm
Anti-agg Mice
LEC
CA1
Sub
CA2
DG
MEC
CA3
PrS
PaS
200 µm
DG
ml
gcl
CA3
50 µm
MEC
PrS
PaS
50 µm

Figure 31 - Expression of tau with pathological conformation in the neuropsin mice at 24 months of age.
Staining with MC1 antibody in brain slices from 24 month old mice showed that only pro-aggregant mice present tau with pathological conformation. Furthermore, MC1 expression was restricted to the EC and perforant pathway up to the axon terminal ends in the middle molecular layer of the DG (middle panel). These results are in agreement with the observations made at previous time points, confirming that tau pathology, even in aged mice, is restricted to the EC and perforant pathway and does not propagate to other cell layers. Anti-aggregant mice (lower panel), as well as WT non-transgenic mice (upper panel), did not express tau with pathological conformation. Scale bar: 200 µm (left figures); 50 µm (right figures).

4.1.5. Inflammatory processes are not altered in pro- or anti-aggregant mice compared to WT non-transgenic mice

As tau pathology has been linked to chronic neuroinflammatory processes, and reactive microglia and astrocytes have been observed in tauopathies (Gerhard et al., 2004; Ishizawa et al., 2004; Vogels et al., 2019), we analyzed the expression of inflammatory markers in the neuropsin mice over time. To monitor the expression of astrocytes in pro- and anti-aggregant mice we used an antibody specific for the glial fibrillary acidic protein (GFAP), an astrocyte-specific intermediate filament protein. As seen in figure 32, there were no significant alterations in GFAP expression in pro- and anti-aggregant mice compared to the WT control animals in the DG at 3 and 6 months of age.

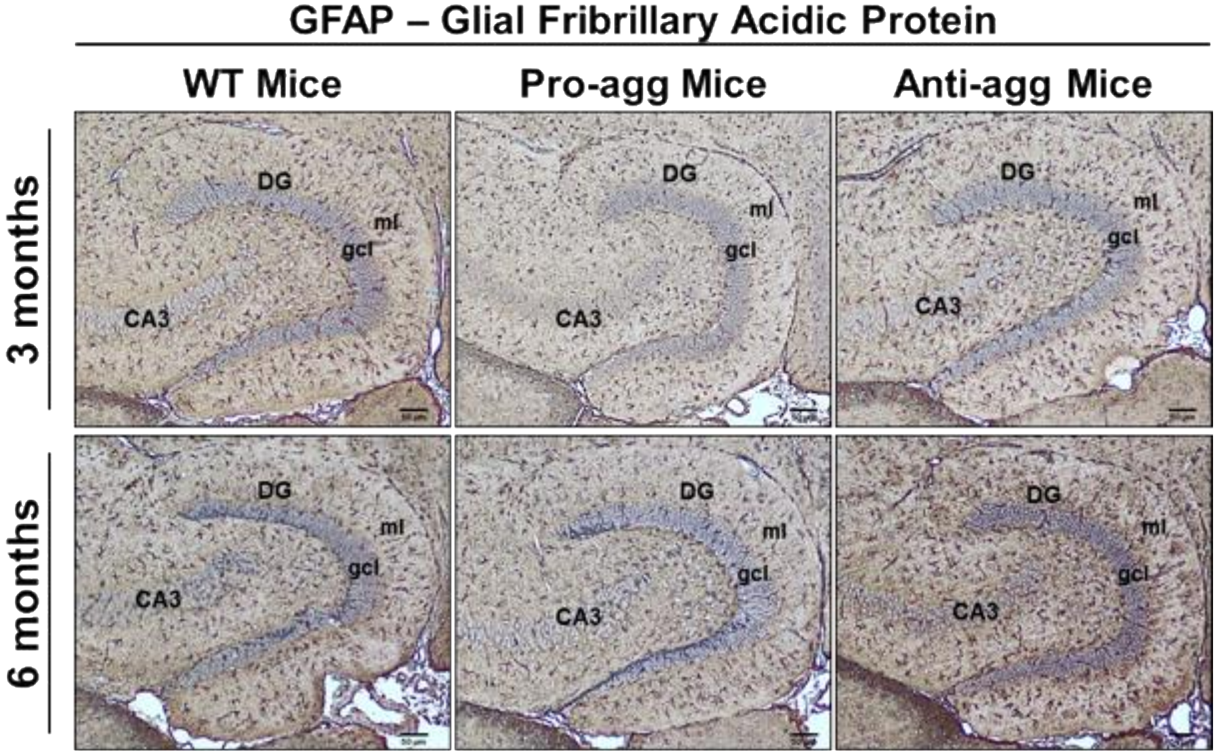

Figure 32 - No significant alterations in astrogliosis observed in the dentate gyrus of pro- and anti-aggregant mice compared to wild-type mice.
Staining with GFAP antibody showed that pro-aggregant mice (middle panel) and anti-aggregant mice (right panel) present no differences in astrogliosis in the DG compared to WT mice (left panel) at 3 and 6 months of age. Scale bar: 50 μm.

Considering its significant putative role in the onset and propagation of tau pathology, we also analyzed the expression of microglia in pro- and anti-aggregant mice. Using the Iba1 antibody, specific for the calcium binding adaptor molecule 1, we detected no differences in microglia levels in the DG of pro- and anti-aggregant mice compared to the WT controls at 3 and 6 months of age (figure 33). To further confirm our results, and extend them to older age, we analyzed the expression of inflammatory markers at 24 months of age in the EC and DG. Similar to the previous time points, no differences were observed in the expression of astrocytes or microglia in the DG of pro- and anti-aggregant mice compared to the WT non-transgenic mice (figure 34A). As the EC is the primary region for the onset of tau pathology and considering the involvement of inflammatory markers on this process, especially microglia, we also monitored the expression of GFAP and Iba1 in the EC of 24 months old mice. No differences in the expression of astrocytes or microglia were detected in the EC region of WT, pro- and anti-aggregant mice (figure 34B). Altogether, these data showed that inflammatory processes present no alterations in the DG and EC of pro- or anti-aggregant mice.

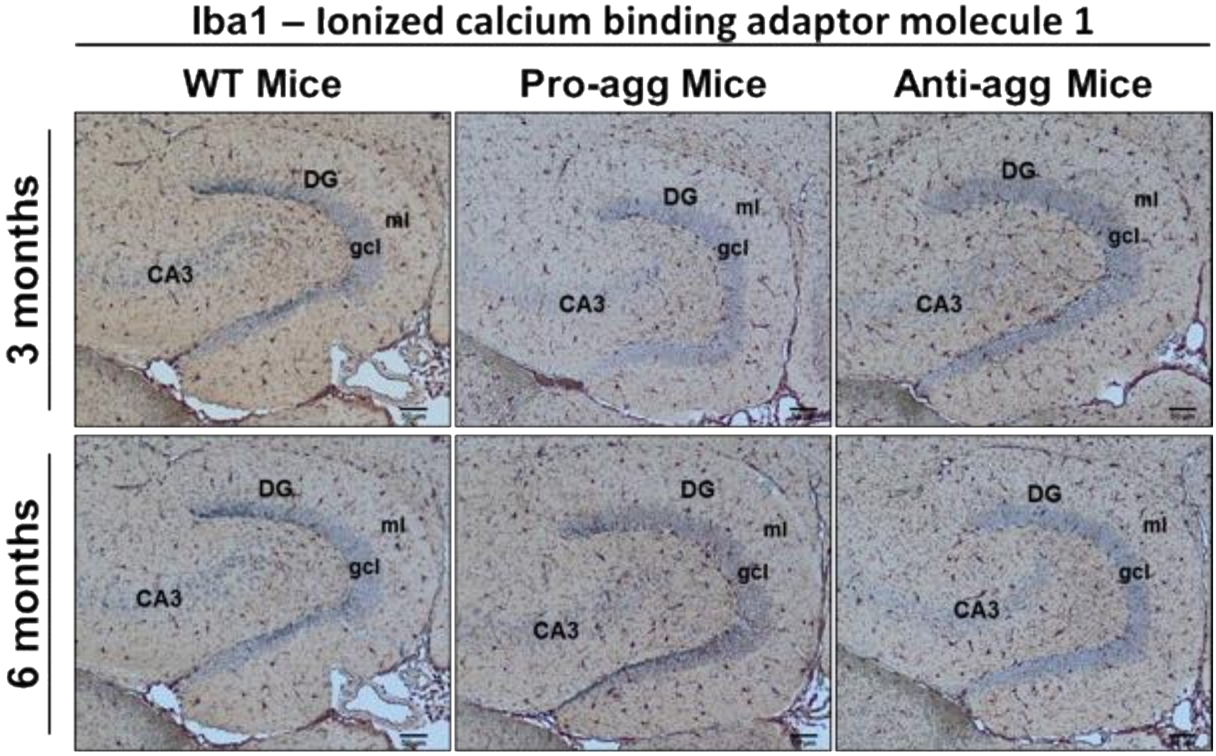

Figure 33 - No significant alterations in microglia expression observed in the dentate gyrus of pro- and anti-aggregant mice compared to wild-type mice.
Staining with Iba1 antibody demonstrated that pro-aggregant mice (middle panel) and anti-aggregant mice (right panel) do not present significant alterations in the expression of microglia in the DG compared to WT mice (left panel) at 3 and 6 months of age. Scale bar: 50 μm.

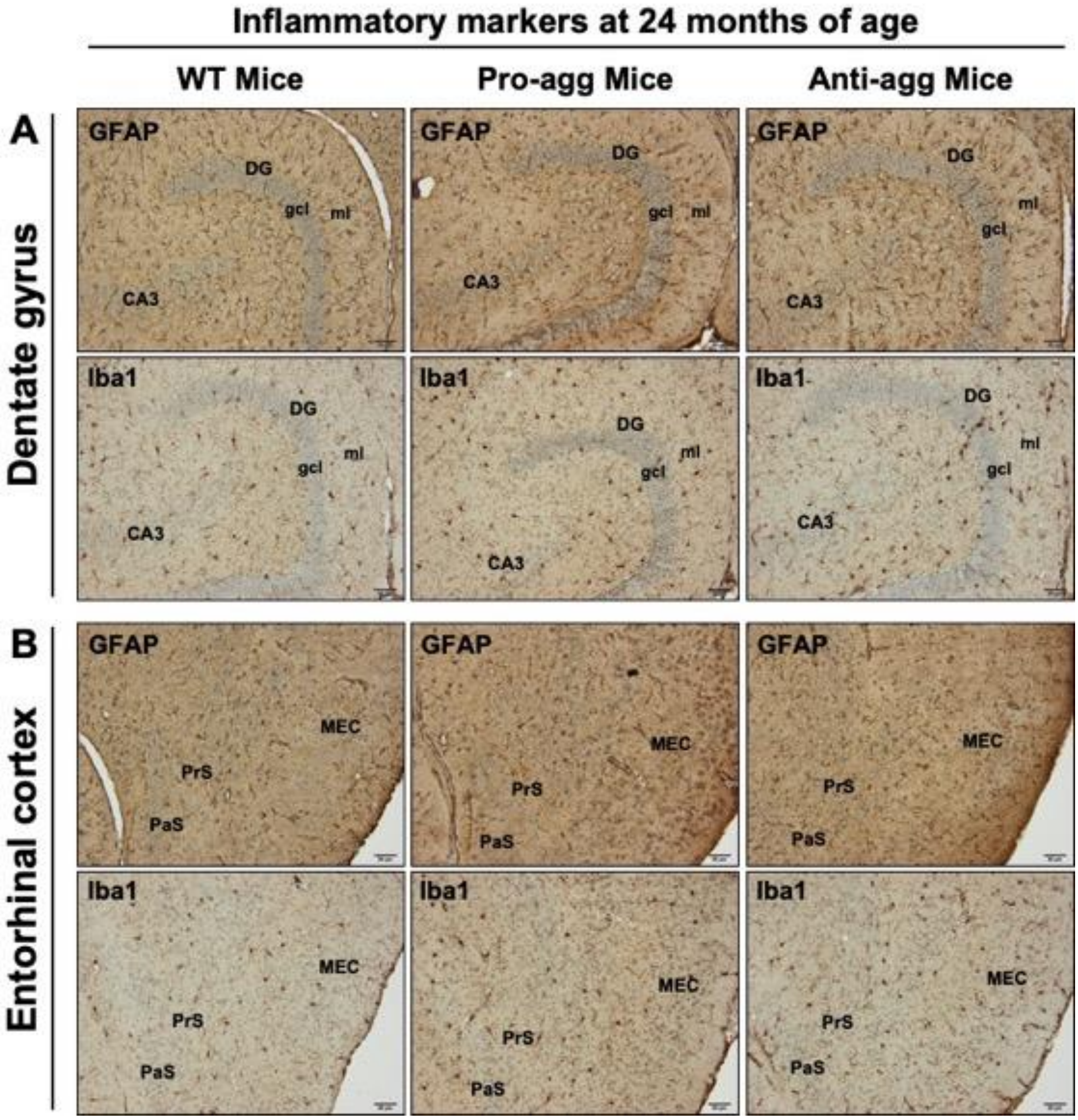
Inflammatory markers at 24 months of age
WT Mice
Pro-agg Mice
Anti-agg Mice
A
Dentate gyrus
GFAP
DG
gcl
ml
CA3
Iba1
B
Entorhinal cortex
MEC
PrS
PaS

Figure 34 - No significant alterations in neuroinflammation markers in the DG and EC of neuropsin mice at 24 months of age.
A. Astrogliosis (GFAP) and microglia (Iba1) were not significantly altered in the DG of pro-aggregant mice (middle panel) or anti-aggregant mice (right panel), compared to WT non-transgenic controls (left panel). **B.** A similar pattern was observed in the EC, with no significant alterations in the GFAP or Iba1 levels in pro-aggregant (middle panel) or anti-aggregant (right panel) mice, compared to controls (right panel). Scale bar: 50 μm.

4.2. Propagation of tau pathology in AAV-injected mice

As no trans-synaptic propagation of tau protein and tau pathology was observed in the neuropsin mice expressing htau in the EC, we aimed to create an accelerated model for the spreading of tau. To achieve this, we injected neuropsin mice in the EC with AAV encoding the same tau mutants that these animals already expressed to increase the expression levels of htau. Therefore, we performed stereotaxic injections of AAV encoding pro-aggregant htau (pAAV-CBA-eGFP-2A-htau40-ΔK280; **AAV-K2**) or anti-aggregant htau (pAAV-CBA-eGFP-2A-htau40-ΔK280-2P; **AAV-K3**) into the EC of 5 months old neuropsin mice (stereotaxic coordinates: AP = -4.7 mm, ML = ±3.6 mm, DV = -3.0 mm). The contralateral hemisphere was injected with PBS as control (figure 35A). Furthermore, WT and tau-KO (TKO) mice were also injected with AAV encoding pro- and anti-aggregant htau. To monitor the propagation of GFP alone, a group of WT mice was injected with AAV-eGFP in the EC. Therefore, the project comprised the following 7 experimental groups (figure 35B): tTA-EC/K2 mice injected with AAV-K2; tTA-EC/K3 mice injected with AAV-K3, WT mice injected with AAV-K2, AAV-K3 or AAV-eGFP; TKO mice injected with AAV-K2 or AAV-K3. At 3 months of age the luciferase BLI was measured in the neuropsin mice, and stereotaxic injections were performed at 5 months of age. Sacrifice and tissue collection were performed at 4 different time points p. i.: 3, 6, 12 and 18 months (figure 35C).

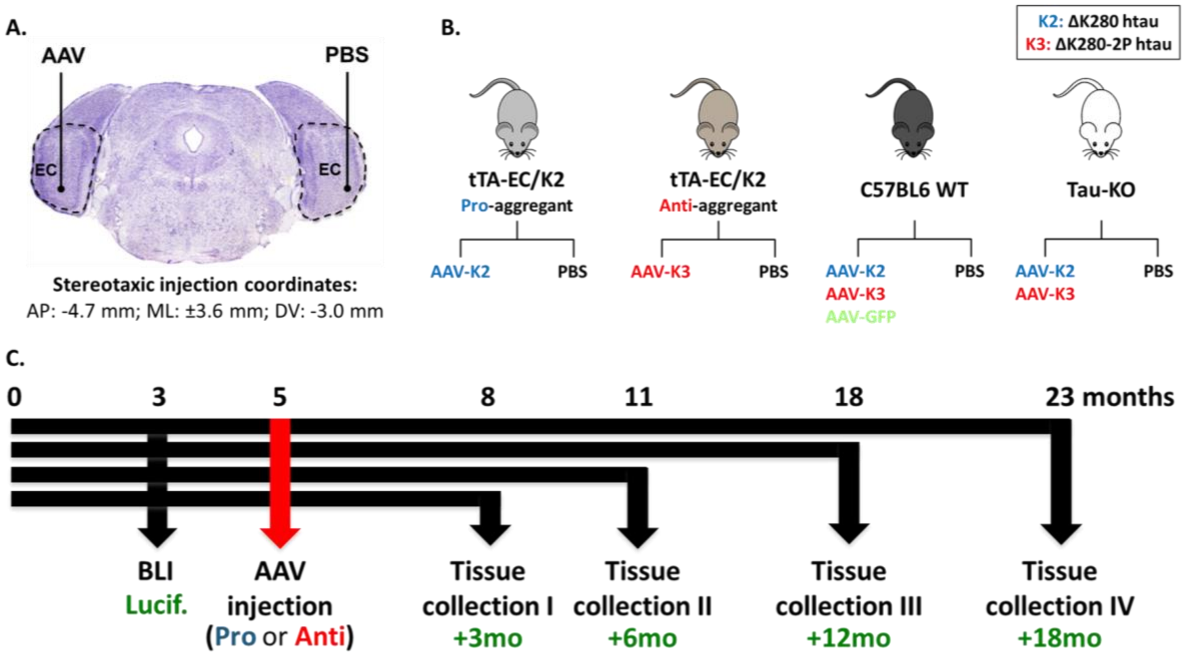
A.
AAV
PBS
EC
EC
Stereotaxic injection coordinates:
AP: -4.7 mm; ML: ±3.6 mm; DV: -3.0 mm
B.
K2: ΔK280 htau
K3: ΔK280-2P htau
tTA-EC/K2
Pro-aggregant
tTA-EC/K2
Anti-aggregant
C57BL6 WT
Tau-KO
AAV-K2
PBS
AAV-K3
PBS
AAV-K2
AAV-K3
AAV-GFP
PBS
AAV-K2
AAV-K3
PBS
C.
0
3
5
8
11
18
23 months
BLI
Lucif.
AAV
injection
(Pro or Anti)
Tissue
collection I
+3mo
Tissue
collection II
+6mo
Tissue
collection III
+12mo
Tissue
collection IV
+18mo

Figure 35 - Experimental design of the project.
A. Representation of the AAV and PBS injection sites in a mouse brain slice, with the description of the stereotaxic coordinates used (AP: -4.7 mm, ML: ±3.6 mm (from Bregma) and DV: -3.0 mm (from the *dura mater*)). **B.** tTA-EC/K2 mice were unilaterally injected with AAV-K2 and tTA-EC/K3 mice were injected with AAV-K3. WT and TKO mice were injected with AAV-K2 or AAV-K3, and a small group of WT mice was injected with AAV-GFP. The contralateral hemisphere of every animal was injected with PBS in the EC as control. **C.** Experimental design; BLI was measured at 3 months of age and stereotaxic injections performed at 5 months of age. Tissue collection was performed at three different time points: 3, 6, 12 and 18 months p. i. (8, 11, 18 and 23 months of age, respectively).

4.2.1. Body weight of all experimental groups

We monitored the BW of the experimental animals weekly from the date of surgery until sacrifice, to obtain insight on the animals' welfare. The BW at 5 months of age (before AAV injection) was similar between all groups (figure 36). However, at 18 months p. i. the BW of WT animals injected with AAV-K2 (pro-aggregant htau) was lower than the BW of WT mice injected with AAV-K3 (anti-aggregant htau). Although not significant, the BW of pro-aggregant mice was also lower than the BW of anti-aggregant mice. This suggests that pro-aggregant htau may play a detrimental effect in the mice. Furthermore, a significant difference between WT and TKO mice injected with AAV-K2 was observed, with the later presenting an increased BW compared to WT mice. This suggests that the absence of endogenous mouse tau may be protective against the detrimental effects of pro-aggregant mutant htau. In addition, in the TKO mice no differences were observed between the group injected with AAV-K2 and the group injected with AAV-K3.

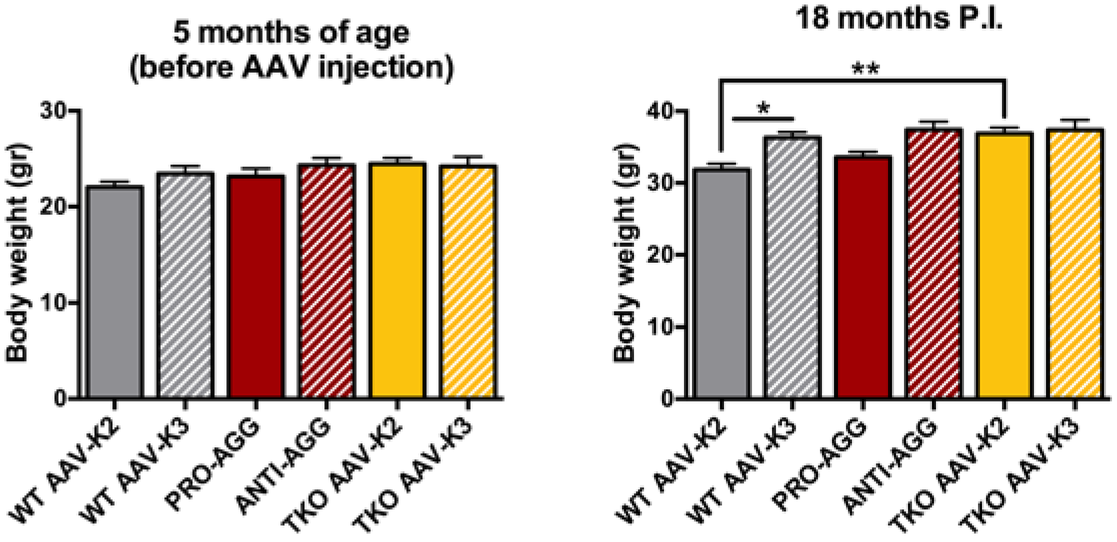

Figure 36 - Body weight in all experimental groups at 5 months of age (before AAV injection) and at 18 months post-injection.
The six distinct experimental groups presented similar BW values at 5 months of age (before AAV injection), allowing us to exclude the possibility of initial differences that could impact the progression of pathology and/or BW over time. On the other hand, at 18 months p. i. the BW of WT mice injected with AAV-K2 was lower than the BW of WT mice injected with AAV-K3 (one-way ANOVA, $p = 0.0157$), suggesting a potential detrimental effect of pro-aggregant htau. A similar tendency was observed in pro- and anti-aggregant mice. Although not significant, pro-aggregant mice presented lower BW compared to anti-aggregant mice. On the other hand, TKO mice injected with AAV-K2 presented a higher BW compared to WT AAV-K2 (one-way ANOVA; $p = 0.0040$), suggesting that the absence of endogenous mouse tau may be protective against the deleterious effects of pro-aggregant htau. Injection of AAV-K2 or AAV-K3 in TKO mice did not affect the BW between both groups. All numerical data are shown as mean +/- SEM. * $p < 0.05$; ** $p < 0.01$.

4.2.2. Tau protein can spread across cells independently of the aggregation propensity

The pattern of expression of htau was analyzed in the brains of AAV-injected mice and compared to the levels of htau in the non-injected neuropsin pro- and anti-aggregant mice. We expected that, by increasing the levels of mutant htau, we would be able to induce an accelerated model of the spreading of tau protein/pathology. The first step was to confirm that, in fact, the AAV injection increased the level of htau in the EC of the neuropsin mice, by comparing the level of htau between AAV-injected neuropsin mice with the contralateral hemisphere injected with PBS. Figure 37A shows that the AAV-injected hemisphere of both pro- or anti-aggregant mice presented a higher level of htau compared to the PBS-injected hemisphere of a neuropsin mouse at 3 months after injection. Quantification of the levels of htau and mtau (figure 37B) showed that in neuropsin (Nop) non-injected mice (or injected with PBS) the level of htau was approximately 20% the level of endogenous mtau, in agreement with the results shown before in figure 26. Injection of these mice with AAV (Nop + AAV) led to a significant increase in the levels of htau to approximately 65% the level of mtau. In WT mice injected with AAV the level of htau was approximately 40% the levels of endogenous mtau, a value lower than in the neuropsin-injected mice, as expected, because these mice already expressed htau under the neuropsin promoter.

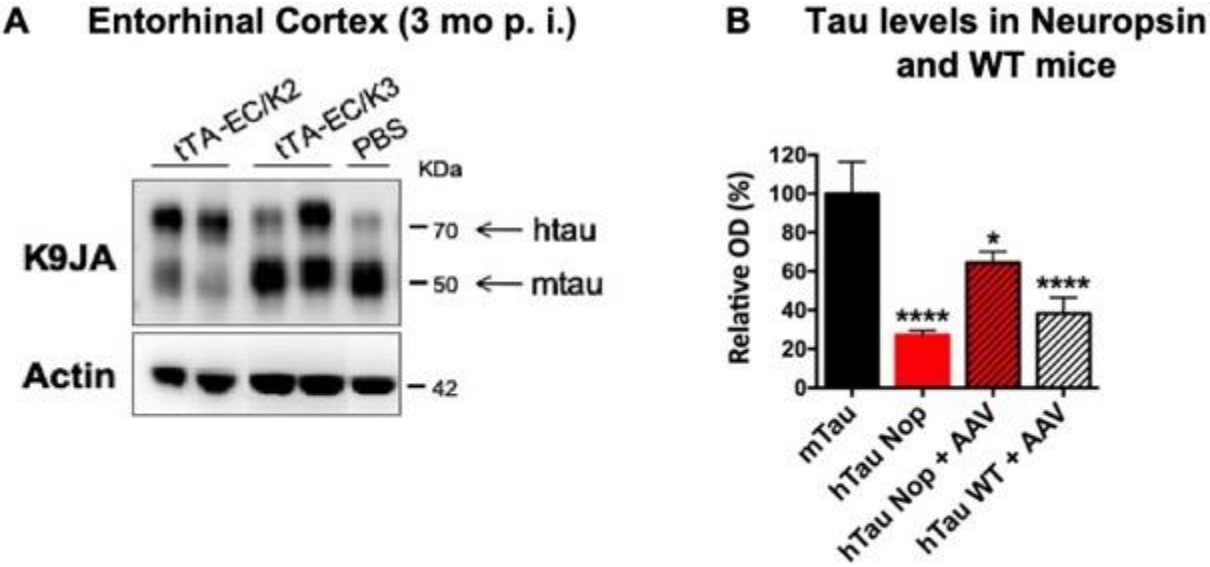

Figure 37 - Total tau levels in non-injected mice and mice injected with AAV-K2 and AAV-K3. **A.** At 3 months p. i., WB analysis of K9JA, an antibody specific for total tau, showed that both tTA-EC/K2 and tTA-EC/K3 mice injected with AAV-K2 and AAV-K3, respectively, presented higher levels of htau compared to the PBS-injected tTA-EC/K2 mouse. **B.** Quantification of the levels of mtau and htau showed that neuropsin (Nop) mice without AAV injection (or injected with PBS) express approximately 20% of htau compared to the endogenous mtau, as previously described ($p < 0.0001$). Neuropsin mice injected with AAV (Nop + AAV) present higher levels of htau compared to the non-injected neuropsin mice (approximately 65% the endogenous mtau; $p < 0.05$). The levels of htau in WT mice injected with AAV are approximately 40% of the endogenous mtau ($p < 0.0001$). One-way ANOVA with uncorrected Fisher's LSD test for multiple comparison. All numerical data are shown as mean +/- SEM; * denotes the significance of the htau levels compared to the endogenous mtau; * $p < 0.05$; **** $p < 0.0001$.

The next step was to observe if the increase in the levels of htau resulting from the AAV injection translates into an increase in the spreading of tau protein and/or tau pathology. Importantly, the AAV constructs used in this study also encode green fluorescent protein (GFP) to facilitate the visualization of transfected cells. Therefore, the cells initially transfected with AAV in the EC are htau$_{+}$/GFP$_{+}$, and named “donor cells”, as they express htau that may be transferred to other cells. Similarly to previous experimental settings (Wegmann et al., 2015), we analyzed the presence of htau$_{+}$/GFP$_{-}$ cells, named tau “recipient cells”. These cells express htau but not GFP, meaning that they were not initially transfected with AAV (hence GFP$_{-}$), but received the htau from the initial donor cells (hence htau$_{+}$). In figure 38A, we observed tau “recipient cells” in the granule cell layer of the DG of 3 month old pro-aggregant mice (arrowheads). Similarly, in figure 38B, we also detected htau$_{+}$/GFP$_{-}$ cells in the granule cell layer of the DG of 3 months old anti-aggregant mice (arrowheads). This indicates that tau protein spreads across cells independently of its aggregation potential, as we observed trans-synaptic spreading of both pro- and anti-aggregant htau.

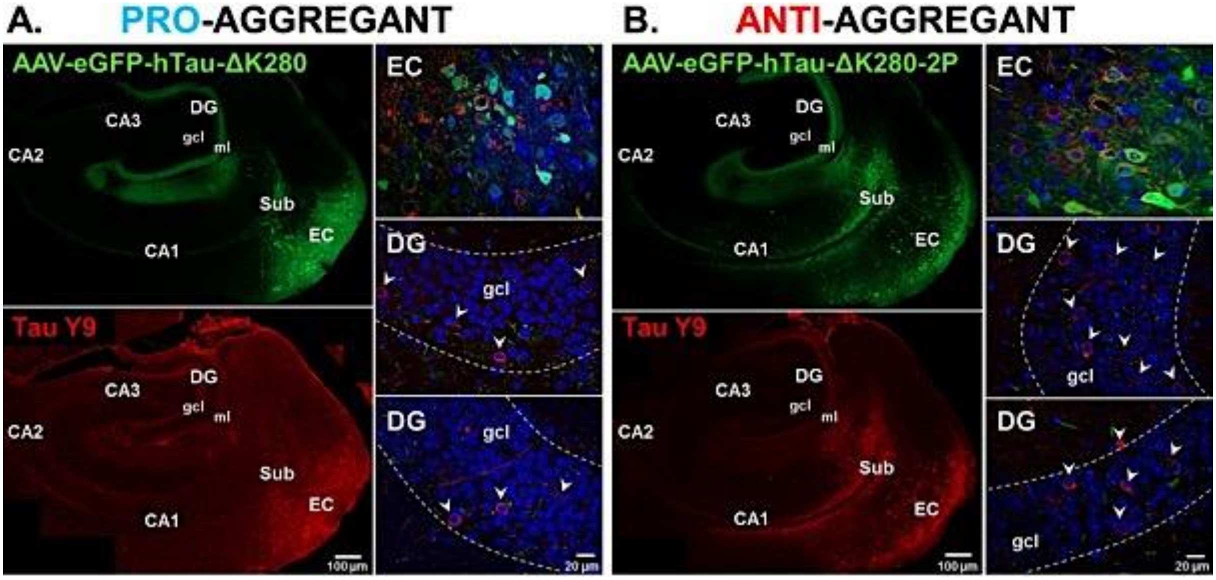

Figure 38 - Trans-synaptic spreading of tau protein in pro- and anti-aggregant neuropsin mice 3 months after AAV injection.
A. Using an htau specific antibody (Tau Y9) we observed cells in the DG of pro-aggregant mice injected with AAV-K2 that express htau, but no GFP (tau “recipient cells”) (arrowheads). **B.** Similarly, we observed tau “recipient cells” (htau+/GFP-) in anti-aggregant mice injected with AAV-K3, showing that the propagation of tau protein is independent of the protein’s aggregation potential. Arrowheads indicate tau recipient cells (htau+/GFP-), which received the htau from tau donor cells (htau+/GFP+) located in the EC region. Scale bar: 100 µm (overview figures); 20 µm (higher magnification figures).

Afterwards, we analyzed the spreading of htau protein in the WT mice injected with AAV-K2 and AAV-K3. These animals, similar to the neuropsin mice, express pro- or anti-aggregant htau in the EC region after injection. Nevertheless, the level of htau is approximately 25% lower than in the injected neuropsin mice (as shown in figure 37), because they lack the protein expressed via the neuropsin promoter. As observed previously in the neuropsin mice, we also detected htau$_{+}$/GFP$_{-}$ cells in the granule cell layer of the DG in WT mice injected with AAV-K2 (figure 39A) and AAV-K3 (figure 39B). The same was observed in the CA1 and CA3 subregions of the hippocampus. This confirms that tau spreads across cells independently of its aggregation potential. Some of the htau+ cells observed were also GFP+ cells, for reasons to discuss later in the present dissertation.

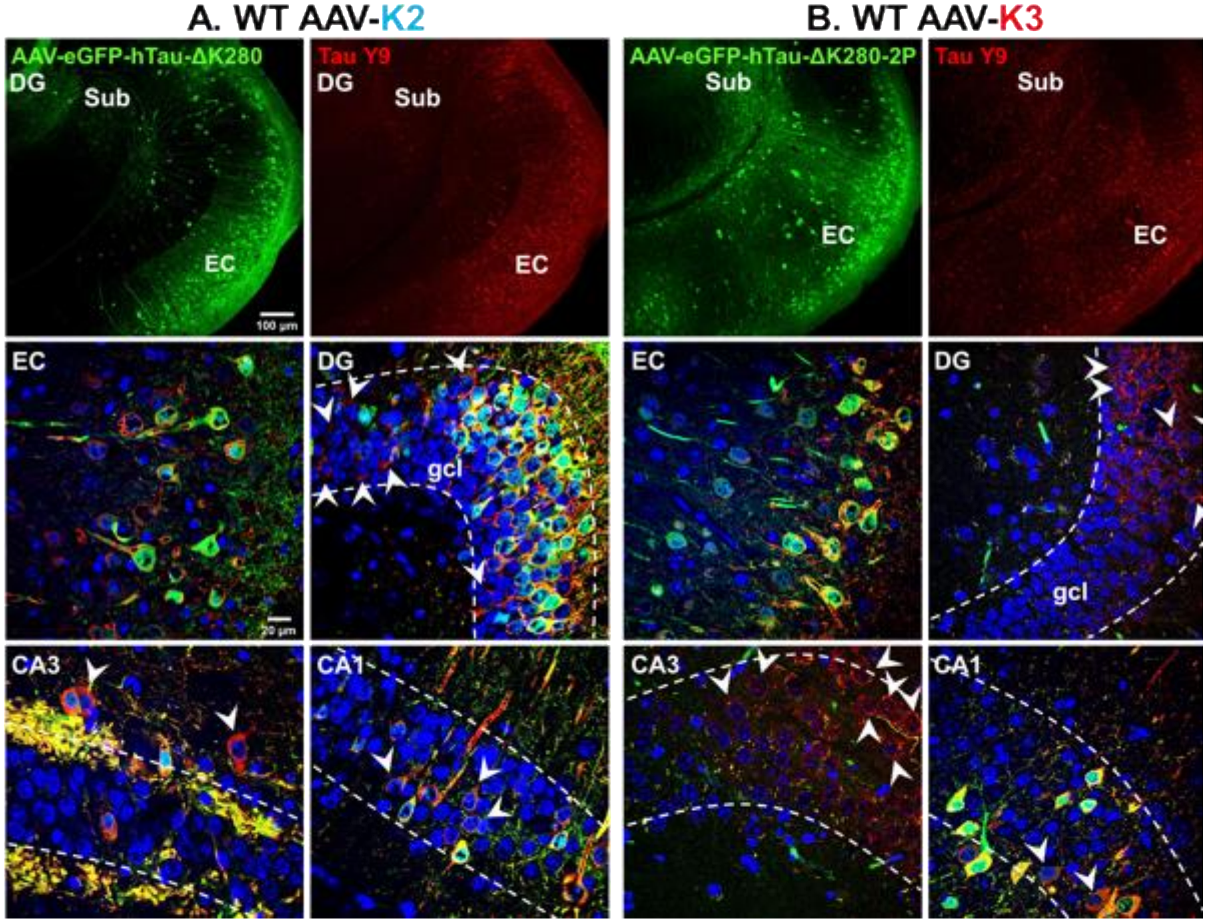

Figure 39 - Trans-synaptic spreading of tau protein in WT mice injected with AAV encoding pro- and anti-aggregant mutant human tau 3 months after AAV injection.
A. Using an htau specific antibody (Tau Y9) we observed the presence of htau positive cells in the DG, CA3 and CA1 regions of WT mice injected with AAV-K2, as highlighted by the arrowheads. **B.** The same observation was made in WT AAV-K3 mice, with tau "recipient cells" detected in the DG, CA3 and CA1 regions of the mice, suggesting once more that the propagation of tau protein is independent of the protein's aggregation potential. Arrowheads indicate tau recipient cells (GFP- / htau+), which received htau from tau donor cells (GFP+ / htau+). Scale bar: 100 µm (overview figures); 20 µm (higher magnification figures).

To extend our findings and gain insights on the role of the endogenous mouse tau in the spreading of tau protein and tau pathology, we additionally injected TKO mice with AAV encoding pro- or anti-aggregant htau. Previous reports demonstrated that the absence of endogenous mouse tau does not interfere the propagation of tau protein, but reduces the extent of tau pathology and toxicity developed (Wegmann et al., 2015). In agreement with this, we observed that both TKO injected with AAV-K2 and AAV-K3 presented tau "recipient cells" (htau$_{+}$/GFP$_{-}$) in the granule cell layer of the DG and CA3 region (figure 40). Furthermore, both groups also presented htau+ cells in the CA1 region, but these cells were GFP+, so we cannot define them as tau "recipient cells", based on our initial definition. Different reasons may explain the observation of tau "donor cells" in this region, as it will be discussed later.

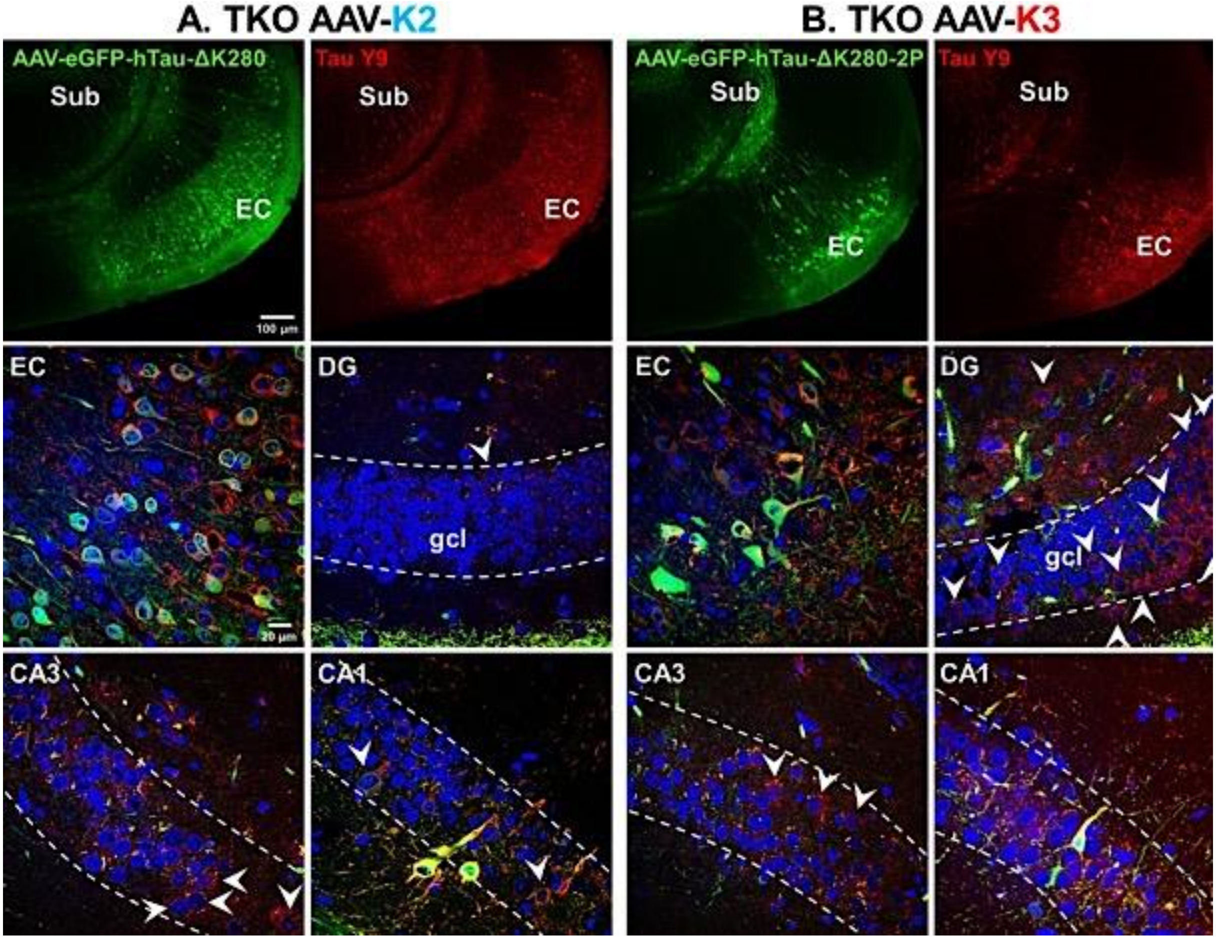

Figure 40 - Trans-synaptic spreading of tau protein in TKO mice injected with AAV encoding pro- and anti-aggregant mutant human tau 3 months after AAV injection.
A. TKO mice injected with AAV-K2 presented tau "donor cells" in the EC region that expressed both htau and GFP. In the hippocampus, these mice presented tau "recipient cells" (htau+/GFP-) in the DG and CA3 regions. Furthermore, htau+ cells were also detected in the CA1 region, but these cells were also GFP+. **B.** The EC of TKO AAV-K3 also displayed tau "donor cells" that express both GFP and htau. In the hippocampus, tau "recipient cells" were detected in the DG and CA3 regions, similarly to the previous group. Furthermore, htau+ cells were detected in the CA1, but these were also GFP+.

Arrowheads indicate tau recipient cells (GFP- / htau+), which received the htau from tau donor cells (GFP+ / htau+). Scale bar: 100 µm (overview figures); 20 µm (higher magnification figures).

4.2.3. Is GFP also spreading across cells?

We observed that, despite using the exact same coordinates and parameters for AAV injection (volume, injection rate, etc.) in all experimental animals, the pattern of htau and GFP expression may be different between the animals. Although EC cells were similarly transfected with AAV in nearly all animals, (as judged by the GFP+ cells), in some animals we observed trans-synaptic spreading of tau protein (as judged by tau "recipient cells" in the DG and other hippocampal regions), whereas in others we did not. Some animals actually presented a significant amount of htau+ cells in the EC and connected brain regions, but these cells were also GFP+, as observed in figure 41. These differences in the propagation of htau (and also GFP) may be related to the intrinsic differences between mice, different neuronal vulnerability, differential targeting of EC layers with the AAV injection, or other reasons, as it will be discussed later. Important to mention is the fact that these observations were random between the experimental groups, i. e., we cannot assign a specific observation (e.g. no trans-synaptic spreading of tau protein) to a specific experimental group.

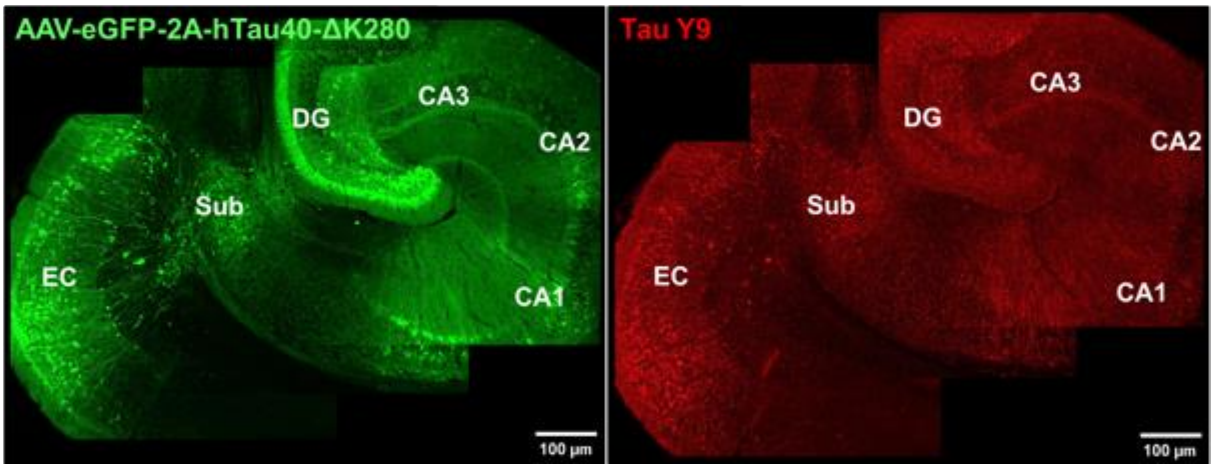

Figure 41 - Expression of GFP and human tau (Tau Y9) in a WT mouse injected with AAV-K2 (pro-aggregant htau) at 18 months post-injection.
The expression of pro-aggregant htau, as well as of GFP, was observed in the EC (the injection site) but also in all the anatomically connected regions through the perforant pathway, namely the granule cell layer of the DG, the CA1 region and also CA3 region, although in a lesser extent. Scale bar: 100 µm.

4.2.4. Phosphorylation of tau is more pronounced in pro-aggregant mice

The phosphorylation of tau at Ser396/Ser404 (an indicator of incipient degeneration), detected by the PHF-1 antibody, was analyzed in all experimental groups of AAV-injected mice. In the EC region, similar to previous observation in non-injected neuropsin mice, the three pro-aggregant models (tTA-EC/K2, WT and TKO injected with AAV-K2) showed a more pronounced phosphorylation of tau compared to the respective anti-aggregant models. WB analysis of EC fractions from the mice with PHF-1 antibody, normalized to the total levels of tau, revealed that pro-aggregant mice express approximately 40% more tau phosphorylation on the Ser396/Ser404 epitope than anti-aggregant (figure 42A and B). WT mice injected with AAV-K2 also presented higher levels of phosphorylation at this epitope compared to WT mice injected with AAV-K3 (approximately 25% higher). Similarly, TKO mice injected with AAV-K3 presented higher levels of phosphorylation than TKO mice injected with AAV-K3 (approximately 45% higher). Staining with PHF-1 antibody (figure 42C) confirmed the WB results, as PHF-1 positive cells were detected in all experimental groups, but more prominent in the pro-aggregant models (tTA-EC/K2, WT AAV-K2 and TKO AAV-K2) compared to the anti-aggregant models (tTA-EC/K3, WT AAV-K3 and TKO AAV-K3).

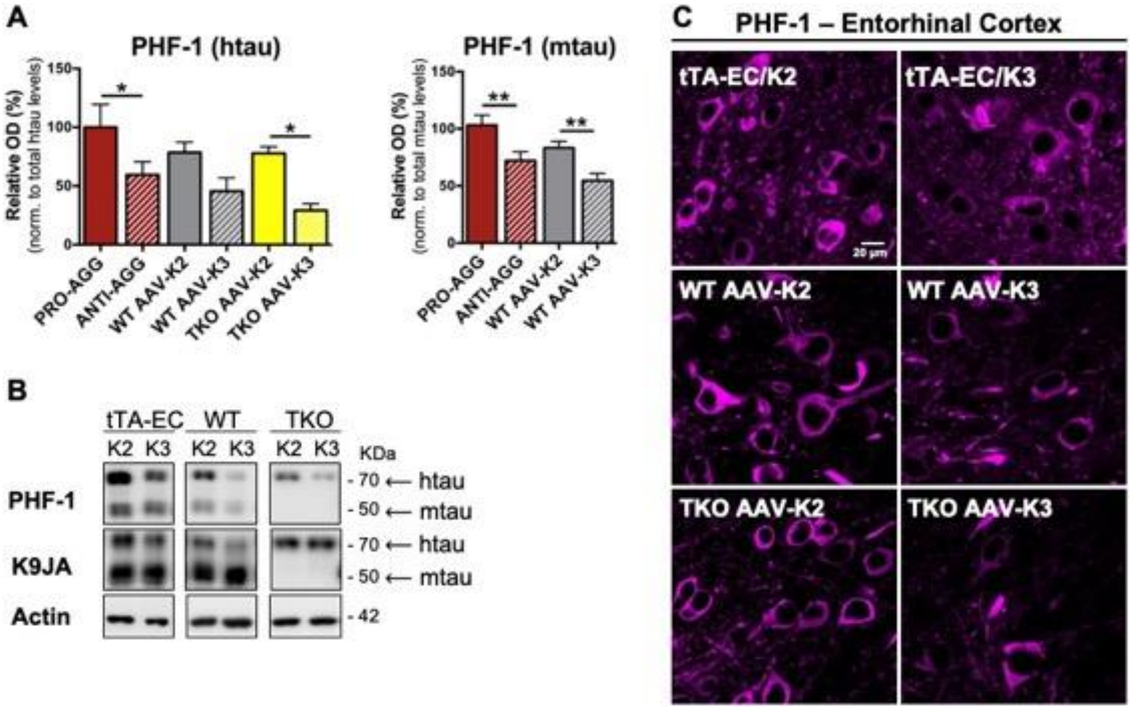

Figure 42 - Phosphorylation of tau at Ser396/Ser404, detected with PHF-1 antibody in the EC region of AAV-injected mice, 3 months after AAV injection.
A. WB analysis of EC fractions from all experimental groups showed that tau phosphorylation is increased in the pro-aggregant models compared to the respective anti-aggregant models. One-way

ANOVA analysis of the means of each group showed statistically significant differences ($p = 0.0064$). Post-hoc analysis with uncorrected Fisher's LSD test for multiple comparisons showed that pro-aggregant mice (tTA-EC/K2 injected with AAV-K2) have significantly higher levels of PHF-1 compared to anti-aggregant mice (tTA-EC/K3 injected with AAV-K3), both at the htau level ($p = 0.0182$) and mtau level ($p = 0.0032$). WT mice injected with AAV-K2 also presented higher levels of PHF-1 compared to WT mice injected with AAV-K3 at the level of htau (not statistically significant; $p = 0.0555$) and at the level of mtau ($p = 0.0079$). TKO AAV-K2 mice also presented higher levels of PHF-1 compared to TKO AAV-K3 mice at the level of htau ($p = 0.0410$). TKO mice do not express endogenous mtau. All numerical data are shown as mean +/- SEM; * denotes the significance of PHF-1 levels of the pro-aggregant group compared to the respective anti-aggregant group for each mouse background; * $p < 0.05$; ** $p < 0.01$. **B.** Representative WB bands for PHF-1 antibody, K9JA (total tau) and actin obtained using the EC fractions from mice of all experimental groups, summarizing the results shown in A. **C.** Staining with PHF-1 antibody showed that, in the EC region, all experimental groups displayed PHF-1+ cells, although phosphorylation of tau was more pronounced in the three pro-aggregant models (tTA-EC/K2, WT AAV-K2 and TKO AAV-K2) compared to the respective anti-aggregant model (tTA-EC/K3, WT AAV-K3 and TKO AAV-K3). Scale bar: 20 µm.

Concerning brain regions outside the EC, WT mice injected with AAV-K2 or AAV-K3 additionally expressed PHF-1+ cells in the DG and CA3 regions, although in a lesser extent than in the EC. On the other hand, tTA-EC/K2 and tTA-EC/K3 mice did not express PHF-1+ cells in other brain region besides the EC. A similar observation was made in TKO mice injected with AAV-K2 and AAV-K3, which only expressed PHF-1 cells in the EC and not in other brain regions (figure 43).

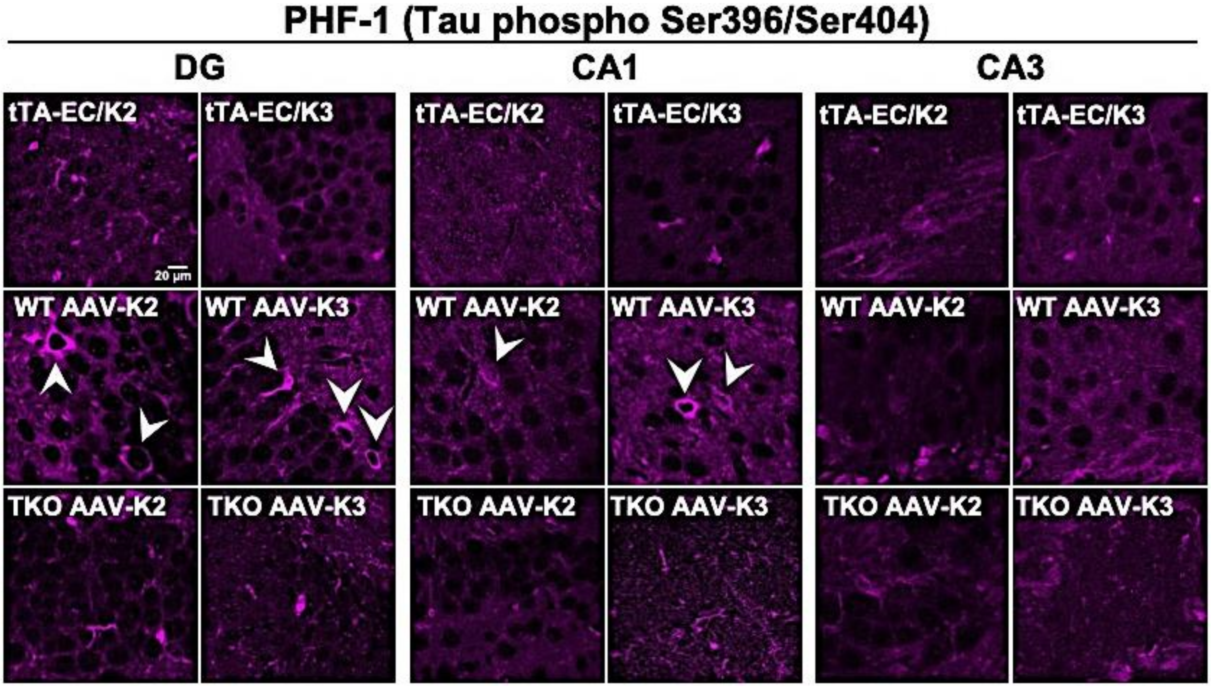

Figure 43 - Phosphorylation of tau at Ser396/Ser404, detected with PHF-1 antibody, only propagates from the EC to other brain regions in WT mice.
Staining with PHF-1 antibody in brain slices of mice 3 moths after AAV injection showed that WT mice, injected with AAV-K2 or AAV-K3, express PHF-1 positive cells in the DG and CA1 region of the hippocampus, which was not observed in the injected neuropsin and TKO mice. Scale bar: 20 µm.

4.2.5. Pathological conformation of tau observed in pro-aggregant mice, but restricted to the EC and perforant pathway

Previously, in the non-injected neuropsin mice we observed that tau with pathological conformation (MC1) was exclusively expressed in pro-aggregant mice, and not propagating to further brain regions besides the EC and perforant pathway up to 24 months of age. The same observation was made in the neuropsin injected mice at 18 months p. i., as we can appreciate in figure 44. Tau with pathological conformation, detected with MC1 antibody, was only expressed in pro-aggregant mice, and restricted to the EC and perforant pathway until the middle molecular layer of the DG. No MC1+ cells were observed outside the mentioned regions, showing that pathological tau is not propagating to other regions of the brain in the tTA-EC/K2 and tTA-EC/K3 mice after AAV injection.

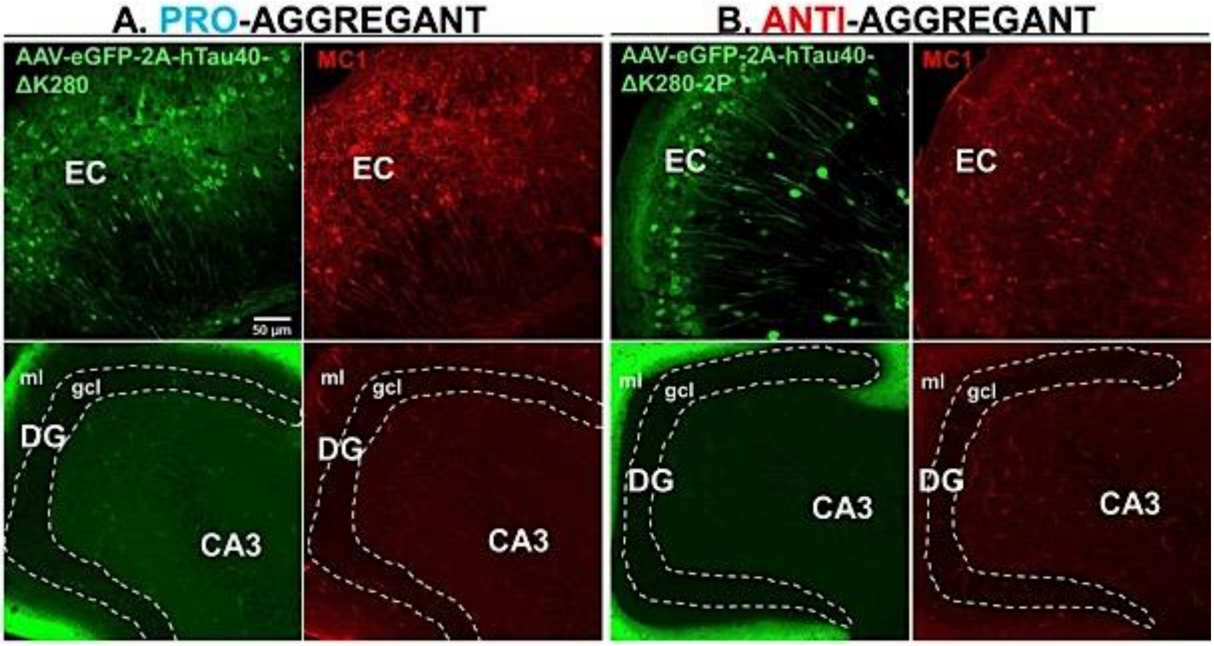

Figure 44 - Expression of tau with pathological conformation (antibody MC1) in neuropsin mice 18 months post-injection.
A. In pro-aggregant mice, tau with pathological conformation (MC1) was present in the EC and perforant pathway axons towards the hippocampus, but not further than the middle molecular layer of the DG, where the axon terminals from the EC are located. Therefore, in the neuropsin pro-aggregant mice no trans-synaptic spreading of tau pathology was observed. **B.** Tau with pathological conformation was not detected in anti-aggregant mice. The granule cell layer (gcl) of the DG is underlined in white; ml = molecular layer. Scale bar: 50 µm.

Next, we analyzed the distribution of the MC1 epitope at 18 months p. i. in WT mice injected with AAV-K2 or AAV-K3. WT AAV-K2 mice presented MC1+ cells in the EC region, similar to the observations made in the tTA-EC/K2 injected mice (figure 45). Furthermore, MC1+ cells were also detected in the granule cell layer of the DG, suggesting that tau with pathological conformation may be propagating in this experimental group. However, these MC1+ cells in the DG were also GFP+, which does not allow us to conclude whether there was in fact trans-synaptic spreading of tau with pathological conformation from the EC to the granule cell layer of the DG, or if the MC1+ cells observed had a different origin. These observations will be discussed in the next section of this thesis. On the other hand, WT mice injected with AAV-K3 did not present MC1+ cells.

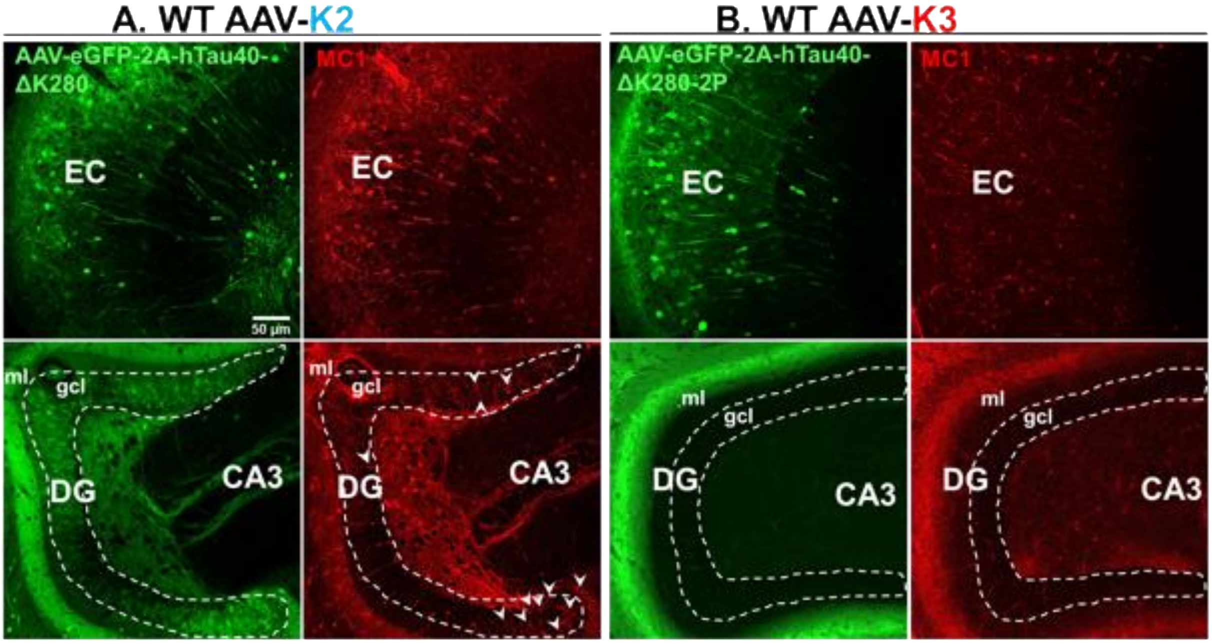

Figure 45 - Expression of tau with pathological conformation in WT mice injected with AAV-K2 or AAV-K3 at 18 months post-injection.
A. Tau with pathological conformation, detected with MC1 antibody, was present in the EC and axons of the perforant pathway in WT mice injected with AAV-K2. In addition, MC1+ cells were observed in the granule cell layer of the DG (arrowheads), but these cells were also GFP+, reason why, according to our definition, it may not be designated as trans-synaptic spreading of tau pathology. **B.** WT mice injected with AAV-K3 did not express MC1+ cells in the EC or hippocampus. The granule cell layer (gcl) of the DG is underlined in white; ml = molecular layer. Arrowheads denote MC1+ cells in the DG. Scale bar: 50 µm.

Subsequently, we analyzed the expression of MC1 in TKO mice injected with AAV-K2 or AAV-K3 which express mutant pro- and anti-aggregant htau but lack endogenous mouse tau. In agreement with the previous experimental groups, TKO mice injected with pro-aggregant tau (AAV-K2) expressed MC1+ cells in the EC region (figure 46A). MC1+ staining was also observed along the perforant pathway axons up to the terminal ends in the middle molecular layer, but no trans-synaptic spreading of tau with pathological conformation was observed. TKO AAV-K3 mice, expressing anti-aggregant htau, did not present MC1+ cells in the EC or other brain regions, in agreement with the previous anti-aggregant experimental groups (figure 46B).

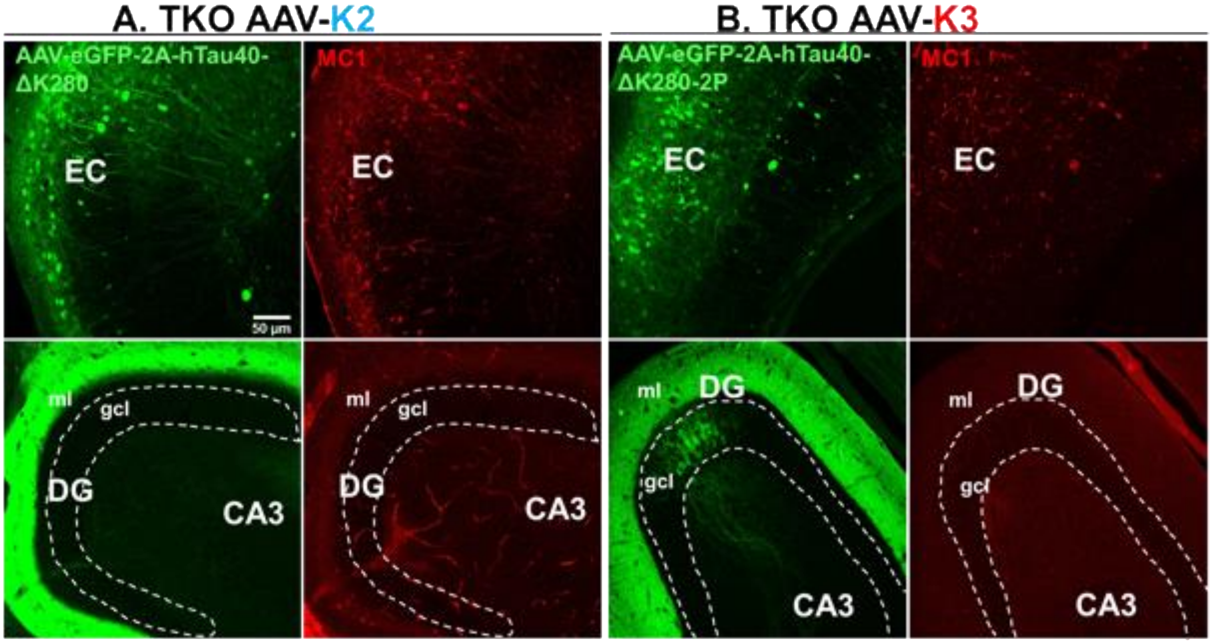

Figure 46 - Expression of tau with pathological conformation in TKO mice injected with AAV-K2 or AAV-K3 at 18 months post-injection.
A. Tau with pathological conformation, detected with MC1 antibody, was observed in the EC and axons of the perforant pathway until the terminal ends in the middle molecular layer in TKO mice injected with AAV-K2, but not in the granule cell layer of the DG (no trans-synaptic spreading). **B.** TKO mice injected with AAV-K3 did not present MC1+ cells in the EC or hippocampal region, although some GFP+ cells were observed in the granule cell layer of the DG. The granule cell layer (gcl) of the DG is underlined in white; ml = molecular layer. Scale bar: 50 µm.

As a summary, although we observed that tau protein can propagate form the EC to connected brain regions (DG) independently of the protein’s aggregation potential, we observed no trans-synaptic spreading of markers of tau pathology (table 1). Tau phosphorylation was mostly confined to the EC region, where most of the htau is expressed, with the exception of WT AAV-K2 and WT AAV-K3 mice, where few PHF-1+ cells were detected in the DG and CA1 region of the hippocampus. Regarding pathological conformation of tau, MC1+ cells were only observed in the EC region of the pro-aggregant experimental groups. This demonstrates that trans-synaptic spreading of markers of tau pathology did not take place in our models and when htau was present in the hippocampal region, this still did not acquire any pathological conformation. An exception was observed in WT AAV-K2 mice, where a sparse number of granule cells in the DG were MC1+, but as these cells were also GFP+, we cannot classify this phenomenon as trans-synaptic spreading of tau pathology, based on our definition previously stated (that cells should be GFP-).

Table 1 - Summary for all experimental groups regarding tau markers: human tau (Tau Y9), phosphorylated tau (PHF-1) and pathological conformation of tau (MC1).

Genotype	AAV injection	htau (Tau Y9)	Phospho tau (PHF-1)	Pathol. Conf. tau (MC1)	Summary
tTA-EC/K2	AAV-K2	EC + Hipp	EC √ DG X CA1 X CA3 X	EC √ Hipp X	Trans-synaptic spreading Tau protein: √ Trans-synaptic spreading Tau pathology: X
tTA-EC/K3	AAV-K3	EC + Hipp	EC √ (less than tTA-EC/K2) DG X CA1 X CA3 X	EC X Hipp X	Trans-synaptic spreading Tau protein: √ Trans-synaptic spreading Tau pathology: X
WT	AAV-K2	EC + Hipp	EC √ DG √ CA1 √ CA3 X	EC √ Hipp √ (but cells are also GFP+)	Trans-synaptic spreading Tau protein: √ Trans-synaptic spreading Tau pathology: ? (MC1+ cells in the hippocampus, but they are also GFP+)
WT	AAV-K3	EC + Hipp	EC √ (less than WT AAV-K2) DG √ CA1 √ CA3 X	EC X Hipp X	Trans-synaptic spreading Tau protein: √ Trans-synaptic spreading Tau pathology: X
TKO	AAV-K2	EC + Hipp	EC √ DG X CA1 X CA3 X	EC √ Hipp X	Trans-synaptic spreading Tau protein: √ Trans-synaptic spreading Tau pathology: X
TKO	AAV-K3	EC + Hipp	EC √ DG X CA1 X CA3 X	EC X Hipp X	Trans-synaptic spreading Tau protein: √ Trans-synaptic spreading Tau pathology: X

4.2.6. Pro-aggregant mice have increased astrogliosis, and this may precede the trans-synaptic spreading of tau pathology

Considering the known functions of microglia and astrocytes in neurodegeneration, together with the potential involvement of neuroinflammation in the spreading of tau pathology, we analyzed the expression of key markers of inflammation in the injected neuropsin mice in both EC and hippocampal fractions. Regarding the expression of the microglial marker Iba1, no differences were observed between pro-aggregant mice (figure 47A) and anti-aggregant mice (figure 47B), neither between the EC and hippocampus. On the other hand, staining with GFAP antibody showed that anti-aggregant mice (figure 47B), expressed lower levels of GFAP compared to pro-aggregant mice (figure 47A). Furthermore, in pro-aggregant mice the expression of the astrocytic marker GFAP was higher in the hippocampal region compared to the EC region. The fact that, in pro-aggregant mice, the increased expression of GFAP is located in the hippocampal region suggests that astrogliosis may precede the propagation of tau pathology from the EC to the hippocampus, possibly through a signaling mechanism originating in the EC that triggers the astrogliosis in the hippocampus, the next region to be affected by tau pathology according to the Braak stages.

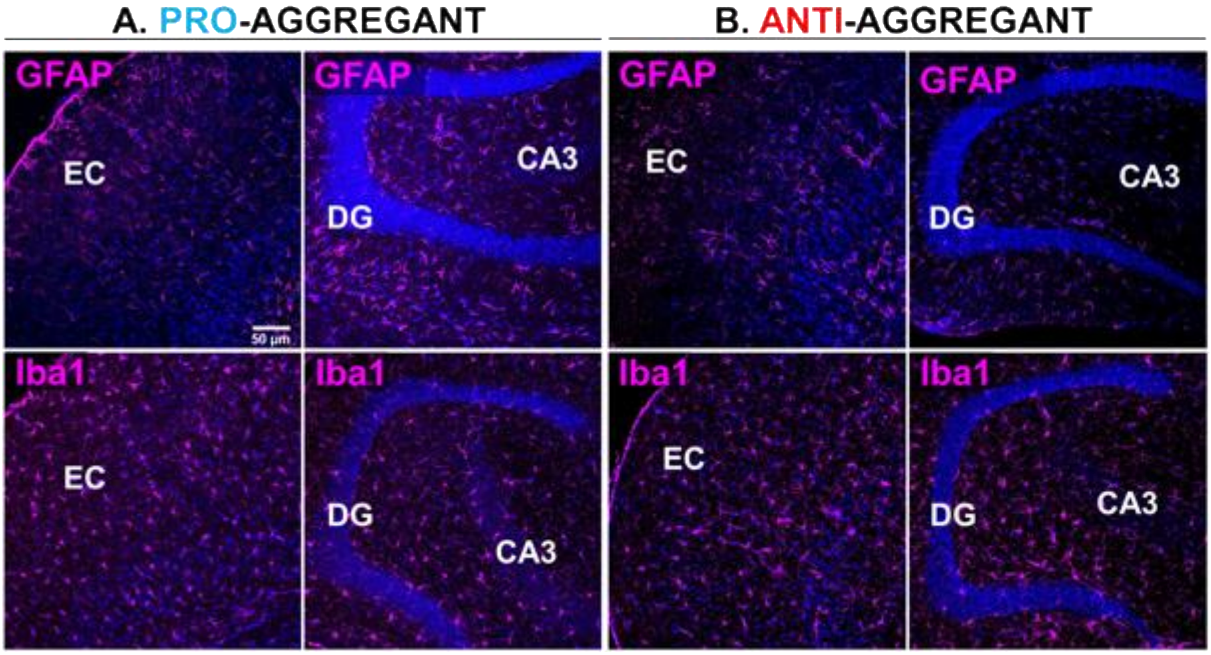

Figure 47 - Expression of GFAP and Iba1 in pro- and anti-aggregant neuropsin mice at 3 months post-injection.
A. In tTA-EC/K2 pro-aggregant mice, the expression of GFAP was mostly restricted to the hippocampal region, as almost no GFAP+ cells were detected in the EC region. Concerning the Iba1 expression, no differences were observed between the EC and hippocampal region in the pro-aggregant mice. **B.** In the tTA-EC/K3 anti-aggregant mice, GFAP+ cells were detected in the hippocampal region, but at a lower level compared to the tTA-EC/K2 mice. Few GFAP+ cells were also detected in the EC region. Regarding Iba1 expression, no differences were observed in the tTA-EC/K3 mice between EC and hippocampal region, as well as no differences compared to Iba1 expression in pro-aggregant mice. Scale bar: 50 µm.

WB analysis of EC fractions from pro- and anti-aggregant mice confirmed the results observed in the staining with Iba1 and GFAP. As shown in figure 48A, in the EC fraction the levels of CD11b, another microglial marker, were not different between pro- and anti-aggregant mice at all time points analyzed (3, 12 and 18 months p. i.). On the other hand, the levels of GFAP were significantly lower in anti-aggregant mice at 12 and 18 months p. i. compared to pro-aggregant mice. In the hippocampal fraction (figure 48B) no significant differences were observed in the levels of CD11b between pro- and anti-aggregant mice. On the other hand, and in agreement with the observation of the GFAP staining from figure 47, anti-aggregant mice presented lower levels of GFAP at 3 and 12 months p. i. compared to pro-aggregant mice, although not significant.

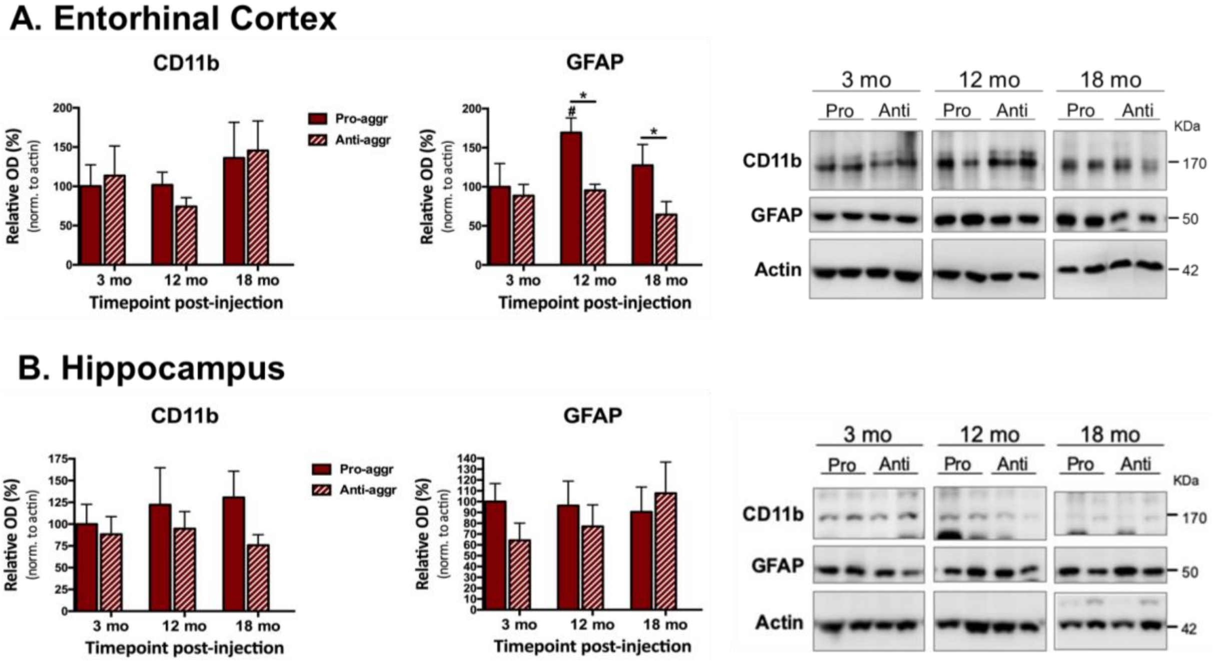

Figure 48 - Levels of inflammatory markers in neuropsin pro- and anti-aggregant mice over time.

A. In the EC, no differences were observed in the microglial marker CD11b between pro- and anti-aggregant mice at the time points analyzed (3, 12 and 18 months p. i.). Regarding the astrocytic marker GFAP, two-way ANOVA denoted an overall effect of the genotype [F(1, 30) = 8.793; p = 0.0059]. Post-hoc analysis with uncorrected Fisher's LSD test showed that, although no significant differences were observed between pro- and anti-aggregant mice at 3 months p. i., the level of GFAP increased in the pro-aggregant mice from 3 to 12 months p. i. (p= 0.0227). Furthermore, at 12 and 18 months p. i., the levels of GFAP were significantly lower in the anti-aggregant mice compared to the pro-aggregant (p = 0.0157 and p = 0.0373, respectively). **B.** In the hippocampal fractions, no significant differences were observed on the levels of CD11b between both genotypes at the time points analyzed. Regarding GFAP, although not significant, anti-aggregant mice presented a tendency for lower levels of GFAP compared to pro-aggregant mice at 3 and 12 months p. i.. All numerical data are shown as mean +/- SEM; * denotes the effect of the genotype; # denotes the effect of time within the same genotype. *, # $p < 0.05$.

We additionally monitored the presence of neuroinflammation markers in the WT and TKO mice injected with AAV to express both pro- or anti-aggregant mutant htau. Similar to the observations in the neuropsin mice, no differences were observed in the expression of Iba1 between WT mice injected with AAV-K2 (figure 49A) or injected with AAV-K3 (figure 49B) at 3 months p. i. On the other hand, the expression of GFAP was increased in the WT AAV-K2 mice (pro-aggregant) compared to the WT AAV-K3 mice (anti-aggregant), similar to the previous observations in the neuropsin mice. Furthermore, recapitulating the observations on neuropsin mice, the expression of GFAP was higher in the hippocampus compared to the EC, once more suggesting that astrogliosis may precede the propagation of markers of tau pathology from the EC to the hippocampus.

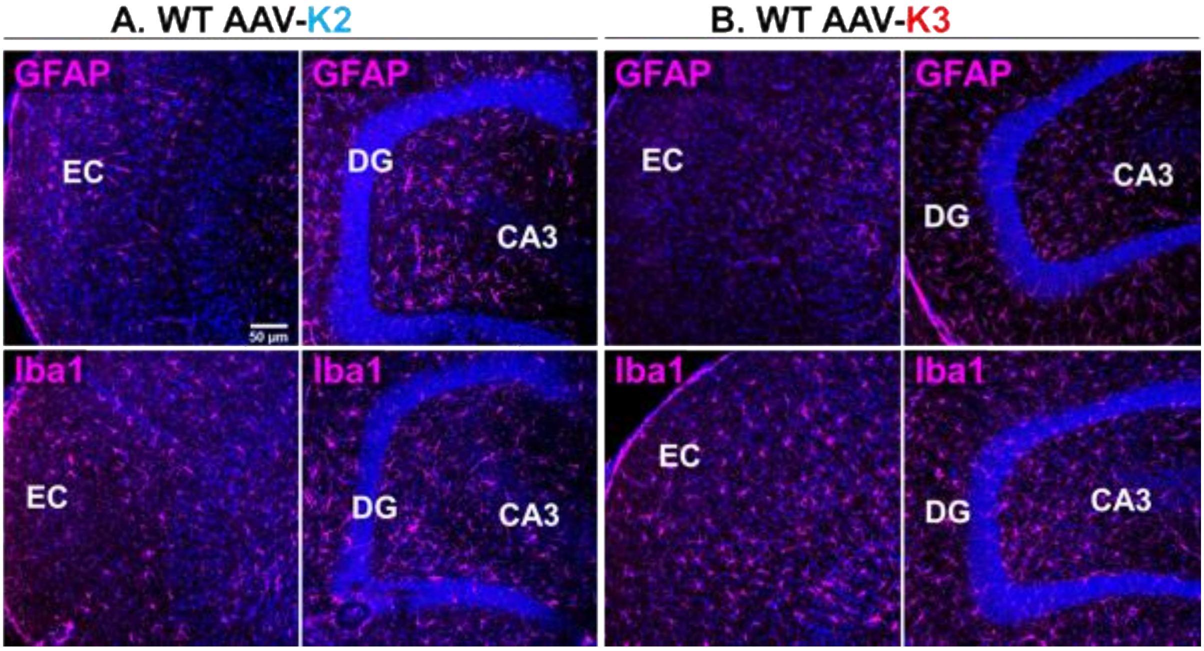

Figure 49 - Expression of GFAP and Iba1 in WT mice injected with AAV-K2 and AAV-K3 at 3 months post-injection.
A. In WT AAV-K2 mice, the expression of GFAP was predominantly observed in the hippocampal region, with only a sparse number of cells in the EC region. The expression of the microglial marker Iba1 was similar between both brain regions. **B.** In WT AAV-K3 mice, and similar to WT AAV-K2, the expression of GFAP is predominantly observed in the hippocampal region, with almost no GFAP+ cells observed in the EC. However, GFAP expression in WT AAV-K3 mice was lower compared to the WT AAV-K2 mice. Regarding Iba1, no differences were observed between EC and hippocampal region, and also in comparison to WT AAV-K2 mice. Scale bar: 50 µm.

WB analysis of CD11b in the EC fraction confirmed the observation made in the staining with Iba1 at 3 months p. i., as no significant differences were detected between WT AAV-K2 and WT AAV-K3 (figure 50A). However, the levels of CD11b significantly increased over time in WT AAV-K2 mice, leading to significant differences between both groups. At 12 and 18 months p. i., WT AAV-K2 mice resented significantly higher levels of CD11b than WT AAV-K3 mice. Similarly, in the hippocampus, no differences were observed on the levels of CD11b between WT AAV-K2 and WT AAV-K3 mice at 3 months p. i., but at 12 months p. i. WT AAV-K2 mice presented significantly higher levels of CD11b compared to WT AAV-K3 (figure 50B). Regarding the levels of GFAP, both in the EC (figure 50A) and hippocampal (figure 50B) fractions we observed that WT AAV-K3 mice presented lower levels of the astrocytic marker at all time points, although not significant, but in agreement with the observation in the staining from figure 49.

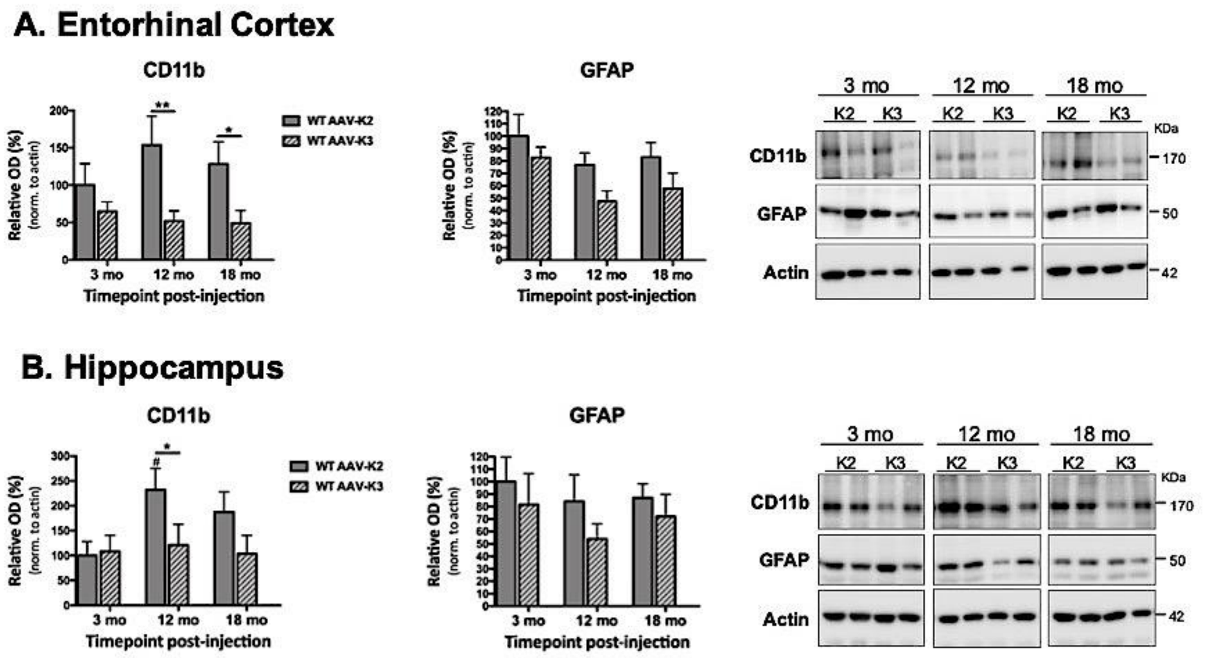

Figure 50 - Levels of inflammatory markers in WT mice injected with AAV-K2 and AAV-K3 over time.
A. In the EC, two-way ANOVA demonstrated an overall effect of the genotype in the levels of CD11b [F(1, 72) = 10.09; p = 0.0022]. Although no significant differences were found between WT AAV-K2 and WT AAV-K3 mice at 3 months p. i., post-hoc analysis with uncorrected Fisher's LSD test showed that CD11b levels were higher in WT AAV-K2 mice at 12 and 18 months p. i. (p = 0.0086 and p = 0.0484, respectively). Regarding astrogliosis, no significant differences were observed between both groups at any time point analyzed, although there was a tendency for lower GFAP levels in the WT AAV-K3 mice. **B.** In the hippocampal fractions, similar to the observations made in the EC region, the levels of CD11b were not different between WT AAV-K2 and WT AAV-K3 mice at 3 months p. i., also in agreement with the Iba1 staining. However, CD11b levels increased over time in the WT AAV-K2 mice, being significantly higher at 12 months p. i. compared to 3 months (p = 0.0155). This increase was not observed in the WT AAV-K3 mice, therefore, WT AAV-K2 mice presented significantly higher levels of CD11b at 12 months p. i. compared to the other group (p = 0.0365) and at 18 months p. i., although not significant. Regarding the levels of GFAP, no significant differences were observed between both genotypes or over time, although there was a tendency for lower GFAP levels in WT AAV-K3 mice compared to WT AAV-K2. All numerical data are shown as mean +/- SEM; * denotes the effect of the genotype; # denotes the effect of time within the same genotype. *, # $p < 0.05$; ** $p < 0.01$.

In TKO mice injected with AAV-K2 (figure 51A), similar to the previous groups, the GFAP expression was increased in the hippocampal region compared to the EC. On the other hand, no differences were observed between both brain regions regarding the expression of Iba1. In TKO AAV-K3 mice (figure 51B) the expression of GFAP was higher in the hippocampal region compared to the EC. Furthermore, in the TKO mice, the expression of GFAP was higher in the TKO AAV-K3 compared to the TKO AAV-K2, contrary to the previous observations in neuropsin and WT mice, where the pro-aggregant model always presented higher GFAP levels than the anti-aggregant.

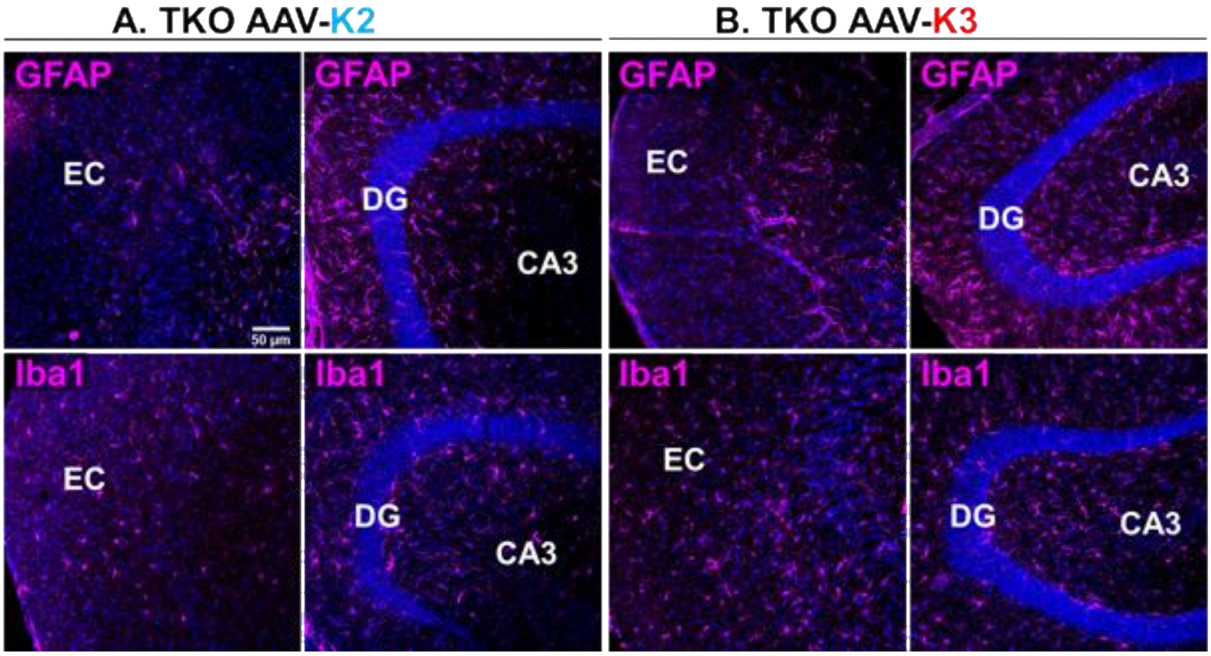

Figure 51 - Expression of GFAP and Iba1 in TKO mice injected with AAV-K2 and AAV-K3 at 3 months post-injection.
A. In TKO AAV-K2 mice, the expression of GFAP was mostly observed in the hippocampal region, and very sparse in the EC. No differences were observed regarding the expression of Iba1 between these two brain regions. **B.** In TKO AAV-K3 mice, the expression of GFAP was also higher in the hippocampal region compared to the EC region, where a scarce number of GFAP+ cells was detected. GFAP expression was also higher in the hippocampus of TKO AAV-K3 mice compared to the hippocampus of TKO AAV-K2 mice. Regarding Iba1, no differences were observed between the EC and hippocampal region of TKO AAV-K3 mice, as well as in comparison with the expression levels of Iba1 in TKO AAV-K2 mice. Scale bar: 50 µm.

In agreement with the results obtained in the staining with Iba1, we observed no differences between TKO AAV-K2 and TKO AAV-K3 on the levels of CD11b in the EC fraction (figure 52A) and in the hippocampal fraction (figure 52B), at the 3 months time point. However, at 12 and 18 months p. i., TKO AAV-K3 mice presented lower levels of CD11b than TKO AAV-K2 mice in both brain regions. Regarding the levels of GFAP, no differences were observed in the expression of the astrocytic marker between TKO AAV-K2 and TKO AAV-K3 in the EC fraction. However, GFAP levels were highly increased in both groups at 18 months p. i. (figure 52A). Furthermore, and contrary to what the staining with GFAP indicated, significant differences were observed in the expression of GFAP in the hippocampal fraction of TKO AAV-K2 and TKO AAV-K3 at 3 months p. i. or any other time point (figure 52B). However, the levels of GFAP, in this brain region, significantly increased over time for both experimental groups.

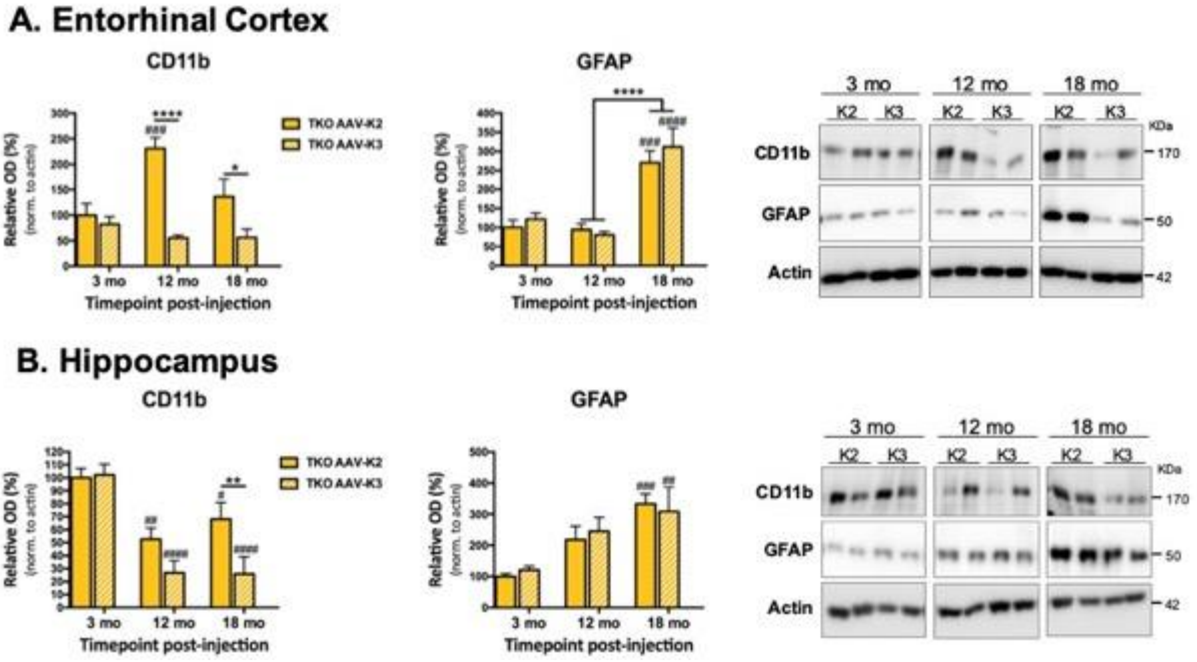

Figure 52 - Levels of inflammatory markers in TKO mice injected with AAV-K2 and AAV-K3 over time.

A. In the EC, two-way ANOVA demonstrated an interaction between the genotype and time in the levels of CD11b [F(2, 30) = 7.024; p = 0.0031]. Post-hoc analysis with uncorrected Fisher's LSD test showed that the levels of CD11b in TKO AAV-K2 mice significantly increased from 3 to 12 months p. i. (p = 0.0001), an effect that was not recapitulated in TKO AAV-K3 mice. Furthermore, when comparing the levels of CD11b in both groups, it was possible to observe that TKO AAV-K2 mice presented higher levels of the microglial marker at 12 and 18 months p. i. than TKO AAV-K3 mice (p < 0.0001 and p = 0.0123). Regarding the levels of GFAP, two-way ANOVA showed an overall effect of time [F(2, 30) = 34.25; p < 0.0001]. Post-hoc analysis with uncorrected Fisher's LSD test showed that, although no significant differences were found between mice injected with AAV-K2 or AAV-K3, the levels of GFAP significantly increased in both groups at 18 months p. i. compared to the first time point (p = 0.0001 and p < 0.0001, respectively), and compared to the 12 months p. i. (p < 0.0001 for both). **B.** In the hippocampus, analyzing the levels of CD11b with a two-way ANOVA denoted an overall effect of time [F(2, 30) = 21.60; p < 0.0001] and an overall effect of the genotype [F(1, 30) = 6.899; p = 0.0135]. Further post-hoc analysis with uncorrected Fisher's LSD test showed that the levels of CD11b were significantly decreased in both TKO injected with AAV-K2 and AAV-K3 at 12 months p. i. (p = 0.0026 and p < 0.0001, respectively), and at 18 months p. i. (p = 0.0353 and p < 0.0001, respectively). As observed, this decrease was more pronounced in the TKO AAV-K3 mice. Indeed, at 18 months p. i., a significant difference is observed between both groups, with TKO AAV-K3 mice presenting lower levels of CD11b compared to TKO AAV-K2 (p = 0.0065). Regarding GFAP, two-way ANOVA denoted an effect of time [F(2, 30) = 11.87; p = 0.0002], with GFAP levels increasing in both groups over time. Post-hoc analysis with uncorrected Fisher's LSD test showed that, at 18 months p. i., the levels of GFAP were significantly higher compared to the 3 months p. i. time point in both TKO AAV-K2 and TKO AAV-K3 (p = 0.0007 and p = 0.0020, respectively). All numerical data are shown as mean +/- SEM; * denotes the effect of the genotype; # denotes the effect of time within the same genotype. *, # p < 0.05; **, ## p < 0.01; ### p < 0.001; ****, #### p < 0.0001.

We also compared WT and TKO mice both injected with AAV-K2 to monitor the impact of the absence of endogenous mouse tau. In the EC fraction (figure 53A) we did not observe differences between both genotypes in terms of CD11b levels within the same time point. However, the levels of CD11b increased over time in the WT AAV-K2 mice, but not in the TKO AAV-K2 mice. Regarding the levels of GFAP in the EC fraction, no significant differences were observed between both genotypes on the time points analyzed. However, the levels of GFAP significantly increased over time in TKO AAV-K2 mice, but not in WT AAV-K2 mice. In the hippocampal fraction (figure 53B), no significant differences were observed between genotypes or over time on the levels of CD11b and GFAP.

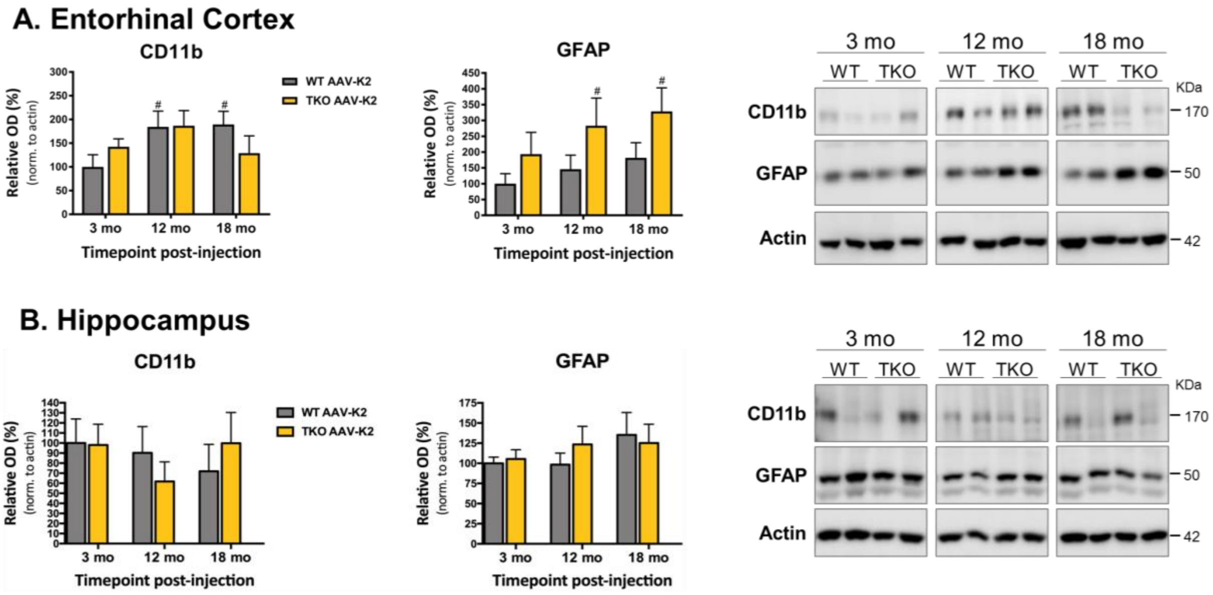

Figure 53 - Levels of inflammatory markers in WT and TKO mice injected with AAV-K2 over time.
A. In the EC, the levels of CD11b increased in WT AAV-K2 mice at 12 months and 18 months p. i. compared to the first time point (p = 0.0475 and p = 0.0364, respectively). This increase was not observed in TKO AAV-K2 mice. However, no significant differences on the level of CD11b were detected between WT AAV-K2 and TKO AAV-K2 mice at all time points. Regarding the levels of GFAP, two-way ANOVA analysis denoted an overall effect of the genotype [F(1, 30) = 6.165; p = 0.0188]. Further post-hoc analysis with uncorrected Fisher's LSD test showed that GFAP increased over time in TKO AAV-K2 mice, being significantly higher at 12 months (p = 0.0457) and 18 months p. i. (p = 0.0143) compared to the initial time point. This significant increase in GFAP levels was not observed in TKO mice. **B.** In the hippocampal fraction, no significant differences were observed in the levels of CD11b and GFAP. All numerical data are shown as mean +/- SEM; # denotes the effect of time within the same genotype. # p < 0.05.

A summary of the results of the distribution of markers for microglia and astroglia in all experimental groups, analyzed by IF and WB, is presented in table 2.

Another parameter we analyzed concerns the levels of pre-synaptic (synaptophysin) and post-synaptic (PSD95) markers in our experimental groups. In the EC fraction of pro- and anti-aggregant mice (figure 54A), the levels of PSD95 were reduced in tTA-EC/K2 mice at 18 months p. i., but not in tTA-EC/K3 mice. Furthermore, the levels of synaptophysin also decreased over time in the pro-aggregant mice, but not in the anti-aggregant mice. Together, this suggests that pro-aggregant mice are more prone to synaptic deficits than anti-aggregant mice in the EC region. In the hippocampal fraction (figure 54B) no significant differences were observed on the levels of synaptophysin over time or between pro- and anti-aggregant mice.

Table 2 - Summary for all experimental groups regarding the expression of the neuroinflammatory markers Iba1/CD11b (for microglia) and GFAP (for astroglia) obtained by immunofluorescence or western blot in different brain regions and time points.

Genotype	AAV injection	Microglia (Iba1/CD11b)		Astroglia (GFAP)	
		IF (3 mo only)	WB	IF (3 mo only)	WB
tTA-EC/K2	AAV-K2	▪ No differences between EC & Hipp at 3 mo	▪ EC & Hipp: no differences over time (3, 12 & 18 mo P.I)	▪ Highly expressed in Hipp compared to EC	▪ EC: increase at 12 mo compared to 3 mo ▪ Hipp: no differences over time
tTA-EC/K3	AAV-K3	▪ No differences between EC & Hipp at 3 mo ▪ No differences compared to tTA-EC/K2	▪ EC & Hipp: no differences over time ▪ Hipp: tendency for lower CD11b in tTA-EC/K3 compared to tTA-EC/K2 at 12 & 18 mo, but n.s.	▪ Very low in both EC & Hipp compared to tTA-EC/K2	▪ EC & Hipp: no differences over time ▪ EC: lower GFAP at 12 & 18 mo compared to tTA-EC/K2 (in Hipp same tendency but n.s.)
WT	AAV-K2	▪ No differences between EC & Hipp at 3 mo	▪ EC: no differences over time ▪ Hipp: CD11b increases at 12 mo compared to 3 mo	▪ Highly expressed in Hipp compared to EC	▪ EC & Hipp: no differences over time
WT	AAV-K3	▪ No differences between EC & Hipp at 3 mo ▪ No differences compared to WT AAV-K2	▪ EC & Hipp: no differences over time ▪ EC: lower CD11b at 12 & 18 mo compared to WT AAV-K2 ▪ Hipp: lower CD11b at 12 mo compared to WT AAV-K2	▪ Lower in both EC & Hipp compared to WT AAV-K2	▪ EC & Hipp: no differences over time ▪ EC & Hipp: tendecy for lower GFAP compared to WT AAV-K2 (all time points), but n.s.
TKO	AAV-K2	▪ No differences between EC & Hipp at 3 mo	▪ EC: CD11b increases at 12 mo compared to 3 mo ▪ Hipp: CD11b decreases at 12 & 18 mo compared to 3 mo	▪ Higher in Hipp at 3 mo compared to EC	▪ EC: GFAP levels increase at 18 mo compared to 3 & 12 mo ▪ Hipp: GFAP increases over time
TKO	AAV-K3	▪ No differences between EC & Hipp at 3 mo ▪ No differences compared to TKO AAV-K2	▪ EC: no differences over time ▪ Hipp: CD11b decreases at 12 & 18 mo cmpared to 3 mo ▪ Compared to TKO AAV-K2, lower CD11b at 12 & 18 mo in EC + at 18 mo in Hipp	▪ Higher in Hipp compared to EC ▪ Higher compared to TKO AAV-K2	▪ EC: GFAP levels increase at 18 mo compared to 3 & 12 mo ▪ Hipp: GFAP increases over time ▪ No difference compared to TKO AAV-K2

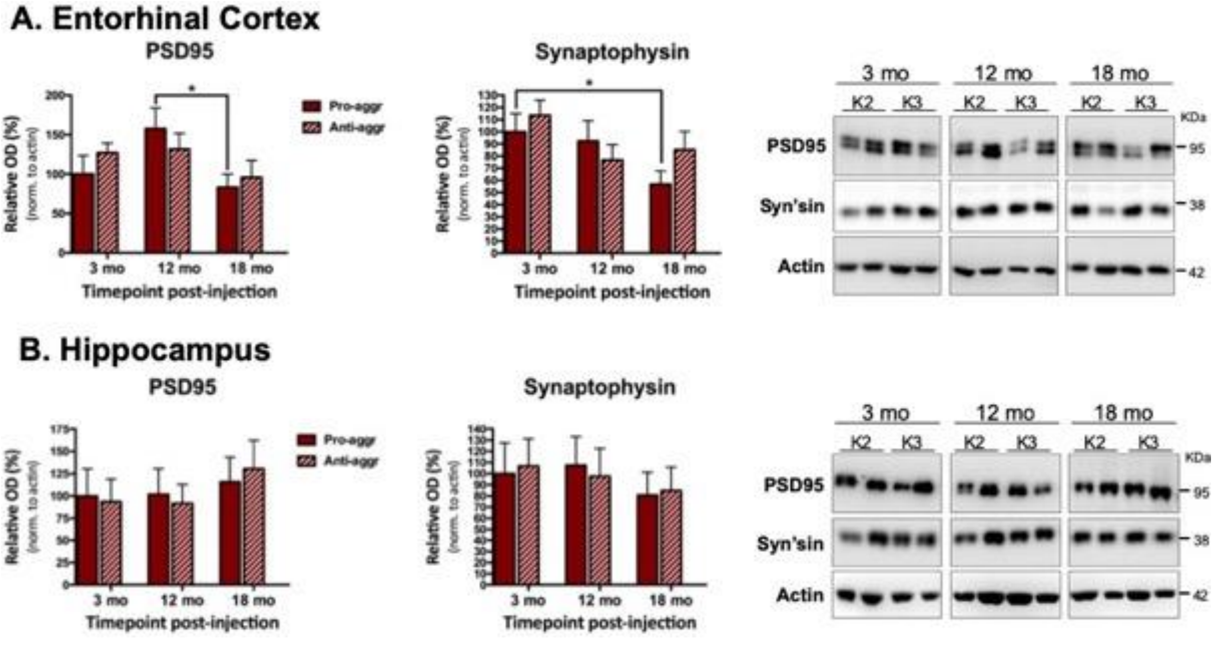

Figure 54 - Levels of pre- and post-synaptic markers in neuropsin pro- and anti-aggregant mice over time.
A. In the EC, two-way ANOVA analysis denoted an overall effect of time on the levels of PSD95 [F(2, 47) = 3.607; p = 0.0349]. Further post-hoc analysis with uncorrected Fisher's LSD test showed that, in tTA-EC/K2 mice, the levels of PSD95 decrease at 18 months p. i. compared to the 12 months time point (p = 0.0127), which was not observed in tTA-EC/K3 mice. Similarly, the levels of synaptophysin

decreased in tTA-EC/K2 mice over time [two-way ANOVA, F(2, 48) = 3.364; p = 0.0429]. Post-hoc analysis with uncorrected Fisher's LSD test showed that the levels of synaptophysin were significantly lower at 18 months p. i. in the pro-aggregant mice compared to the initial time point (p = 0.0329). This decrease in synaptophysin over time was not observed in the anti-aggregant mice. **B.** In the hippocampal fraction, no significant differences were observed in the levels of PSD95 and synaptophysin. All numerical data are shown as mean +/- SEM; * denotes the effect of time. * p < 0.05.

The expression of synaptic markers was also analyzed in EC and hippocampal fractions of WT mice injected with AAV-K2 and AAV-K3. In the EC fraction (figure 55A), the levels of PSD95 were significantly lower in WT AAV-K2 mice at 12 and 18 months p. i. compared to the 3 month time point, a decrease not observed in WT AAV-K3 mice. No differences were detected between the two groups or over time regarding the levels of synaptophysin. On the hippocampal fractions (figure 55B), the levels of PSD95 were also decreased in WT AAV-K2 mice at 12 months p. i. compared to the initial time point, a decrease not observed in WT AAV-K3 mice. Similar to the EC fractions, no differences were observed in the levels of synaptophysin in the hippocampus.

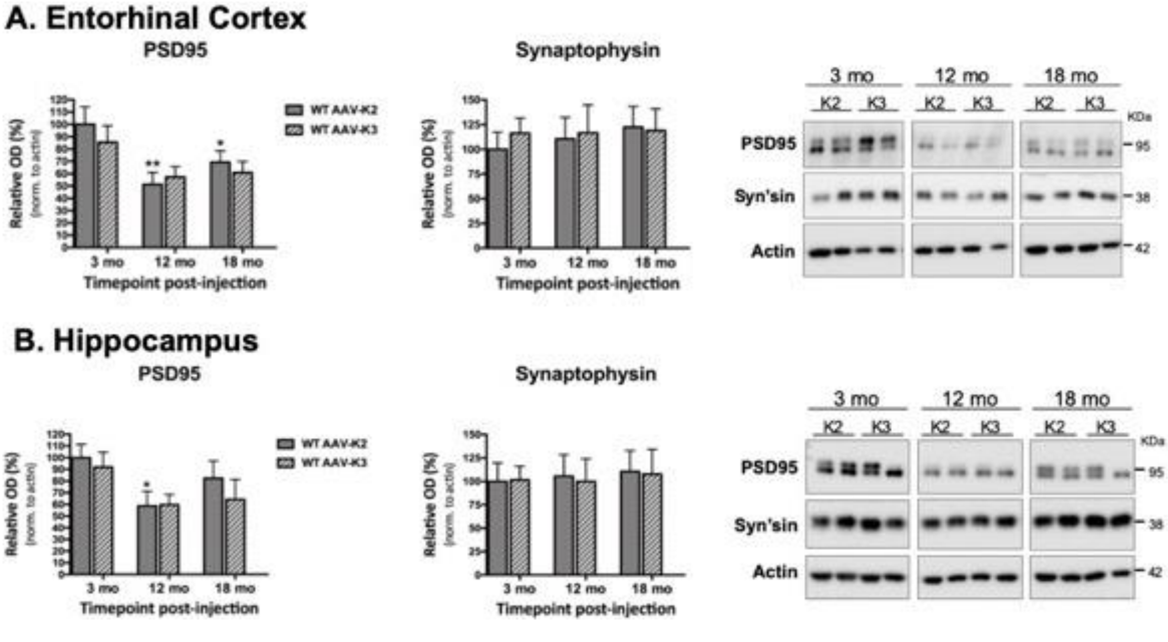

Figure 55 - Levels of pre- and post-synaptic markers in WT mice injected with AAV-K2 and AAV-K3 over time.
A. In the EC, two-way ANOVA analysis denoted an overall effect of time on the levels of PSD95 [F(2, 46) = 6.542; p = 0.0032]. Further post-hoc analysis with uncorrected Fisher's LSD test showed that PSD95 levels decreased in WT AAV-K2 mice at 12 months p. i. (p = 0.0024) and 18 months p. i. (p = 0.0487) compared to the initial time point, a decrease not observed in WT AAV-K3 mice. No significant differences were observed on the levels of synaptophysin. **B.** In the hippocampal fraction, two-way ANOVA analysis denoted an overall effect of time on the levels of PSD95 [F(2, 47) = 4.064; p = 0.0236]. Post-hoc analysis with uncorrected Fisher's LSD test showed that PSD95 levels were decreased at 12 months p. i. in WT AAV-K2 mice (p = 0.0294) compared to the 3 months time point, a decrease that was not recapitulated in WT AAV-K3 mice. No significant differences were observed on the levels of synaptophysin. All numerical data are shown as mean +/- SEM; * denotes the effect of time within the same group. * p < 0.05; ** p < 0.01.

Similar to what was performed before, the levels of pre- and post-synaptic markers were also analyzed in TKO mice injected with AAV-K2 and AAV-K3. In the EC fractions (figure 56A), no significant differences were observed in the levels of PSD95. However, the levels of synaptophysin decreased over time in TKO AAV-K2 mice, but not in TKO AAV-K3 mice. Regarding the hippocampal fractions (figure 56B), the levels of PSD95 significantly increased over time in TKO AAV-K2 mice, which was not recapitulated in TKO AAV-K3 mice. Contrarily, the levels of synaptophysin significantly increased over time in the TKO AAV-K3 mice, but not in the TKO AAV-K2 mice.

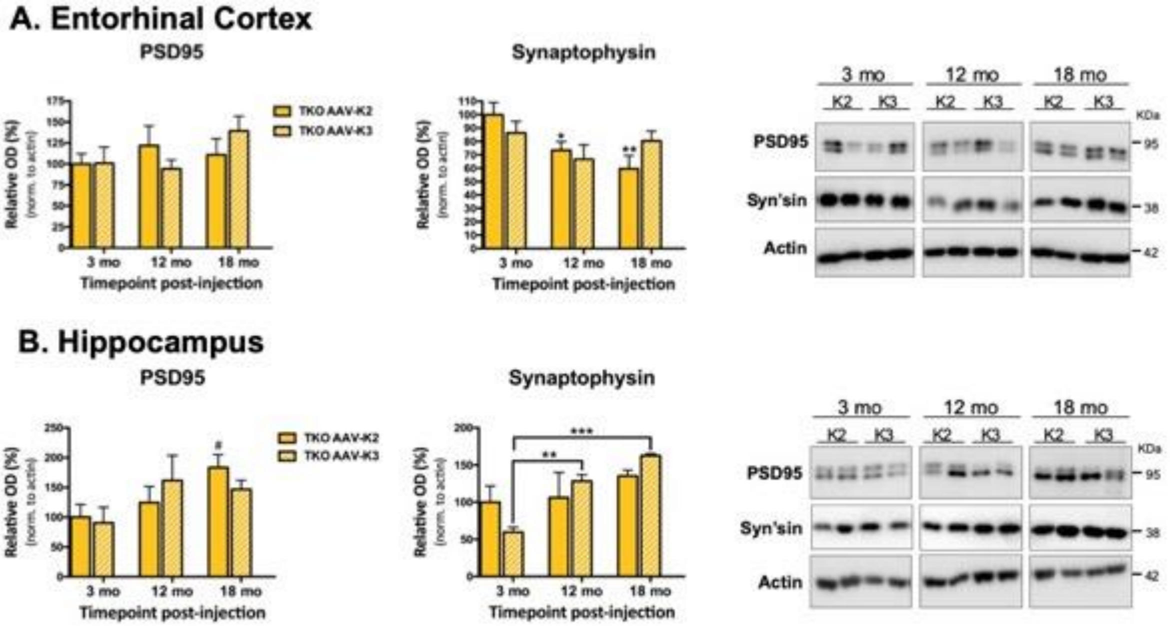

Figure 56 - Levels of pre- and post-synaptic markers in TKO mice injected with AAV-K2 and AAV-K3 over time.
A. In the EC fraction no significant differences were observed on the levels of PSD95 between TKO mice injected with AAV-K2 or AAV-K3. On the other hand, two-way ANOVA denoted an overall effect of time on the levels of synaptophysin [F(2, 30) = 4.628; p = 0.0177]. Further post-hoc analysis showed a significant decrease in the levels of synaptophysin in TKO AAV-K2 mice at 12 (p = 0.0412) and 18 months p. i. (p = 0.0029), compared to the initial time point. **B.** In the hippocampal fraction, two-way ANOVA denoted an overall effect of time on the levels of PSD95 [F(2, 30) = 3.550; p = 0.0413]. Post-hoc analysis with uncorrected Fisher's LSD test showed that PSD95 levels increase over time in TKO AAV-K2 mice (p = 0.0358 at 18 months p. i.), which was not observed in TKO AAV-K3. Regarding the levels of synaptophysin, two-way ANOVA showed an overall effect of time [F(2, 30) = 7.872]. Further post-hoc analysis showed a significant increase on the levels of synaptophysin in TKO AAV-K3 mice at 12 (p = 0.0092) and 18 months p. i. (p = 0.0002), compared to the initial time point. All numerical data are shown as mean +/- SEM; * denotes the effect of time within the same group. * p < 0.05; ** p < 0.01; *** p < 0.001.

To finalize, we also compared the levels of synaptic markers between WT and TKO mice both injected with AAV-K2 to express pro-aggregant htau. In the EC fractions (figure 57A), the levels of PSD95 significantly decreased in WT AAV-K2 mice at 18 months p. i. compared to 3 months p. i., which was not observed in the TKO AAV-K2 mice. On the other hand, the levels of synaptophysin increased in TKO AAV-K2 mice at 12 months p. i. compared to 3 months p. i., which did not occur in the WT AAV-K2 mice. In the hippocampal fraction (figure 57B), no significant differences were observed on the levels of PSD95 and synaptophysin over time or between genotypes.

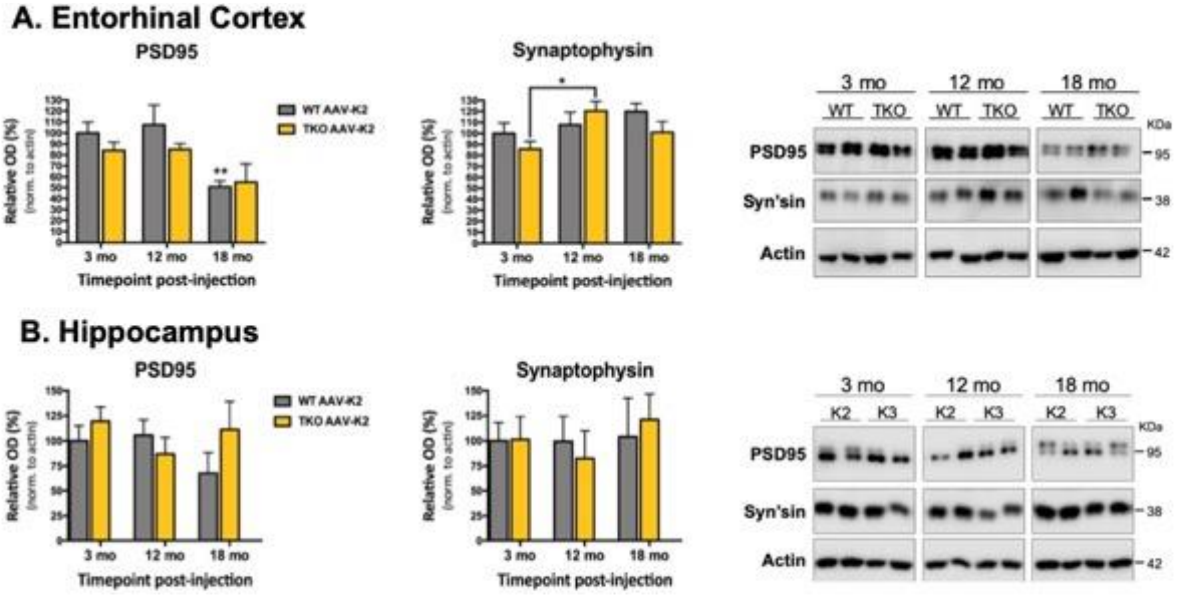

Figure 57 - Levels of pre- and post-synaptic markers in WT and TKO mice injected with AAV-K2 over time.
A. In the EC fraction, two-way ANOVA showed an overall effect of time on the levels of PSD95 [F(2, 30) = 8.162; p = 0.0015]. Post-hoc analysis with uncorrected Fisher's LSD test showed that the levels of PSD95 decreased at 18 months p. i. in WT AAV-K2 mice compared to 3 months p. i. (p = 0.0060), which was not detected in TKO AAV-K3 mice. The levels of synaptophysin increased at 12 months p. i. in TKO AAV-K2 mice (p = 0.0107), which was not observed in WT AAV-K2 mice. **B.** In the hippocampal fraction, no significant differences were observed on the levels of PSD95 and synaptophysin over time or between genotypes. All numerical data are shown as mean +/- SEM; * denotes the effect of time within the same group. * $p < 0.05$; ** $p < 0.01$.

A summary of the results regarding the expression of synaptic markers in the pro- and anti-aggregant mouse models used in the study is given in table 3.

Table 3 - Summary of the expression of pre-synaptic (synaptophysin) and post-synaptic (PSD95) markers in the entorhinal cortex and hippocampus in all experimental groups.

Genotype	AAV injection	Pre-synaptic (synaptophysin)	Post-synaptic (PSD95)
tTA-EC/K2	AAV-K2	▪ EC: decrease over time ▪ Hipp: no significant differences over time	▪ EC: decrease at 18 mo compared to 12 mo P.I. ▪ Hipp: no significant differences over time
tTA-EC/K3	AAV-K3	▪ EC: no significant differences over time ▪ Hipp: no significant differences over time ▪ No differences compared to tTA-EC/K2	▪ EC: no significant differences over time ▪ Hipp: no significant differences over time ▪ No differences compared to tTA-EC/K2
WT	AAV-K2	▪ EC: no significant differences over time ▪ Hipp: no significant differences over time	▪ EC: decrease at 18 mo & 12 mo compared to 3 mo P.I. ▪ Hipp: decrease at 12 mo compared to 3mo P.I.
WT	AAV-K3	▪ EC: no significant differences over time ▪ Hipp: no significant differences over time ▪ No differences compared to tTA-EC/K2	▪ EC: decrease at 18 mo & 12 mo compared to 3 mo P.I. ▪ Hipp: decrease at 12 mo compared to 3mo P.I. ▪ No differences compared to WT AAV-K2
TKO	AAV-K2	▪ EC: decrease over time ▪ Hipp: no significant differences over time	▪ EC: no significant differences over time ▪ Hipp: increase at 18 mo compared to 3 mo P.I.
TKO	AAV-K3	▪ EC: decrease at 12 mo compared to 3 mo P.I. ▪ Hipp: increase over time ▪ No differences compared to TKO AAV-K2	▪ EC: no significant differences over time ▪ Hipp: no significant differences over time ▪ No differences compared to TKO AAV-K2

4.3. Therapeutic intervention to halt the propagation of tau pathology by a tau aggregation inhibitor

Considering that both pro- and anti-aggregant tau can propagate along the perforant pathway from the EC to other brain regions of the brain, but only pro-aggregant tau induces pathological alterations in the mouse brain, we hypothesized that targeting tau aggregation may represent a potential therapeutic strategy for AD neurodegeneration. Indeed, a drug screening of ~200 000 compounds performed by our group (Pickhardt et al., 2005, 2007), showed that BSc3094, a potent inhibitor of tau aggregation, may have beneficial effects in *in vitro* and *in vivo* models of tauopathy. However, one of the challenges regarding the treatment of brain pathologies is the BBB, which represents an obstacle to compounds. Therefore, strategies to bypass the BBB are of major relevance for the treatment of CNS disorders. Our drug of interest, BSc3094, is effective as an inhibitor of tau aggregation, but has poor BBB permeability. For this reason, we decided to administer the drug via Alzet osmotic pumps, which enabled the direct delivery of BSc3094 into the brain of transgenic mice, thus overcoming the BBB. The selection of the most appropriate mouse model was also a critical point on the experimental design. As BSc3094 is a potent inhibitor of tau aggregation, a mouse model with pronounced formation of NFTs at a young age was necessary.

Furthermore, as the Alzet pump model used was operational for 28 days, and could only be replaced once, this means that the treatment could last only 2 months. As we wanted to start the treatment at a preliminary stage when no aggregates would be present still in the mice, we needed a model that within the two months of treatment would develop NFTs and cognitive deficits. The transgenic mouse model rTg4510 (Ramsden et al., 2005; SantaCruz et al., 2005), expressing human tau containing the P301L mutation, linked with familial FTD, was the most appropriate for this study. rTg4510 mice express high levels of mutant htau compared to the levels of endogenous mouse tau (approximately 13 times higher), and develop progressive age-related NFTs, neuronal loss, and behavioral deficits, which start as early as 2.5 months of age. Therefore, we implanted the Alzet pumps to start the treatment at ~2 months of age (lasting until 4 months of age), in order to test BSc3094.

4.3.1. BSc3094 has poor BBB permeability, but direct intraventricular administration reduces sarkosyl-insoluble tau in transgenic mice

Administration of BSc3094 through i.v. injection (3mg/kg, in PEG400/ddH$_2$O (60:40)) showed that the compound has poor BBB permeability, as the concentration reaching the brain was very low (approximately 70 ng/mL). Furthermore, the half-life of the drug in the brain corresponded to 0.8h (figure 58A), meaning that it is not suitable for a brain-related disease therapeutic approach. Nevertheless, taking into account the optimistic results obtained in our previous experiments (mentioned in the introduction of this thesis), we hypothesized that local delivery of BSc3094 into the brain could produce therapeutic effects. We used a novel state-of-the-art technology for targeted delivery to the CNS, which comprises the use of Alzet osmotic pumps combined with a brain infusion kit (figure 58B). This allowed us to directly infuse BSc3094, at a constant rate of 0.11µL/h over 28 days, into the lateral ventricles of the brain. With this, we expose a variety of brain regions to the drug via the cerebrospinal fluid that bathes the brain. The first step was to determine the appropriate coordinates for the implantation of the cannula in the lateral ventricle of 1.5-2 month old rTg4510 mice. This was made by testing different coordinates for placing the cannula and infusing the brain with a dye (bromophenol blue) followed by dissection and sectioning of the brain (figure 58C). After determining the appropriate coordinates (AP = -0.5 mm; ML = +0.8 mm; DV = -2.5 mm), we tested three different doses of the tau aggregation inhibitor and monitored the effect on the levels of sarkosyl-insoluble tau. The highest dose tested (1.5mM) led to a significant reduction (approximately 70%) in the levels of sarkosyl-insoluble tau in rTg4510 mice (figure 58D), giving us a good indication of the potential therapeutic effect of the drug in this transgenic mouse model of AD.

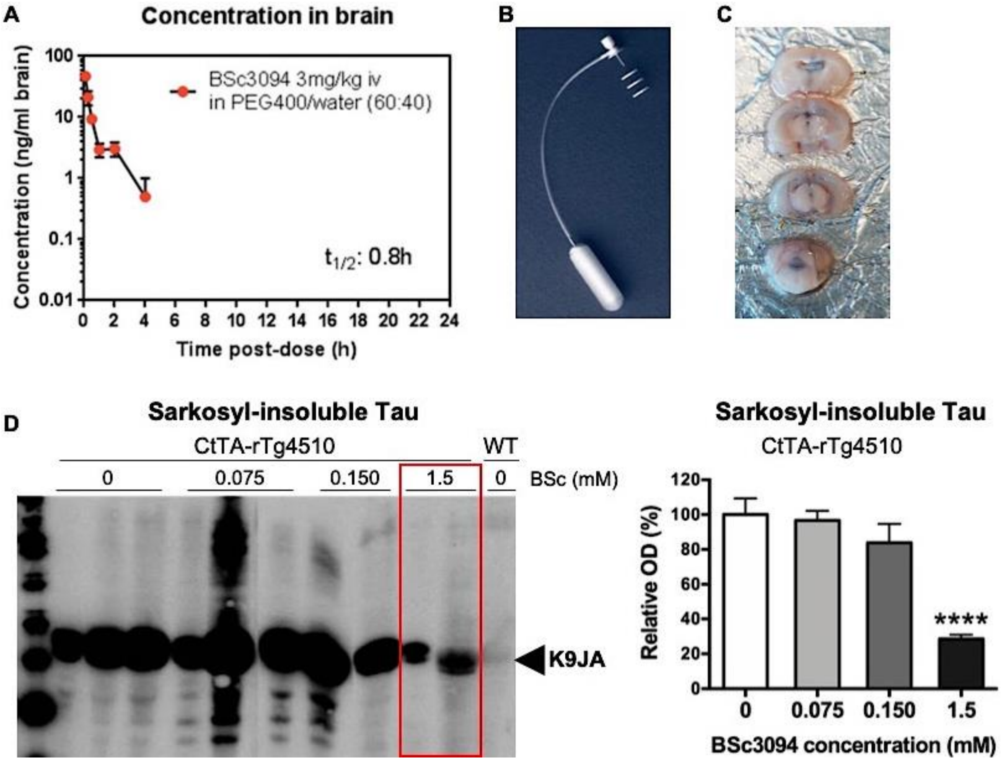

Figure 58 - Intravenous administration of BSc3094 demonstrates poor blood-brain-barrier permeability, but direct intracerebral administration of the drug significantly reduces sarkosyl-insoluble tau.
A. I.v. administration of BSc3094 (3mg/kg in PEG400/water (60:40)) demonstrated poor BBB permeability, as the concentration of drug in the brain was very low compared to the initial administered drug concentration, and the half-life of the drug in the brain equaled 0.8h, meaning its potential therapeutic effect wears off in an extremely short period of time. **B.** Model of a fully assembled Alzet osmotic pump with brain infusion kit, which allows the intracerebral delivery of BSc3094 to a desired brain region. **C.** Sections of a mouse brain infused with bromophenol blue to determine the appropriate coordinates for the implantation of the cannula into the lateral ventricle. The lateral ventricles, as well as the fourth ventricle, were filled with the blue dye. **D.** Direct intraventricular administration of 3 increasing doses of BSc3094 over 28 days into the brains of rTg4510 mice led to a significant reduction (approximately 70%) of sarkosyl-insoluble tau achieved with the 1.5 mM drug concentration (one-way ANOVA with uncorrected Fisher's LSD post-hoc test; $p < 0.0001$). All numerical data are shown as mean +/- SEM; * denotes the significance compared to 100% (no drug). **** $p < 0.0001$.

Based on these findings, we designed an experiment to test BSc3094 on a mouse model of tauopathy. rTg4510 mice expressing the P301L tau mutation were used in the study, as they recapitulate the tau pathology and pronounced neurodegeneration observed in human tauopathies. rTg4510 mice and littermate controls (figure 59A) were treated with BSc3094 (1.5mM in PEG400/ddH_2O (60:40)) or vehicle (PEG400/ddH_2O (60:40)) for 2 months. Briefly, Alzet osmotic pumps (containing drug or vehicle) were implanted at 2 months of age. The treatment was performed over 28 days, after which Alzet osmotic pumps were replaced by new ones to extend the treatment for further 28 days. One week after the pump was replaced, the behavioral assessment started, lasting until the end of the treatment, when mice were sacrificed at 4 months of age (figure 59B).

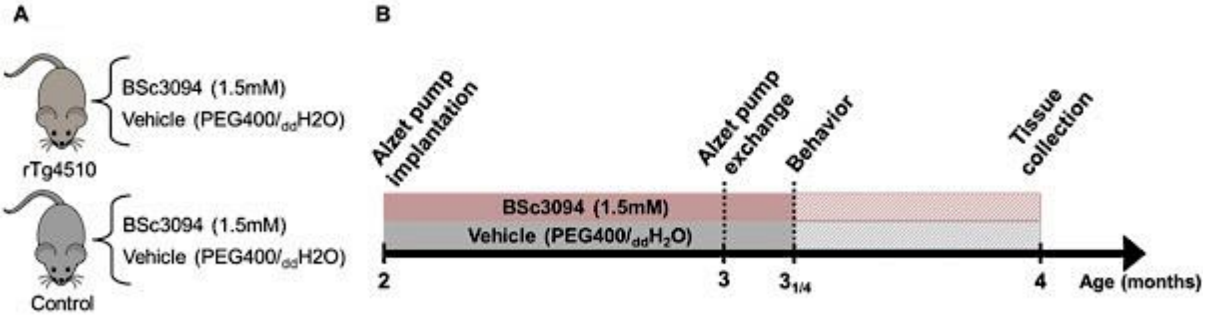
A
B
BSc3094 (1.5mM)
Vehicle (PEG400/ddH2O)
rTg4510
BSc3094 (1.5mM)
Vehicle (PEG400/ddH2O)
Control
Alzet pump implantation
Alzet pump exchange
Behavior
Tissue collection
BSc3094 (1.5mM)
Vehicle (PEG400/ddH2O)
2
3
3 1/4
4
Age (months)

Figure 59 - Experimental design for testing the putative therapeutic effect of BSc3094.
A. Experimental groups used in the study. Double transgenic rTg4510 mice, expressing the htau P301L mutation, and littermate non-transgenic controls were treated with BSc3094 (1.5mM per day) or with the vehicle solution (PEG400/$_{dd}H_2O$ (60:40)). **B.** Experimental timeline of the project. The Alzet osmotic pumps were implanted in control and transgenic animals at 2 months of age to begin the administration of BSc3094 or vehicle. After 28 days (3 months of age), the osmotic pumps were replaced by new ones to continue the treatments and, one week later, the behavioral assessment started, lasting until the end of the treatment (tissue collection at 4 months of age).

4.3.2. rTg4510 mice have decreased brain and body weight compared to littermate controls, which is not reversed by BSc3094 treatment

Previous results demonstrated that rTg4510 transgenic mice present lower total brain weight compared to littermate controls (Ramsden et al., 2005; SantaCruz et al., 2005), which was found to correlate with a concomitant lower body weight (Helboe et al., 2017). Similar to previous reports, we observed a significant decrease in the total brain weight of rTg4510 mice compared to control mice (figure 60A). This effect was not reversed by treatment with BSc3094. Furthermore, the BW of transgenic animals was significantly lower than the BW of controls (figure 60B), an effect not reversed by treatment with BSc3094.

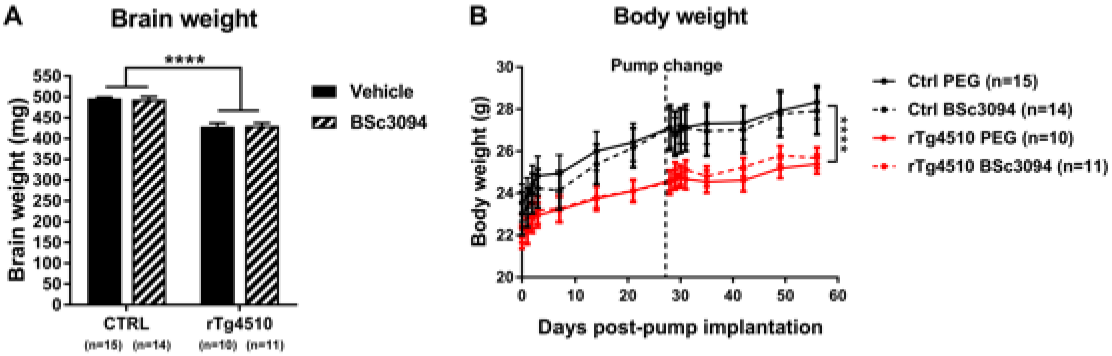

Figure 60 - Total brain and body weight in rTg4510 and control mice used in the study. **A.** Representation of the total brain weight (in mg) at the moment of sacrifice. A two-way ANOVA analysis showed an overall effect of the genotype [F(1, 46) = 112.8; $p < 0.0001$], with double transgenic rTg4510 mice presenting a lower brain weight compared to control mice. Further post-hoc analysis with Tukey's multiple comparison test showed that vehicle-treated rTg4510 mice had significantly lower brain weight than vehicle-treated controls ($p < 0.0001$). Similarly, BSc3094-treated rTg4510 mice also presented lower brain weight than BSc3094-treated controls ($p < 0.0001$). There was no effect of the drug treatment. **B.** Representation of the BW over time, from the pump implantation until the sacrifice date, showed that double transgenic mice had a decreased BW compared to the control littermates [F(1, 472) = 69.92; $p < 0.0001$]. Similar to the brain weight, the drug treatment did not reverse the BW loss observed in the transgenic mice. All numerical data are shown as mean +/- SEM; * denotes the effect of the genotype; **** $p < 0.0001$.

4.3.3. BSc3094 treatment does not reverse the impairments in burrowing and nest building in rTg4510 mice

Despite not reversing the brain weight and BW loss in transgenic mice, we analyzed the effect of BSc3094 treatment in the behavior of the animals. Nest building and burrowing performance, assessed in the home cage, are tools for evaluating brain malfunction, as well as neurodegenerative diseases (Deacon, 2012). Reduction of these behaviors is an early sign of dysfunction and disease progression. Therefore, changes in nest building and burrowing performance provides a global idea of the mouse's state and aids monitoring animal well-being. rTg4510 mice presented a significantly lower percentage of burrowing compared to control animals (figure 59A). Treatment with BSc3094 did not reverse the impairment in burrowing behavior. Similarly, in the nesting test we observed that rTg4510 mice present a significantly lower nesting scores at 2h and 6h after the introduction of the new nest compared to control mice (figure 61B), which was not reversed by treatment with BSc3094.

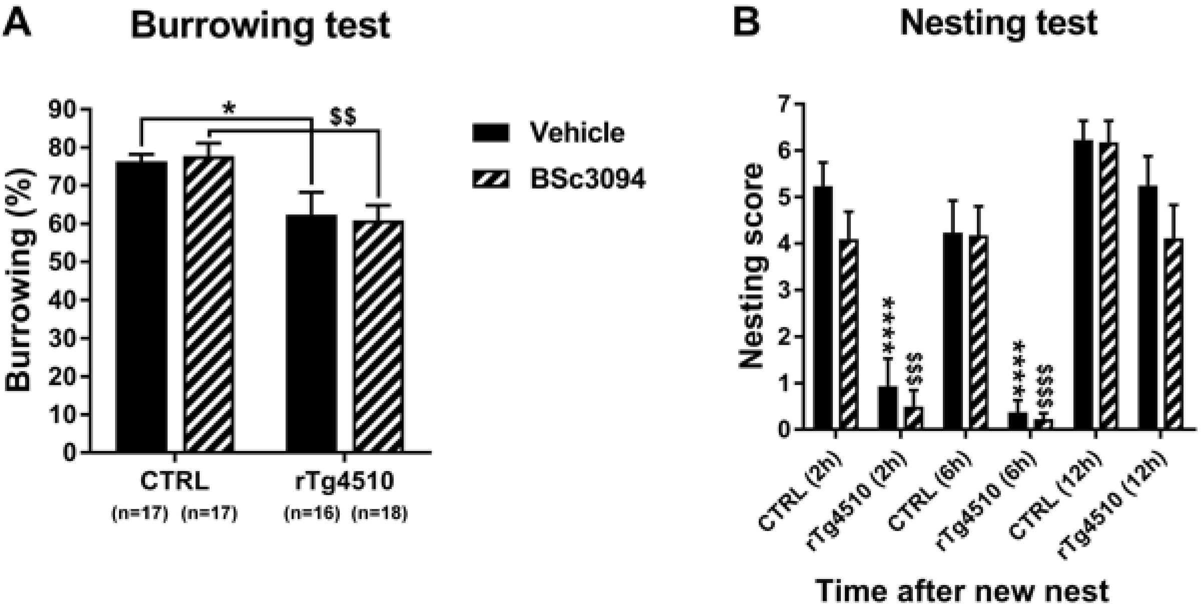

Figure 61 - Burrowing and nesting tests showed that BSc3094 does not rescue the behavioral deficits in rTg4510 mice.
A. rTg4510 mice presented a significant reduction in the percentage of burrowing compared to control animals, an effect that was not reversed with Bsc3094 treatment. Two-way ANOVA revealed an overall effect of the genotype [F(1, 62) = 15.2; p = 0.0002]. Further post-hoc analysis with uncorrected Fisher's LSD test showed that vehicle-treated rTg4510 mice presented lower percentage of burrowing compared to vehicle-treated controls (p = 0.0153). Similarly, BSc3094-treated transgenic mice also presented lower percentage of burrowing than BSc3094-treated controls (p = 0.0037). **B.** rTg4510 mice presented lower nesting scores at 2 and 6 hours after the introduction of the new nest, which was not reversed by BSc3094 treatment [overall effect of genotype, F(5, 191) = 41.53]. Vehicle-treated rTg4510 presented lower nesting scores compared to vehicle-treated controls at 2h (p < 0.0001) and 6h (p < 0.0001) after the introduction of the new nest. Similarly, BSc3094-treated mice presented lower nesting score compared to BSc3094-treated controls at 2h (p = 0.0002) and 6h (p < 0.0001) after introduction of the new nest. At 12 hours after the introduction of the new nest, rTg4510 perform as good as control animals, and BSc3094 treatment produces a reduction on the nesting score, although not significant. All numerical data are shown as mean +/- SEM; * denotes the effect of the genotype in vehicle-treated mice; $ denotes the effect of the genotype in BSc3094-treated mice. * p < 0.05; ** p < 0.01; ***, $$$ p < 0. 001; ****, $$$$ p < 0.0001.

4.3.4. rTg4510 transgenic mice do not show motor impairment, but anxiety-like behavior in the open field

Assessing motor impairment in experimental animals is important because this could affect the result of behavioral tests that rely on locomotor activity (e.g. MWM), simply because the mice cannot move as well as controls. The OF test was used to evaluate general locomotor activity levels, anxiety and willingness to explore in rodent models for scientific research (Seibenhener and Wooten, 2015). Mice display a natural aversion to bright open areas, but they have a drive to explore a perceived threatening stimulus. Increased levels of anxiety in the mice result in a lower distance traveled and a preference to stay near the walls of the OF arena instead of in the center. Our results showed that rTg4510 transgenic mice did not display locomotor impairments, as no significant differences were found between control and transgenic mice in the distance traveled in the OF on both days of the test (figure 62A and B). On the other hand, analyzing the time spent in the center of the OF arena showed that vehicle-treated rTg4510 mice spent a significant lower percentage of time in the center of the arena compared to vehicle-treated controls on day 1 (figure 62C). Similarly, on day 2, vehicle-treated rTg4510 mice presented a lower percentage of time spent in the center of the arena compared to vehicle-treated controls, confirming the anxiety-like behavior in transgenic mice (figure 62D). This phenotype was not observed in rTg4510 mice after treatment with BSc3094, showing that the drug produced a positive effect in anxiety-like behavior.

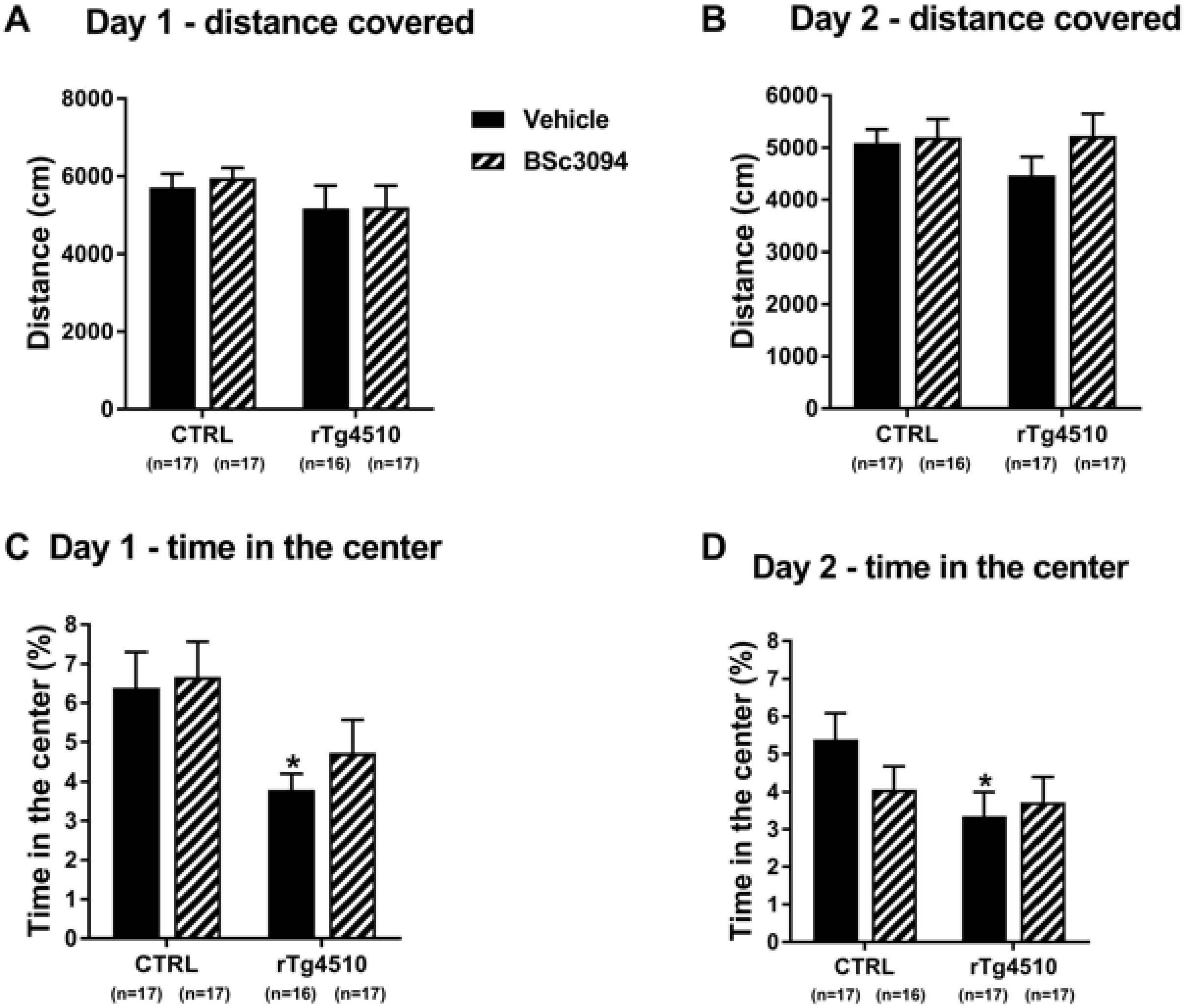

Figure 62 - No motor impairments observed in rTg4510 mice, but a slight increase in anxiety-like behavior compared to control mice.
rTg4510 mice presented similar distance covered values on days 1 **(A)** and 2 **(B)** of the OF test compared to control mice, showing that they did not have significant motor impairments that could affect the results of the behavioral assessment. On the other hand, an overall effect of the genotype was observed in the time spent in the center of the arena on day 1 **(C)** (two-way ANOVA, [F(1, 62) = 7.745; p = 0.0071]). Uncorrected Fisher's LSD post-hoc test revealed that vehicle-treated rTg4510 mice presented lower percentage of time in the center of the arena compared to vehicle-treated

controls (p = 0.0306), which is an indicator of anxiety behavior. On day 2, a similar pattern was observed, with vehicle-treated rTg4510 mice presenting a lower percentage of time spent in the center of the arena **(D)** compared to vehicle-treated controls (p = 0.0330). This reduction in the time spent in the center of the arena was not observed in rTg4510 mice on days 1 and 2 after treatment with BSc3094, showing that the drug produced a positive effect in anxiety-like behavior. All numerical data are shown as mean +/- SEM; * denotes the effect of the genotype; * p < 0.05.

4.3.5. BSc3094 treatment reverses the memory impairment in rTg4510 mice in the novel object recognition test, but not in the y-maze test

To assess recognition memory in the experimental animals, the NOR test was performed. This test is based on the assumption that when animals are exposed to a familiar and a novel object, they typically spend more time exploring the novel rather than the familiar one, due to their natural propensity for novelty (Ennaceur, 2010). rTg4510 mice treated with vehicle spent a significantly lower percentage of time in the novel object during the NOR test (figure 63). This effect was reversed by treatment with the aggregation inhibitor, as BSc3094-treated rTg4510 mice spent a significantly higher percentage of time exploring the new object than vehicle-treated rTg4510 mice.

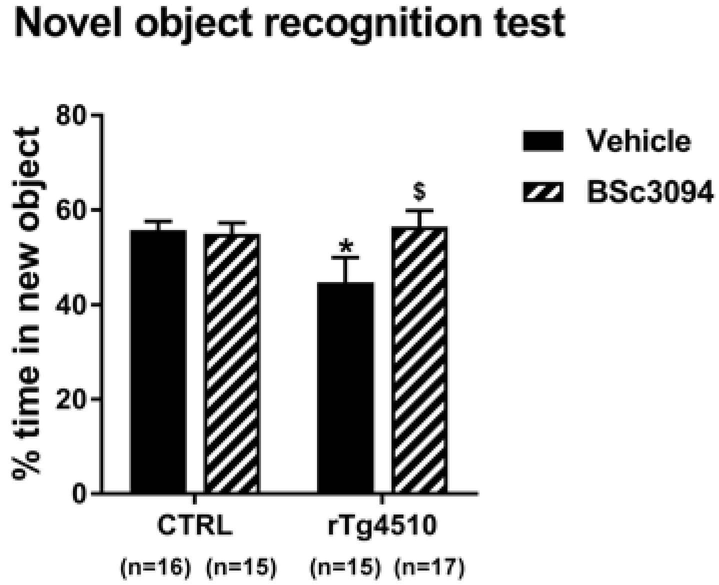

Figure 63 - BSc3094 treatment reversed the memory deficits in rTg4510 mice in the novel object recognition test.
A two-way ANOVA analysis followed by uncorrected Fisher's LSD post-hoc test revealed that vehicle-treated rTg4510 mice spent a lower percentage of time exploring the novel object in the NOR test compared to controls (p = 0.0291). This memory impairment was reversed by BSc3094 treatment, as drug-treated rTg4510 mice spent a significantly higher percentage of time exploring the novel object compared to vehicle-treated transgenic mice (p = 0.0171). All numerical data are shown as mean +/- SEM; * denotes the effect of the genotype; $ denotes the effect of BSc3094 treatment. *, $ p < 0.05.

On the other hand, despite the positive results obtained in the NOR test, the drug failed to revert the memory impairment in the y-maze test. By analyzing the arm preference in the y-maze test (figure 64), we observed that control mice, either treated with vehicle or BSc3094, presented a significantly lower preference for the old arm. Transgenic mice treated with vehicle did not show any preference for the old or new arm of the y-maze, a sign of memory impairment. This was also observed in BSc3094-treated rTg4510, showing that the drug did not revert the memory impairments that rTg4510 mice present in the y-maze test.

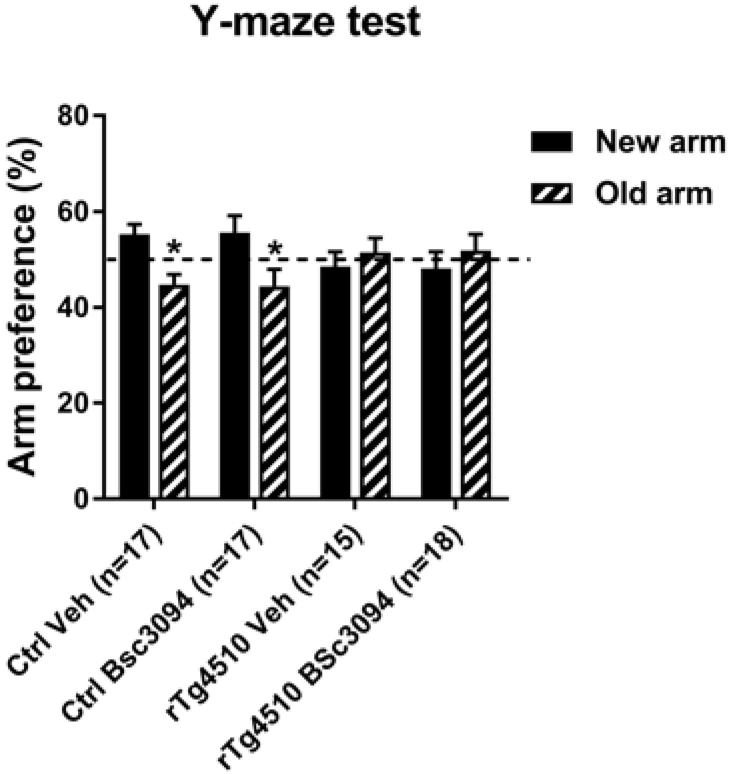

Figure 64 - BSc3094 did not improve spatial reference memory in rTg4510 mice.
Vehicle- and BSc3094-treated control mice presented a lower preference for the old arm in the y-maze test. A two-way ANOVA analysis revealed an interaction between genotype and treatment [F(3, 122) = 3.414; p = 0.0197]. Further post-hoc analysis with uncorrected Fisher's LSD test showed a decreased preference for the old arm in vehicle-treated control mice (p = 0.024) and in BSc3094-treated control mice (p = 0.0112). In contrast, vehicle-treated rTg4510 mice showed no preference for the new or old arm, reflecting impaired spatial reference memory. These deficits in the transgenic mice were not reversed by BSc3094 treatment. All numerical data are shown as mean +/- SEM. * p < 0.05 when compared to new arm preference.

4.3.6. BSc3094 improves long-term memory in the Morris Water Maze test

Another behavioral test performed to evaluate the therapeutic effects of BSc3094 was the MWM test, which assesses spatial memory and learning. We observed that control mice presented a significantly lower latency to escape than transgenic mice throughout all days of learning (figure 65A). Indeed, vehicle-treated transgenic mice presented an increased latency to escape compared to vehicle-treated controls. A similar effect was observed in BSc3094-treated rTg4510 in comparison to BSc3094-treated controls, with transgenic mice performing worse in the MWM, showing that BSc3094 treatment did not reverse the increased escape latency observed in transgenic mice during MWM. During the probe trials (figure 65B) control mice, either treated with vehicle or BSc3094, spent a significantly increased percentage of time in the target quadrant compared to transgenic mice, once more reflecting the impaired spatial memory in rTg4510 mice. This effect was not reversed by BSc3094 treatment in rTg4510 mice, as no significant differences were observed between vehicle-treated and rTg4510-treated transgenic mice. On the other hand, analyzing the percentage of time in the target quadrant in the long-term probe trial (72 hours after the last training trial) (figure 65C) showed that, although vehicle-treated rTg4510 mice spent a significantly lower percentage of time in the target quadrant compared to controls, this memory impairment was reversed by BSc3094 treatment.

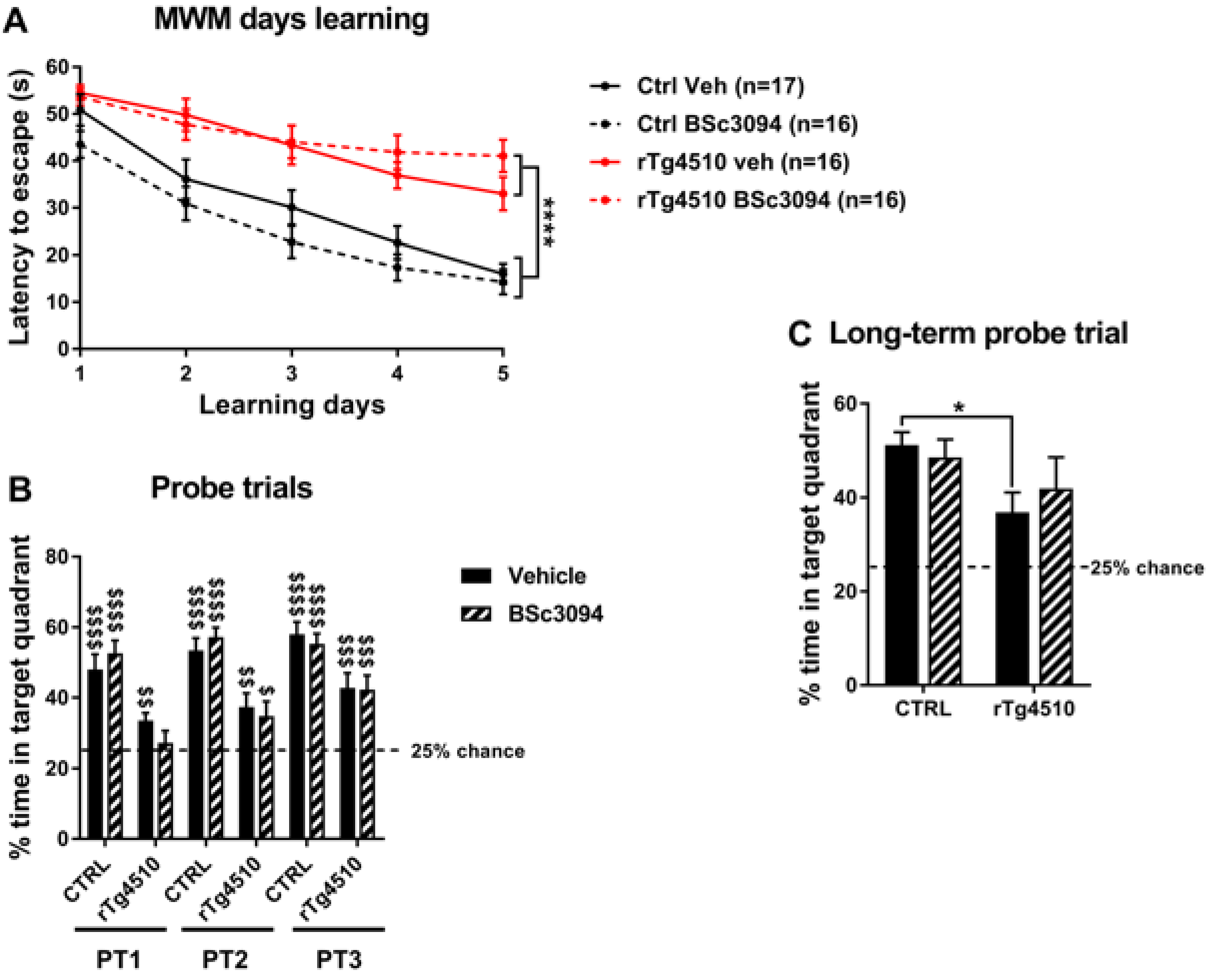

Figure 65 - BSc3094 treatment slightly improved long-term memory in the MWM test.
A. Two-way ANOVA analysis revealed an overall effect of the genotype on the latency to escape in the MWM [F(3, 305) = 42.88]. Vehicle-treated rTg4510 mice presented a significantly increased latency to

escape in the MWM test compared to vehicle-treated controls ($p < 0.0001$). This memory deficit was not reversed by BSc3094 treatment, as drug-treated rTg4510 mice also presented an increased latency to escape compared to BSc3094-treated controls ($p < 0.0001$). **B.** By comparing the percentage of time of the animals in the target quadrant with the 25% chance of exploration we observed that transgenic mice spent a lower percentage of time in the target quadrant of the MWM in the 3 probe trials performed compared to control mice, and effect that was not reversed by treatment with BSc3094. **C.** A two-way ANOVA analysis of the percentage of time in the target quadrant in the long-term probe trial denoted an overall effect of the genotype [$F(1, 62) = 5.309$; $p = 0.0246$]. Further post-hoc analysis with uncorrected Fisher's LSD test showed that vehicle-treated rTg4510 mice spent a significantly lower percentage of time in the target quadrant in the long-term probe trial compared to vehicle-treated controls ($p = 0.0246$), an effect that was partially reversed by BSc3094 treatment. All numerical data are shown as mean +/- SEM; * denotes the effect of the genotype; $ denotes the significance compared to 25% chance of exploration of the target quadrant. *, $ $p < 0.05$; $$ $p < 0.01$; $$$ $p < 0.001$; ****, $$$$ $p < 0.0001$.

4.3.7. BSc3094 treatment reduces the level of phosphorylated tau species in rTg4510 mice

Besides analyzing the potential therapeutic effect of BSc3094 by monitoring different behavioral tasks in the mice, including memory, we also assessed the effect of the drug in markers of tau pathology. As expected, rTg4510 mice treated with vehicle presented significantly higher levels of phosphorylated tau at Ser262, detected with 12E8 antibody, compared to control mice (figure 66A). Interestingly, BSc3094 treatment was able to revert the increase in tau phosphorylation levels. A similar pattern was observed when analyzing the phosphorylation levels at another epitope, Ser396/Ser404 (detected by PHF-1 antibody). Vehicle-treated transgenic mice presented a significant increase in the phosphorylation levels at this epitope compared to control mice (figure 66B), which was reversed by treatment with BSc3094.

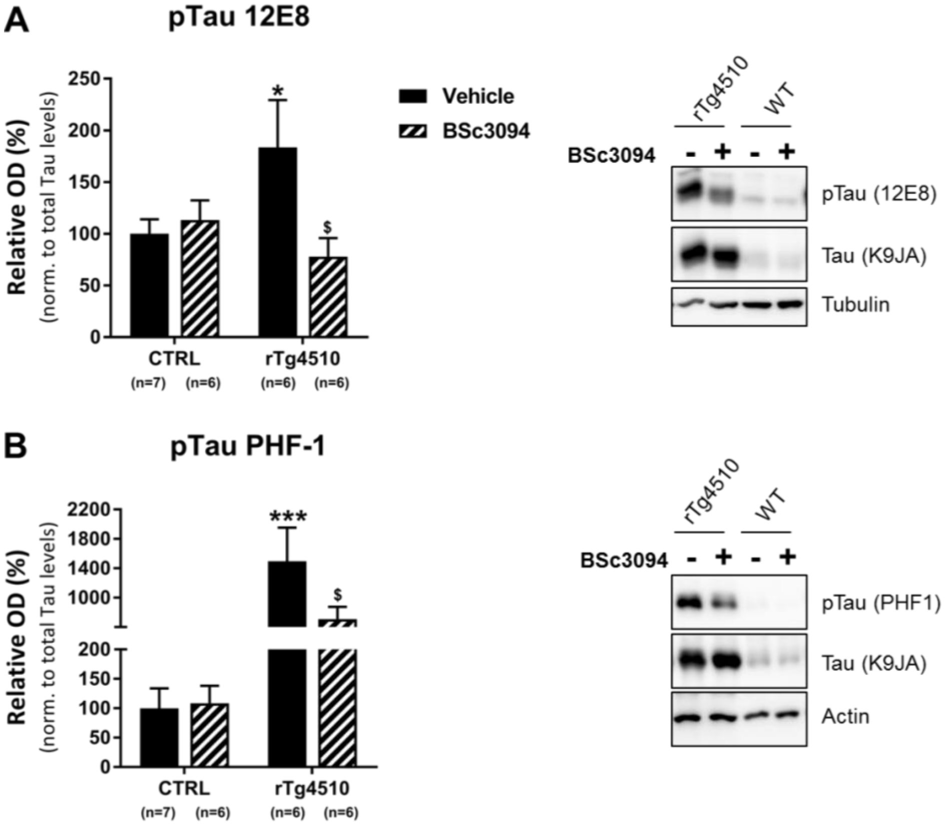

Figure 66 - Treatment with BSc3094 significantly reduced tau phosphorylation in rTg4510 mice. **A.** A two-way ANOVA analysis demonstrated an interaction between genotype and treatment on the levels of 12E8 [F(1, 22) = 4.32; p = 0.0495]. Further post-hoc analysis with uncorrected Fisher's LSD test showed that rTg4510 mice presented an increase in the levels of 12E8 compared to control animals (p = 0.429), an effect that was reversed by BSc3094 treatment (p = 0.0160). **B.** An overall effect of the genotype was detected regarding the levels of PHF-1 [F(1, 22) = 14.58; p = 0.0009]. Uncorrected Fisher's LSD post-hoc test showed that the phosphorylation at the epitope Ser396/ser404, detected with PHF-1 antibody, was increased in vehicle-treated rTg4510 compared to controls (p = 0.0007). This effect was reversed by treatment with BSc3094 (p = 0.0452). All numerical data are shown as mean +/- SEM; * denotes the effect of the genotype; $ denotes the effect of BSc3094 treatment. *, $ p < 0.05; *** p < 0. 001.

4.3.8. BSc3094 treatment has no effect on the expression of glutamate receptor and synaptic markers

We also analyzed the levels of GluR1 in the experimental animals (figure 67). Transgenic mice presented significantly lower levels of GluR1compared to control mice. BSc3094-treated rTg4510 mice also presented significantly lower levels of GluR1 compared to control mice, showing that the anti-aggregant drug did not revert the loss of GluR1 observed in rTg4510 mice.

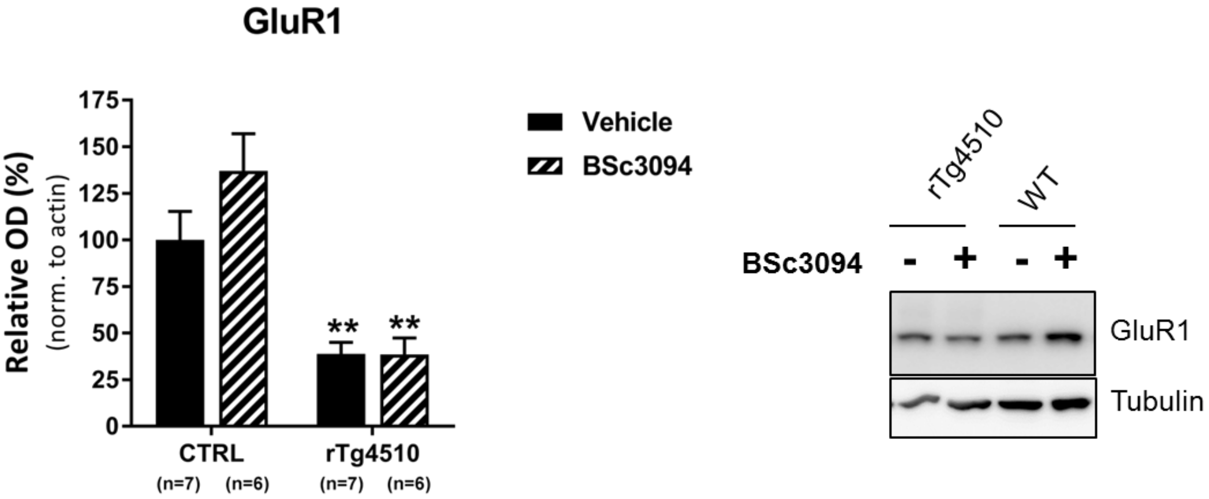

Figure 67 - BSc3094 did not reverse the loss of glutamate receptor 1 in rTg4510 mice. A two-way ANOVA analysis denoted an overall effect of the genotype on the levels of GluR1 [F(1, 22) = 35.08; p < 0.0001]. Further uncorrected Fisher's LSD post-hoc test showed that vehicle-treated rTg4510 mice presented significantly lower levels of GluR1 compared to vehicle-treated control mice (p = 0.0030), a decrease that was also observed in BSc3094-treated rTg4510 mice (p = 0.0039), demonstrating the inefficacy of the drug to reverse the loss of GluR1 observed in the transgenic mice. All numerical data are shown as mean +/- SEM; * denotes the effect of the genotype; ** p < 0.01.

In addition, we analyzed the potential effect of BSc3094 in reversing the loss in pre- and post-synaptic markers typically observed in rTg4510 mice. Our results showed that rTg4510 mice have lower levels of PSD95 (figure 68A) and synaptophysin (figure 68B), compared to control mice. Treatment with BSc3094 did not reverse the decrease in pre- and post-synaptic markers observed in the transgenic mice, as drug-treated rTg4510 mice presented lower levels of PSD95 and synaptophysin compared to control mice.

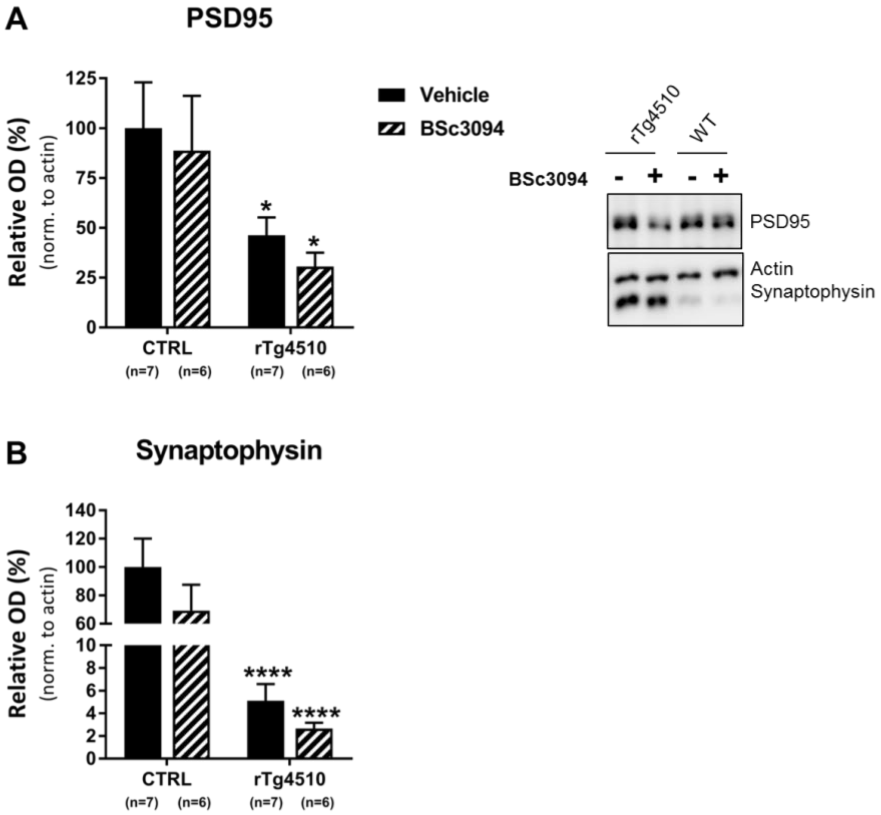

Figure 68 - BSc3094 treatment did not reverse the loss in the expression of synaptic markers in rTg4510 mice.

A. Two-way ANOVA analysis showed an overall effect of the genotype [F(1, 22) = 8.982; p = 0.0066] on the levels of PSD95. Further uncorrected Fisher’s LSD post-hoc test indicated that vehicle-treated rTg4510 mice presented significantly lower levels of PSD95 compared to vehicle-treated control mice (p = 0.0456), a decrease that was also observed in BSc3094-treated rTg4510 mice (p = 0.0153), demonstrating that the drug treatment did not reverse the loss in the expression of PSD95. **B.** Analysis of synaptophysin expression with two-way ANOVA showed an overall effect of the genotype [F(1, 22) = 34.24; p < 0.0001]. Further post-hoc analysis with uncorrected Fisher’s LSD test showed that vehicle-treated rTg4510 mice presented significantly lower levels of synaptophysin compared to control mice (p < 0.0001), an effect that was not reversed by BSc3094 treatment (p < 0.0001). All numerical data are shown as mean +/- SEM; * denotes the effect of the genotype; * p < 0.05; **** p < 0.0001.

5

DISCUSSION

5. Discussion

Despite considerable progress in our understanding of the pathophysiology of neurodegenerative diseases, AD remains a complex and multifactorial disorder with undefined course(s). Over the last years, several theories arose to explain the onset and propagation of tau pathology throughout the brain. Still, studies using *in vitro* and *in vivo* models were not able to answer some of the fundamental questions in the field. Understanding the mechanisms underlying the initiation and progression of tau pathology, as well as the potential involvement of external factors, including neuroinflammation, is important towards the prevention and treatment of the disease.

AD, the most common neurodegenerative disorder, is characterized by the intraneuronal aggregation of the MT-associated protein tau (Grundke-Iqbal et al., 1986) and deposition of Aβ plaques (Price et al., 1991). In contrast to AD, where mutations have not been found in the tau gene (MAPT), patients presenting FTD with parkinsonism associated with chromosome 17 (FTDP-17) exhibit tau mutations (Buée et al., 2000; Dujardin et al., 2014). These mutations have been used to develop animal models with tau aggregation to study the role of this protein in tauopathies (Duyckaerts et al., 2008; Götz and Ittner, 2008). However, the relevance of using these mutations for AD research is debatable, as mutated tau has different properties than WT tau (e.g. higher nucleation process). Furthermore, in FTDP-17 there is not a specific unique neuronal network affected by tau pathology, while certain sporadic tauopathies display hierarchical pathways of degeneration (Chang et al., 2008). An example is AD, where tau pathology follows a well-established pathway defined by the Braak stages, beginning in the EC, spreading to the hippocampal formation and eventually invading the entire cerebral cortex over time (Braak and Braak, 1991; Duyckaerts et al., 1997; Delacourte et al., 1999). Other tauopathies, like PSP or argyrophilic grain disease, also follow a specific hierarchical pathway of fibrillary degeneration (Verny et al., 1996; Saito et al., 2004). Despite its debatable relevance, tau mutations have been widely used for the development of cellular and animal models of AD.

5.1. Propagation of tau pathology in mouse models of early Alzheimer disease

To study the spreading of tau pathology throughout the brain, different models expressing mutant htau have been used over the last years. An important aspect to consider while studying this mechanism is the fact that htau must be initially restricted to a brain region, and the spreading of the protein or pathology is studied from that region onwards. Mainly two strategies have been used so far: 1) transgenic mouse models with tau transgene expression under the regulation of the neuropsin promoter, which restricts the expression of mutant htau to the EC; 2) stereotaxic injections into a specific brain region of WT or transgenic mice with AAV encoding different tau mutants, PFFs, or brain homogenates from patients or mouse models of AD. Regarding the first example, the rTgTauEC mouse has been widely used as a model of early AD (de Calignon et al., 2012). These transgenic mice overexpress htau P301L restricted to EC layer II neurons, where tau pathology starts developing in transgene-expressing neurons. Over time, tau pathology propagates first to neighboring neurons in the EC region without transgene expression, and later to neurons in synaptically connected regions such as the DG, CA fields of the hippocampus, and cingulate cortex.

5.1.1. Transgenic mice expressing pro- and anti-aggregant human tau under the neuropsin promoter as models of tau spreading

Similarly, we used transgenic tTA-EC/K2 and tTA-EC/K3 mice, which express htau-ΔK280 (pro-aggregant) and htau-ΔK280-2P (anti-aggregant), respectively, under the neuropsin promoter (restricted to the EC). Using a specific antibody for htau (HT7) and BLI measurements in *ex vivo* brain slices we confirmed the EC-restricted expression of both pro- and anti-aggregant htau in the neuropsin mice. Furthermore, our results partly recapitulated the findings of de Calignon et al., 2012, as we observed phosphorylated tau (12E8 and AT180 antibodies) and pathological conformation (MC1 antibody) in the EC region of pro-aggregant mice at different ages. Anti-aggregant neuropsin mice did not present tau with pathological conformation, but presented tau phosphorylation in the EC, although in a lesser extent than pro-aggregant mice. Contrary to the findings of de Calignon et al., 2012, our animals did not express Gallyas or ThioS positive neurons in the EC (results not shown). In addition, mutant htau was present in the EC region and along the perforant pathway, but no trans-synaptic spreading of tau protein was observed in the neuropsin mice up to 24 months of age. We also did not observe propagation of the markers of tau pathology (phosphorylation and pathological conformation) from the EC to other brain regions, contrasting with the observations in rTgTauEC mice. Therefore, pro- and anti-aggregant htau, initially restricted to the EC, was transported along the EC axons via the perforant pathway up to the axon terminals in the outer molecular layer of the DG, where the synapses between EC axon terminals and apical dendrites from DG granule cells occur, but did not move forward to the next cell layer (the granule cell layer of the DG).

The expression of markers of astrogliosis (GFAP) and microgliosis (Iba1) in the EC and DG presented no differences between pro-aggregant, anti-aggregant and WT non-transgenic mice up to 24 months of age. In contrary, de Calignon et al., 2012 observed a higher number of GFAP labeled astrocytes in the brains of rTgTauEC mice compared to controls and increased microglial activation at 24 months of age in the molecular layer of the DG. As the neuropsin mice and the rTgTauEC mice express similar levels of htau compared to the endogenous mtau (approximately 20%), the different experimental outcome cannot be explained by differences on the expression level of htau. However, the fact that the models contain two distinct tau mutations (htau-ΔK280 and htau-P301L) may contribute to the differences observed in the development of pathology and its propagation. Besides the differences in the mouse models, the use of different brain embedding methods, tissue preparation and staining protocols could also contribute to the differences. Specifically, we used 5 μm-thick paraffin sections and performed IHC with DAB, while in the other study frozen 40 μm-thick sections and IF were used.

Despite the advantages of the neuropsin model, recently the robustness of the promoter has been questioned (Yetman et al., 2016). By performing a systematic analysis of Nop-tTA expression using a LacZ reporter, the authors confirmed that the highest density of tTA expression is observed in the EC and pre-/parasubiculum, but also revealed considerable expression in several other cortical areas. Indeed, expression was found to be robust in occipital, temporal and cortical areas, with weaker expression in several other brain regions. Contrary to these findings, we did not find htau positive cells outside the EC and perforant pathway in the neuropsin model up to 24 months of age. The discrepancy between the results might be accounted for by several factors, including the use of different methods to check the specificity of Nop-tTA expression. Most groups, including ours, rely on *in situ* hybridization, RT-PCR, or immunohistology to detect expression of the tet-responsive mRNA or protein of interest (Harris et al., 2010; de Calignon et al., 2012; Liu et al., 2012; Rowland et al., 2013), instead of checking the specificity of Nop-tTA expression using colorimetric or fluorescent responder lines. Furthermore, other factors may influence the expression pattern of some promoters, including age (Long and Rossi, 2009), epigenetic modifications (Swain et al., 1987; Akitake et al., 2011), and the strain background on which the transgene is expressed (Opsahl et al., 2002; Robertson et al., 2002; Lehman et al., 2003; Han et al., 2012; Strong et al., 2012).

5.1.2. Combining AAV-directed gene transfer with neuropsin mice to boost the propagation of tau pathology

We assumed that the fact that we did not observe trans-synaptic spreading of tau protein and tau pathology in the tTA-EC/K2 and tTA-EC/K3 mouse models was related to the low expression of the mutant htau transgene. To create an accelerated model for the spreading of tau pathology, we combined the neuropsin mouse models with stereotaxic injections of AAV in the EC encoding the same tau mutants (ΔK280 and ΔK280-2P) that the mice already expressed. This led to a successful increase in the levels of htau compared to the PBS-injected hemisphere or non-injected mice. The AAVs used also encoded GFP besides htau-ΔK280 or htau-ΔK280-2P, and both sequences were separated by a 2A self-cleaving peptide, which ensures the independent expression of both proteins (GFP and htau). To monitor the spreading of htau protein, we considered the htau$_+$/GFP$_-$ cells as htau "recipient cells", which received htau from the "donor cells" that were initially transfected by the AAV and were, therefore, htau$_+$/GFP$_+$.

Other authors injected K18 tau seeds in the hippocampal CA1 region of rTg4510 mice and analyzed the spreading of tau pathology from the injection site to interconnected areas (Peeraer et al., 2015). The K18 tau seeds are PFFs consisting of an aggregated synthetic htau fragment containing the MT-binding repeat domain with a P301L mutation (Barghorn et al., 2005). Similarly, other authors injected K18 tau seeds in PS19 transgenic mice expressing the P301S mutation (Iba et al., 2013). Both studies showed that intracerebral inoculation of rTg4510 or PS19 mice results in a rapid induction of NFT-like inclusions around the injection site, which can propagate from this region to anatomically connected brain areas distant from the injection site in a time-dependent manner.

Despite the relevance of these approaches as models of fast spreading of tau pathology, several aspects should be considered. First, the injection of PFFs usually only produces an effect when injected into the brain of a transgenic mouse. Injection of PFFs into the brain of control non-transgenic mice does not induce tau aggregation and propagation of tau pathology (Peeraer et al., 2015). Therefore, besides injecting a relatively high amount of synthetic tau fibrils, a background where high levels of mutant htau and tau pathology are present is also necessary for the effects observed. These conditions are more artificial than what happens in the brains of sporadic AD patients and, therefore, we believe that our model represents a more physiological condition. Furthermore, the fact that in our study htau was initially restricted to the EC mimics the initial stages of tau pathology in AD, while other authors performed injections in the hippocampus or cortex and studied the propagation of the pathology from these injection sites to interconnected regions. In addition, injection into a relatively small region like the CA1 may increase the possibility of errors during the injection procedure. These errors can be due to an incorrect injection site, but also because the volume to be injected may be greater than what the CA1 layer can accommodate, which would lead to part of the injected solution flowing to other regions. Besides this, the withdrawal of the stereotaxic syringe may cause backflow of the injected solution to other regions, giving a false positive for the spreading of tau pathology.

Hence, small differences in experimental design might account for the conflicting results, but the observed differences are also likely to be related to genetic background differences in the mouse strains employed in these studies. Furthermore, mice may also recover differently, and distinct levels of inflammation may be induced during/after stereotaxic surgery, which can affect the course of tau pathology developed. As a conclusion, both neuropsin and injection models have pros and cons which we need to be aware of to be critical about the experimental results.

5.1.3. The propagation of tau protein is independent of the aggregation potential

In the neuropsin injected mice (tTA-EC/K2 and tTA-EC/K3), both pro-aggregant htau (ΔK280) and anti-aggregant htau (ΔK280-2P) propagated from the EC to other brain regions. This was confirmed by the presence of tau “recipient cells” ($htau_+/GFP_-$) in brain regions anatomically connected with the EC, like the granule cell layer of the DG. The fact that these cells express htau but not GFP means that they were not initially transfected with the AAV but received htau from a “donor cell”, located in the EC and initially transfected with the AAV. As both pro- and anti-aggregant htau can propagate from the EC this demonstrates that the ability of tau protein to spread across cells is independent of the protein's aggregation potential. Similarly, in WT and TKO mice injected with AAV-K2 (pro-aggregant htau) and AAV-K3 (anti-aggregant htau), tau "recipient cells" (htau$_{+}$/GFP$_{-}$) were observed in brain regions anatomically connected to the EC, including the granule cell layer of the DG, and pyramidal cells of CA1 and CA3. This confirms that pro- and anti-aggregant htau was able to spread from one cell layer to the next, meaning that the ability of tau protein to spread across cells is independent of its aggregation potential. Moreover, our observations also corroborate the idea that tau does not spread in a "prion-like" manner, as tau does not need to have a pathological conformation to be transferred from cell to cell, as it is necessary in the case of PrP$_{Sc}$.

Although in several experimental animals we observed the propagation of htau alone, which easily allowed us to detect the trans-synaptic spreading of tau, we also observed the expression of GFP in several other brain regions rather than the EC in other animals. This adds a confounding parameter because if a cell outside the EC is htau$_{+}$ we have to be careful when considering this as trans-synaptic spreading of tau protein if the cell is also GFP$_{+}$. Our data suggests that GFP itself may also be able to spread independently from cell to cell, as the AAV constructs used contain the cleaving agent 2A, which ensures the independent expression of GFP and the htau transgene. In fact, if the spreading of tau occurs via synaptic connections it is expected that GFP, if it can be released and taken up by cells, will most likely follow the same stereotypical pattern for propagation. We also cannot exclude that errors in the injection site/injection procedure may have occurred, leading to the presence of GFP$_{+}$ cells where they were not expected, although this is unlikely.

To further monitor the impact of the presence of pro- and anti-aggregant htau, the BW of the animals was monitored weekly from the date of stereotaxic surgery. At 5 months of age, before AAV injection, no differences were observed on the BW between groups. On the other hand, at 18 months p. i., the BW of WT AAV-K2 mice was significantly lower than the BW of WT AAV-K3 mice. A similar tendency was observed between the injected tTA-EC/K2 and tTA-EC/K3 mice, with the mice expressing pro-aggregant htau presenting a lower BW, although not significant. This suggests a potential deleterious effect of the expression of pro-aggregant mutant htau in tTA-EC/K2 and WT AAV-K2 mice, due to the lower BW compared to the animals expressing anti-aggregant htau.

The BW of TKO AAV-K2 mice was significantly higher than the BW of WT AAV-K2 mice, suggesting that the absence of endogenous mouse tau might protect against the BW loss caused by the expression of pro-aggregant htau. Other studies have shown that, although the absence of endogenous mouse tau does not prevent the spreading of mutant tau from the EC to the rest of the brain, it reduces the extent of pathology developed (Wegmann et al., 2015). The authors also revealed features of tau that differ from expectations based on the prion-like model of tau propagation and toxicity (previously described in this thesis). In particular, mutant htau, either in ECrTgTau mice or AAV-mediated P301L tau expression, could be released by donor neurons and taken up and be detected weeks to months later in recipient neurons, even if endogenous tau was missing. Therefore, aggregated tau remains for substantial periods of time in the recipient cells without a requirement for templated misfolding of endogenous tau to “maintain” the aggregate, as is necessary in case of PrP (Weissmann, 2004). However, the absence of endogenous mouse tau markedly reduced the extent of pathology in rTg4510 mice, showing that although the absence of endogenous mouse tau does not alter the propagation of tau protein, it reduces tau pathology. An explanation is that the conformational changes resulting from the co-aggregation of endogenous mouse tau with human P301L tau may create toxic strains of tau aggregates (Sanders et al., 2014).

5.1.4. Absence of trans-synaptic propagation of markers of tau pathology

Although we observed that tau protein was able to spread from the EC to the next interconnected brain region in both pro- and anti-aggregant mouse models, we did not observe spreading of markers of tau pathology in our mouse models. Similar to the observations in neuropsin non-injected mice, we detected phosphorylated tau (with PHF-1 antibody, Ser396/Ser404) in the EC of the pro-aggregant models (tTA-EC/K2, WT AAV-K2 and TKO AAV-K2) and anti-aggregant models (tT-EC/K3, WT AAV-K3 and TKO AAV-K3). Once more, the expression of phosphorylated tau was more prominent in the pro-aggregant models, as expected based on the previous evidences. Despite observing phosphorylated tau in the EC region of the mice, phosphorylated tau species were not observed in other brain regions but were confined to the injection site. An exception was observed in WT mice injected with AAV-K2 or AAV-K3, where

PHF-1+ cells were additionally detected in the granule cell layer of the DG and pyramidal cell layer of the CA1, although in a sparse number.

On the other hand, staining with MC1 antibody, specific for pathological conformation of tau, showed that only pro-aggregant mouse models present tau with pathological conformation. This was restricted to EC neurons and perforant pathway up to the axon terminals in the outer molecular layer of the DG, not spreading to any further cell layer. Therefore, if there was htau in the DG or other brain region in these mice, it still did not acquire any pathological conformation/features. Thus, in our mouse models there is no propagation of tau pathology from the EC to other brain regions. Although pathological alterations in tau are observed in the EC, these remain confined to this area and do not propagate to the rest of the brain. Worth mentioning is that in WT AAV-K2 and TKO AAV-K3 mice MC1$_+$ cells were detected in the DG, but due to the fact of being also GFP$_+$ we cannot consider this as spreading of pathology, based on our initial definition of spreading (cells must be GFP$_-$).

Our results diverge from other studies previously mentioned, where AT8$_+$ neurons, as well as MC1$_+$ and ThioS$_+$ cells have been found in regions connected to the injection site (Iba et al., 2013; Peeraer et al., 2015). These differences may be related to the fact that our mutated htau is initially restricted in the EC, while on these studies PFFs were injected in the hippocampus or cortex from where tau pathology may spread more easily, although this hypothesis still needs to be tested. Also, the fact that we are using animals with different genetic background and different tau mutations, as well as the differences in the injected solutions (AAV *vs.* PFFs) may account for the discrepancies in the experimental outcome. Since we are using a pro-aggregant mutant form of tau, we hypothesize that the protein may aggregate readily on the injection site (EC) and is not so easily released and taken up by cells, preventing the pathology from propagating. Indeed, a recent study analyzed the impact of distinct tau isoforms or mutations on the process of tau aggregation and tau propagation (Dujardin et al., 2018). In human neuropathological material MAPT mutations induce a faster protein misfolding compared to the non-mutated tau found in sporadic AD patients. Furthermore, in the rat brain, the species of tau has an impact in the propagation of markers of tau pathology like hyperphosphorylation and misfolding. In fact, the spreading rate of misfolded and hyperphosphorylated tau protein is different in the presence of a tau mutation or when the isoform composition is altered. In agreement, a previous study using different immunological tools to follow phospho-tau species, showed that tau pathology generated using mutated htau remains near the injection site, whereas it spreads much further using WT htau, resembling the propagation of pathology happening in AD brains (Dujardin et al., 2014). These results clearly demonstrate the presence of specific folding properties of tau, related to the isoform composition or mutations present, that affect the behavior of pathological tau species. It is also important to highlight that the fact that tau aggregates are the toxic tau species responsible for the pathology is still debatable. Indeed, recent evidences have weakened this hypothesis and suggested that other factors, like neuroinflammation, may be the culprit for the pathology observed in the AD brain (Ishizawa et al., 2004; Ising et al., 2019; Vogels et al., 2019).

5.2. Role of neuroinflammation in the onset and propagation of tau pathology

Increasing evidences suggest that the pathological mechanisms in AD are not restricted to the neuronal compartment, but strongly interact with immunological mechanisms in the brain (Heneka et al., 2018). Indeed, neuroinflammation in AD is not a simple bystander activated by the appearance of senile plaques or NFTs, but actually contributes to the same extent or more to the pathogenesis as plaques and tangles themselves (Zhang et al., 2013; Heneka et al., 2018). This is emphasized by recent findings that genes for immune receptors, including TREM2 (Guerreiro et al., 2013) and CD33 (Bradshaw et al., 2013), are associated with AD. Activated microglia, astrocytes and increased levels of proinflammatory molecules are additional pathological hallmarks observed in the brain regions affected by tau pathology (Leyns and Holtzman, 2017). In recent years, there has been abundant research to understand the role of gliosis and neuroinflammation in neurodegenerative diseases, particularly AD. It has been shown that both microglia and astroglia contribute to the onset and propagation of tau pathology throughout the brain. As an example, the assembly of the NLRP3 inflammasome inside microglia upon activation leads to the downstream release of IL-1β, which regulates the activity of kinases and phosphatases, having a direct impact on the pathogenesis of tau protein and contributing to the worsening of tau pathology (Ising et al., 2019). Furthermore, microglia activation positively correlates with tau pathology, and microglia can spread tau via exosome secretion, contributing to the progression of the pathology (Asai et al., 2015; Wang et al., 2017). Indeed, the same study showed that depletion of microglia suppressed the propagation of tau, providing robust evidence for the involvement of microglia in the pathogenesis of AD. Furthermore, several transgenic mouse models of AD present astrocyte activation in the affected brain regions, frequently before the development of mature plaques and/or tangles. This suggests that astrocytosis is involved in AD pathogenesis, possibly preceding the development of tangles or plaques (Garwood et al., 2010, 2011).

5.2.1. Neuroinflammation may precede the propagation of tau pathology

Based on the hypothetical involvement of neuroinflammation in the onset and propagation of tau pathology, we analyzed the expression of markers for astrocytosis (GFAP) and microgliosis (Iba-1 or CD11b) both by immunofluorescence and WB. In tTA-EC/K2 mice, at 3 months p. i., staining for GFAP was more pronounced in the hippocampal region compared to the EC, although most of the htau and tau with pathological changes is located in the EC. This suggests that the activation of astrocytes in the hippocampus might precede the propagation of tau pathology form the EC to the hippocampus and be the result of a signaling mechanism arising in the EC that induces astrogliosis. In tTA-EC/K3 mice we did not observe differences in the expression of GFAP between the EC and hippocampus and, overall, the animals expressed lower levels of GFAP than the pro-aggregant mice. This difference was further confirmed by WB using the GFAP antibody, which showed that pro-aggregant mice express higher levels of astrogliosis compared to anti-aggregant mice at 12 and 18 months after AAV injection. Regarding the expression of microglia, both immunofluorescence with Iba1 antibody and WB with CD11b antibody revealed no differences in the levels of microglia between the injected pro- and anti-aggregant mice at the time points analyzed.

Similar to the findings in neuropsin-injected mice, in WT mice staining with GFAP antibody was more pronounced in the hippocampal region of WT AAV-K2 mice than in the EC region. In WT AAV-K3 mice we did not observe a differential expression of GFAP between the EC and the hippocampus, and again these animals had an overall lower expression of GFAP compared to WT AAV-K2 mice. This observation was further confirmed by WB analysis using the GFAP antibody, with WT AAV-K2 mice presenting higher levels of GFAP compared to WT AAV-K3 mice in the EC and hippocampus at all time points analyzed, although not significant. Together with the results from the neuropsin injected mice, this shows that in mice expressing pro-aggregant htau there is increased astrogliosis in the hippocampal region compared to the anti-aggregant models, which is likely to be correlated with the pathological changes in tau observed in the EC of these mice. We hypothesize that the appearance of the first signs of pathology in the EC signals other brain regions, possibly through the release of proinflammatory cytokines. This would then lead to the initiation of inflammatory processes in those brain regions (like the hippocampus), starting the pathological cascade that will later contribute to neurodegeneration. In addition, immunofluorescence and WB analysis of microglia levels in WT mice showed that, at 3 months after AAV injection, no significant differences exist between WT AAV-K2 and WT AAV-K3 mice. However, the levels of the microglial marker CD11b increased over time in the EC and hippocampus of WT AAV-K2 mice, which was not observed in the WT AAV-K3 mice. This increase in the levels of microglia is likely to be a response to the development of tau pathology in the EC region of these mice.

Regarding the levels of microglia and astrogliosis in injected TKO mice a different tendency was observed. Staining with GFAP was still more prominent in the hippocampal region of TKO AAV-K2 mice compared to the EC region, in agreement with the previous mouse lines. However, the same was observed in TKO AAV-K3 mice. WB analysis with the GFAP antibody showed no differences between TKO AAV-K2 and TKO AAV-K3 at the time points analyzed, but a similar increase in GFAP levels over time in the EC and hippocampal fractions of both experimental groups. Regarding the levels of microglia, WB with the CD11b antibody showed no significant differences at 3 months p. i. between TKO AAV-K2 and TKO AAV-K3 mice. However, at 12 and 18 months p. i., TKO AAV-K2 mice present significantly higher levels of CD11b compared to TKO AAV-K3 mice, both in the EC and hippocampal fractions. This is likely to be a response to the development of pathological alterations in these animals, due to the expression of mutant pro-aggregant htau in the EC.

Overall, the increase in the levels of GFAP in the pro-aggregant mouse models is likely to be a consequence of the expression of mutant htau that induces pathological alterations in the EC of these mice, which in turn activates neuroinflammatory pathways. However, based on the evidences implicating microglia in the pathogenesis and spreading of tau, we expected to observe higher levels of microglia in the pro-aggregant models too compared to the anti-aggregant mice. Furthermore, despite in neuropsin and WT mice we observed that GFAP levels were higher in the mice expressing pro-aggregant tau compared to the ones expressing anti-aggregant tau, a different pattern was observed in TKO mice. The fact that the same level of GFAP was observed in TKO AAV-K2 and TKO AAV-K3 mice may result from the absence of endogenous mouse tau. Indeed, when we compared WT AAV-K2 with TKO AAV-K2 mice, we also observed that the levels of GFAP increase over time in the EC fraction of TKO mice, which was not observed in WT mice. This again reinforces that the absence of endogenous mouse tau may induce a higher activation of astrocytes. However, further studies are needed to shed light on the relation between astrogliosis and the different forms of tau. Other studies also analyzed the expression of inflammatory markers upon induction of tau pathology. Indeed, Peeraer et al., 2015, observed abundant astrogliosis and microgliosis after PFF injection, closely correlating with the induced tau pathology. Similarly, Ahmed et al., 2014 also identified a subtle increase in microgliosis in tau transgenic mice 2.5 months after infusion with P301S brain extracts. Despite no obvious nerve cell loss in this model, the increase in Iba1 staining might be indicative of an early inflammatory response to neurodegeneration. Since neuroinflammation occurs before we see apparent cell loss in the model of Peeraer et al., 2015, the authors hypothesized that aggregated tau stresses the neurons triggering microglial and astroglial phagocytosis as an early inflammatory response in a pathogenic mechanism.

Finally, we analyzed the levels of pre- and post-synaptic markers in all experimental groups over time. In the tTA-EC/k2 mice, the levels of PSD95 and synaptophysin decreased over time in the EC fraction, which was not observed in tTA-EC/K3 mice. This suggests the presence of synaptic deficits, likely as a result of the presence of pro-aggregant mutant htau which induces pathological changes in the EC of these mice. In WT mice we did not detect differences on the levels of synaptophysin at all time points analyzed. However, WT mice injected with AAV-K2 presented a significant decrease on the levels of PSD95 over time in the EC and hippocampal fractions, which was not observed in WT AAV-K3 mice and is once more likely to be a consequence of the expression of mutant pro-aggregant htau and concomitant pathological changes.

The analysis of pre- and post-synaptic markers in TKO originated conflicting results. In the EC fraction we observed a significant decrease over time in the levels of synaptophysin in TKO AAV-K2 mice, which was not observed in TKO AAV-K3 mice. However, in the hippocampal fraction the levels of synaptophysin remained unchanged in TKO AAV-K2 mice, but significantly increased over time in TKO AAV-K3 mice. Regarding the postsynaptic markers, we did not observe differences between TKO AAV-K2 and TKO AAV-K3 mice in the EC fraction, but the levels of PSD95 significantly increased over time in TKO AAV-K2 mice. Previous studies showed that knockout of tau protein leads to an upregulation of the tau homolog protein MAP1A and modification of the axon caliber to one typically found in dendrites (Harada et al., 1994). Furthermore, other authors have shown an age-dependent reduction of synaptophysin levels in TKO mice, along with a significant reduction of post-synaptic excitatory markers (NR2B, PSD95, Fyn, drebrin), especially in aged TKO mice (Ma et al., 2014), concomitant with deficits in the MWM test and loss of functional MAPS. Further studies have to be performed to understand the impact of the absence of endogenous mouse tau in the spreading of tau pathology and in its effect on the expression of synaptic markers.

In summary, we observed that in the AAV-injected mouse models both pro- and anti-aggregant htau propagate between cells from the EC to other regions. This shows that the aggregation propensity of tau does not interfere with its ability to spread across cells. However, only pro-aggregant tau induces pathological changes, and these remain mostly confined to the EC and perforant pathway. No trans-synaptic spreading of markers of tau pathology to the next layer of cells (DG) was observed, as these remained around the injection site. Furthermore, no differences were observed in the levels of microglia between pro- and anti-aggregant models, but astrogliosis was increased in the pro-aggregant models compared to the anti-aggregant. These evidences suggest that the activation of astrocytes in the hippocampal region may be an early event that precedes the propagation of tau pathology from the EC to the hippocampus. More studies are needed to shed light on the inflammatory mechanisms in the pathogenesis of AD, with potential implications for the development of novel therapeutic strategies. Furthermore, it is of major relevance to clearly distinguish between the spreading of tau protein across cells and the propagation of pathology throughout the brain (figure 69).

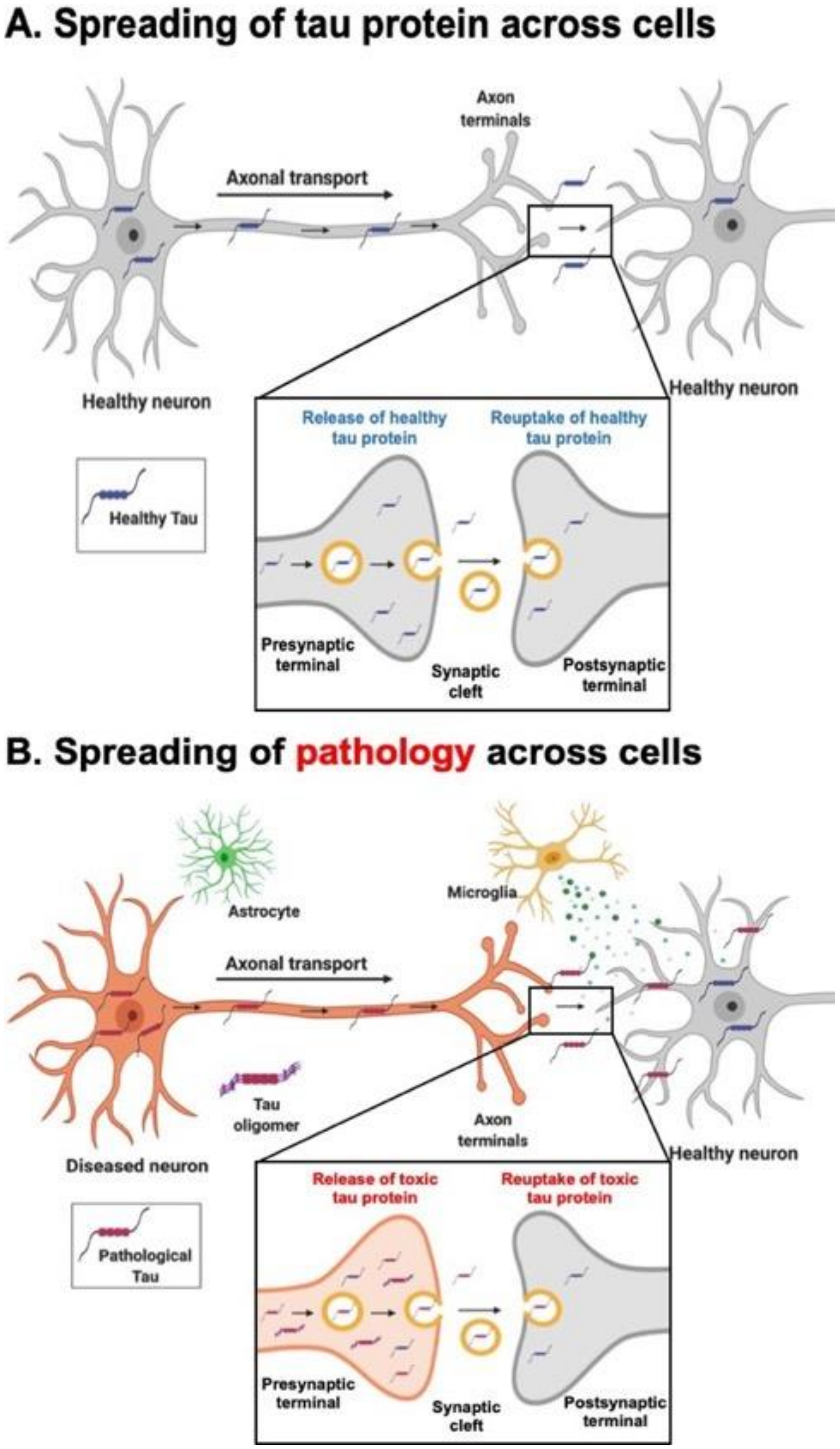
A. Spreading of tau protein across cells
Axon terminals
Axonal transport
Healthy neuron
Healthy neuron
Healthy Tau
Release of healthy tau protein
Reuptake of healthy tau protein
Presynaptic terminal
Synaptic cleft
Postsynaptic terminal
B. Spreading of pathology across cells
Astrocyte
Microglia
Axonal transport
Tau oligomer
Axon terminals
Diseased neuron
Healthy neuron
Pathological Tau
Release of toxic tau protein
Reuptake of toxic tau protein
Presynaptic terminal
Synaptic cleft
Postsynaptic terminal

Figure 69 - Schematic representation of the spreading of tau protein and tau pathology.
A. Healthy tau protein (in blue) can be transported along an axon up to the axon terminals of the neuron. This process of axonal transport is unrelated to the trans-synaptic spreading of the protein. The healthy tau in the axon terminals of a donor neuron may be released to the extracellular space via different mechanisms (e.g. exocytosis, exosome release), and be taken up by the next acceptor cell

(e.g. endocytosis, exosome uptake). This process of trans-synaptic spreading of tau protein does not involve spreading of pathology. Note that any event of exocytosis or endocytosis can transfer proteins across cell boundaries. **B.** Under certain conditions, tau (or some other factor X) may acquire toxic properties (e.g. misfolded tau, red). This pathological agent may also be transported along the axon, then released and taken up by other cells. In the acceptor neurons, the pathological tau (or agent) will produce a toxic effect and possibly convert the healthy tau into a misfolded toxic species to propagate the toxic cascade. Importantly, other players may also contribute to the spreading of pathology and their role cannot be ruled out (e.g. microglia releasing pro-inflammatory cytokines, etc.). In that case, misfolding of tau may be a hallmark rather than the cause of pathology.

5.3. Therapeutic intervention to halt the propagation of tau pathology

In light of the increased understanding of the physiological and pathological roles of tau, and advances in animal models of tauopathy, novel targets have been identified contributing to the development of new drug candidates. Several drug candidates targeting tau have so far progressed into clinical testing, including anti-tau vaccines and aggregation blockers. Other strategies have been developed that do not target tau directly, but targets involved in pathways with a putative role in tau-mediated toxicity, such as MT stabilizers and small molecules to block tau hyperphosphorylation and acetylation (Li and Götz, 2017).

5.3.1. Tau aggregation inhibitors as therapeutical agents for AD and other tauopathies

Although controversial, it is believed that tau-mediated neurodegeneration arises, at least partly, from the protein’s aggregation capacity. As a consequence, tau aggregation inhibitors became potential therapeutic agents for diseases encompassing tau pathology, including AD. Two major approaches have been followed for tau aggregation: 1) the search for inhibitors of kinases that phosphorylate tau, based on the assumption that phosphorylation promotes tau aggregation (Kosik and Shimura, 2005; Kelleher et al., 2007; Bulic et al., 2009); 2) the search for direct inhibitors of the tau aggregation process. Regarding the latter, methylene blue has been tested to reverse the proteolytic stability of protease-resistant tau filaments by blocking the tau-tau interaction thought the MT-binding domain (Wischik et al., 1996; Hochgräfe et al., 2015). Several studies explored the efficacy of methylene blue and, although the drug failed to inhibit tau-dependent toxicity in zebrafish (van Bebber et al., 2010), the drug efficiently induced autophagy and attenuated tauopathy *in vitro* and *in vivo* (Congdon et al., 2012) and blocked tau aggregation in *C. elegans* (Fatouros et al., 2012). Unfortunately, the drug did not show treatment benefit when tested at two doses in phase III trials involving 891 participants with mild-to-moderate AD (Gauthier et al., 2016), for reasons that remain unclear.

Another potential inhibitor of tau aggregation is BSc3094. Since previous *in vitro* studies from our group showed positive results using this drug, we moved forward into testing BSc3094 in an *in vivo* model of tau pathology, the rTg4510 mouse line. First, we assessed the BBB permeability of BSc3094 through i. v. administration of the drug at a dose of 3 mg/kg. This resulted in a maximum concentration in the brain of around 70 ng/ml, and the half-life of the drug was 0.8h, clearly showing that it does not efficiently cross the BBB. For this reason, we delivered the drug directly into the brains of rTg4510 and control littermate mice using Alzet osmotic pumps with brain infusion kit.

5.3.2. BSc3094 as a promising therapeutical agent for tau-related neurodegeneration

BSc3094 monohydrobromide (2-[4-(4-Nitrophenyl)-2-thiazolyl]hydrazide-1H-benzimidazole-6-carboxylic acid monohydrobromide) is a phenylthiazolyl-hydrazide derivative (Pickhardt et al., 2007). BSc3094 has been used in tau protein research to study the processes underlying the aggregation of the protein, as it has the ability to inhibit tau aggregation and dissolve tau PFFs (Pickhardt et al., 2007). Previous studies from our group showed that this compound efficiently reduced tau phosphorylation and aggregation (>82%), increasing at the same time cell viability and having no cytotoxic effects in N2a cells expressing pro-aggregant mutant htau (Pickhardt et al., 2015, 2017). Further studies showed that BSc3094 was capable of reducing the levels of insoluble tau and increase the locomotion speed in a *C. elegans* model of tauopathy expressing pro-aggregant mutant htau (Fatouros et al., 2012). Recently, BSc3094 reversed the pre-synaptic impairment observed in organotypic hippocampal slices from pro-aggregant tau transgenic mice, by reversing the paired-pulse depression observed in non-treated pro-aggregant tau transgenic slices after applying a paired-pulse stimulus of the Schaffer collaterals (Dennissen et al., 2016). Taken together, these results strengthen the hypothesis that BSc3094, a tau aggregation inhibitor, could be a potential therapeutical agent used to reverse tau pathology and, possibly, exert a beneficial effect in AD.

A pilot study performed by us using three different test doses of BSc3094 administered via direct intraventricular infusion using Alzet osmotic pumps showed that the highest dose (1.5 mM) reduced the levels of sarkosyl-insoluble tau in rTg4510 mice, compared to non-treated rTg4510 mice. Therefore, we used this drug dosage for the final experimental design. As BSc3094 is an inhibitor of tau aggregation, it was important to select an appropriate mouse model to test this drug, with extensive NFT pathology at a young age, reason why we selected rTg4510 mice. These animals express the P301L tau mutation, and develop pretangles as early as 2.5 months of age, accompanied by impaired spatial memory (Ramsden et al., 2005; SantaCruz et al., 2005).

5.3.3. Treatment with BSc3094 failed to reverse the body and brain weight loss in rTg4510 mice

The first outcome from the treatment, which was monitored weekly, was the BW of the mice. BSc3094 did not reverse the BW loss typically observed in this transgenic mouse line. Furthermore, at the day of sacrifice, the brain weight was measured. Again, BSc3094 failed to reverse the brain weight loss characteristic in rTg4510 mice. Previous studies showed that rTg4510 mice present a loss of 60% of CA1 neurons at 5.5 months of age, which results in a significant loss in brain weight (Ramsden et al., 2005; SantaCruz et al., 2005). A likely explanation is that pathological alterations that culminate in this extensive neuronal loss start very early in life, so that it reaches a massive reduction in CA1 cells at 5.5 months of age. Therefore, starting the treatment with BSc3094 at 2 months of age may have been too late to reverse or slow down the neuronal loss characteristic of rTg4510 mice, explaining why BSc3094-treated mice also presented a lower brain weight compared to control littermate mice.

5.3.4. Treatment with BSc3094 significantly reduced the levels of phosphorylated and insoluble tau, and partially improved cognition

Despite this, treatment with BSc3094 strongly reduced the levels of phosphorylated tau (detected with both 12E8 and PHF-1 antibodies), as well as the levels of sarkosyl-insoluble tau, which is in agreement with previous *in vitro* studies from our group, plus an indicator that pathological hallmarks may be reduced upon BSc3094 treatment.

In terms of behavioral assessment, treatment with BSc3094 resulted in a reversal of anxiety-like behavior and improvement in certain cognitive tests. Initially, we analyzed locomotor activity in the OF test, to ensure that transgenic mice do not have motor impairments that could lead to differences in the behavioral performance. Although no significant motor impairment was found in rTg4510 mice, we observed an increase in anxiety-like behavior in vehicle-treated transgenic mice, shown by a reduction in the time the mice spent exploring the center of the arena. This phenotype was ameliorated in the BSc3094-treated rTg4510 mice, showing that the drug reduced anxiety-like behavior. Furthermore, BSc3094 treatment reversed the memory impairment in rTg4510 mice in the NOR test, based on the assumption that mice have an innate tendency for exploring a novel environment or object. Vehicle-treated rTg4510 mice spent a significantly lower percentage of time in the new object compared to control mice, showing that they cannot distinguish between the familiar and novel object. On the other hand, BSc3094-treated mice spent a significantly higher percentage of time in the new object compared to the vehicle-treated transgenic mice. Treatment with BSc3094 also improved long-term memory in the MWM maze, as vehicle-treated rTg4510 mice spent a significantly lower percentage of time in the target quadrant during the long-term probe trial (72h after the last training session) compared to control mice. This was partly reversed by treatment with BSc3094, although no beneficial effect was observed on the latency to escape from the water during the MWM learning days or during the other probe trials. Besides this, BSc3094 also failed to reverse the impairments in burrowing and nest building in rTg4510 mice. The treatment with the tau aggregation inhibitor also did not reverse memory deficits observed in the y-maze test, as well as the loss in synaptic markers GluR1, synaptophysin and PSD95 in rTg4510 mice.

Several reasons may explain these conflicting results, including the fact that the different behavioral tasks performed to assess cognition in rTg4510 mice involve different types of memory that require distinct neuronal networks and brain regions for their storage and retrieval (Thompson and Kim, 1996; Ben-Yakov et al., 2015). Furthermore, the extent of tau pathology and the concentration of BSc3094 reaching each part of the mouse brain may be different, which could contribute to the differences. In addition, the implantation of Alzet osmotic pumps and brain infusion kit in young mice (2 months of age) is a delicate surgery, which may also contribute to an increased variability and the conflicting results. As already mentioned, rTg4510 mice develop tangles and memory deficits at a very young age (2.5 months). The levels of mutant htau in this mouse model are also extremely high compared to the levels of endogenous mouse tau (approximately 13 times higher) (Ramsden et al., 2005; SantaCruz et al., 2005). Based on this, the window for a therapeutical intervention in rTg4510 mice is short. We started the treatment as early as possible, as we wanted to avoid the development of pathological changes in the brain that may be irreversible. However, we could not start before 2 months of age because, even using the smaller model of Alzet osmotic pumps, the animals needed to weight at least 20 grams to be able to cope with the subcutaneous implantation of the Alzet pump. This may have been a late start for the therapeutic intervention, which further contributes to the conflicting results.

In a future approach, a different mouse model that develops tau aggregates and pathology at a later stage in life could be considered, as this would allow us to perform an earlier interventional approach. Furthermore, it would also facilitate the implantation of the Alzet osmotic pump, as the use of adult animals would prevent certain issues we experienced. Specifically, as the animals were relatively small at 2 months of age, we had problems during and after the implantation of the Alzet pump because the animals were too small and still growing. This led to the skin opening around the cannula, as it was stretched extensively, allowing the mice to remove the Alzet pump or to disconnect the catheter. Another possibility would be to make use of the regulatable expression of the transgene in the rTg4510 mice. Administration of Doxycycline, a tetracycline analog, would lead to the inactivation of the transgene expression, allowing the animals to grow without developing any pathological changes. This would allow us to perform the BSc3094 treatment later in life, very shortly after stopping the administration of Doxycycline, ensuring that the treatment starts early enough before any pathological changes occur. This would prevent the problems related to the surgery, as older mice could be used.

Another important aspect to mention is the fact that, although BSc3094 treatment resulted in a strong reduction of tau phosphorylation and in the levels of sarkosyl-insoluble tau, there was no robust improvement in terms of memory and cognition. This again suggests that tau aggregates may not be the toxic tau species, but intermediate forms of tau could be causing the pathology and neurodegeneration. Indeed, although inhibiting tau aggregation seems a valid therapeutical strategy for halting tau-mediated neurodegeneration in AD, based on the premise that this protein has a crucial role in tauopathies and drives pathology, this assumption has been questioned over the last years. Currently, it is still unclear which form of tau is pathological and if tau aggregates are the toxic tau species or not. If tau aggregates are not deleterious, this means that tau aggregation inhibitors will produce little or no effect, or even be harmful as we may be reducing the tangle load but increasing the number of small oligomers, which are now proposed to be toxic (Cheng et al., 2007; Necula et al., 2007; Kaniyappan et al., 2017).

Due to the multifactorial nature of AD pathogenesis, which involves a host of environmental and genetic factors, it may be necessary to personalize the preventive or therapeutic approach and combine different strategies that target distinct hallmarks of the disease to achieve a therapeutic effect.

6

Conclusions

6. Conclusions

Histopathological analysis of the brains of AD patients suggests a detrimental role for tau protein, especially in the form of NFTs, in the onset and progression of AD pathology. Recent experimental studies demonstrate that intermediate tau species and the activation of neuroinflammation may also contribute to the disease pathomechanisms. Yet, the mechanistic contribution of different tau species, astrocytes, microglia and pro-inflammatory molecules (including cytokines) remains unclear.

The research presented here provides novel insights regarding the spreading of tau pathology, showing that:

- The spreading of tau protein was independent of the aggregation propensity of tau;
- Only pro-aggregant tau induced pathological alterations;
- Markers of tau pathology did not propagate throughout the brain, but remained in the EC and perforant pathway up to the axon terminals in the molecular layer of the DG;
- The expression of pro-aggregant htau induced an early activation of astrocytes in the hippocampal region that precedes the propagation of tau pathology from the EC to the hippocampus.

The second part of our study, testing the potential therapeutic role of the tau aggregation inhibitor BSc3094, showed that:

- BSc3094 decreased tau phosphorylation at 12E8 and PHF-1 epitopes;
- BSc3094 reduced the levels of sarkosyl-insoluble tau;
- BSc3094 improved cognitive performance in the NOR test and in the long-term probe trial in the MWM test, although it failed to reverse the deficits observed in the MWM learning phase, Y-maze, burrowing and nesting tests;
- BSc3094 did not reverse the BW and brain weight loss characteristic of rTg4510 mice.

Overall, these studies add novel evidence to our understanding of the molecular pathways underlying the spreading of tau pathology, which correlates with cognitive decline, as described in the Braak stages (Braak and Braak, 1991). In addition, we also proposed the use of the tau aggregation inhibitor BSc3094 as a potential therapeutic agent to halt the propagation of tau pathology, although we do not exclude the potential contribution of intermediate oligomeric tau species for the development and progression of pathology (Kaniyappan et al., 2017).

While more studies are necessary, our findings highlight that tau alone is not sufficient for causing the extensive pathology typically observed in AD patients, and inflammatory pathways may be involved as well. This opens new roads to investigate inflammation as a novel therapeutical approach, not only for AD but for other tauopathies beyond AD. However, given the complex pathology of AD, it can be anticipated that combinatorial and individualized treatments should be explored, which could be designed for each patient. These strategies could target tau and Aβ, and also add agents to modulate inflammation, enhance synaptic activity and stimulate neurogenesis and neurite regrowth. Furthermore, improving methods for drug delivery into the brain, combined with the optimization of antibody formats and specificity, would also highly contribute to the success of future therapeutical interventions.

7

References

7. References

Ahmed, Z., J. Cooper, T. K. Murray, K. Garn, E. McNaughton, H. Clarke, S. Parhizkar, M. A. Ward, A. Cavallini, S. Jackson, S. Bose, F. Clavaguera, M. Tolnay, I. Lavenir, M. Goedert, M. L. Hutton, and M. J. O'Neill, 2014, A novel in vivo model of tau propagation with rapid and progressive neurofibrillary tangle pathology: The pattern of spread is determined by connectivity, not proximity: Acta Neuropathologica, v. 127, no. 5, p. 667–683, doi:10.1007/s00401-014-1254-6.

Ahmed, T., A. Van der Jeugd, D. Blum, M. C. Galas, R. D'Hooge, L. Buee, and D. Balschun, 2014, Cognition and hippocampal synaptic plasticity in mice with a homozygous tau deletion: Neurobiology of Aging, v. 35, no. 11, p. 2474–2478, doi:10.1016/j.neurobiolaging.2014.05.005.

Akitake, C., M. Macurak, M. Halpern, and M. Goll, 2011, Transgenerational analysis of transcriptional silencing in zebrafish: Dev. Biol., v. 352, no. 2, p. 191–201, doi:10.1016/j.ydbio.2011.01.002.

Allen, W., 1948, Fiber degeneration in Ammon's horn resulting from extirpations of the pyriform lobe and other cortical areas and from transection of the horn at various levels: J Comp Neurol, v. 88, no. 3, p. 425–438, doi:10.1002/cne.900880305.

Alzheimer's Association, 2017, 2017 Alzheimer's facts and figures: Alzheimer's & Dementia, v. 13, no. 4, p. 325–373, doi:10.1016/j.jalz.2017.02.001.

Alzheimer's Association, 2019, 2019 Alzheimer's Disease Facts and Figures: Alzheimer's & Dementia, v. 15, no. 3, p. 321–387, doi:https://doi.org/10.1016/j.jalz.2019.01.010.

Alzheimer's Disease International, 2018, World Alzheimer Report 2018. The state of the art of dementia research: new frontiers: doi:10.1111/j.0033-0124.1950.24_14.x.

Amaral, D. G., H. E. Scharfman, and P. Lavenex, 2007, The dentate gyrus: fundamental neuroanatomical organization (dentate gyrus for dummies): Progress in Brain Research, v. 163, p. 3–22, doi:10.1016/S0079-6123(07)63001-5.

Andersen, P., B. Holmqvist, and P. E. Voorhoeve, 1966, Entorhinal activation of dentate granule cells: Acta Physiol Scan, v. 66, p. 448–460, doi:10.1038/ncb2299.

Andreadis, A., 2005, Tau gene alternative splicing: expression patterns, regulation and modulation of function in normal brain and neurodegenerative diseases: Biochimica et biophysica acta, v. 1739, no. 2–3, p. 91–103, doi:10.1016/j.bbadis.2004.08.010.

Arendt, T., J. Stieler, A. M. Strijkstra, R. A. Hut, J. Rüdiger, E. A. Van der Zee, T. Harkany, M. Holzer, and W. Härtig, 2003, Reversible paired helical filament-like phosphorylation of tau is an adaptive process associated with neuronal plasticity in hibernating animals: Journal of Neuroscience, v. 23, no. 18, p. 6972–6981, doi:10.1523/jneurosci.23-18-06972.2003.

Aronov, S., G. Aranda, L. Behar, and I. Ginzburg, 2001, Axonal tau mRNA localization coincides with tau protein in living neuronal cells and depends on axonal targeting signal: Journal of Neuroscience, v. 21, no. 17, p. 6577–6587, doi:10.1523/jneurosci.21-17-06577.2001.

Asai, H., S. Ikezu, S. Tsunoda, M. Medalla, J. Luebke, B. Wolozin, O. Butovsky, T. Ikezu, and E. Therapeutics, 2015, Depletion of microglia and inhibition of exosome synthesis halt tau propagation: Nature neuroscience, v. 18, no. 11, p. 1584–1593, doi:10.1038/nn.4132.Depletion.

Audrain, M., J. V. Haure-Mirande, M. Wang, S. H. Kim, T. Fanutza, P. Chakrabarty, P. Fraser, P. H. St George-Hyslop, T. E. Golde, R. D. Blitzer, E. E. Schadt, B. Zhang, M. E. Ehrlich, and S. Gandy, 2018, Integrative approach to sporadic Alzheimer's disease: deficiency of TYROBP in a tauopathy mouse model reduces C1q and normalizes clinical phenotype while increasing spread and state of phosphorylation of tau: Molecular Psychiatry, p. 1383–1397, doi:10.1038/s41380-018-0258-3.

Balaji, V., S. Kaniyappan, E. Mandelkow, Y. Wang, and E. M. Mandelkow, 2018, Pathological missorting of endogenous MAPT/Tau in neurons caused by failure of protein degradation systems: Autophagy, v. 14, no. 12, p. 2139–2154, doi:10.1080/15548627.2018.1509607.

Ballatore, C., K. R. Brunden, D. M. Huryn, J. Q. Trojanowski, V. M. Y. Lee, and A. B. S. III, 2012, Microtubule Stabilizing Agents as Potential Treatment for Alzheimer's Disease and Related Neurodegenerative Tauopathies: Journal of Medicinal Chemistry, v. 55, no. 21, p. 8979–8996, doi:10.1038/jid.2014.371.

Barghorn, S., J. Biernat, and E. Mandelkow, 2005, Purification of Recombinant Tau Protein and Preparation of Alzheimer-Paired Helical Filaments In Vitro, *in* E. M. Sigurdsson, ed., Amyloid Proteins: Methods and Protocols: Totowa, NJ, Humana Press, p. 35–51, doi:10.1385/1-59259-874-9:035.

Barghorn, S., Q. Zheng-Fischhofer, M. Ackmann, J. Biernat, M. Von Bergen, E. M. Mandelkow, and E. Mandelkow, 2000, Structure, microtubule interactions, and paired helical filament aggregation by tau mutants of frontotemporal dementias: Biochemistry, v. 39, no. 38, p. 11714–11721, doi:10.1021/bi000850r.

van Bebber, F., D. Paquet, A. Hruscha, B. Schmid, and C. Haass, 2010, Methylene blue fails to inhibit Tau and polyglutamine protein dependent toxicity in zebrafish: Neurobiology of Disease, v. 39, no. 3, p. 265–271, doi:10.1016/j.nbd.2010.03.023.

Ben-Yakov, A., Y. Dudai, and M. R. Mayford, 2015, Memory retrieval in mice and men: Cold Spring Harbor Perspectives in Biology, v. 7, no. 12, p. 1–28, doi:10.1101/cshperspect.a021790.

Biernat, J., N. Gustke, G. Drewes, E. Mandelkow, and E. Mandelkow, 1993, Phosphorylation of Ser262 strongly reduces binding of tau to microtubules: Distinction between PHF-like immunoreactivity and microtubule binding: Neuron, v. 11, no. 1, p. 153–163, doi:10.1016/0896-6273(93)90279-Z.

Blackmore, T., S. Meftah, T. K. Murray, P. J. Craig, A. Blockeel, K. Phillips, B. Eastwood, M. J. O'Neill, H. Marston, Z. Ahmed, G. Gilmour, and F. Gastambide, 2017, Tracking progressive pathological and functional decline in the rTg4510 mouse model of tauopathy: Alzheimer's Research and Therapy, v. 9, no. 1, p. 1–15, doi:10.1186/s13195-017-0306-2.

Blackstad, T. W., 1956, Commissural connections of the hippocampal region in the rat, with special reference to their mode of termination: Journal of Comparative Neurology, v. 105, no. 3, p. 417–537, doi:10.1002/cne.901050305.

Boutajangout, A., A. Boom, K. Leroy, and J. P. Brion, 2004, Expression of tau mRNA and soluble tau isoforms in affected and non-affected brain areas in Alzheimer's disease: FEBS Letters, v. 576, no. 1–2, p. 183–189, doi:10.1016/j.febslet.2004.09.011.

Boutajangout, A., J. Ingadottir, P. Davies, and E. Sigurdsson, 201AD, Passive immunization targeting pathological phospho-tau protein in a mouse model reduces functional decline and clears tau aggregates from the brain: J Neurochem, v. 118, no. 4, p. 658–67, doi:10.1111/j.1471-4159.2011.07337.x.

Braak, H., and E. Braak, 1996, Development of Alzheimer-related neurofibrillary changes in the neocortex inversely recapitulates cortical myelogenesis: Acta Neuropathologica, v. 92, no. 2, p. 197–201, doi:10.1007/s004010050508.

Braak, H., and E. Braak, 1991, Neuropathological stageing of Alzheimer-related changes: Acta Neuropathologica, v. 82, no. 4, p. 239–259, doi:10.1007/BF00308809.

Braak, H., and E. Braak, 1992, The human entorhinal cortex: normal morphology and lamina-specific pathology in various diseases: Neuroscience Research, v. 15, no. 1–2, p. 6–31, doi:10.1016/0168-0102(92)90014-4.

Braak, F., H. Braak, and E. M. Mandelkow, 1994, A sequence of cytoskeleton changes related to the formation of neurofibrillary tangles and neuropil threads: Acta Neuropathologica, v. 87, no. 6, p. 554–567, doi:10.1007/BF00293315.

Braak, H., and K. Del Tredici, 2011, Alzheimer's pathogenesis: Is there neuron-to-neuron propagation? Acta Neuropathologica, v. 121, no. 5, p. 589–595, doi:10.1007/s00401-011-0825-z.

Bradshaw, E., L. Chibnik, B. Keenan, L. Ottoboni, T. Raj, A. Tang, L. Rosenkrantz, S. Imboywa, M. Lee, A. Von Korff, D. N. I. Alzheimer, M. Morris, D. Evans, K. Johnson, R. Sperling, J. Schneider, D. Bennett, and P. De Jager, 2013, CD33 Alzheimer's disease locus: Altered monocyte function and amyloid biology: Nature Neuroscience, v. 16, no. 7, p. 848–50, doi:10.1126/science.1246980.Common.

Brodmann, K., 1909, Vergleichende Lokalisationslehre der Grosshirnrinde in ihren Prinzipien dargestellt auf Grund des Zellenbaues: Leipzig : Barth, 324 p.

Buée, L., T. Bussière, V. Buée-Scherrer, A. Delacourte, and P. R. Hof, 2000, Tau protein isoforms, phosphorylation and role in neurodegenerative disorders: Brain research. Brain research reviews, v. 33, no. 2, p. 95–130, doi:10.1016/s0165-0173(00)00019-9.

Bulic, B., M. Pickhardt, B. Schmidt, E. M. Mandelkow, H. Waldmann, and E. Mandelkow, 2009, Development of tau aggregation inhibitors for alzheimer's disease: Angewandte Chemie - International Edition, v. 48, no. 10, p. 1740–1752, doi:10.1002/anie.200802621.

Bussian, T. J., A. Aziz, C. F. Meyer, B. L. Swenson, J. M. van Deursen, and D. J. Baker, 2018, Clearance of senescent glial cells prevents tau-dependent pathology and cognitive decline: Nature, v. 562, no. 7728, p. 578–582, doi:10.1038/s41586-018-0543-y.

Caceres, A., and K. S. Kosik, 1990, Inhibition of neurite polarity by Tau antisense oligonucleotides in primary cerebellar neurons: Nature, v. 343, no. 1, p. 461–463, doi:10.1038/343461a0.

Calafate, S., A. Buist, K. Miskiewicz, V. Vijayan, G. Daneels, B. de Strooper, J. de Wit, P. Verstreken, and D. Moechars, 2015, Synaptic Contacts Enhance Cell-to-Cell Tau Pathology Propagation: Cell Reports, v. 11, no. 8, p. 1176–1183, doi:10.1016/j.celrep.2015.04.043.

de Calignon, A., M. Polydoro, M. Suarez-Calvet, C. William, D. Adamowicz, K. Kopeikina, R. Pitstick, N. Sahara, K. Ashe, G. Carlson, T. Spires-Jones, and B. Hyman, 2012, Propagation of tau pathology in a model of early Alzheimer's disease: Neuron, v. 73, no. 4, p. 685–697, doi:10.1016/j.neuron.2011.11.033.Propagation.

Catania, Sotiropoulos, Silva, C. Onofri, K. C. Breen, N. Sousa, and O. F. X. Almeida, 2009, The amyloidogenic potential and behavioral correlates of stress.: Molecular psychiatry, v. 14, no. 1, p. 95–105, doi:10.1038/sj.mp.4002101.

Chai, X., S. Wu, T. K. Murray, R. Kinley, C. V. Cella, H. Sims, N. Buckner, J. Hanmer, P. Davies, M. J. O'Neill, M. L. Hutton, and M. Citron, 2011, Passive immunization with anti-tau antibodies in two transgenic models: Reduction of tau pathology and delay of disease progression: Journal of Biological Chemistry, v. 286, no. 39, p. 34457–34467, doi:10.1074/jbc.M111.229633.

Chang, E., S. Kim, H. Yin, H. N. Nagaraja, and J. Kuret, 2008, Pathogenic missense MAPT mutations differentially modulate tau aggregation propensity at nucleation and extension steps: Journal of Neurochemistry, v. 107, no. 4, p. 1113–1123, doi:10.1111/j.1471-4159.2008.05692.x.

Cheng, I. H., K. Scearce-Levie, J. Legleiter, J. J. Palop, H. Gerstein, N. Bien-Ly, J. Puoliväli, S. Lesné, K. H. Ashe, P. J. Muchowski, and L. Mucke, 2007, Accelerating amyloid-β fibrillization reduces oligomer levels and functional deficits in Alzheimer disease mouse models: Journal of Biological Chemistry, v. 282, no. 33, p. 23818–23828, doi:10.1074/jbc.M701078200.

Chesser, A. S., S. M. Pritchard, and G. V. W. Johnson, 2013, Tau Clearance Mechanisms and Their Possible Role in the Pathogenesis of Alzheimer Disease: Frontiers in neurology, v. 4, no. September, p. 122, doi:10.3389/fneur.2013.00122.

Clavaguera, F., T. Bolmont, R. A. Crowther, D. Abramowski, S. Frank, A. Probst, G. Fraser, A. K. Stalder, M. Beibel, M. Staufenbiel, M. Jucker, M. Goedert, and M. Tolnay, 2009, Transmission and spreading of tauopathy in transgenic mouse brain: Nature Cell Biology, v. 11, no. 7, p. 909–913, doi:10.1038/ncb1901.

Clavaguera, F., F. Grueninger, and M. Tolnay, 2014, Intercellular transfer of tau aggregates and spreading of tau pathology: Implications for therapeutic strategies: Neuropharmacology, v. 76, no. PART A, p. 9–15, doi:10.1016/j.neuropharm.2013.08.037.

Congdon, E., J. Wu, N. Myeku, Y. Figueroa, M. Herman, P. Marinec, J. Gestwicki, C. Dickey, W. Yu, and K. Duff, 2012, Methylthioninium chloride (methylene blue) induces autophagy and attenuates tauopathy in vitro and in vivo: Autophagy, v. 4, p. 609–22, doi:10.4161/auto.19048.

Coppola, G. … D. H. Geschwind, 2012, Evidence for a role of the rare p.A152T variant in mapt in increasing the risk for FTD-spectrum and Alzheimer's diseases: Human Molecular Genetics, v. 21, no. 15, p. 3500–3512, doi:10.1093/hmg/dds161.

Le Corre, S., H. W. Klafki, N. Plesnila, G. Hübinger, A. Obermeier, H. Sahagún, B. Monse, P. Seneci, J. Lewis, J. Eriksen, C. Zehr, M. Yue, E. McGowan, D. W. Dickson, M. Hutton, and H. M. Roder, 2006, An inhibitor of tau hyperphosphorylation prevents severe motor impairments in tau transgenic mice: Proceedings of the National Academy of Sciences of the United States of America, v. 103, no. 25, p. 9673–9678, doi:10.1073/pnas.0602913103.

Couchie, D., C. Mavilia, I. S. Georgieff, R. K. H. Liemi, M. L. Shelanski, J. Nunez, I. National, D. Sant, R. Medicale, U. N. De, R. Scientifique, H. H. Mondor, C. A. M. Occ, C. C. A. Bat, and T. I. G. Acc, 1992, Primary structure of high molecular weight tau present in the peripheral nervous system: Proceedings of the National Academy of Sciences of the United States of America, v. 89, no. 10, p. 4378–4381, doi:10.1073/pnas.89.10.4378.

Cragg, B. G., 1961, Olfactory and other afferent connections of the hippocampus in the rabbit, rat, and cat: Experimental Neurology, v. 3, no. 6, p. 588–600, doi:10.1016/S0014-4886(61)80007-1.

Crary, J. F., J. Q. Trojanowski, J. A. Schneider, J. F. Abisambra, L. Erin, I. Alafuzoff, S. E. Arnold, J. Attems, T. G. Beach, H. Bigio, N. J. Cairns, D. W. Dickson, M. Gearing, and L. T. Grinberg, 2014, Primary age-related tauopathy (PART): a common pathology associated with human aging: Acta Neuropathol, v. 128, no. 6, p. 755–766, doi:10.1007/s00401-014-1349-0.Primary.

Cras, P., M. Kawai, S. Siedlak, and G. Perry, 1991, Microglia are associated with the extracellular neurofibrillary tangles of alzheimer disease: Brain Research, v. 558, no. 2, p. 312–314, doi:10.1016/0006-8993(91)90783-R.

D'Hooge, R., R. Lüllmann-Rauch, T. Beckers, D. Balschun, M. Schwake, K. Reiss, K. Von Figura, and P. Saftig, 2005, Neurocognitive and psychotiform behavioral alterations and enhanced hippocampal long-term potentiation in transgenic mice displaying neuropathological features of human α-mannosidosis: Journal of Neuroscience, v. 25, no. 28, p. 6539–6549, doi:10.1523/JNEUROSCI.0283-05.2005.

Dawson, H. N., A. Ferreira, M. V Eyster, N. Ghoshal, L. I. Binder, and M. P. Vitek, 2001, Inhibition of neuronal maturation in primary hippocampal neurons from tau deficient mice: Journal of cell science, v. 114, no. Pt 6, p. 1179–87.

Deacon, R. M., 2012, Assessing Burrowing, Nest Construction, and Hoarding in Mice: Journal of Visualized Experiments, v. 59, p. e2607, doi:10.1016/j.pbb.2009.01.016.Neurobehavioral.

Deacon, R. M., 2006, Assessing nest building in mice.: Nature Protocols, v. 1, no. 3, p. 1117–1119, doi:10.1038/nprot.2006.170.

Deacon, R. M., 2009, Burrowing: A sensitive behavioral assay, tested in five species of laboratory rodents: Behavioural brain research, v. 200, no. 1, p. 128–133, doi:10.1016/j.bbr.2009.01.007.

Dehmelt, L., and S. Halpain, 2005, The MAP2/Tau family of microtubule-associated proteins: Genome biology, v. 6, no. 1, p. 1–10, doi:10.1186/gb-2004-6-1-204.

Delacourte, A., J. P. David, N. Sergeant, L. Buée, A. Wattez, P. Vermersch, F. Ghozali, C. Fallet-Bianco, F. Pasquier, F. Lebert, H. Petit, and C. Di Menza, 1999, The biochemical pathway of neurofibrillary degeneration in agind and Alzheimer's disease: Neurology, v. 52, no. 6, p. 1158–65, doi:https://doi.org/10.1212/WNL.52.6.1158.

Demaegd, K., J. Schymkowitz, and F. Rousseau, 2018, Transcellular Spreading of Tau in Tauopathies: ChemBioChem, v. 19, no. 23, p. 2424–2432, doi:10.1002/cbic.201800288.

Dennissen, F., M. Anglada-Huguet, A. Sydow, E. Mandelkow, and E.-M. Mandelkow, 2016, Adenosine A 1 receptor antagonist rolofylline alleviates axonopathy caused by human Tau ΔK280: Proceedings of the National Academy of Sciences, v. 113, no. 41, p. 11597–11602, doi:10.1073/pnas.1603119113.

Despres, C., C. Byrne, H. Qi, F. X. Cantrelle, I. Huvent, B. Chambraud, E. E. Baulieu, Y. Jacquot, I. Landrieu, G. Lippens, and C. Smet-Nocca, 2017, Identification of the Tau phosphorylation pattern that drives its aggregation: Proceedings of the National Academy of Sciences of the United States of America, v. 114, no. 34, p. 9080–9085, doi:10.1073/pnas.1708448114.

DeVos, S. L., D. K. Goncharoff, G. Chen, C. S. Kebodeaux, K. Yamada, F. R. Stewart, D. R. Schuler, S. E. Maloney, D. F. Wozniak, F. Rigo, C. F. Bennett, J. R. Cirrito, D. M. Holtzman, and T. M. Miller, 2013, Antisense reduction of tau in adult mice protects against seizures: Journal of Neuroscience, v. 33, no. 31, p. 12887–12897, doi:10.1523/JNEUROSCI.2107-13.2013.

DeVos, S. L., B. T. Corjuc, D. H. Oakley, C. K. Nobuhara, R. N. Bannon, A. Chase, C. Commins, J. A. Gonzalez, P. M. Dooley, M. P. Frosch, and B. T. Hyman, 2018, Synaptic tau seeding precedes tau pathology in human Alzheimer's disease brain: Frontiers in Neuroscience, v. 12, no. APR, p. 1–15, doi:10.3389/fnins.2018.00267.

DeVos, S. L., and T. Miller, 2013, Direct Intraventricular Delivery of Drugs to the Rodent Central Nervous System: Journal of Visualized Experiments, v. 50326, no. 75, p. 1–10, doi:10.3791/50326.

Ding, H., P. J. Dolan, and G. V. W. Johnson, 2008, Histone deacetylase 6 interacts with the microtubule-associated protein tau: Journal of neurochemistry, v. 106, no. 5, p. 2119–30, doi:10.1111/j.1471-4159.2008.05564.x.

DiPatre, P., and B. Gelman, 1997, Microglial cell activation in aging and Alzheimer disease: partial linkage with neurofibrillary tangle burden in the hippocampus: J Neuropathol Exp Neurol, v. 56, no. 2, p. 143–9, doi:10.1097/00005072-199702000-00004.

Dixit, R., J. L. Ross, Y. E. Goldman, and E. L. F. Holzbaur, 2008, Differential Regulation of Dynein and Kinesin Motor Proteins by Tau: Science, v. 319, no. 5866, p. 1086–1089, doi:10.1126/science.1152993.Differential.

Drewes, G., A. Ebneth, U. Preuss, E. M. Mandelkow, and E. Mandelkow, 1997, MARK, a novel family of protein kinases that phosphorylate microtubule- associated proteins and trigger microtubule disruption: Cell, v. 89, no. 2, p. 297–308, doi:10.1016/S0092-8674(00)80208-1.

Drubin, D. G., D. Caput, and M. W. Kirschner, 1984, Studies on the expression of the microtubule-associated protein, tau, during mouse brain development, with newly isolated complementary DNA probes: Journal of Cell Biology, v. 98, no. 3, p. 1090–1097, doi:10.1083/jcb.98.3.1090.

Dujardin, S., S. Bégard, R. Caillierez, C. Lachaud, S. Carrier, S. Lieger, J. A. Gonzalez, V. Deramecourt, N. Déglon, C. A. Maurage, M. P. Frosch, B. T. Hyman, M. Colin, and L. Buée, 2018, Different tau species lead to heterogeneous tau pathology propagation and misfolding: Acta neuropathologica communications, v. 6, no. 1, p. 132, doi:10.1186/s40478-018-0637-7.

Dujardin, S., K. Lécolle, R. Caillierez, S. Bégard, N. Zommer, C. Lachaud, S. Carrier, N. Dufour, G. Aurégan, J. Winderickx, P. Hantraye, N. Déglon, M. Colin, and L. Buée, 2014, Neuron-to-neuron wild-type Tau protein transfer through a trans-synaptic mechanism: Relevance to sporadic tauopathies: Acta Neuropathologica Communications, v. 2, no. 1, p. 1–14, doi:10.1186/2051-5960-2-14.

Duyckaerts, C., M. Bennecib, Y. Grignon, T. Uchihara, Y. He, F. Piette, and J. J. Hauw, 1997, Modeling the relation between neurofibrillary tangles and intellectual status: Neurobiology of Aging, v. 18, no. 3, p. 267–273, doi:10.1016/S0197-4580(97)80306-5.

Duyckaerts, C., M. C. Potier, and B. Delatour, 2008, Alzheimer disease models and human neuropathology: Similarities and differences: Acta Neuropathologica, v. 115, no. 1, p. 5–38, doi:10.1007/s00401-007-0312-8.

Eckermann, K., M. M. Mocanu, I. Khlistunova, J. Biernat, A. Nissen, A. Hofmann, K. Schönig, H. Bujard, A. Haemisch, E. Mandelkow, L. Zhou, G. Rune, and E. M. Mandelkow, 2007, The β-propensity of tau determines aggregation and synaptic loss in inducible mouse models of tauopathy: Journal of Biological Chemistry, v. 282, no. 43, p. 31755–31765, doi:10.1074/jbc.M705282200.

Ennaceur, a, 2010, One-trial object recognition in rats and mice: methodological and theoretical issues.:

Behavioural brain research, v. 215, no. 2, p. 244–54, doi:10.1016/j.bbr.2009.12.036.

Esquerda-Canals, G., L. Montoliu-Gaya, J. Güell-Bosch, and S. Villegas, 2017, Mouse Models of Alzheimer's Disease: Journal of Alzheimer's Disease, v. 57, no. 4, p. 1171–1183, doi:10.3233/JAD-170045.

Fatouros, C., G. J. Pir, J. Biernat, S. P. Koushika, E. Mandelkow, E.-M. Mandelkow, E. Schmidt, and R. Baumeister, 2012, Inhibition of tau aggregation in a novel Caenorhabditis elegans model of tauopathy mitigates proteotoxicity: Human Molecular Genetics, v. 21, no. 16, p. 3587–3603, doi:10.1093/hmg/dds190.

Flores-Rodríguez, P., M. A. Ontiveros-Torres, M. C. Cárdenas-Aguayo, J. P. Luna-Arias, M. A. Meraz-Ríos, A. Viramontes-Pintos, C. R. Harrington, C. M. Wischik, R. Mena, B. Florán-Garduño, and J. Luna-Muñoz, 2015, The relationship between truncation and phosphorylation at the C-terminus of tau protein in the paired helical filaments of Alzheimer's disease: Frontiers in Neuroscience, v. 9, no. 33, p. 1–10, doi:10.3389/fnins.2015.00033.

Frandemiche, M. L., S. De Seranno, T. Rush, E. Borel, A. Elie, I. Arnal, F. Lanté, and A. Buisson, 2014, Activity-dependent tau protein translocation to excitatory synapse is disrupted by exposure to amyloid-beta oligomers: Journal of Neuroscience, v. 34, no. 17, p. 6084–6097, doi:10.1523/JNEUROSCI.4261-13.2014.

Frederick, C., K. Ando, K. Leroy, C. Héraud, V. Suain, L. Buée, and J. P. Brion, 2015, Rapamycin ester analog CCI-779/Temsirolimus alleviates tau pathology and improves motor deficit in mutant tau transgenic mice: Journal of Alzheimer's Disease, v. 44, no. 4, p. 1145–1156, doi:10.3233/JAD-142097.

Friedhoff, P., M. Von Bergen, E. M. Mandelkow, P. Davies, and E. Mandelkow, 1998, A nucleated assembly mechanism of Alzheimer paired helical filaments: Proceedings of the National Academy of Sciences of the United States of America, v. 95, no. 26, p. 15712–15717, doi:10.1073/pnas.95.26.15712.

Frost, B., R. L. Jacks, and M. I. Diamond, 2009, Propagation of Tau misfolding from the outside to the inside of a cell: Journal of Biological Chemistry, v. 284, no. 19, p. 12845–12852, doi:10.1074/jbc.M808759200.

Fu, H., J. Hardy, and K. E. Duff, 2018, Selective vulnerability in neurodegenerative diseases: Nature Neuroscience, v. 21, no. 10, p. 1350–1358, doi:10.1038/s41593-018-0221-2.

Funk, K. E., H. Mirbaha, H. Jiang, D. M. Holtzman, and M. I. Diamond, 2015, Distinct therapeutic mechanisms of Tau antibodies: Promoting microglial clearance versus blocking neuronal uptake: Journal of Biological Chemistry, v. 290, no. 35, p. 21652–21662, doi:10.1074/jbc.M115.657924.

Furman, J. L., J. Vaquer-Alicea, C. L. White Iii, N. J. Cairns, P. T. Nelson, M. I. Diamond, and A. N. Author, 2017, Widespread Tau Seeding Activity at Early Braak Stages HHS Public Access Author manuscript: Acta Neuropathol, v. 133, no. 1, p. 91–100, doi:10.1007/s00401-016-1644-z.

Fuster-Matanzo, A., E. G. de Barreda, H. N. Dawson, M. P. Vitek, J. Avila, and F. Hernández, 2009, Function of tau protein in adult newborn neurons: FEBS Letters, v. 583, no. 18, p. 3063–3068, doi:10.1016/j.febslet.2009.08.017.

G. Almeida, C., D. Tampellini, R. H.Takahashi, P. Greengard, M. T. Lin, E. M. Snyder, and G. K. Gouras, 2005, Beta-amyloid accumulation in APP mutant neurons reduces PSD-95 and GluR1 in synapses: Neurobiology of d, v. 20, no. 2, p. 187–198, doi:10.1016/j.pnpbp.2012.11.007.

García-Sierra, F., S. Mondragón-Rodríguez, and G. Basurto-Islas, 2008, Truncation of tau protein and its pathological significance in Alzheimer's disease: Journal of Alzheimer's Disease, v. 14, no. 4, p. 401–409, doi:10.3233/JAD-2008-14407.

Gauthier, S., H. H. Feldman, L. S. Schneider, G. K. Wilcock, B. Giovanni, J. H. Hardlund, H. J. Moebius, P. Bentham, K. A. Kook, D. J. Wischik, B. O. Schelter, C. S. Davis, R. T. Staff, L. Bracoud, K. Shamsi, M. D. John, C. R. Harrington, and C. M. Wischik, 2016, Efficacy and safety of tau-aggregation inhibitor therapy in patients with mild or moderate Alzheimer's disease: a randomised, controlled, double-blind, parallel-arm, phase 3 trial: Lancet, v. 388, no. 10062, p. 2873–2884, doi:10.1016/S0140-6736(16)31275-2.Efficacy.

Gerhard, A., J. Watts, I. Trender-Gerhard, F. Turkheimer, R. B. Banati, K. Bhatia, and D. J. Brooks, 2004, In vivo imaging of microglial activation with [11C](R -PK11195 PET in corticobasal degeneration: Movement Disorders, v. 19, no. 10, p. 1221–1226, doi:10.1002/mds.20162.

Gheyara, A. L., R. Ponnusamy, B. Djukic, R. J. Craft, K. Ho, W. Guo, M. M. Finucane, P. E. Sanchez, and L. Mucke, 2014, Tau reduction prevents disease in a mouse model of Dravet syndrome: Annals of Neurology, v. 76, no. 3, p. 443–456, doi:10.1002/ana.24230.

Goedert, M., and R. Jakes, 1990, Expression of separate isoforms of human Tau protein: correlation with the Tau pattern in brain and effects on tubulin polymerization: The EMBO journal, v. 9, no. 13, p. 4225–4230, doi:10.1002/j.1460-2075.1990.tb07870.x.

Gomez-Isla, T., R. Hollister, H. West, S. Mui, J. Growdon, R. Petersen, J. Parisi, and B. Hyman, 1997, Neurond Loss Correlates with but Exceeds Newofibriiary Tangles in Alzheimer's Disease: Annals of Neurology, v. 41, no. 1, p. 17–24, doi:10.1002/ana.410410106.

Gong, C.-X., 2000, Phosphorylation of Microtubule-associated Protein Tau Is Regulated by Protein Phosphatase

2A in Mammalian Brain. Implications for neurofibrillary degeneration in Alzheimer’s disease: Journal of Biological Chemistry, v. 275, no. 8, p. 5535–5544, doi:10.1074/jbc.275.8.5535.

Gong, C.-X., and K. Iqbal, 2008, Hyperphosphorylation of Microtubule-Associated Protein Tau: A Promising Therapeutic Target for Alzheimer Disease: Current Medicinal Chemistry, v. 15, no. 23, p. 2321–2328, doi:10.2174/092986708785909111.

Goode, B. L., and S. C. Feinstein, 1994, Identification of a Novel Microtubule Binding and Assembly Domain in the Developmentally Regulated Inter-repeat Region of Tau: The Journal of Cell Biology, v. 124, no. 5, p. 769–782, doi:10.1083/jcb.124.5.769.

Goodson, H. V., and E. M. Jonasson, 2018, Microtubules and microtubule-associated proteins: Cold Spring Harbor perspectives in biology, v. 10, no. 6, p. 57–70, doi:10.1101/cshperspect.a022608.

Gorath, M., T. Stahnke, T. Mronga, O. Goldbaum, and C. Richter-Landsberg, 2001, Developmental changes of tau protein and mRNA in cultured rat brain oligodendrocytes: Glia, v. 36, no. 1, p. 89–101, doi:10.1002/glia.1098.

Gorlovoy, P., S. Larionov, T. T. H. Pham, and H. Neumann, 2009, Accumulation of tau induced in neurites by microglial proinflammatory mediators: FASEB journal : official publication of the Federation of American Societies for Experimental Biology, v. 23, no. 8, p. 2502–13, doi:10.1096/fj.08-123877.

Götz, J., and L. M. Ittner, 2008, Animal models of Alzheimer’s disease and frontotemporal dementia: Nature Reviews Neuroscience, v. 9, no. 7, p. 532–544, doi:10.1038/nrn2420.

Götz, J., D. Xia, G. Leinenga, Y. L. Chew, and H. Nicholas, 2013, What Renders TAU Toxic: Frontiers in neurology, v. 4, no. June, p. 72, doi:10.3389/fneur.2013.00072.

Green, J. D., and W. R. Adey, 1955, Electrophysiological studies of hippocampal connections and excitability: EEG Clin Neurophysiol, v. 8, p. 245–262, doi:10.1016/0013-4694(56)90117-1.

Greenberg, S. G., and P. Davies, 2006, A preparation of Alzheimer paired helical filaments that displays distinct tau proteins by polyacrylamide gel electrophoresis.: Proceedings of the National Academy of Sciences, v. 87, no. 15, p. 5827–5831, doi:10.1073/pnas.87.15.5827.

Grundke-Iqbal, I., J. Fleming, Y.-C. Tung, H. Lassmann, K. Iqbal, and J. G. Joshi, 1990, Ferritin is a component of the neuritic (senile) plaque in Alzheimer dementia: Acta Neuropathologica, v. 81, no. 2, p. 105–110, doi:10.1007/BF00334497.

Grundke-Iqbal, I., K. Iqbal, Y. Tung, M. Quinlan, H. M. Wisniewski, and L. I. Bindert, 1986, Abnormal phosphorylation of the microtubule-associated protein tau in Alzheimer cytoskeletal pathology: Proceedings of the National Academy of Sciences of the United States of America, v. 83, no. 13, p. 4913–4917, doi:10.1073/pnas.83.13.4913.

Grüning, C. S. R., E. A. Mirecka, A. N. Klein, E. Mandelkow, D. Willbold, S. F. Marino, M. Stoldt, and W. Hoyer, 2014, Alternative conformations of the tau repeat domain in complex with an engineered binding protein: Journal of Biological Chemistry, v. 289, no. 33, p. 23209–23218, doi:10.1074/jbc.M114.560920.

Guerreiro, R., A. Wojtas, J. Bras, M. Carrasquillo, E. Rogaeva, E. Majounie, C. Cruchaga, J. S. K. Kauwe, S. Younkin, L. Hazrati, J. Lambert, P. Amouyel, A. Goate, A. Singleton, and J. Hardy, 2013, TREM2 variants in Alzheimer’s Disease: New England Journal of Medicine, v. 368, no. 2, p. 117–127, doi:10.1056/NEJMoa1211851.TREM2.

Guo, J. L., and V. M. Y. Lee, 2011, Seeding of normal tau by pathological tau conformers drives pathogenesis of Alzheimer-like tangles: Journal of Biological Chemistry, v. 286, no. 17, p. 15317–15331, doi:10.1074/jbc.M110.209296.

Guo, T., W. Noble, and D. P. Hanger, 2017, Roles of tau protein in health and disease: Acta Neuropathologica, v. 133, no. 5, p. 665–704, doi:10.1007/s00401-017-1707-9.

Gustke, N., B. Trinczek, J. Biernat, E. M. Mandelkow, and E. Mandelkow, 1994, Domains of τ Protein and Interactions with Microtubules: Biochemistry, v. 33, no. 32, p. 9511–9522, doi:10.1021/bi00198a017.

Haass, C., and D. J. Selkoe, 2007, Soluble protein oligomers in neurodegeneration: lessons from the Alzheimer’s amyloid beta-peptide: Nature Reviews Molecular Cell Biology, v. 8, no. 2, p. 101–112, doi:10.1016/j.biocel.2004.04.010.

Han, H. J., C. C. Allen, C. M. Buchovecky, M. J. Yetman, H. A. Born, M. A. Marin, S. P. Rodgers, B. J. Song, H. C. Lu, M. J. Justice, F. J. Probst, and J. L. Jankowsky, 2012, Strain background influences neurotoxicity and behavioral abnormalities in mice expressing the tetracycline transactivator: Journal of Neuroscience, v. 32, no. 31, p. 10574–10586, doi:10.1523/JNEUROSCI.0893-12.2012.

Hanger, D. P., J. C. Betts, T. L. F. Loviny, W. P. Blackstock, and B. H. Anderton, 2002, New Phosphorylation Sites Identified in Hyperphosphorylated Tau (Paired Helical Filament-Tau) from Alzheimer’s Disease Brain Using Nanoelectrospray Mass Spectrometry: Journal of Neurochemistry, v. 71, no. 6, p. 2465–2476, doi:10.1046/j.1471-4159.1998.71062465.x.

Hansen, D. V, J. E. Hanson, and M. Sheng, 2018, Microglia in Alzheimer's disease: Journal of Cell Biology, v. 217, no. 2, p. 459–472, doi:10.1083/jcb.201709069.

Harada, A., K. Oguchi, S. Okabe, J. Kuno, S. Terada, T. Ohshima, R. Sato-Yoshitake, Y. Takei, T. Noda, and N. Hirokawa, 1994, Altered microtubule organization in small-calibre axons of mice lacking tau protein: Nature, v. 369, no. 6480, p. 488–491, doi:10.1038/369488a0.

Harris, J., N. Devidze, L. Verret, K. Ho, B. Halabisky, M. Thwin, D. Kim, P. Hamto, I. Lo, G. Yu, J. Palop, E. Masliah, and L. Mucke, 2010, Transsynaptic progression of amyloid-β-induced neuronal dysfunction within the entorhinal-hippocampal network: Neuron, v. 68, no. 3, p. 428–41, doi:10.1016/j.neuron.2010.10.020.

Heinrich, S., M. Berwig, A. Simon, J. Jänichen, N. Hallensleben, W. Nickel, A. Hinz, E. Brähler, and H.-J. Gertz, 2014, German adaptation of the Resources for Enhancing Alzheimer's Caregiver Health II: study protocol of a single-centred, randomised controlled trial.: BMC geriatrics, v. 14, p. 21, doi:10.1186/1471-2318-14-21.

Helboe, L., J. Egebjerg, P. Barkholt, and C. Volbracht, 2017, Early depletion of CA1 neurons and late neurodegeneration in a mouse tauopathy model: Brain Research, v. 1665, p. 22–35, doi:10.1016/j.brainres.2017.04.002.

Heneka, M. T., M. J. Carson, J. El Khoury, E. Gary, F. Brosseron, D. L. Feinstein, A. H. Jacobs, T. Wyss-coray, J. Vitorica, and R. M. Ransohoff, 2018, Neuroinflammation in Alzheimer's Disease: Lancet Neurol, v. 14, no. 4, p. 388–405, doi:10.1016/S1474-4422(15)70016-5.Neuroinflammation.

Himmler, A., 1989, Structure of the bovine Tau gene: alternatively spliced transcripts generate a protein family: Molecular and cellular biology, v. 9, no. 4, p. 1389–1396, doi:10.1128/mcb.9.4.1389.

Hirokawa, N., T. Funakoshi, R. Sato-Harada, and Y. Kanai, 1996, Selective stabilization of tau in axons and microtubule-associated protein 2C in cell bodies and dendrites contributes to polarized localization of cytoskeletal proteins in mature neurons: Journal of Cell Biology, v. 132, no. 4, p. 667–679, doi:10.1083/jcb.132.4.667.

Hochgräfe, K., A. Sydow, D. Matenia, D. Cadinu, S. Könen, O. Petrova, M. Pickhardt, P. Goll, F. Morellini, E. Mandelkow, and E.-M. Mandelkow, 2015, Preventive methylene blue treatment preserves cognition in mice expressing full-length pro-aggregant human Tau: Acta Neuropathologica Communications, v. 3, no. 1, p. 25, doi:10.1186/s40478-015-0204-4.

Hochgräfe, K., and E. M. Mandelkow, 2013, Making the brain glow: In vivo bioluminescence imaging to study neurodegeneration: Molecular Neurobiology, v. 47, no. 3, p. 868–882, doi:10.1007/s12035-012-8379-1.

Hoesen, G. W. V., and D. N.Pandya, 1975, Some connections of the entorhinal (area 28) and perirhinal (area 35) cortices of the rhesus monkey. III. Efferent connections: Brain Research, v. 95, p. 39–59, doi:10.1016/0006-8993(75)90206-1.

Holmes, B. B., and M. I. Diamond, 2014, Prion-like properties of Tau protein: The importance of extracellular Tau as a therapeutic target: Journal of Biological Chemistry, v. 289, no. 29, p. 19855–19861, doi:10.1074/jbc.R114.549295.

Holth, J. K., V. C. Bomben, J. Graham Reed, T. Inoue, L. Younkin, S. G. Younkin, R. G. Pautler, J. Botas, and J. L. Noebels, 2013, Tau loss attenuates neuronal network hyperexcitability in mouse and drosophila genetic models of epilepsy: Journal of Neuroscience, v. 33, no. 4, p. 1651–1659, doi:10.1523/JNEUROSCI.3191-12.2013.

Holtzman, D. M., J. C. Morris, and A. Goate, 2012, Alzheimer's disease: the challenge of the second century: Sci Transl Med, v. 3, no. 77, p. 1–35, doi:10.1515/cclm.1985.23.7.399.

Hong, M., V. Zhukareva, V. Vogelsberg-Ragaglia, Z. Wszolek, L. Reed, B. I. Miller, D. H. Geschwind, T. D. Bird, D. McKeel, A. Goate, J. C. Morris, K. C. Wilhelmsen, G. D. Schellenberg, J. Q. Trojanowski, and V. M.-Y. Lee, 1998, Mutation-specific functional impairments in distinct tau isoforms of hereditary FTDP-17: Science, v. 282, no. 5395, p. 1914–1917, doi:10.1126/science.282.5395.1914.

Hong, X. P., C. X. Peng, W. Wei, Q. Tian, Y. H. Liu, X. Q. Yao, Y. Zhang, F. Y. Cao, Q. Wang, and J. Z. Wang, 2010, Essential role of tau phosphorylation in adult hippocampal neurogenesis: Hippocampus, v. 20, no. 12, p. 1339–1349, doi:10.1002/hipo.20712.

Hoover, B. R., M. N. Reed, J. Su, R. D. Penrod, A. Linda, M. K. Grant, R. Pitstick, G. a Carlson, and L. M. Lanier, 2010, Tau mislocalization to dendritic spines mediates synaptic dysfunction independently of neurodegeneration: Neuron, v. 68, no. 6, p. 1067–1081, doi:10.1016/j.neuron.2010.11.030.Tau.

Hopp, S. C., Y. Lin, D. Oakley, A. D. Roe, S. L. Devos, D. Hanlon, and B. T. Hyman, 2018, The role of microglia in processing and spreading of bioactive tau seeds in Alzheimer's disease: Journal of Neuroinflammation, v. 15, no. 1, p. 1–15, doi:10.1186/s12974-018-1309-z.

Huang, H.-C., and Z.-F. Jiang, 2009, Accumulated amyloid-beta peptide and hyperphosphorylated tau protein: relationship and links in Alzheimer's disease.: Journal of Alzheimer's disease : JAD, v. 16, no. 1, p. 15–27, doi:10.3233/JAD-2009-0960.

Humpel, C., 2018, Organotypic Brain Slice Cultures: Current Protocols in Immunology, v. 123, no. 1, p. 1–17, doi:10.1002/cpim.59.

Hyman, B., G. W. Van Hoesen, A. R. Damasio, and C. L. Barnes, 1984, Alzheimer’s Disease: Cell-Specific Pathology Isolates the Hippocampal Formation: Science, v. 225, no. 4667, p. 1168–1170, doi:10.1126/science.6474172.

Iba, M., J. L. Guo, J. D. McBride, B. Zhang, J. Q. Trojanowski, and V. M. Y. Lee, 2013, Synthetic tau fibrils mediate transmission of neurofibrillary tangles in a transgenic mouse model of alzheimer’s-like tauopathy: Journal of Neuroscience, v. 33, no. 3, p. 1024–1037, doi:10.1523/JNEUROSCI.2642-12.2013.

Ishizawa, K., T. Komori, S. Sasaki, N. Arai, T. Mizutani, and T. Hirose, 2004, Microglial Activation Parallels System Degeneration in Multiple System Atrophy: Journal of Neuropathology and Experimental Neurology, v. 63, no. 1, p. 43–52, doi:10.1093/jnen/63.1.43.

Ising, C. … M. T. Heneka, 2019, NLRP3 inflammasome activation drives tau pathology: Nature, v. 575, no. November, doi:10.1038/s41586-019-1769-z.

Ittner, L. M., Y. D. Ke, F. Delerue, M. Bi, A. Gladbach, J. van Eersel, H. Wölfing, B. C. Chieng, M. J. Christie, I. a. Napier, A. Eckert, M. Staufenbiel, E. Hardeman, and J. Götz, 2010, Dendritic function of tau mediates amyloid-β toxicity in alzheimer’s disease mouse models: Cell, v. 142, no. 3, p. 387–397, doi:10.1016/j.cell.2010.06.036.

Ittner, L. M., Y. D. Ke, and J. Götz, 2009, Phosphorylated Tau interacts with c-Jun N-terminal kinase-interacting protein 1 (JIP1) in Alzheimer disease: Journal of Biological Chemistry, v. 284, no. 31, p. 20909–20916, doi:10.1074/jbc.M109.014472.

Jackson, W. S., 2014, Selective vulnerability to neurodegenerative disease: The curious case of Prion Protein: DMM Disease Models and Mechanisms, v. 7, no. 1, p. 21–29, doi:10.1242/dmm.012146.

Jeganathan, S., A. Hascher, S. Chinnathambi, J. Biernat, E. M. Mandelkow, and E. Mandelkow, 2008, Proline-directed pseudo-phosphorylation at AT8 and PHF1 epitopes induces a compaction of the paperclip folding of tau and generates a pathological (MC-1) conformation: Journal of Biological Chemistry, v. 283, no. 46, p. 32066–32076, doi:10.1074/jbc.M805300200.

Van der Jeugd, A., K. Hochgräfe, T. Ahmed, and J. M. Decker, 2012, Cognitive defects are reversible in inducible mice expressing pro-aggregant full-length human Tau: Acta neuropathologica, v. 123, no. 6, p. 787–805, doi:10.1007/s00401-012-0987-3.Cognitive.

Johnson, G. V. W., and W. H. Stoothoff, 2004, Tau phosphorylation in neuronal cell function and dysfunction: Journal of cell science, v. 117, no. Pt 24, p. 5721–5729, doi:10.1242/jcs.01558.

Kadavath, H., R. V Hofele, J. Biernat, S. Kumar, K. Tepper, and H. Urlaub, 2015, Tau stabilizes microtubules by binding at the interface between tubulin heterodimers: Proceedings of the National Academy of Sciences of the United States of America, v. 112, no. 24, p. 7501–7506, doi:10.1073/pnas.1504081112.

Kanaan, N. M., G. A. Morfini, N. E. LaPointe, G. F. Pigino, K. R. Patterson, Y. Song, A. Andreadis, Y. Fu, S. T. Brady, and L. I. Binder, 2011, Pathogenic forms of tau inhibit kinesin-dependent axonal transport through a mechanism involving activation of axonal phosphotransferases: Journal of Neuroscience, v. 31, no. 27, p. 9858–9868, doi:10.1523/JNEUROSCI.0560-11.2011.

Kaniyappan, S., R. R. Chandupatla, E.-M. Mandelkow, and E. Mandelkow, 2017, Extracellular low-n oligomers of tau cause selective synaptotoxicity without affecting cell viability: Alzheimer’s & Dementia, v. 13, no. 11, p. 1270–1291, doi:10.1002/ana.21548.The.

Kaufman, S. K., T. L. Thomas, K. Del Tredici, H. Braak, and M. I. Diamond, 2017, Characterization of tau prion seeding activity and strains from formaldehyde-fixed tissue: Acta neuropathologica communications, v. 5, no. 1, p. 41, doi:10.1186/s40478-017-0442-8.

Kaufman, S. K., K. Del Tredici, T. L. Thomas, H. Braak, and M. I. Diamond, 2018, Tau seeding activity begins in the transentorhinal/entorhinal regions and anticipates phospho-tau pathology in Alzheimer’s disease and PART: Acta Neuropathologica, v. 136, no. 1, p. 57–67, doi:10.1007/s00401-018-1855-6.

Kelleher, I., C. Garwood, D. P. Hanger, B. H. Anderton, and W. Noble, 2007, Kinase activities increase during the development of tauopathy in htau mice: Journal of Neurochemistry, v. 103, no. 6, p. 2256–2267, doi:10.1111/j.1471-4159.2007.04930.x.

Kfoury, N., B. B. Holmes, H. Jiang, D. M. Holtzman, and M. I. Diamond, 2012, Trans-cellular propagation of Tau aggregation by fibrillar species: Journal of Biological Chemistry, v. 287, no. 23, p. 19440–19451, doi:10.1074/jbc.M112.346072.

Kilgore, M., C. a Miller, D. M. Fass, K. M. Hennig, S. J. Haggarty, J. D. Sweatt, and G. Rumbaugh, 2010, Inhibitors of class 1 histone deacetylases reverse contextual memory deficits in a mouse model of Alzheimer’s disease.: Neuropsychopharmacology, v. 35, no. 4, p. 870–80, doi:10.1038/npp.2009.197.

Kimura, T., T. Fukuda, N. Sahara, S. Yamashita, M. Murayama, T. Mizoroki, Y. Yoshiike, B. Lee, I. Sotiropoulos, S.

Maeda, and A. Takashima, 2010, Aggregation of detergent-insoluble tau is involved in neuronal loss but not in synaptic loss: Journal of Biological Chemistry, v. 285, no. 49, p. 38692–38699, doi:10.1074/jbc.M110.136630.

Kimura, T., D. J. Whitcomb, J. Jo, P. Regan, T. Piers, S. Heo, C. Brown, T. Hashikawa, M. Murayama, H. Seok, I. Sotiropoulos, E. Kim, G. L. Collingridge, A. Takashima, and K. Cho, 2014, Microtubule-associated protein tau is essential for long-term depression in the hippocampus: Philosophical transactions of the Royal Society of London. Series B, Biological sciences, v. 369, no. 1633, p. 20130144, doi:10.1098/rstb.2013.0144.

Kimura, T., S. Yamashita, T. Fukuda, J.-M. Park, M. Murayama, T. Mizoroki, Y. Yoshiike, N. Sahara, and A. Takashima, 2007, Hyperphosphorylated tau in parahippocampal cortex impairs place learning in aged mice expressing wild-type human tau: The EMBO journal, v. 26, no. 24, p. 5143–5152, doi:10.1038/sj.emboj.7601917.

Knops, J., K. S. Kosik, G. Lee, J. D. Pardee, L. Cohen-Gould, and L. McConlogue, 1991, Overexpression of tau in a nonneuronal cell induces long cellular processes: Journal of Cell Biology, v. 114, no. 4, p. 725–733, doi:10.1083/jcb.114.4.725.

Kontsekova, E., N. Zilka, B. Kovacech, P. Novak, and M. Novak, 2014, First-in-man tau vaccine targeting structural determinants essential for pathological tau-tau interaction reduces tau oligomerisation and neurofibrillary degeneration in an Alzheimer's disease model: Alzheimer's Research and Therapy, v. 6, no. 4, p. 1–12, doi:10.1186/alzrt278.

Konzack, S., E. Thies, A. Marx, E. M. Mandelkow, and E. Mandelkow, 2007, Swimming against the tide: Mobility of the microtubule-associated protein tau in neurons: Journal of Neuroscience, v. 27, no. 37, p. 9916–9927, doi:10.1523/JNEUROSCI.0927-07.2007.

Kosik, K. S., J. E. Crandall, E. J. Mufson, and R. L. Neve, 1989, Tau in situ hybridization in normal and alzheimer brain: Localization in the somatodendritic compartment: Annals of Neurology, v. 26, no. 3, p. 352–361, doi:10.1002/ana.410260308.

Kosik, K. S., and H. Shimura, 2005, Phosphorylated tau and the neurodegenerative foldopathies: Biochimica et Biophysica Acta - Molecular Basis of Disease, v. 1739, no. 2, p. 298–310, doi:10.1016/j.bbadis.2004.10.011.

Kouri, N., Y. Carlomagno, M. Baker, A. M. Liesinger, J. Richard, Z. K. Wszolek, L. Petrucelli, B. F. Boeve, J. E. Parisi, K. A. Josephs, R. J. Uitti, O. A. Ross, N. R. Graff-radford, M. A. Deture, D. W. Dickson, and R. Rademakers, 2014, Novel mutation in MAPT exon 13 (p. N410H) causes corticobasal degeneration: Acta Neuropathol, v. 127, no. 2, p. 271–282, doi:10.1007/s00401-013-1193-7.Novel.

Lasagna-Reeves, C., M. de Haro, S. Hao, J. Park, M. Rousseaux, I. Al-Ramahi, P. Jafar-Nejad, L. Vilanova-Velez, L. See, A. De Maio, L. Nitschke, Z. Wu, J. Troncoso, T. Westbrook, J. Tang, J. Botas, and H. Zoghbi, 2016, Reduction of Nuak1 Decreases Tau and Reverses Phenotypes in a Tauopathy Mouse Model: Neuron, v. 92, no. 2, p. 407–418, doi:10.1016/j.neuron.2016.09.022.

Lasagna-Reeves, C. A., D. L. Castillo-Carranza, U. Sengupta, J. Sarmiento, J. Troncoso, G. R. Jackson, and R. Kayed, 2012, Identification of oligomers at early stages of tau aggregation in Alzheimer's disease: FASEB J, v. 26, no. 5, p. 1946–1959, doi:10.1096/fj.11-199851.

Lee, V M-Y; Brunden, KR; Hutton, M; Trojanowski, J., 2011, Developing therapeutic approaches to tau, selected kinases, and related neuronal protein targets: Cold Spring Harbor perspectives in Medicine, v. 1, p. 1–20, doi:10.1101/cshperspect.a006437.

Lehman, E. J. H., L. S. Kulnane, Y. Gao, M. C. Petriello, K. M. Pimpis, L. Younkin, G. Dolios, R. Wang, S. G. Younkin, and B. T. Lamb, 2003, Genetic background regulates β-amyloid precursor protein processing and β-amyloid deposition in the mouse: Human Molecular Genetics, v. 12, no. 22, p. 2949–2956, doi:10.1093/hmg/ddg322.

Lei, P., S. Ayton, D. I. Finkelstein, L. Spoerri, G. D. Ciccotosto, D. K. Wright, B. X. W. Wong, P. A. Adlard, R. A. Cherny, L. Q. Lam, B. R. Roberts, I. Volitakis, G. F. Egan, C. A. McLean, R. Cappai, J. A. Duce, and A. I. Bush, 2012, Tau deficiency induces parkinsonism with dementia by impairing APP-mediated iron export: Nature Medicine, v. 18, no. 2, p. 291–295, doi:10.1038/nm.2613.

Leinenga, G., C. Langton, R. Nisbet, and J. Götz, 2016, Ultrasound treatment of neurological diseases-current and emerging applications: Nature Reviews Neurology, v. 12, no. 3, p. 161–174, doi:10.1038/nrneurol.2016.13.

Leroy, K., K. Ando, V. Laporte, R. Dedecker, V. Suain, M. Authelet, C. Héraud, N. Pierrot, Z. Yilmaz, J. N. Octave, and J. P. Brion, 2012, Lack of tau proteins rescues neuronal cell death and decreases amyloidogenic processing of APP in APP/PS1 mice: American Journal of Pathology, v. 181, no. 6, p. 1928–1940, doi:10.1016/j.ajpath.2012.08.012.

Leyns, C. E. G., and D. M. Holtzman, 2017, Glial contributions to neurodegeneration in tauopathies: Molecular Neurodegeneration, v. 12, no. 1, p. 1–16, doi:10.1186/s13024-017-0192-x.

Li, C., and J. Götz, 2017, Tau-based therapies in neurodegeneration: Opportunities and challenges: Nature Reviews Drug Discovery, v. 16, no. 12, p. 863–883, doi:10.1038/nrd.2017.155.

Li, X., Y. Kumar, H. Zempel, E.-M. Mandelkow, J. Biernat, and E. Mandelkow, 2011, Novel diffusion barrier for axonal retention of Tau in neurons and its failure in neurodegeneration.: The EMBO journal, v. 30, no. 23, p. 4825–37, doi:10.1038/emboj.2011.376.

Litman, P., J. Barg, L. Rindzoonski, and I. Ginzburg, 1993, Subcellular localization of tau mRNA in differentiating neuronal cell culture: Implications for neuronal polarity: Neuron, v. 10, no. 4, p. 627–638, doi:10.1016/0896-6273(93)90165-N.

Liu, L., V. Drouet, J. W. Wu, M. P. Witter, S. A. Small, C. Clelland, and K. Duff, 2012, Trans-synaptic spread of tau pathology in vivo: PLoS ONE, v. 7, no. 2, p. 1–9, doi:10.1371/journal.pone.0031302.

Liu, C., and J. Götz, 2013, Profiling murine tau with 0N, 1N and 2N isoform-specific antibodies in brain and peripheral organs reveals distinct subcellular localization, with the 1N isoform being enriched in the nucleus: PLoS ONE, v. 8, no. 12, p. 1–18, doi:10.1371/journal.pone.0084849.

Long, M. A., and F. M. V. Rossi, 2009, Silencing Inhibits Cre-Mediated Recombination of the Z/AP and Z/EG Reporters in Adult Cells: PLoS ONE, v. 4, no. 5, doi:10.1371/journal.pone.0005435.

Loomis, P. A., T. H. Howard, R. P. Castleberry, and L. I. Binder, 1990, Identification of nuclear T isoforms in human neuroblastoma cells: Proceedings of the National Academy of Sciences of the United States of America, v. 87, no. 21, p. 8422–8426, doi:10.1073/pnas.87.21.8422.

Lopresti, P., S. Szuchet, S. C. Papasozomenos, R. P. Zinkowski, and L. I. Binder, 1995, Functional implications for the microtubule-associated protein Tau: localization in oligodendrocytes: Proceedings of the National Academy of Sciences of the United States of America, v. 92, no. October, p. 10369–10373, doi:10.1073/pnas.92.22.10369.

Lorente de Nó, R., 1934, Studies on the structure of the cerebral cortex. II. Continuation of the study of the ammonic system: Journal für Psychologie und Neurologie, v. 46, p. 113–177, doi:10.1213/ane.0b013e31817330cf.

Lovestone, S., and C. H. Reynolds, 1997, The phosphorylation of Tau: a critical stage in neurodevelopment and neurodegenerative processes: Neuroscience, v. 78, no. 2, p. 309–324, doi:10.1016/s0306-4522(96)00577-5.

Ma, Q. L., X. Zuo, F. Yang, O. J. Ubeda, D. J. Gant, M. Alaverdyan, N. C. Kiosea, S. Nazari, P. P. Chen, F. Nothias, P. Chan, E. Teng, S. A. Frautschy, and G. M. Cole, 2014, Loss of MAP function leads to hippocampal synapse loss and deficits in the morris water maze with aging: Journal of Neuroscience, v. 34, no. 21, p. 7124–7136, doi:10.1523/JNEUROSCI.3439-13.2014.

Maeda, S., N. Sahara, Y. Saito, M. Murayama, Y. Yoshiike, H. Kim, T. Miyasaka, S. Murayama, A. Ikai, and A. Takashima, 2007, Granular tau oligomers as intermediates of tau filaments: Biochemistry, v. 46, no. 12, p. 3856–3861, doi:10.1021/bi061359o.

Magnani, E., J. Fan, L. Gasparini, M. Golding, M. Williams, G. Schiavo, M. Goedert, L. A. Amos, and M. G. Spillantini, 2007, Interaction of tau protein with the dynactin complex: EMBO Journal, v. 26, no. 21, p. 4546–4554, doi:10.1038/sj.emboj.7601878.

Mandelkow, E.-M., and E. Mandelkow, 2012, Biochemistry and cell biology of tau protein in neurofibrillary degeneration.: Cold Spring Harbor perspectives in medicine, v. 2, no. 7, p. a006247, doi:10.1101/cshperspect.a006247.

Maphis, N., G. Xu, O. N. Kokiko-Cochran, A. Cardona, R. M. Ransohoff, B. T. Lamb, and K. Bhaskar, 2015, Loss of tau rescues inflammation-mediated neurodegeneration: Frontiers in Neuroscience, v. 9, no. 5, p. 1–12, doi:10.3389/fnins.2015.00196.

Maphis, N., G. Xu, O. N. Kokiko-Cochran, S. Jiang, A. Cardona, R. M. Ransohoff, B. T. Lamb, and K. Bhaskar, 2015, Reactive microglia drive tau pathology and contribute to the spreading of pathological tau in the brain: Brain, v. 138, no. 6, p. 1738–1755, doi:10.1093/brain/awv081.

Martini-Stoica, H., A. L. Cole, D. B. Swartzlander, F. Chen, Y. W. Wan, L. Bajaj, D. A. Bader, V. M. Y. Lee, J. Q. Trojanowski, Z. Liu, M. Sardiello, and H. Zheng, 2018, TFEB enhances astroglial uptake of extracellular tau species and reduces tau spreading: Journal of Experimental Medicine, v. 215, no. 9, p. 2355–2377, doi:10.1084/jem.20172158.

Mattson, M., and T. Magnus, 2014, Ageing and neuronal vulnerability: Nature reviews. Neuroscience, v. 7, p. 278–294, doi:10.1037/a0032811.Child.

Mausbach, B. T., E. A. Chattillion, S. K.- Roepke, T. Patterson, and I. Grant, 2014, A comparison of psychosocial outcomes in elderly Alzheimer's caregivers and non-caregivers: Am J Geriatr Psychiatry, v. 21, no. 1, p. 1–13, doi:10.1016/j.jagp.2012.10.001.A.

Mcgeer, P. L., H. Akiyama, S. Itagaki, and E. G. Mcgeer, 1989, Immune System Response in Alzheimer's Disease: Canadian Journal of Neurological Sciences / Journal Canadien des Sciences Neurologiques, v. 16, no. S4, p. 516–527, doi:10.1017/S0317167100029863.

McInnes, J., K. Wierda, A. Snellinx, L. Bounti, Y. C. Wang, I. C. Stancu, N. Apóstolo, K. Gevaert, I. Dewachter, T. L. Spires-Jones, B. De Strooper, J. De Wit, L. Zhou, and P. Verstreken, 2018, Synaptogyrin-3 Mediates

Presynaptic Dysfunction Induced by Tau: Neuron, v. 97, no. 4, p. 823-835.e8, doi:10.1016/j.neuron.2018.01.022.

Mirbaha, H., D. Chen, O. A. Morazova, K. M. Ruff, A. M. Sharma, X. Liu, M. Goodarzi, R. V. Pappu, D. W. Colby, H. Mirzaei, L. A. Joachimiak, and M. I. Diamond, 2018, Inert and seed-competent tau monomers suggest structural origins of aggregation: eLife, v. 7, p. 1–29, doi:10.7554/eLife.36584.

Miyasaka, T., C. Xie, S. Yoshimura, Y. Shinzaki, S. Yoshina, E. Kage-Nakadai, S. Mitani, and Y. Ihara, 2016, Curcumin improves tau-induced neuronal dysfunction of nematodes: Neurobiology of Aging, v. 39, p. 69–81, doi:10.1016/j.neurobiolaging.2015.11.004.

Mocanu, M.-M., A. Nissen, K. Eckermann, I. Khlistunova, J. Biernat, D. Drexler, O. Petrova, K. Schonig, H. Bujard, E. Mandelkow, L. Zhou, G. Rune, and E.-M. Mandelkow, 2008, The Potential for -Structure in the Repeat Domain of Tau Protein Determines Aggregation, Synaptic Decay, Neuronal Loss, and Coassembly with Endogenous Tau in Inducible Mouse Models of Tauopathy: Journal of Neuroscience, v. 28, no. 3, p. 737–748, doi:10.1523/jneurosci.2824-07.2008.

Morishima-Kawashima, M. Hasegawa, K. Takio, M. Suzuki, H. Yoshida, K. Titani, and Y. Ihara, 1995, Proline-directed and non-proline-directed phosphorylation of PHF-tau: The Journal of biological chemistry, v. 270, no. 2, p. 823–829, doi:10.1074/jbc.270.2.823.

Morita, T., and K. Sobuě, 2009, Specification of neuronal polarity regulated by local translation of CRMP2 and tau via the mTOR-p70S6K pathway: Journal of Biological Chemistry, v. 284, no. 40, p. 27734–27745, doi:10.1074/jbc.M109.008177.

Morsch, R., W. Simon, and P. Coleman, 1999, Neurons may live for decades with neurofibrillary tangles: J Neuropathol Exp Neurol, v. 58, no. 2, p. 188–197, doi:10.1097/00005072-199902000-00008.

Mroczko, B., M. Groblewska, and A. Litman-Zawadzka, 2019, The role of protein misfolding and tau oligomers (TauOs) in Alzheimer's disease (AD): International Journal of Molecular Sciences, v. 20, no. 19, doi:10.3390/ijms20194661.

Mudher, A., M. Colin, S. Dujardin, M. Medina, I. Dewachter, S. M. Alavi Naini, E. M. Mandelkow, E. Mandelkow, L. Buée, M. Goedert, and J. P. Brion, 2017, What is the evidence that tau pathology spreads through prion-like propagation? Acta neuropathologica communications, v. 5, no. 1, p. 99, doi:10.1186/s40478-017-0488-7.

Mukrasch, M. D., S. Bibow, J. Korukottu, S. Jeganathan, J. Biernat, C. Griesinger, E. Mandelkow, and M. Zweckstetter, 2009, Structural polymorphism of 441-residue Tau at single residue resolution: PLoS Biology, v. 7, no. 2, p. 0399–0414, doi:10.1371/journal.pbio.1000034.

Murayama, S., and Y. Saito, 2004, Neuropathological diagnostic criteria for Alzheimer's disease: Neuropathology, v. 24, no. 3, p. 254–260, doi:10.1111/j.1440-1789.2004.00571.x.

Nave, K.-A., and H. B. Werner, 2014, Myelination of the Nervous System: Mechanisms and Functions: Annual Review of Cell and Developmental Biology, v. 30, no. 1, p. 503–533, doi:10.1146/annurev-cellbio-100913-013101.

Necula, M., R. Kayed, S. Milton, and C. G. Glabe, 2007, Small molecule inhibitors of aggregation indicate that amyloid β oligomerization and fibrillization pathways are independent and distinct: Journal of Biological Chemistry, v. 282, no. 14, p. 10311–10324, doi:10.1074/jbc.M608207200.

Neddens, J., M. Temmel, S. Flunkert, B. Kerschbaumer, C. Hoeller, T. Loeffler, V. Niederkofler, G. Daum, J. Attems, and B. Hutter-Paier, 2018, Phosphorylation of different tau sites during progression of Alzheimer's disease: Acta Neuropathologica Communications, v. 6, no. 52, p. 1–15, doi:10.1186/s40478-018-0557-6.

Neve, R. L., P. Harris, K. S. Kosik, D. M. Kurnit, and T. a. Donlon, 1986, Identification of cDNA clones for the human microtubule-associated protein Tau and chromosomal localization of the genes for Tau and microtubule-associated protein 2: Molecular Brain Research, v. 1, no. 3, p. 271–280, doi:10.1016/0169-328X(86)90033-1.

Nilson, A. N., K. C. English, J. E. Gerson, T. Barton Whittle, C. Nicolas Crain, J. Xue, U. Sengupta, D. L. Castillo-Carranza, W. Zhang, P. Gupta, and R. Kayed, 2017, Tau oligomers associate with inflammation in the brain and retina of tauopathy mice and in neurodegenerative diseases: Journal of Alzheimer's Disease, v. 55, no. 3, p. 1083–1099, doi:10.3233/JAD-160912.

Novak, P. … M. Novak, 2017, Safety and immunogenicity of the tau vaccine AADvac1 in patients with Alzheimer's disease: a randomised, double-blind, placebo-controlled, phase 1 trial: The Lancet Neurology, v. 16, no. 2, p. 123–134, doi:10.1016/S1474-4422(16)30331-3.

Oh, S. J., J. Cheng, J. H. Jang, J. Arace, M. Jeong, C. H. Shin, J. Park, J. Jin, P. Greengard, and Y. S. Oh, 2019, Hippocampal mossy cell involvement in behavioral and neurogenic responses to chronic antidepressant treatment: Molecular Psychiatry, doi:10.1038/s41380-019-0384-6.

Opsahl, M. L., M. McClenaghan, A. Springbett, S. Reid, R. Lathe, A. Colman, and C. B. A. Whitelaw, 2002, Multiple effects of genetic background on variegated transgene expression in mice: Genetics, v. 160, no. 3, p. 1107–

1112.

Ozcelik, S., G. Fraser, P. Castets, V. Schaeffer, Z. Skachokova, K. Breu, F. Clavaguera, M. Sinnreich, L. Kappos, M. Goedert, M. Tolnay, and D. T. Winkler, 2013, Rapamycin Attenuates the Progression of Tau Pathology in P301S Tau Transgenic Mice: PLoS ONE, v. 8, no. 5, p. 2–8, doi:10.1371/journal.pone.0062459.

Papasozomenos, S. C., and L. I. Binder, 1987, Phosphorylation determines two distinct species of Tau in the central nervous system.: Cell motility and the cytoskeleton, v. 8, no. 3, p. 210–226, doi:10.1002/cm.970080303.

Peeraer, E., A. Bottelbergs, K. Van Kolen, I. Stancu, B. Vasconcelos, M. Mahieu, H. Duytschaever, L. Ver Donck, A. Torremans, E. Sluydts, N. Van Acker, J. Kemp, M. Mercken, K. Brunden, J. Trojanowski, I. Dewachter, V. Lee, and D. Moechars, 2015, Intracerebral injection of preformed synthetic tau fibrils initiates widespread tauopathy and neuronal loss in the brains of tau transgenic mice: Neurobiology of disease, v. 73, no. 1, p. 83–95, doi:10.1016/j.nbd.2014.08.032.

Perea, J. R., M. Llorens-Martín, J. Ávila, and M. Bolós, 2018, The role of microglia in the spread of Tau: Relevance for tauopathies: Frontiers in Cellular Neuroscience, v. 12, no. July, p. 1–8, doi:10.3389/fncel.2018.00172.

Pickhardt, M., T. Neumann, D. Schwizer, K. Callaway, M. Vendruscolo, D. Schenk, P. George-Hyslop, Eva Mandelkow, C. Dobson, L. McConlogue, Eckhard Mandelkow, and G. Toth, 2015, Identification of Small Molecule Inhibitors of Tau Aggregation by Targeting Monomeric Tau As a Potential Therapeutic Approach for Tauopathies: Current Alzheimer Research, v. 12, no. 9, p. 814–828, doi:10.2174/156720501209151019104951.

Pickhardt, M., J. Biernat, S. Hübschmann, F. J. A. Dennissen, T. Timm, A. Aho, E. M. Mandelkow, and E. Mandelkow, 2017, Time course of Tau toxicity and pharmacologic prevention in a cell model of Tauopathy: Neurobiology of Aging, v. 57, p. 47–63, doi:10.1016/j.neurobiolaging.2017.04.022.

Pickhardt, M., Z. Gazova, M. Von Bergen, I. Khlistunova, Y. Wang, A. Hascher, E. M. Mandelkow, J. Biernat, and E. Mandelkow, 2005, Anthraquinones inhibit tau aggregation and dissolve Alzheimer's paired helical filaments in vitro and in cells: Journal of Biological Chemistry, v. 280, no. 5, p. 3628–3635, doi:10.1074/jbc.M410984200.

Pickhardt, M., G. Larbig, I. Khlistunova, A. Coksezen, B. Meyer, E. M. Mandelkow, B. Schmidt, and E. Mandelkow, 2007, Phenylthiazolyl-hydrazide and its derivatives are potent inhibitors of τ aggregation and toxicity in vitro and in cells: Biochemistry, v. 46, no. 35, p. 10016–10023, doi:10.1021/bi700878g.

Planel, E., K. E. G. Richter, C. E. Nolan, J. E. Finley, L. Liu, Y. Wen, P. Krishnamurthy, M. Herman, L. Wang, J. B. Schachter, R. B. Nelson, L.-F. Lau, and K. E. Duff, 2007, Anesthesia leads to tau hyperphosphorylation through inhibition of phosphatase activity by hypothermia.: The Journal of neuroscience : the official journal of the Society for Neuroscience, v. 27, no. 12, p. 3090–7, doi:10.1523/JNEUROSCI.4854-06.2007.

Price, J., P. Davis, J. Morris, and D. White, 1991, The distribution of tangles, plaques and related immunohistochemical markers in healthy aging and Alzheimer's disease: Neurobiology of aging, v. 12, no. 4, p. 295–312, doi:10.1016/0197-4580(91)90006-6.

Probst, A., J. Ulrich, and P. U. Heitz, 1982, Senile dementia of Alzheimer type: Astroglial reaction to extracellular neurofibrillary tangles in the hippocampus - An immunocytochemical and electron-microscopic study: Acta Neuropathologica, v. 57, no. 1, p. 75–79, doi:10.1007/BF00688880.

Prusiner, S. B., 1998, Prions: Proceedings of the National Academy of Sciences of the United States of America, v. 95, no. 23, p. 13363–13383, doi:10.1073/pnas.95.23.13363.

Ramón y Cajal S., 1893, Estructura del asta de Ammon y fascia dentata: Ann Soc Esp Hist Nat, v. 22, doi:10.1016/j.neubiorev.2005.02.002.

Ramón y Cajal S., 1902, Sobre un ganglio especial de la corteza esfeno-occipital: Trab del Lab de Invest Biol Univ Madrid, v. 1, p. 189–206, doi:10.1111/j.1460-9592.2010.03506.x.

Ramsden, M., L. Kotilinek, C. Forster, J. Paulson, E. McGowan, K. SantaCruz, A. Guimaraes, M. Yue, J. Lewis, G. Carlson, M. Hutton, and K. H. Ashe, 2005, Age-dependent neurofibrillary tangle formation, neuron loss, and memory impairment in a mouse model of human tauopathy (P301L): Journal of Neuroscience, v. 25, no. 46, p. 10637–10647, doi:10.1523/JNEUROSCI.3279-05.2005.

Rapoport, M., H. N. Dawson, L. I. Binder, M. P. Vitek, and A. Ferreira, 2002, Tau is essential to beta -amyloid-induced neurotoxicity: Proceedings of the National Academy of Sciences of the United States of America, v. 99, no. 9, p. 6364–6369, doi:10.1073/pnas.092136199.

Roberson, E. D., K. Scearce-Levie, J. J. Palop, F. Yan, I. H. Cheng, T. Wu, H. Gerstein, G.-Q. Yu, and L. Mucke, 2007, Reducing endogenous tau ameliorates amyloid beta-induced deficits in an Alzheimer's disease mouse model.: Science, v. 316, no. 5825, p. 750–4, doi:10.1126/science.1141736.

Robertson, A., J. Perea, T. Tolmachova, P. K. Thomas, and C. Huxley, 2002, Effects of mouse strain, position of integration and tetracycline analogue on the tetracycline conditional system in transgenic mice: Gene, v. 282, no. 1–2, p. 65–74, doi:10.1016/S0378-1119(01)00793-4.

Roselli, F., M. Tirard, J. Lu, P. Hutzler, P. Lamberti, P. Livrea, M. Morabito, and O. F. X. Almeida, 2005, Soluble β-amyloid1-40 induces NMDA-Dependent Degradation of Postsynaptic Density-95 at Glutamatergic Synapses: Journal of Neuroscience, v. 25, no. 48, p. 11061–11070, doi:10.1523/JNEUROSCI.3034-05.2005.

Rowland, D. C., A. P. Weible, I. R. Wickersham, H. Wu, M. Mayford, M. P. Witter, and C. G. Kentros, 2013, Transgenically targeted rabies virus demonstrates a major monosynaptic projection from hippocampal area CA2 to medial entorhinal layer II neurons: Journal of Neuroscience, v. 33, no. 37, p. 14889–14898, doi:10.1523/JNEUROSCI.1046-13.2013.

Saito, Y., N. N. Ruberu, M. Sawabe, T. Arai, N. Tanaka, Y. Kakuta, H. Yamanouchi, and S. Murayama, 2004, Staging of argyrophilic grains: An age-associated tauopathy: Journal of Neuropathology and Experimental Neurology, v. 63, no. 9, p. 911–918, doi:10.1093/jnen/63.9.911.

Salehi, A., J.-D. Delcroix, and W. C. Mobley, 2003, Traffic at the intersection of neurotrophic factor signaling and neurodegeneration: Trends in neurosciences, v. 26, no. 2, p. 73–80, doi:10.1016/S0166-2236(02)00038-3.

Sanders, D. W., S. K. Kaufman, S. L. Devos, A. M. Sharma, A. Li, S. J. Barker, A. Foley, J. R. Thorpe, L. C. Serpell, T. M. Miller, L. T. Grinberg, W. W. Seeley, and M. I. Diamond, 2014, Distinct tau prion strains propagate in cells and mice and define different tauopathies: Neuron, v. 82, no. 6, p. 1271–1288, doi:10.1016/j.neuron.2014.04.047.Distinct.

SantaCruz, K. … K. H. Ashe, 2005, Tau Suppression in a Neurodegenerative Mouse Model Improves Memory Function: Science, v. 309, no. 5733, p. 476–481, doi:10.1037/a0013262.Open.

Saura, C. A., A. Parra-Damas, and L. Enriquez-Barreto, 2015, Gene expression parallels synaptic excitability and plasticity changes in Alzheimer’s disease: Frontiers in Cellular Neuroscience, v. 9, no. 318, p. 1–14, doi:10.3389/fncel.2015.00318.

Scharfman, H. E., 2006, Epileptogenesis in the Parahippocampal Region: Parallels with the Dentate Gyrus: Annals of the New York Academy of Sciences, v. 911, no. 1, p. 305–327, doi:10.1111/j.1749-6632.2000.tb06734.x.

Scharfman, H., and M. Chao, 2013, The entorhinal cortex and neurotrophin signaling in Alzheimer’s disease and other disorders: Cogn Neurosci, v. 4, no. 3, p. 123–135, doi:10.1038/jid.2014.371.

Schneider, A., J. Biernat, M. Von Bergen, E. Mandelkow, and E. M. Mandelkow, 1999, Phosphorylation that detaches tau protein from microtubules (Ser262, Ser214) also protects it against aggregation into Alzheimer paired helical filaments: Biochemistry, v. 38, no. 12, p. 3549–3558, doi:10.1021/bi981874p.

Seibenhener, M. L., and M. C. Wooten, 2015, Use of the open field maze to measure locomotor and anxiety-like behavior in mice: Journal of Visualized Experiments, v. 3, no. 96, p. 1–6, doi:10.3791/52434.

Selkoe, D. J., 2006, Toward a Comprehensive Theory for Alzheimer’s Disease: Annals of the New York Academy of Sciences, v. 924, no. 1, p. 17–25, doi:10.1111/j.1749-6632.2000.tb05554.x.

Shahani, N., and R. Brandt, 2002, Functions and malfunctions of the Tau proteins: Cell. Mol. Life Sci, v. 59, p. 1668–1680, doi:10.1007/pl00012495.

Sharma, A. M., T. L. Thomas, D. R. Woodard, O. M. Kashmer, and M. I. Diamond, 2018, Tau monomer encodes strains: eLife, v. 7, p. 1–20, doi:10.7554/eLife.37813.

Sheffield, L. G., J. G. Marquis, and N. E. J. Berman, 2000, Regional distribution of cortical microglia parallels that of neurofibrillary tangles in Alzheimer’s disease: Neuroscience Letters, v. 285, no. 3, p. 165–168, doi:10.1016/S0304-3940(00)01037-5.

Simon, E., J. Obst, and D. Gomez-Nicola, 2019, The Evolving Dialogue of Microglia and Neurons in Alzheimer’s Disease: Microglia as Necessary Transducers of Pathology: Neuroscience, v. 405, p. 24–34, doi:10.1016/j.neuroscience.2018.01.059.

Sjöberg, M. K., E. Shestakova, Z. Mansuroglu, R. B. Maccioni, and E. Bonnefoy, 2006, Tau protein binds to pericentromeric DNA: A putative role for nuclear tau in nucleolar organization: Journal of Cell Science, v. 119, no. 10, p. 2025–2034, doi:10.1242/jcs.02907.

Spires, T. L., J. D. Orne, K. SantaCruz, R. Pitstick, G. a Carlson, K. H. Ashe, and B. T. Hyman, 2006, Region-specific dissociation of neuronal loss and neurofibrillary pathology in a mouse model of tauopathy: The American journal of pathology, v. 168, no. 5, p. 1598–1607, doi:10.2353/ajpath.2006.050840.

Stamer, K., R. Vogel, E. Thies, E. Mandelkow, and E. M. Mandelkow, 2002, Tau blocks traffic of organelles, neurofilaments, and APP vesicles in neurons and enhances oxidative stress: Journal of Cell Biology, v. 156, no. 6, p. 1051–1063, doi:10.1083/jcb.200108057.

Streit, W. J., H. Braak, K. Del Tredici, J. Leyh, J. Lier, H. Khoshbouei, C. Eisenlöffel, W. Müller, and I. Bechmann, 2018, Microglial activation occurs late during preclinical Alzheimer’s disease: Glia, v. 66, no. 12, p. 2550–2562, doi:10.1002/glia.23510.

Strong, M., A. Southwell, J. Yonan, M. Hayden, G. Macgregor, L. Thompson, and O. Steward, 2012, Age-Dependent Resistance to Excitotoxicity in Htt CAG140 Mice and the Effect of Strain Background: J

Huntingtons Dis., v. 1, no. 2, p. 221–41, doi:10.3233/JHD-129005.

Sultan, A., F. Nesslany, M. Violet, S. Bégard, A. Loyens, S. Talahari, Z. Mansuroglu, D. Marzin, N. Sergeant, S. Humez, M. Colin, E. Bonnefoy, L. Buée, and M. C. Galas, 2011, Nuclear Tau, a key player in neuronal DNA protection: Journal of Biological Chemistry, v. 286, no. 6, p. 4566–4575, doi:10.1074/jbc.M110.199976.

Swain, J. L., T. A. Stewart, and P. Leder, 1987, Parental legacy determines methylation and expression of an autosomal transgene: A molecular mechanism for parental imprinting: Cell, v. 50, no. 5, p. 719–727, doi:10.1016/0092-8674(87)90330-8.

Swaminathan, A., I. Wichert, D. Schmitz, and N. Maier, 2018, Involvement of Mossy Cells in Sharp Wave-Ripple Activity In Vitro: Cell Reports, v. 23, no. 9, p. 2541–2549, doi:10.1016/j.celrep.2018.04.095.

Sydow, A., A. Van der Jeugd, F. Zheng, T. Ahmed, D. Balschun, O. Petrova, D. Drexler, L. Zhou, G. Rune, E. Mandelkow, R. D'Hooge, C. Alzheimer, and E.-M. Mandelkow, 2011, Tau-Induced Defects in Synaptic Plasticity, Learning, and Memory Are Reversible in Transgenic Mice after Switching Off the Toxic Tau Mutant: Journal of Neuroscience, v. 31, no. 7, p. 2511–2525, doi:10.1523/jneurosci.5245-10.2011.

Sydow, A., K. Hochgräfe, S. Könen, D. Cadinu, D. Matenia, O. Petrova, M. Joseph, F. J. Dennissen, and E. M. Mandelkow, 2016, Age-dependent neuroinflammation and cognitive decline in a novel Ala152Thr-Tau transgenic mouse model of PSP and AD: Acta neuropathologica communications, v. 4, p. 17, doi:10.1186/s40478-016-0281-z.

Szymczak, A. L., C. J. Workman, Y. Wang, K. M. Vignali, S. Dilioglou, E. F. Vanin, and D. A. A. Vignali, 2004, Correction of multi-gene deficiency in vivo using a single "self-cleaving" 2A peptide–based retroviral vector: Nature Biotechnology, v. 22, no. 5, p. 589–594, doi:10.1038/nbt957.

Tai, H. C., B. Y. Wang, A. Serrano-Pozo, M. P. Frosch, T. L. Spires-Jones, and B. T. Hyman, 2014, Frequent and symmetric deposition of misfolded tau oligomers within presynaptic and postsynaptic terminals in Alzheimer's disease: Acta Neuropathologica Communications, v. 2, no. 1, p. 1–14, doi:10.1186/s40478-014-0146-2.

Takashima, A., 2015, Toxic Tau aggregation in AD: Advances in Experimental Medicine and Biology, v. 822, p. 3–9, doi:10.1007/978-3-319-08927-0.

Thies, W., and L. Bleiler, 2011, Alzheimer's Disease Facts and Figures: Alzheimers Dement, v. 7:208, no. 44.

Thies, E., and E. M. Mandelkow, 2007, Missorting of tau in neurons causes degeneration of synapses that can be rescued by the kinase MARK2/Par-1: Journal of Neuroscience, v. 27, no. 11, p. 2896–2907, doi:10.1523/JNEUROSCI.4674-06.2007.

Thompson, R. F., and J. J. Kim, 1996, Memory systems in the brain and localization of a memory: Proceedings of the National Academy of Sciences of the United States of America, v. 93, no. 24, p. 13438–13444, doi:10.1073/pnas.93.24.13438.

Trabzuni, D., S. Wray, J. Vandrovcova, A. Ramasamy, R. Walker, C. Smith, C. Luk, J. R. Gibbs, A. Dillman, D. G. Hernandez, S. Arepalli, A. B. Singleton, M. R. Cookson, A. M. Pittman, R. De silva, M. E. Weale, J. Hardy, and M. Ryten, 2012, MAPT expression and splicing is differentially regulated by brain region: Relation to genotype and implication for tauopathies: Human Molecular Genetics, v. 21, no. 18, p. 4094–4103, doi:10.1093/hmg/dds238.

Tran, H., L. Sanchez, and D. Brody, 2012, Inhibition of JNK by a peptide inhibitor reduces traumatic brain injury-induced tauopathy in transgenic mice: J Neuropathol Exp Neurol, v. 71, no. 2, p. 116–29, doi:10.1097/NEN.0b013e3182456aed.

Tsao, A., J. Sugar, L. Lu, C. Wang, J. J. Knierim, M. B. Moser, and E. I. Moser, 2018, Integrating time from experience in the lateral entorhinal cortex: Nature, v. 561, no. 7721, p. 57–62, doi:10.1038/s41586-018-0459-6.

Utton, M. A., W. J. Noble, J. E. Hill, B. H. Anderton, and D. P. Hanger, 2005, Molecular motors implicated in the axonal transport of tau and α-synuclein: Journal of Cell Science, v. 118, no. 20, p. 4645–4654, doi:10.1242/jcs.02558.

Verny, M., C. Duyckaerts, Y. Agid, and J. J. Hauw, 1996, The significance of cortical pathology in progressive supranuclear palsy. Clinico-pathological data in 10 cases: Brain, v. 119, no. 4, p. 1123–1136, doi:10.1093/brain/119.4.1123.

Vershinin, M., B. C. Carter, D. S. Razafsky, S. J. King, and S. P. Gross, 2007, Multiple-motor based transport and its regulation by Tau: Proceedings of the National Academy of Sciences of the United States of America, v. 104, no. 1, p. 87–92, doi:10.1073/pnas.0607919104.

Violet, M., L. Delattre, M. Tardivel, A. Sultan, A. Chauderlier, R. Caillierez, S. Talahari, F. Nesslany, B. Lefebvre, E. Bonnefoy, L. Buée, and M. C. Galas, 2014, A major role for Tau in neuronal DNA and RNA protection in vivo under physiological and hyperthermic conditions: Frontiers in Cellular Neuroscience, v. 8, no. MAR, p. 1–11, doi:10.3389/fncel.2014.00084.

Vitale, F., L. Giliberto, S. Ruiz, K. Steslow, P. Marambaud, and C. d'Abramo, 2018, Anti-tau conformational scFv

MC1 antibody efficiently reduces pathological tau species in adult JNPL3 mice: Acta neuropathologica communications, v. 6, no. 1, p. 82, doi:10.1186/s40478-018-0585-2.

Vogels, T., A.-N. Murgoci, and T. Hromádka, 2019, Intersection of pathological tau and microglia at the synapse: Acta Neuropathologica Communications, v. 7, no. 1, p. 1–25, doi:10.1186/s40478-019-0754-y.

Vossel, K. a., J. C. Xu, V. Fomenko, T. Miyamoto, E. Suberbielle, J. a. Knox, K. Ho, D. H. Kim, G.-Q. Yu, and L. Mucke, 2015, Tau reduction prevents Abeta-induced axonal transport deficits by blocking activation of GSK3: The Journal of Cell Biology, v. 209, no. 3, p. 419–433, doi:10.1083/jcb.201407065.

Wang, Y., V. Balaji, S. Kaniyappan, L. Krüger, S. Irsen, K. Tepper, R. Chandupatla, W. Maetzler, A. Schneider, E. Mandelkow, and E.-M. Mandelkow, 2017, The release and trans-synaptic transmission of Tau via exosomes: Molecular Neurodegeneration, v. 12, p. 5, doi:10.1186/s13024-016-0143-y.

Wang, Y., and P. A. Loomis, 1993, A Novel Tau Transcript in Cultured Human Neuroblastoma Cells Expressing Nuclear Tau: The Journal of Cell Biology, v. 121, no. 2, p. 257–267, doi:10.1083/jcb.121.2.257.

Wang, Y., and E. Mandelkow, 2012, Degradation of tau protein by autophagy and proteasomal pathways: Biochemical Society transactions, v. 40, no. 4, p. 644–52, doi:10.1042/BST20120071.

Wang, Y., and E. Mandelkow, 2016, Tau in physiology and pathology: Nature Reviews Neuroscience, v. 17, no. 1, p. 5–21, doi:10.1038/nrn.2015.1.

Wegmann, S., E. A. Maury, M. J. Kirk, L. Saqran, A. Roe, S. L. DeVos, S. Nicholls, Z. Fan, S. Takeda, O. Cagsal-Getkin, C. M. William, T. L. Spires-Jones, R. Pitstick, G. A. Carlson, A. M. Pooler, and B. T. Hyman, 2015, Removing endogenous tau does not prevent tau propagation yet reduces its neurotoxicity: The EMBO Journal, v. 34, no. 24, p. 3028–3041, doi:10.15252/embj.201592748.

Weingarten, M. D., A. H. Lockwood, S. Hwo, and M. W. Kirschner, 1975, A protein factor essential for microtubule assembly: Proceedings of the National Academy of Sciences of the United States of America, v. 72, no. 5, p. 1858–1862, doi:10.1073/pnas.72.5.1858.

Weissmann, C., 2004, The state of the prion: Nature Reviews Microbiology, v. 2, no. 11, p. 861–871, doi:10.1038/nrmicro1025.

Wischik, C. M., P. C. Edwards, R. Y. K. Lai, M. Roth, and C. R. Harrington, 1996, Selective inhibition of Alzheimer disease-like tau aggregation by phenothiazines: Proceedings of the National Academy of Sciences of the United States of America, v. 93, no. 20, p. 11213–11218, doi:10.1073/pnas.93.20.11213.

Witter, M., and D. Amaral, 1991, Entorhinal cortex of the monkey: V. Projections to the dentate gyrus, hippocampus, and subicular complex.: Journal of Comparative Neurology, v. 307, p. 437–459, doi:10.1002/cne.903070308.

Witter, Menno P., T. P. Doan, B. Jacobsen, E. S. Nilssen, and S. Ohara, 2017, Architecture of the entorhinal cortex a review of entorhinal anatomy in rodents with some comparative notes: Frontiers in Systems Neuroscience, v. 11, no. 46, p. 1–12, doi:10.3389/fnsys.2017.00046.

Witter, M. P., H. J. Groenewegen, F. H. Lopes da Silva, and A. H. M. Lohman, 1989, Functional organization of the extrinsic and intrinsic circuitry of the parahippocampal region: Progress in Neurobiology, v. 33, no. 3, p. 161–253, doi:10.1016/0301-0082(89)90009-9.

Witter, M. P., G. W. Van Hoesen, and D. G. Amaral, 1989, Topographical organization of the entorhinal projection to the dentate gyrus of the monkey: Journal of Neuroscience, v. 9, no. 1, p. 216–228, doi:https://doi.org/10.1523/JNEUROSCI.09-01-00216.1989.

Witter, M.P., H. Kleven, and A. K. Flatmoen, 2017, Comparative contemplations on the hippocampus: Brain Behav Evol, v. 90, no. 1, p. 15–24, doi:10.1093/bja/aet177.

Wu, J. W., S. A. Hussaini, I. M. Bastille, G. A. Rodriguez, A. Mrejeru, K. Rilett, D. W. Sanders, C. Cook, H. Fu, R. A.C.M., M. I. Boonen1, Mathieu Herman1, Eden Nahmani1, Sheina Emrani1, Y. Helen Figueroa1, and 7 Diamond4, Catherine L. Clelland1, Selina Wray6, and Karen E. Duff1, 2, 2016, Neuronal activity enhances tau propagation and tau pathology in vivo: Nat Neurosci, v. 19, no. 8, p. 1085–1092, doi:10.1038/nn.4328.

Xu, H., T. W. Rosler, T. Carlsson, A. de Andrade, O. Fiala, M. Hollerhage, W. H. Oertel, M. Goedert, A. Aigner, and G. U. Hoglinger, 2014, Tau silencing by siRNA in the P301S mouse model of tauopathy: Current Gene Therapy, v. 14, no. 5, p. 343–351, doi:10.2174/156652321405140926160602.

Yan, M., X. Wang, and X. Zhu, 2013, Mitochondrial defects and oxidative stress in Alzheimer disease and Parkinson disease: Free Radic Biol Med, v. 62, p. 90–101, doi:10.1016/j.freeradbiomed.2012.11.014.

Yasuda, M., and M. R. Mayford, 2006, CaMKII Activation in the Entorhinal Cortex Disrupts Previously Encoded Spatial Memory: Neuron, v. 50, no. 2, p. 309–318, doi:10.1016/j.neuron.2006.03.035.

Yetman, M., S. Lillehaug, J. Bjaalie, T. Leergaard, and J. Jankowsky, 2016, Transgene expression in the Nop-tTA driver line is not inherently restricted to the entorhinal cortex: Brain Struct Funct., v. 221, no. 4, p. 2231–2249, doi:10.1007/s00429-015-1040-9.

Yoshida, H., and Y. Ihara, 1993, Tau in Paired Helical Filaments Is Functionally Distinct from Fetal Tau: Assembly

Incompetence of Paired Helical Filament-Tau: Journal of neurochemistry, v. 61, no. 3, p. 1183–1186, doi:10.1111/j.1471-4159.1993.tb03642.x.

Zanier, E. R., I. Bertani, E. Sammali, F. Pischiutta, M. A. Chiaravalloti, G. Vegliante, A. Masone, A. Corbelli, D. H. Smith, D. K. Menon, N. Stocchetti, F. Fiordaliso, M. G. De Simoni, W. Stewart, and R. Chiesa, 2018, Induction of a transmissible tau pathology by traumatic brain injury: Brain, v. 141, no. 9, p. 2685–2699, doi:10.1093/brain/awy193.

Zempel, H., F. J. A. Dennissen, Y. Kumar, J. Luedtke, J. Biernat, E. M. Mandelkow, and E. Mandelkow, 2017, Axodendritic sorting and pathological missorting of Tau are isoform-specific and determined by axon initial segment architecture: Journal of Biological Chemistry, v. 292, no. 29, p. 12192–12207, doi:10.1074/jbc.M117.784702.

Zempel, H., J. Luedtke, Y. Kumar, J. Biernat, H. Dawson, E. Mandelkow, and E.-M. Mandelkow, 2013, Amyloid-β oligomers induce synaptic damage via Tau-dependent microtubule severing by TTLL6 and spastin.: The EMBO journal, v. 32, no. 22, p. 2920–37, doi:10.1038/emboj.2013.207.

Zempel, H., and E. Mandelkow, 2014, Lost after translation: missorting of Tau protein and consequences for Alzheimer disease: Trends in Neurosciences, v. 37, no. 12, p. 721–732, doi:10.1016/j.tins.2014.08.004.

Zempel, H., E. Thies, E. Mandelkow, and E.-M. Mandelkow, 2010, Abeta oligomers cause localized Ca(2+) elevation, missorting of endogenous Tau into dendrites, Tau phosphorylation, and destruction of microtubules and spines: The Journal of neuroscience, v. 30, no. 36, p. 11938–50, doi:10.1523/JNEUROSCI.2357-10.2010.

Zhang, B. … V. Emilsson, 2013, Integrated systems approach identifies genetic nodes and networks in late-onset Alzheimer's disease: Cell, v. 153, no. 3, p. 19–22, doi:10.1109/WISNET.2018.8311553.

Zhang, B., A. Maiti, S. Shively, F. Lakhani, G. McDonald-Jones, J. Bruce, E. B. Lee, S. X. Xie, S. Joyce, C. Li, P. M. Toleikis, V. M. Y. Lee, and J. Q. Trojanowski, 2005, Microtubule-binding drugs offset tau sequestration by stabilizing microtubules and reversing fast axonal transport deficits in a tauopathy model: Proceedings of the National Academy of Sciences of the United States of America, v. 102, no. 1, p. 227–231, doi:10.1073/pnas.0406361102.

8. Appendix

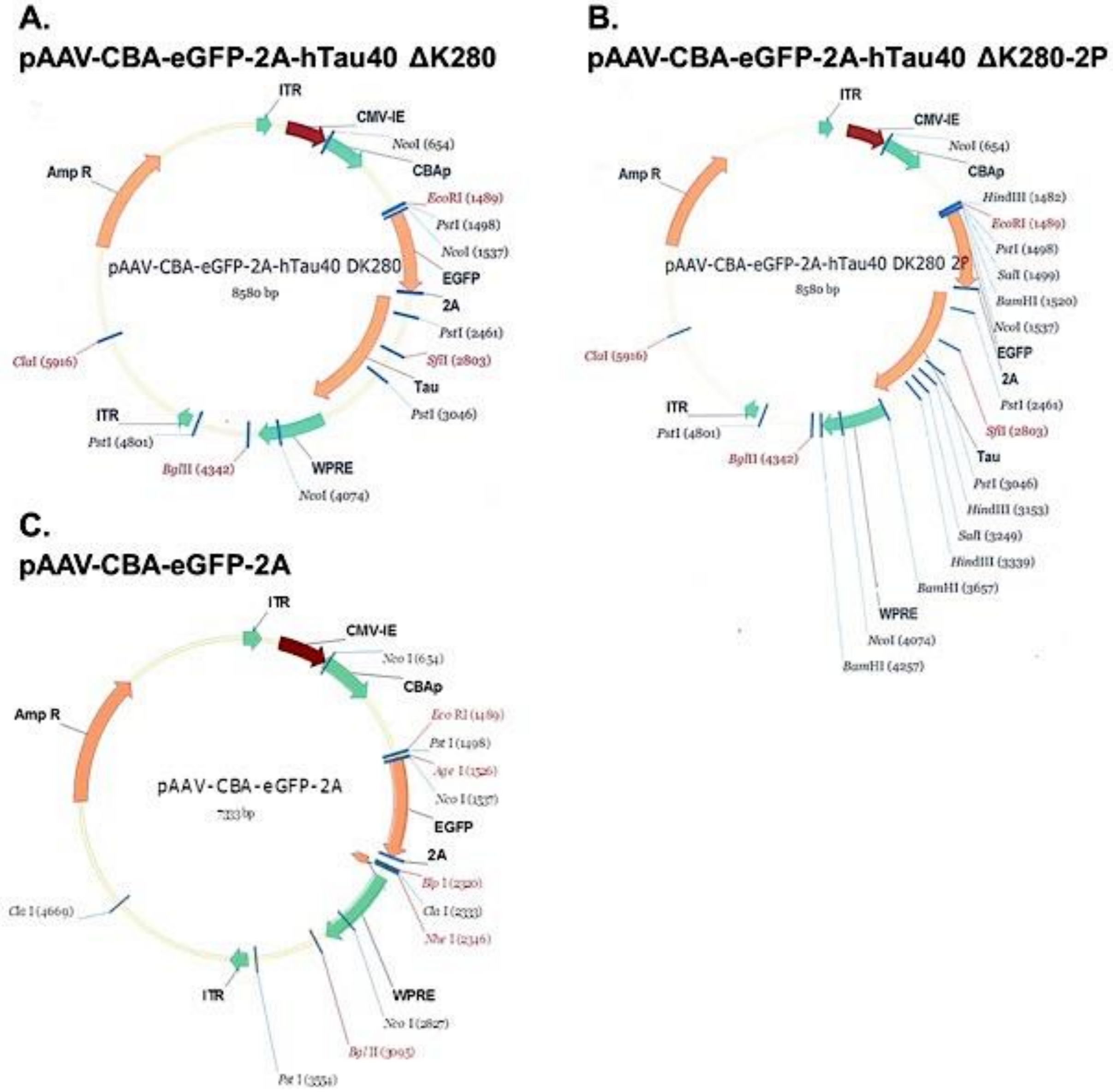
A.
pAAV-CBA-eGFP-2A-hTau40 ΔK280
ITR
CMV-IE
NcoI (654)
CBAp
Amp R
EcoRI (1489)
PstI (1498)
NcoI (1537)
pAAV-CBA-eGFP-2A-hTau40 DK280
8580 bp
EGFP
2A
PstI (2461)
ClaI (5916)
SfiI (2803)
Tau
ITR
PstI (3046)
PstI (4801)
BglII (4342)
WPRE
NcoI (4074)
B.
pAAV-CBA-eGFP-2A-hTau40 ΔK280-2P
ITR
CMV-IE
NcoI (654)
CBAp
Amp R
HindIII (1482)
EcoRI (1489)
PstI (1498)
pAAV-CBA-eGFP-2A-hTau40 DK280 2P
8580 bp
SalI (1499)
BamHI (1520)
NcoI (1537)
ClaI (5916)
EGFP
2A
ITR
PstI (2461)
PstI (4801)
SfiI (2803)
BglII (4342)
Tau
PstI (3046)
HindIII (3153)
SalI (3249)
HindIII (3339)
BamHI (3657)
WPRE
NcoI (4074)
BamHI (4257)
C.
pAAV-CBA-eGFP-2A
ITR
CMV-IE
Neo I (654)
CBAp
Amp R
Eco RI (1489)
Pst I (1498)
Age I (1526)
pAAV-CBA-eGFP-2A
7333 bp
Nco I (1537)
EGFP
2A
Blp I (2320)
Cla I (4669)
Cla I (2333)
Nhe I (2346)
ITR
WPRE
Nco I (2827)
Bgl II (3005)
Pst I (3554)

Suppl. fig. 1 - Plasmid maps of the adeno-associated virus used in the study.
A. pAAV-CBA-eGFP-2A-hTau40 ΔK280, for the expression of pro-aggregant Tau (full length mutant human Tau with the ΔK280 mutation); **B.** pAAV-CBA-eGFP-2A-hTau40 ΔK280-2P for the expression of anti-aggregant Tau (full length mutant human Tau with the ΔK280 mutation and 2 prolines); **C.** pAAV-CBA-eGFP-2A for the expression of GFP in the cells.

SDS gel composition

Reagent	Resolving 10%	Resolving 17%	Stacking 4%
Acrylamide 40%	18mL	30mL	5.4mL
1M Tris HCl pH 8.8	26	26	-
0.25M Tris HCl pH 6.8	-	-	27mL
H_2O + Bromophenol Blue	-	-	2mL
MiliQ H_2O	25mL	13mL	18.9
SDS 10%	700µL	700µL	540µL
TEMED	70µL	70µL	150µL
APS 10%	700µL	700µL	200µL

5x SDS sample buffer

0.32 M Tris-HCl, pH 6.8; 10% SDS; 50% glycerol; 1.43 M β-Mercaptoethanol and 10% bromophenol blue

1x SDS running buffer (5 liters)

0.025 M Tris; 0.192 M glycine; 0.1% SDS; Adjust volume to 5 liters with ddH_2O

10x blotting buffer (2.5 liters)

73.25 g glycine; 145.3 g Tris; 7.5 g SDS
Adjust volume to 2.5 liters with ddH_2O.

1x blotting buffer (1 liter)

80 mL 10x blotting buffer; 870 mL MiliQ H_2O 50 mL MeOH

10x TBS-T (2.5 liters)

30.27 g Tris; 220 g NaCl
Adjust pH to 7.5 and add 12.5 mL Tween 20. Fill up to 2.5 liters.

2x lysis buffer (40 mL)

50 mM Tris-Hcl pH 7.4; 10& glycerol; 1% NP40; 5 mM DTT;M 1 mM NaEGTA; 20 mM NaF; 1 mM Na_3VO_4
Adjust to 40 mL with ddH_2O.

Working lysis buffer (8 mL)

4 mL 2x lysis stock; 150 mM NaCl; 1x complete mini 25x conc.; 5 mM CHAPS; 100 U Benzonase; 5 µM okadaic acid; 2 mM MiliQ H_2O; 1 mM PMSF

10x PBS (1 liter)

80 g NaCl; 2 g KCl; 14.4 g Na_2HPO_4; 2.4 g KH_2PO_4
Set pH to 7.4 and adjust volume to 1liter with ddH_2O.

10x TBS (1 liter)

24 g Tris; 88 g NaCl
Set pH to 7.4 and adjust volume to 1liter with ddH_2O.

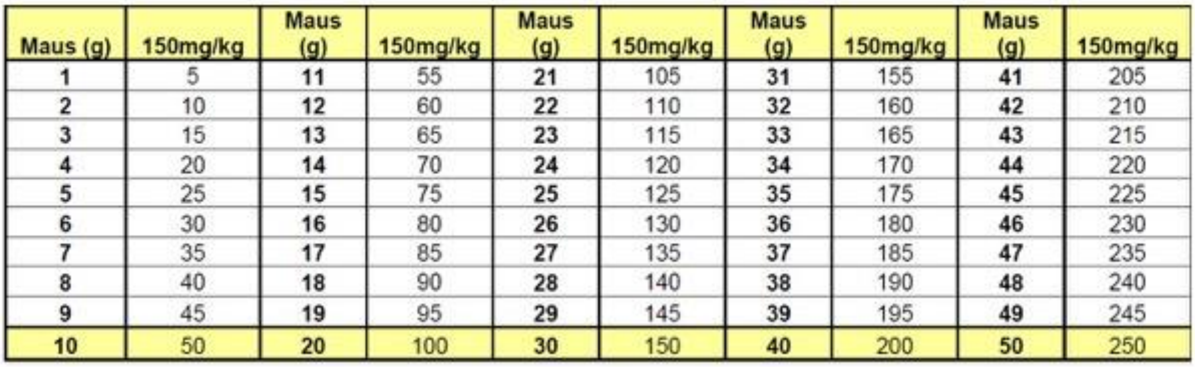

Maus (g)	150mg/kg	Maus (g)	150mg/kg	Maus (g)	150mg/kg	Maus (g)	150mg/kg	Maus (g)	150mg/kg
1	5	**11**	55	**21**	105	**31**	155	**41**	205
2	10	**12**	60	**22**	110	**32**	160	**42**	210
3	15	**13**	65	**23**	115	**33**	165	**43**	215
4	20	**14**	70	**24**	120	**34**	170	**44**	220
5	25	**15**	75	**25**	125	**35**	175	**45**	225
6	30	**16**	80	**26**	130	**36**	180	**46**	230
7	35	**17**	85	**27**	135	**37**	185	**47**	235
8	40	**18**	90	**28**	140	**38**	190	**48**	240
9	45	**19**	95	**29**	145	**39**	195	**49**	245
10	50	**20**	100	**30**	150	**40**	200	**50**	250

Suppl. fig. 2 - Volume of luciferin to be injected in the mice before BLI measurement according to the body weight to achieve an injection concentration of 150 mg/kg.

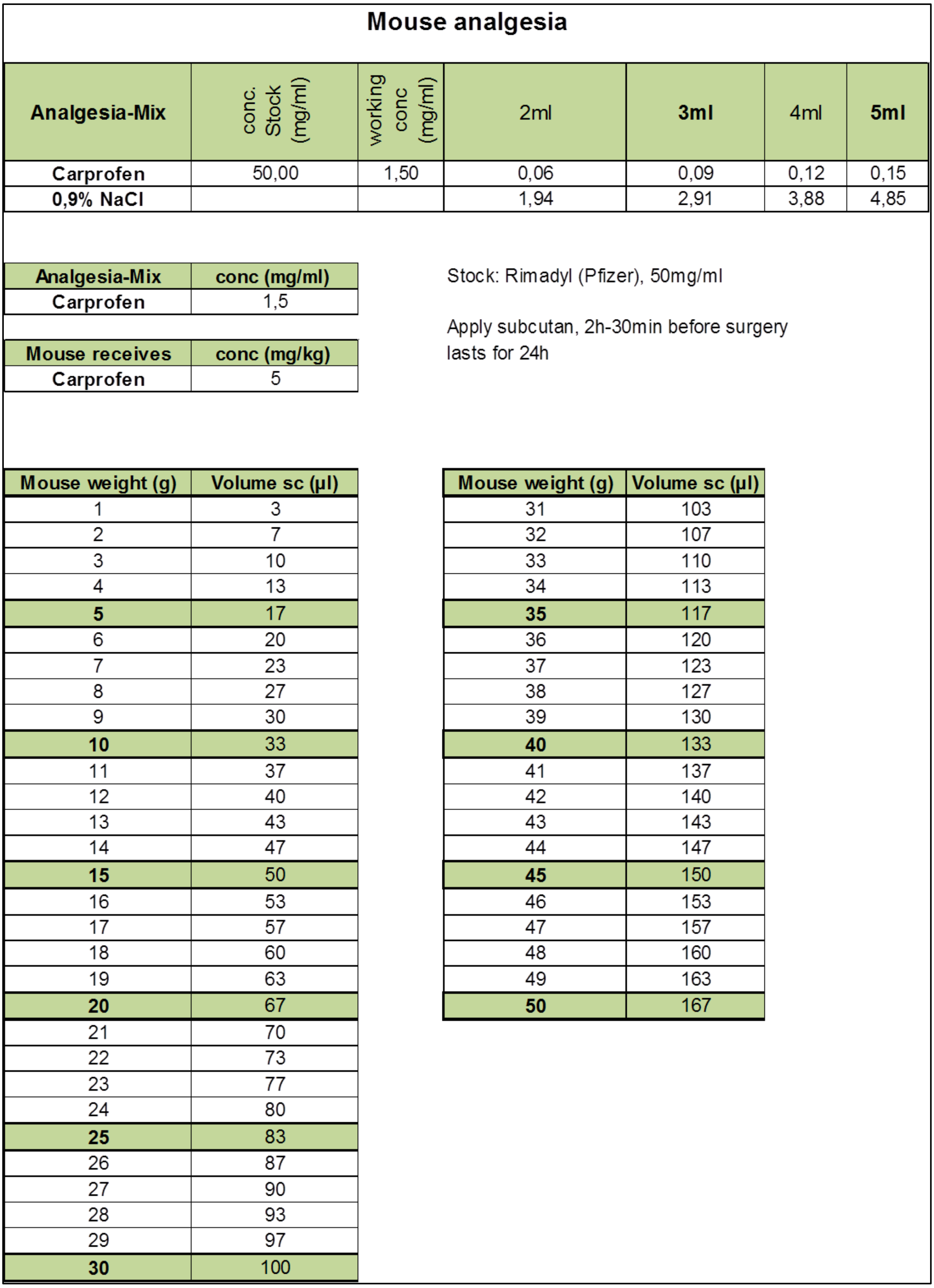

Mouse analgesia

Analgesia-Mix	conc. Stock (mg/ml)	working conc (mg/ml)	2ml	**3ml**	4ml	**5ml**
Carprofen	50,00	1,50	0,06	0,09	0,12	0,15
0,9% NaCl			1,94	2,91	3,88	4,85

Analgesia-Mix	**conc (mg/ml)**
Carprofen	1,5

Stock: Rimadyl (Pfizer), 50mg/ml

Mouse receives	**conc (mg/kg)**
Carprofen	5

Apply subcutan, 2h-30min before surgery
lasts for 24h

Mouse weight (g)	**Volume sc (µl)**
1	3
2	7
3	10
4	13
5	17
6	20
7	23
8	27
9	30
10	33
11	37
12	40
13	43
14	47
15	50
16	53
17	57
18	60
19	63
20	67
21	70
22	73
23	77
24	80
25	83
26	87
27	90
28	93
29	97
30	100

Mouse weight (g)	**Volume sc (µl)**
31	103
32	107
33	110
34	113
35	117
36	120
37	123
38	127
39	130
40	133
41	137
42	140
43	143
44	147
45	150
46	153
47	157
48	160
49	163
50	167

Suppl. fig. 3 - Dosage of analgesia (Carprofen) to be administrated to the mice before surgery, according to the animal's body weight.

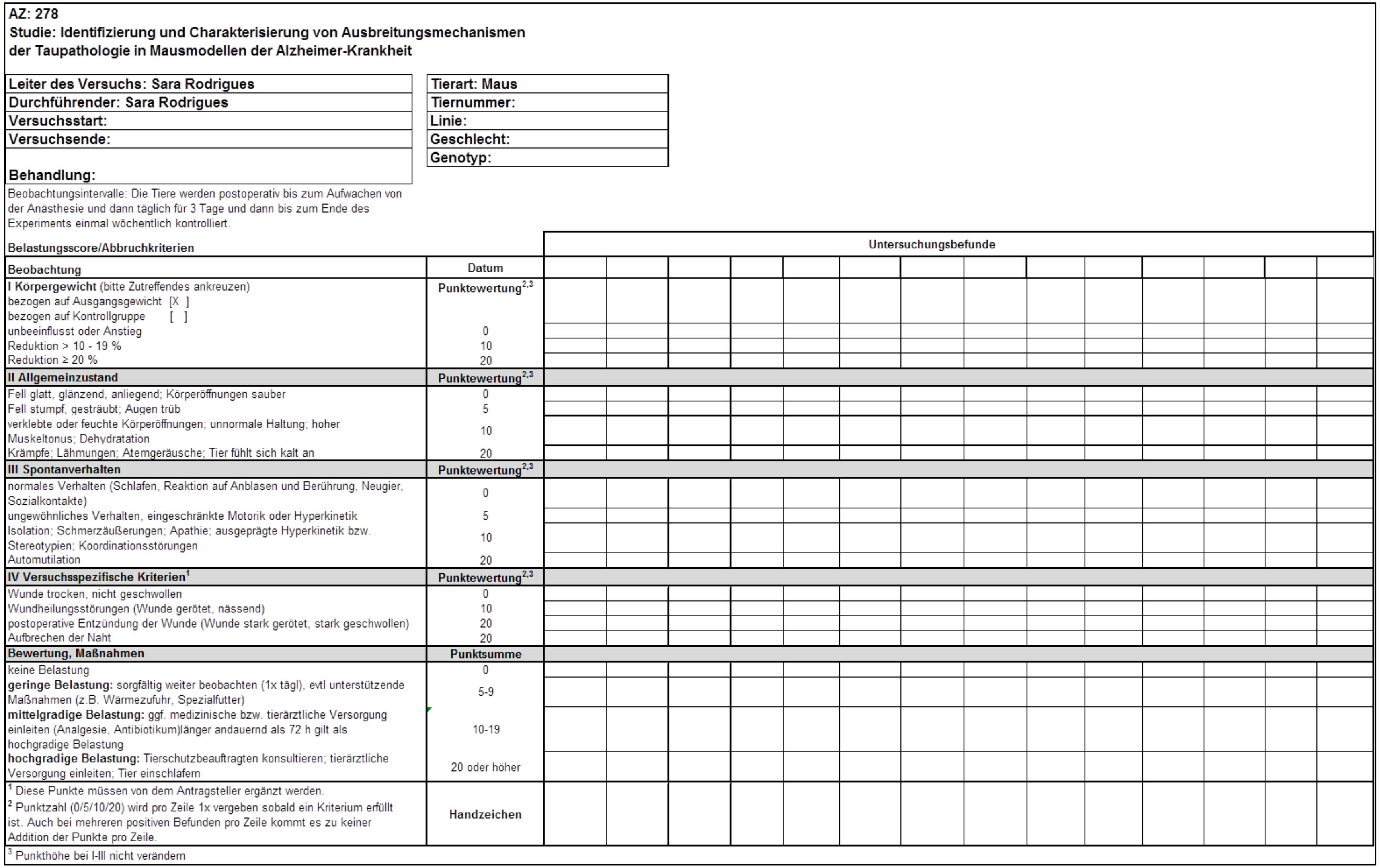

AZ: 278

Studie: Identifizierung und Charakterisierung von Ausbreitungsmechanismen der Taupathologie in Mausmodellen der Alzheimer-Krankheit

Leiter des Versuchs: Sara Rodrigues
Durchführender: Sara Rodrigues
Versuchsstart:
Versuchsende:

Behandlung:

Tierart: Maus
Tiernummer:
Linie:
Geschlecht:
Genotyp:

Beobachtungsintervalle: Die Tiere werden postoperativ bis zum Aufwachen von der Anästhesie und dann täglich für 3 Tage und dann bis zum Ende des Experiments einmal wöchentlich kontrolliert.

Belastungsscore/Abbruchkriterien		**Untersuchungsbefunde**													
Beobachtung	**Datum**														
I Körpergewicht (bitte Zutreffendes ankreuzen) bezogen auf Ausgangsgewicht [X] bezogen auf Kontrollgruppe [ ]	**Punktewertung[2,3]**														
unbeeinflusst oder Anstieg	0														
Reduktion > 10 - 19 %	10														
Reduktion ≥ 20 %	20														
II Allgemeinzustand	**Punktewertung[2,3]**														
Fell glatt, glänzend, anliegend; Körperöffnungen sauber	0														
Fell stumpf, gesträubt; Augen trüb	5														
verklebte oder feuchte Körperöffnungen; unnormale Haltung; hoher Muskeltonus; Dehydratation	10														
Krämpfe; Lähmungen; Atemgeräusche; Tier fühlt sich kalt an	20														
III Spontanverhalten	**Punktewertung[2,3]**														
normales Verhalten (Schlafen, Reaktion auf Anblasen und Berührung, Neugier, Sozialkontakte)	0														
ungewöhnliches Verhalten, eingeschränkte Motorik oder Hyperkinetik	5														
Isolation; Schmerzäußerungen; Apathie; ausgeprägte Hyperkinetik bzw. Stereotypien; Koordinationsstörungen	10														
Automutilation	20														
IV Versuchsspezifische Kriterien[1]	**Punktewertung[2,3]**														
Wunde trocken, nicht geschwollen	0														
Wundheilungsstörungen (Wunde gerötet, nässend)	10														
postoperative Entzündung der Wunde (Wunde stark gerötet, stark geschwollen)	20														
Aufbrechen der Naht	20														
Bewertung, Maßnahmen	**Punktsumme**														
keine Belastung	0														
geringe Belastung: sorgfältig weiter beobachten (1x tägl), evtl unterstützende Maßnahmen (z.B. Wärmezufuhr, Spezialfutter)	5-9														
mittelgradige Belastung: ggf. medizinische bzw. tierärztliche Versorgung einleiten (Analgesie, Antibiotikum)länger andauernd als 72 h gilt als hochgradige Belastung	10-19														
hochgradige Belastung: Tierschutzbeauftragten konsultieren; tierärztliche Versorgung einleiten; Tier einschläfern	20 oder höher														
[1] Diese Punkte müssen von dem Antragsteller ergänzt werden. [2] Punktzahl (0/5/10/20) wird pro Zeile 1x vergeben sobald ein Kriterium erfüllt ist. Auch bei mehreren positiven Befunden pro Zeile kommt es zu keiner Addition der Punkte pro Zeile.	**Handzeichen**														

[3] Punkthöhe bei I-III nicht verändern

Suppl. fig. 4 - Score sheet for evaluating the mice after stereotaxic injection of AAV, as approved by the German authority for animal welfare LANUV under the animal application number 84-02.04.2016-A278.

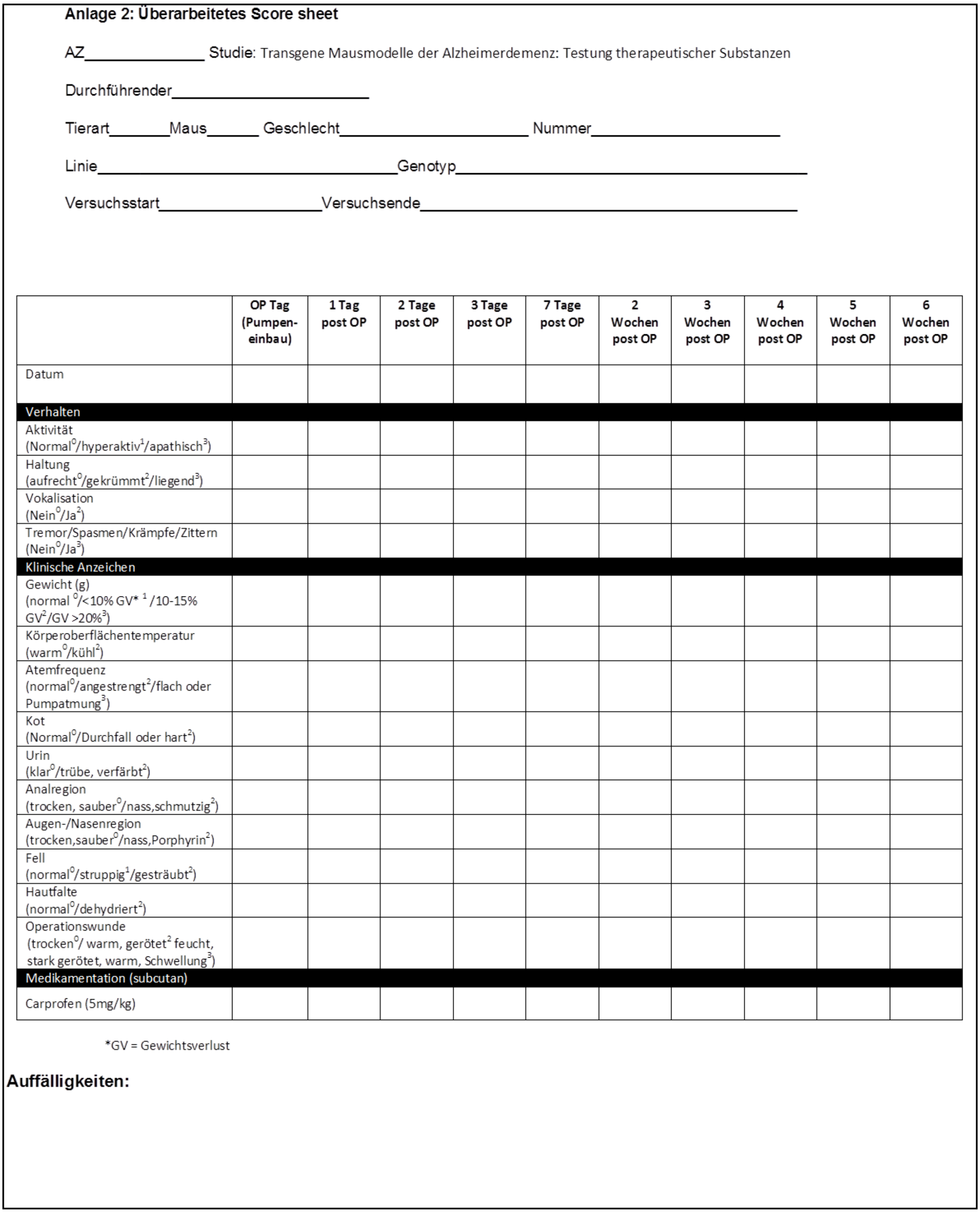

Anlage 2: Überarbeitetes Score sheet

AZ_______________ Studie: Transgene Mausmodelle der Alzheimerdemenz: Testung therapeutischer Substanzen

Durchführender________________________

Tierart_______Maus______ Geschlecht______________________ Nummer______________________

Linie__________________________________Genotyp____

Versuchsstart___________________Versuchsende____

	OP Tag (Pumpen-einbau)	1 Tag post OP	2 Tage post OP	3 Tage post OP	7 Tage post OP	2 Wochen post OP	3 Wochen post OP	4 Wochen post OP	5 Wochen post OP	6 Wochen post OP
Datum										
Verhalten										
Aktivität (Normal^0/hyperaktiv^1/apathisch^3)										
Haltung (aufrecht^0/gekrümmt^2/liegend^3)										
Vokalisation (Nein^0/Ja^2)										
Tremor/Spasmen/Krämpfe/Zittern (Nein^0/Ja^3)										
Klinische Anzeichen										
Gewicht (g) (normal ^{0}/<10% GV* ^{1} /10-15% GV^2/GV >20%^{3})										
Körperoberflächentemperatur (warm^0/kühl^2)										
Atemfrequenz (normal^0/angestrengt^2/flach oder Pumpatmung^3)										
Kot (Normal^0/Durchfall oder hart^2)										
Urin (klar^0/trübe, verfärbt^2)										
Analregion (trocken, sauber^0/nass,schmutzig^2)										
Augen-/Nasenregion (trocken,sauber^0/nass,Porphyrin^2)										
Fell (normal^0/struppig^1/gesträubt^2)										
Hautfalte (normal^0/dehydriert^2)										
Operationswunde (trocken^0/ warm, gerötet^2 feucht, stark gerötet, warm, Schwellung^3)										
Medikamentation (subcutan)										
Carprofen (5mg/kg)										

*GV = Gewichtsverlust

Auffälligkeiten:

Suppl. fig. 5 - Score sheet for evaluating the mice after implantation and replacement of Alzet osmotic pumps, as approved by the German authority for animal welfare LANUV under the animal application number 84-02.04.2017-A405.

Acknowledgements

I am very grateful to a number of people who contributed to the successful completion of this doctoral thesis. Some, however, deserve special attention:

First, I would like to express my sincere gratitude to my supervisors Prof. Dr. Eckhard Mandelkow and Dr. Eva Mandelkow for their continuous support during my PhD research, for the knowledge, motivation, and opportunity to grow scientifically.

A special acknowledgement to Marta Anglada for her prompt and useful advice during my research, but also in life. She gives me a lifetime unforgettable memory of laughter and joy, and I truly value her friendship.

I wish to express my deepest gratitude to the funding agencies: the European Union's Horizon 2020 research and innovation program under grant agreement No 676144, and the DZNE

Furthermore, I would like to sincerely acknowledge Sabrina Hübschmann for her outstanding technical assistance and for being always available to help me.

I am also thankful to Laiq-Jan, Ronja and Julia for their friendship and for making my time in the lab so enjoyable.

A special thank you to all previous and current members of the Mandelkow group for receiving so well in the group and for being always available to help me.

A sincere acknowledgement to the members of the SyDAD PhD program. I am grateful for being part of this program and for all the knowledge and moments we shared.

A special thank you to the DZNE Light Microscope Facility (LMF), and the animal facility staff for their continuous support throughout my research, and to Susanne Birnmeyer for her support with administrative tasks.

I wish to show my gratitude to Sven for the unconditional love, patience and support. Thank you for all the wonderful ways you make me happy.

Last, but definitely not the least, I am greatly indebted to the most important persons in my life, my parents and brother. An endless thank you for providing me every opportunity to do what I love and for your continuous support, even when that means being thousand miles away. Thank you for your love and dedication.